Development of Methods to Improve Subsurface Injection Project Site-Suitability Assessments Conducted in the Alberta Basin

by

Mahendra Samaroo

A thesis submitted in partial fulfillment of the requirements for the degree of

Doctor of Philosophy

in

Geotechnical Engineering

Department of Civil and Environmental Engineering
University of Alberta

Abstract

Drastic changes in the scale and type of fluid injection required to support the implementation of a net-zero energy economy have introduced risks previously not considered in existing site screening processes conducted for industrial-scale injection projects. A scale of injection unprecedented in human history into underexplored injection target formations is being considered, with limited knowledge of potential cumulative or long-term consequences. New methods are required to complement existing site screening and risk assessment procedures for such projects, to account for the potential to impact other (current and future) subsurface users, to trigger induced seismicity and the likelihood of achieving long-term injectivity goals.

This research adapted an existing method (developed for hydrocarbon resource assessment) and used this adaptation along with over 63 million fluid extraction and injection records from over 610,000 wells over the last 60 years to calculate the net fluid balance (a new capacity estimation parameter, equivalent to the upper limit of sustainable injection capacity) at various stratigraphic intervals in the Alberta Basin. This new workflow enables the use of high confidence, publicly available volumetric data to evaluate the in-situ net fluid balance in various geographic locations and stratigraphic intervals in the Alberta Basin. The results indicate that significant sustainable injection capacity may exist within the extensively depleted Mesozoic formations (legacy oil and gas reservoirs) in several geographic locations in the basin, while limited sustainable injection capacity appears to exist in Paleozoic formations in contact with the Precambrian basement.

A novel fluid-injection project site selection screening method was then developed. This method is designed to evaluate and rank the brittleness/ductility and the potential for fault slip associated seismogenicity in geologic formations, based on current in-situ stress state and rock

geomechanical properties. The application of this new method to evaluate and rank the potential for seismogenic/aseismic fault slip was then demonstrated, by evaluating over 3,000 laboratory core triaxial tests along with the in-situ (minimum horizontal, vertical) stress and pore pressure measurements available for 51 injection and confining formations in the Alberta Basin. This analysis indicates that most of the major formations evaluated in the Alberta Basin were ductile (at the time of the in-situ measurements) and likely to display low potential for seismogenicity (i.e., fault slip likely to be aseismic), which is consistent with induced seismicity observations in the Alberta Basin over the past decade.

A workflow was then developed for generating high confidence estimates of long-term (20 year) sustained regional-scale carbon dioxide (CO_2) injectivity rates in key disposal formations in the Alberta Basin. The utility of this workflow was demonstrated by first using the results of over 3,000 laboratory core tests to construct 22 regional-scale 3D geological, geomechanical and petrophysical models. These models were then calibrated with calculated regional-scale injectivity data obtained from disposal operations conducted in over 4,000 wells over the last 60 years, and the calibrated models used to simulate the effects of 20 years of CO_2 injection in these (22) formations. This analysis indicates that several of the ductile (legacy, depleted hydrocarbon reservoir) Mesozoic formations in the Alberta Basin are also capable of supporting sustained CO_2 injection at the rates needed to enable commercial-scale sequestration activities (in addition to the main virgin pressure Paleozoic saline aquifer currently targeted) and that CO_2 presence and material formation pressure increases can be expected at distances of at least 12 km from the injector.

The three workflows developed and demonstrated in this research may be useful complementary criteria for project proponents and regulators to consider during project site

suitability studies conducted at the site screening stages of industrial-scale fluid disposal project development in any sedimentary basin. Consideration of the net fluid balance, brittle-ductile state, and long-term sustained injectivity rates could improve the site selection process, help reduce project risks and thereby enhance the chances of successful commercial-scale CO_2 injection project development and operations.

Preface

All sections of this thesis have been published in the Special Issue State-of-the-Art Geo-Energy Technology in North America of the journal Energies (ISSN 1996-1073). I developed the concepts for the net fluid balance and the regional-scale CO_2 injection rate simulation workflow, designed the research methodologies, conducted the formal analysis, designed and executed all simulations and wrote the manuscripts for all papers contained in this thesis. Dr. Rick Chalaturnyk developed the conceptual model for the brittle-ductile state method and assisted with manuscript reviews and editing. Dr. Maurice Dusseault assisted with design of research methodology, manuscript reviews and editing. The published journal papers are listed below, and the relevant paper is referenced in the corresponding footnote for each chapter.

(1) Samaroo, M.; Chalaturnyk, R.; Dusseault, M.; Jackson, R.; Buhlmann, A.; Custers, H. An Assessment of the Net Fluid Balance in the Alberta Basin. Energies 2022, 15, 1081. https://doi.org/10.3390/en15031081.

(2) Samaroo, M.; Chalaturnyk, R.; Dusseault, M.; Chow, J.F.; Custers, H. Assessment of the Brittle–Ductile State of Major Injection and Confining Formations in the Alberta Basin. Energies 2022, 15, 6877. https://doi.org/10.3390/en15196877.

(3) Samaroo, M.; Chalaturnyk, R.; Dusseault, M. Estimating Sustainable Long-Term Fluid Disposal Rates in the Alberta Basin. Energies 2023, 16(6), 2532, https://doi.org/10.3390/en16062532.

Acknowledgements

I would like to express my sincere appreciation for the people around me that have helped to make this effort possible and memorable. Most importantly, I would like to thank my family (Juliana and Matthew) for the support, patience and understanding displayed over the countless evenings and weekends I spent in the basement, and for the many others spent whining about incomprehensible data and uncooperative software.

This work would not have been possible without the guidance and support of my supervisor, Dr. Rick Chalaturnyk, to whom I am grateful for the wealth of wisdom selflessly dispensed in times of frustration. I am also immensely grateful for the invaluable insights of Dr. Maurice Dusseault, Dr. Richard Jackson and the guidance of Dr. Derek Martin, Dr. Renato Macciotta, Dr. Chris Hawkes. The encouragement and support of Chris Holly, Hans Custers, Stephen Wills, Steve Tkalcic, Rodney Anderson, Patti Humphrey, Mary Jane Fedor, Jordan and Vicki Lightbown and Jesse Toor are also gratefully acknowledged. The generous assistance of Garrett Fowler and Dr. Mark McClure (ResFrac^{TM} Corporation) with the use of the ResFrac^{TM} simulator is also gratefully appreciated. Additionally, the support of the Alberta Department of Energy over the years was instrumental for the completion of this study.

This journey was made enjoyable by the many friends I made along the way. My appreciation to Dr. Juan Arias, Susan Navas, Hope Walls, Dr. Gonzalo Zambrano, Dr. Amir Haghi, and the many others at the Reservoir Geomechanics Research Group and the Alberta Department of Energy for the support and encouragement over the (many) years.

Table of Contents

List of Tables

List of Figures

1.0 Introduction

Historically, fluid injection and waste disposal into the subsurface has largely been successful in oil and gas basins partly because volumes of fluid injected into the subsurface have been insignificant compared to the volumes of fluid extracted, the fluids injected have been principally native oil and gas associated waste and the receiving formations have been competent (low leakage) geologic fluid traps for at least millennia. Hydrocarbon production-associated fluid extraction from such basins over the last century has resulted in massive pressure depletion, with these depleted formations becoming subsurface pressure sinks ideal for storage of unwanted fluids. Regulatory requirements in such basins typically help to ensure that large-scale fluid injection is directed back to the original source formation, to mitigate subsurface hydrogeologic impacts.

The future implementation of energy transition and net-zero energy policies is expected to drastically reduce hydrocarbon fluid extraction, while substantially increasing the volumes of fluid waste disposed into the subsurface. A net-zero energy economy, for instance, is likely to result in an unprecedented scale of CO_2 injection into the subsurface in the Alberta Basin, which has the potential to overwhelm the pore space available and increase receiving formation pore pressures considerably at a regional scale [1]. Concurrently, it is being increasingly recognized globally that pore space is a finite, depleting resource that requires active management for the public good [2], and that current methods for estimating pore space resource for sequestration capacity in deep saline formations do not account for conflicting uses of pore space and the potential for CO_2 migration and subsurface pressure effects to extend over hundreds to thousands of square kilometers [3]. However, recent energy policy strategies have assumed that annual gigaton scale injection of CO_2 into such aquifers is unremarkable and can be successfully maintained for decades in existing sedimentary basins without significant adverse effects [4]–[6]. Conversely, the operations of CO_2 injection projects can be prematurely terminated if large magnitude induced seismic events and/or the loss of (lateral or vertical) containment occurs [7], which could consequently handicap essential (net zero) industrial operations that depend on availability of sequestration capacity. Proactive assessment of major risks to sequestration capacity availability is therefore important to mitigate the impacts of a loss of sequestration capacity and major unplanned industrial disruptions in a future net-zero economy.

Current pore space capacity estimation methods have focused on determination of gross pore space volume, with limited ability to account for diverse risks posed to other subsurface users by (sustained) gigaton scale displacement of pore fluids (brines) and basin-scale increase in subsurface pressure. The impacts of such pressure increase may be important to consider, particularly in sedimentary basins such as Alberta, where regionally interconnected mega-hydrodynamic flow systems and their existing hydraulic gradients enable operation of the economically important hydrocarbon extraction and associated industries. Additionally, such capacity estimation methods have not yet evolved to enable (i) proactive consideration of pressure constraints which may be required to mitigate the potential for generating induced seismicity of concern, and (ii) a high confidence assessment of the likelihood that the required disposal volumes can be continuously injected into the targeted receiving formation at economically feasible rates. Development of methods to help evaluate sustainable disposal capacity, which is the subset of subsurface pore space into which disposal is unlikely to affect current/future pore space users, is unlikely to trigger induced seismicity of concern and can be continuously conducted at economic rates can therefore be a valuable complement to existing site screening criteria for industrial-scale fluid-injection projects. The availability of such methods can help to inform the design of future pore space and energy policy, as well as the site selection and design process for industrial-scale CO_2 injection projects.

1.1 Problem Statement

There are existing precedents in other industries that provide principles that can be useful for estimating sustainable capacity in the subsurface fluid-injection industry. These include the (mass-balance based) concept of sustainable yield commonly used in groundwater extraction, which is defined as the maximum amount of water that can be withdrawn from a specified aquifer system with acceptable physical, economic, environmental, social, cultural, institutional, and legal consequences [8]. The difference between the amount of fluid injected into and the amount of fluid removed from the same stratigraphic zone in the subsurface (i.e., the net fluid balance) has the most impact on changing the subsurface pore pressure, with projects that maintain a zero or negative net fluid balance generating fewer seismic events [9]. Regional or basin-scale fluid budgets that maintain a zero or negative net fluid balance, particularly within 1

km of the Precambrian basement, could help to reduce the potential for generating seismic events of concern in industrial-scale injection projects [10], [11].

Another key engineering principle used to (maintain hydraulic containment and) mitigate containment risk in large industrial waste sites involves the maintenance of a permanent negative (inward) or zero hydraulic (pressure) gradient between non-native (contaminant) fluids in the subsurface and the surrounding environment at the end of project operations [12]–[14]. However, no (known) publicly available calculation-based method currently exists for the estimation of sustainable injection capacity, despite the existence of extensive (high confidence) fluid input (injection) and output (withdrawal) volumetric data for sedimentary basins with many decades of hydrocarbon extraction activities. Additionally, best practice (hydraulic containment) design principles for managing (fluid injection) containment risks require an evaluation of all likely alternatives to the proposed widespread use of only virgin pressure saline aquifers for multi-decade gigaton scale CO_2 sequestration.

In addition to sustainable capacity, the ability to maintain sufficiently high long-term injection rates is critical for commercial-scale CO_2 sequestration projects to operate continuously at the economy of scale required to provide cost-effective service rates for industrial emitter clients [15]–[17]. However, limited efforts have been focused on developing high confidence methods to evaluate this key parameter (especially at a regional scale) despite its importance [18]. The development of methods to provide reliable long-term CO_2 injectivity estimates can therefore contribute to reducing economic risks for sequestration project developers, industrial emitters, policy makers and regulators. High confidence estimates of capacity and injectivity can help mitigate commercial risk in contractual obligations such as long-term offtake agreements (e.g., take or pay contracts) between emitters and sequestration service providers and help improve cost effectiveness of future commercial sequestration rates.

1.2 Research Objectives and Methodology

The main objectives of this research were to develop methods to evaluate sustainable capacity, potential for induced seismicity occurrence and long-term regional formation injection rates that can be used to complement existing site screening and selection assessments conducted for industrial-scale fluid-injection projects. These include a calculation-based materials balance

method for assessing regional scale formation net fluid balance, a geomechanics-based method to assess formation brittleness and a calibrated, validated numerical simulation-based method to assess long-term regional formation injectivity. The results presented in this thesis suggests that, in the Alberta Basin the regionally extensive intermediate-depth Mesozoic (depleted legacy oil and gas reservoir) formations appear to have greater sustainable capacity, a lower potential for generating induced seismicity, and injectivity comparable to the Paleozoic saline aquifers currently considered prime targets for industrial-scale CO_2 sequestration.

A calculation-based material balance method was first developed by adapting a method developed by the United States Geological Survey for the assessment of undiscovered hydrocarbon resources [19], [20] to estimate the in-situ net fluid balance in specific geographic regions and stratigraphic horizons in the Alberta Basin using surface-measured (i.e., stock-tank) fluid volumes. This involved the extraction, data cleansing and processing of the entire production and fluid-injection data set available for the Alberta Basin for the period 1962-2020, consisting of approximately 63 million fluid injection and production and approximately 610,000 well location, well depth, and depth-to-Precambrian basement records. Well records were subsequently grouped by common geologic setting and characteristics into specific geographic areas and by depth to the Precambrian basement, and then in-situ fluid injected minus in-situ fluid extracted calculated for each stratigraphic and geographic zone using the corresponding stock-tank volume measurements. The results obtained were then graphically presented for each geographic area and stratigraphic zone, with the stratigraphic zone located within 1 km of the Precambrian basement corresponding to the zone into which formation pressure increases were most likely to result in generation of induced seismicity of concern.

Next, a method and two parameters (χ and I_{BD}) were developed for assessment of the brittle-ductile state of a formation, based on its in-situ stress state, the Mogi-equivalent ductility parameter [21] for the specific lithology and the definition of the critical state concept applied to rock [22]. First, historical fluid production and injection volumetric data was used to identify 51 of the major injection and confining formations in the Alberta Basin. Subsequently, all publicly available well core laboratory triaxial test data for the Alberta Basin (approximately 3,000 core tests covering the period 1960-2021) was manually extracted, processed, examined, and re-interpreted in some cases, and then used to assess the Mogi-equivalent ductility parameter of

these 51 injection and confining formations. The in-situ stress states for these formations were then determined, and the most recent in-situ stress data used along with the calculated Mogi-equivalent ductility parameter to assess the χ and I_{BD} of these 51 major injection and confining formations.

A workflow to generate estimates of regional-scale CO_2 injection rates in major disposal formations was then developed, calibrated, and validated. First, all water disposal volumetric data for the approximately 4,000 disposal wells in the Alberta Basin (over the period 1960-2022) was extracted, processed, scrubbed, and analyzed to identify the recipient geologic formation. The injection rate data was then grouped by geologic formation and injection rate statistical distribution parameters calculated for each of the 66 disposal formations identified. The results of over 3,000 laboratory core data analyses were then used, to construct 3D regional-scale geological, geomechanical and petrophysical models for 22 of these disposal formations. The injection rate statistical distribution parameters were then used to history-match the water injection rates and derive regional-scale formation permeability for each disposal formation. The history-matched regional-scale permeability and the 3D models were subsequently used in a three-dimensional physics-based, coupled, integrated hydraulic fracturing and reservoir simulation numerical model (ResFrac^{TM}) to evaluate the geomechanical effects of long-term CO_2 injection and likely sustained long-term CO_2 injected rates. The modeled CO_2 injection rate for a specific saline aquifer was then compared to the actual injection rate of a commercial-scale sequestration project operating in the same aquifer in the Alberta Basin, with close agreement obtained between the modeled and actual rates.

1.3 Thesis Organization

This thesis uses a paper-based structure format, since the main chapters contained have been published as individual papers in the peer-reviewed journal Energies. A succinct summary of the contents of each chapter is provided below.

1.3.1 Chapter 2 - An Assessment of the Net Fluid Balance in the Alberta Basin

This chapter provides details on the need for a method to assess sustainable capacity in the Alberta Basin and on the development process of the Net Fluid Balance method. This chapter

also demonstrates the application of the Net Fluid Balance method to estimate sustainable injection capacity in the Alberta Basin.

1.3.2 Chapter 3 – Assessment of the Brittle-Ductile State of Major Injection and Confining Formations in the Alberta Basin

This chapter provides details on the need for a method to assess the potential for fault slip to be aseismic/seismic, on the implications for seismic hazard, on the development of the method to assess the brittle-ductile state of injection and confining formations and demonstrates the use of this method to assess the potential for seismogenic fault slip in major injection and confining formations in the Alberta Basin.

1.3.3 Chapter 4 – Estimating Sustainable Long-Term Disposal Rates in the Alberta Basin

This chapter provides details on the importance of long-term regional injection rates for mitigating commercial-scale CO_2 injection project economic risk, the development of the workflow to estimate, calibrate and validate regional injection rates and the geomechanical effects of sustained long-term injection on 22 disposal formations in the Alberta Basin.

1.3.4 Chapter 5 – Conclusions and Recommendations

2.0 Assessment of the Net Fluid Balance in the Alberta Basin[1]

Abstract

Net fluid balance in the Alberta Basin has been negative over the last 60 years because extensive fluid production has consistently exceeded injection during this period. However, future gigaton-scale carbon sequestration, among other activities, can result in future cumulative fluid injection exceeding extraction (i.e., a positive net fluid balance). The in-situ net fluid balance (i.e., total fluids produced minus total fluids injected at in-situ conditions) in this basin over the period 1960-2020 shows that a liquids deficit of 4.53×10^9 m^3 and a gas deficit of 6.05×10^{12} m^3 currently exist. However, fluid deficits are more significant in the upper stratigraphic intervals (located more than 1 km above the Precambrian basement) than in the stratigraphic intervals located within 1 km of the Precambrian basement in most geographic regions. This observation indicates that greater sustainable injection capacity for large-scale fluid injection may exist in the upper stratigraphic intervals (located at more than 1 km above the Precambrian basement), reducing the potential for generating induced seismicity of concern. Additionally, while fluid depletion rates consistently increased over most of the last 60 years in the Alberta Basin, this trend appears to have changed over the past few years. Such analysis of regional net fluid balance and trends may be useful in assessing regional sustainable fluid storage capacity and managing induced seismicity hazards.

2.1 Introduction

Public policy developed on the basis of foundational science and evidence is essential for managing societal risk [23]. Empowering policymakers with sufficient information to make informed decisions significantly improves the likelihood of developing and implementing strategic public policies that mitigate risk, improves community resilience, and enhances public trust. Effective critical information for such purposes focuses on what results are known rather than the uncertainties or the process by which such information is derived [24].

[1] This chapter was published in the Special Issue State of the Art Geo-Energy Technology in North America of Energies: Samaroo, M.; Chalaturnyk, R.; Dusseault, M.; Jackson, R.; Buhlmann, A.; Custers, H. An Assessment of the Net Fluid Balance in the Alberta Basin. Energies 2022, 15, 1081. https://doi.org/10.3390/en15031081

Significant research has been conducted on developing methods to quantify the hazards associated with large-volume subsurface fluid injection and storage over the last century (e.g., [25]). These efforts intensified over the last two decades, focusing on developing methods to assess site performance risks and enhance public confidence in (future) large-scale carbon capture and storage activities [26]. These methods and frameworks have traditionally focused on project-scale injected fluid containment assurance, conformance, injection pressure and injectivity risks, with limited emphasis on the potential for generating felt-induced seismicity (e.g., [27]–[29]). Such emphasis on containment and conformance with little focus on induced seismicity generation and its impacts on infrastructure and inhabitants is reflected in the published risk assessments for major fluid-injection projects conducted in the Western Canada Sedimentary Basin (WCSB) (e.g., [30]–[39]).

The potential to generate induced seismicity that can affect surface infrastructure and population is a key hazard that should also be considered in risk assessments conducted for large-volume fluid-injection projects. Fluid injection into formations hydraulically connected to the geologic basement (including underpressured formations) significantly increases seismicity risk even in stable intraplate areas, and minor increases in pore pressure (as low as 0.8 kPa in some cases) are capable of reactivating critically stressed faults and triggering seismicity [40]–[42]. Meanwhile, over its lifetime, an industrial-scale carbon dioxide injection project has the potential to pressurize basin-scale radii of up to 100 km by more than 100 kPa, even though the actual injected fluid plume may be constrained to linear dimensions of under 10 km [43]–[45].

A common element in current seismicity root-cause hypotheses is that deep basement faults pose the greatest hazard [46]–[49], and the existence of a hydraulic connection from the injection horizon to the Precambrian basement greatly increases the likelihood of seismicity of concern [50]–[55]. A principal hazard factor identified to date is the proximity of the injection horizon to the crystalline basement (i.e., a proxy that considers the probability of hydraulic connection and poroelastic stress transfer between the injection horizon and the crystalline basement), with a threshold vertical distance of 1 km or less considered hazardous [10], [47], [48], [56]–[58]. The other hazard factor is the volume of fluid injected, with the number and size of potential seismic events generally proportional to the cumulative volume of fluid injected [59]–[63]. Management of these two factors has been shown to be a practical tool for managing

the potential for occurrence and controlling induced seismicity of concern in high-volume fluid-injection projects [64]–[67]. In addition, the net fluid balance (the difference between fluid injected into and fluid removed from the same zone in the subsurface) has the most impact on changing subsurface pore pressure over time; projects that maintain a balance between fluid injection and withdrawal generate fewer seismic events [9]. Regional or basin-scale fluid budgets that maintain a zero or negative net fluid balance, particularly within 1 km of the Precambrian basement, could help reduce the potential for generating seismic events of concern in large-scale injection projects [10], [68].

Deep injection of large fluid volumes is likely to increase significantly in the WCSB, arising from a substantial increase in energy-related carbon sequestration activities. Concurrently, a future energy transition is expected to substantially reduce the amount of hydrocarbon fluids removed from this basin. These macro-trends have the potential to increase injection-formation pore pressures in this basin. Consequently, there is a need to evaluate the net fluid budget in this basin to assess and sustainably manage its fluid-injection capacity. In cases of industrial-scale fluid injection, even in underpressured reservoirs, basin-wide fluid injection budget assessment (and management) is an essential requirement to mitigate the potential for generating induced seismicity of concern [10], [66].

This paper uses widely available measured (high confidence) volumetric data collected regularly for production and royalty accounting to construct a regional-scale net fluid balance for the Alberta Basin (a sub-basin within the WCSB) for the period 1960–2020. Such regional-scale net fluid balance assessments may be useful to policymakers and regulators for determining sustainable regional and basin-scale subsurface fluid storage capacity, managing basin-scale fluid budgets, and mitigating fluid-injection-related hazards such as induced seismicity. This evaluation shows that the largest fluid deficits (and sustainable fluid injection capacity) in the Alberta Basin exist in the stratigraphic horizons located more than 1 km above the Precambrian basement in select geographic locations. In addition, this evaluation also demonstrates that regional-scale fluid budget assessments can be conducted with relative ease using available information collected for production (volumetric) accounting purposes.

2.2 Materials and Methods

The considerable extent of the Alberta Basin and the geological and stratigraphic variations across its geography necessitates the use of a sector-based approach to isolate regional net fluid balance trends and identify areas in which proactive subsurface basin fluid management may be required. The use of production and royalty accounting data to estimate in-situ volumes requires conversion of surface volumes to subsurface volumes to account for differences between the surface measurement and subsurface reservoir conditions.

2.2.1 Subdivision of the Alberta Basin into Distinct Geology/Industrial Activity Regions

The Petroleum Services Association of Canada (PSAC) subdivision of the geographic regions within the Alberta Basin defines seven areas that are geologically distinct and/or have common (unique) resource characteristics. Each of these seven areas corresponds to a specific (predominant) type of geologic interest in the oil and gas industry [69], [70]. This subdivision has been used since the early 1970s to characterize geographic patterns of oil and gas activity across the Alberta Basin. These include oil and natural gas exploration, drilling, production, reserves, and cost statistics (e.g., the annual AER ST98 industry activity statistical reports) as well as PSAC-area specific benchmarks for well depths, drilling, and completion costs (e.g., the semi-annual PSAC Well Cost study). This subdivision is therefore suitable for characterizing trends in net fluid balance and industrial activity patterns within the Alberta Basin since each area is illustrative of the underlying geology and industrial activity types and is used to benchmark its historical, current, and future industrial activity levels [70], [71]. Figure 1 shows the seven PSAC areas in Alberta.

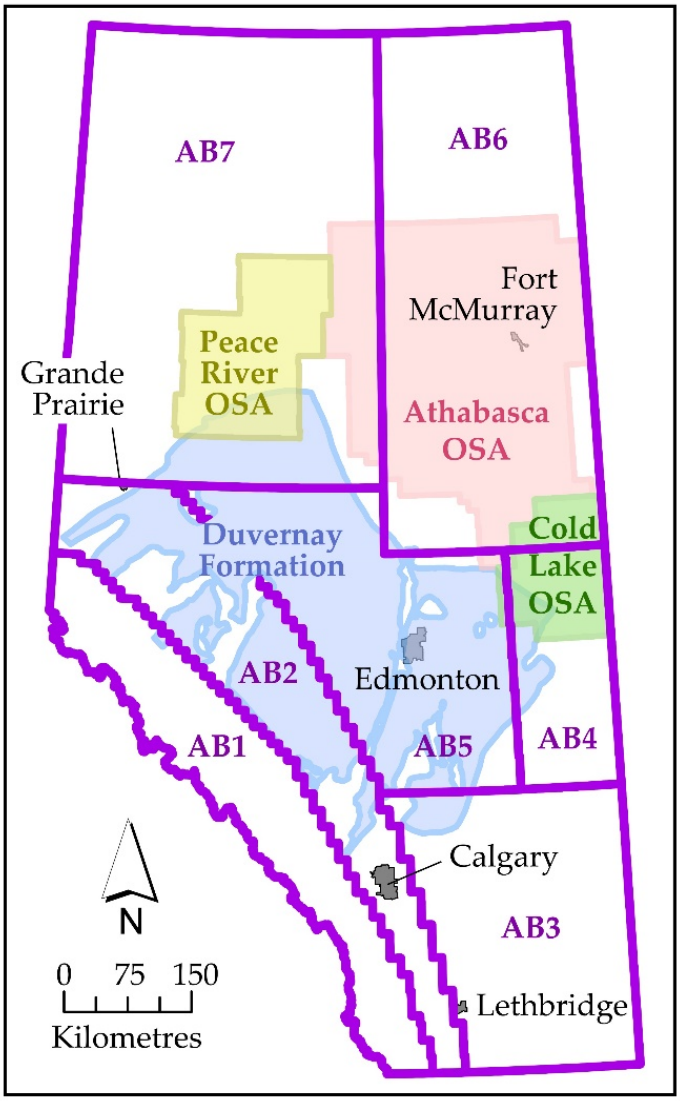

Figure 1. Map of the PSAC Areas, oil sands areas (OSA) and the Duvernay Shale Formation in Alberta. Courtesy of the Alberta Department of Energy.

Within the Alberta Basin, the thickness of the package of dipping sedimentary rocks exceeds 6 km in the southwest (adjacent to the Rocky Mountain Foothills). However, it thins to zero in the northeast due to depositional thinning and erosion [72], [73]. Consequently, common (median) well depths to the formations of interest in each region vary, with well depths being the shallowest in the northeast (in AB6) and increasing to the southwest (in AB1) as the thickness of the sedimentary package increases.

Since the predominant type of geologic interest in each area varies, the levels of industrial activity in each area also vary as a function of the market conditions during each

period for the specific type of oil and gas products. Major (current) geologic interest in areas AB1, AB2, AB3, AB5, and AB7 are the deep (km-scale) natural gas liquids-rich Duvernay Formation shale (Figure 1), with AB2 accounting for more than half of Alberta's natural gas production and most of its condensate production in 2019 [71]. These areas are expected to account for most of Alberta's industrial activity for higher-value light crude oil, natural gas, and natural gas liquids production over the next decade [71]. The availability of ample low-cost nearby subsurface pore space for the disposal of the large quantities of produced waste fluids (flowback) is vital for the commercial feasibility of hydraulic fracturing technology currently used to extract natural gas and condensates from shale formations such as the Duvernay [74], [75].

Shallow (around 500 m deep) bitumen deposits are the predominant geologic interest in AB4, AB6, and much of AB7. Approximately three million barrels per day of crude bitumen were produced from these areas in 2020 [71]. Mining and steam-based oil extraction technologies used to produce bitumen in these areas dispose of large quantities of liquid process wastes (such as produced fluids, mine dewatering fluids, and boiler blow-down) by injection into saline aquifers, while the in-situ thermal facilities in this region extract large quantities of water from these saline aquifers to generate steam used in bitumen production. However, current understanding of the hydrologic link between surface water bodies, shallow groundwater, and deep saline aquifers is limited at the regional scale, and detailed studies are required to assess the scale of anthropogenic-induced changes (if any) on the regional hydrologic balance of this area [76], [77].

Historic oil and gas activity in AB5 has consisted of the exploitation of conventional oil and natural gas deposits, which have now been largely depleted [71]. While this area also contains liquid-rich shale formations, production activity over the next decade is anticipated to be lower than in other areas, because of lower well-productivity rates and higher production/supply costs associated with industrial-scale operations near urban environments [71].

2.2.2 Calculation of Formation Volume Factors for Each Injection/Production Horizon in the Alberta Basin

The net fluid balance (also referred to as the net cumulative volume) is often used to characterize the fluid storage capacity of a formation. It consists of the cumulative volume of fluids (oil, gas, and water) removed from a formation minus the cumulative volume of fluid injected (liquids and gases) injected into the same formation over its production history [78]. Alberta maintains an extensive (auditable) dataset containing the monthly volumes of fluids removed from and injected into each well drilled in the province since 1960, with such volumetric measurements collected under surface (often referred to as stock tank) conditions. However, calculation of the net fluid balance within each formation requires correction of the volumes of fluids measured at surface conditions to the volumes they occupied in the subsurface, using the respective formation volume factors (FVF) for each fluid and corresponding formation depth (i.e., temperature and pressure) [78]. Schuenemeyer (2005) provides a method for conversion of stock-tank volumes to in-situ volumes shown in Equation 1 below [19]:

$$RV = FVF * ST, \qquad (1)$$

where RV and ST are the reservoir and stock-tank volumes of fluid (in the same volume units), FVF is the (dimensionless) formation volume factor specific to the corresponding formation (temperature and pressure) from which the fluid was removed. Estimates of formation volume factors for oil and gas extracted from each formation can be calculated using (empirical, imperial-unit specific) relationships developed by Verma and Bird (2005), providing that the depth at which such fluids have been extracted from or injected into and the corresponding American Petroleum Institute (API) oil gravity (in the case of oil) are known, and assuming formations are normally pressured [20]. These relationships are provided below, as Equations 2 to 13:

$$FVF_o = 0.972 + 0.000147 * (F)^{1.175}, \qquad (2)$$

$$F = GOR * (sgg/og)^{0.5} + 1.25 * t, \qquad (3)$$

$$og = 141.5 / (ag + 131.5), \qquad (4)$$

$$GOR = 0.86\ GOR_u \text{ (when } GOR_u \leq 1200), \qquad (5)$$

$$GOR = (0.86 + 0.24 * \sin^2 [(GOR_u - 1200) * \pi / (2000)] \text{ (when } 1200 < GOR_u < 2250), \qquad (6)$$

$$GOR = 1.1 * GOR_u \text{ (when } GOR_u \geq 2250), \quad (7)$$

$$GOR_u = sgg * [(p + 14.7) * 10^{0.0125 * ag} / (18 * 10^{0.00091 * t})]^{1.2}, \quad (8)$$

$$sgg = ((0.1402 * \ln(p+14.7) - 0.4227) + (0.1369 * \ln(t) + 0.0156) + (0.1704 * \ln(ag) + 0.1469))/3, \quad (9)$$

$$p = 1000 * TD/2, \quad (10)$$

$$t = 19 * TD + 30, \quad (11)$$

$$FVF_g = 752.2 * (1 - e^{-0.05728 * TD}), \text{ when } 0 < TD \leq 5.67, \quad (12)$$

$$FVF_g = 113.3 + 21.1 * TD - 0.81 * TD^2 + 0.0116 * TD^3, \text{ when } 5.67 < TD \leq 30, \quad (13)$$

where FVF_o and FVF_g are the formation volume factors for oil and (non-associated) gas, respectively. F is a correction factor, GOR is the corrected solution gas/oil ratio (in ft^3/barrel), *sgg* is the formation solution specific gravity, *og* is the corrected oil gravity (in API units), *t* is the formation-specific temperature (in degrees Fahrenheit), *ag* is the API oil gravity, GOR_u is the uncorrected solution gas/oil ratio (in ft^3/barrel), *p* is the formation pressure (in psi), and TD is the formation depth (in thousands of feet). While this empirical conversion method was developed specifically for estimating regional-scale quantities of undiscovered in-situ oil and (associated and non-associated) gas volumes in Alaskan oil deposits, it is anticipated to also provide a reasonable approximation in Alberta's geological environment, since there are many structural similarities in the petroleum bearing provinces in both locations [79]. Additionally, the main interest in this research is comparability of relative differences between injected and extracted in-situ volumes at different stratigraphic depths and geographic zones, and therefore accurate determination of the absolute value of in-situ volumes is of limited interest in this case. The use of the same method for all stratigraphic depths is anticipated to result in consistency (and comparability) in computed differences between the relative corrected injected and extracted volumes across the stratigraphic depths of interest.

The commercially available geoSCOUT® database contains well-specific monthly fluid injection and production stock-tank volume, production, injection, and well perforation depth records for over 610,000 wells in the Alberta Basin. The total vertical depth (TVD) of the well perforations was assumed to be equivalent to the formation depth, for calculation purposes. The average API gravity of oil produced from each PSAC area is characteristic of that area because

of its unique geological setting, with an average API oil gravity of 10 within AB6 and AB7, average API oil gravity of 25 within AB1, AB2, AB3, and AB5 and an average API oil gravity of 15 within AB4 [80].

The monthly measured production and injection (stock-tank) fluid volume records for each of the approximately 610,000 wells in Alberta for January 1960-December 2020, were extracted from the geoSCOUT® database (about 63 million production records) for each PSAC area, along with the respective total vertical depth (TVD) of each well. Data cleaning consisted of automated identification of outlier (production and injection volume and well run-time) values, followed by a manual review of the corresponding entry in the detailed well record in geoSCOUT® for the corresponding period. Anomalous values without a logical corresponding supporting well record for that period were then eliminated from the database. The TVD, characteristic API gravity of the corresponding PSAC area and Equations 2 to 13 were then used to calculate oil and gas FVFs for the stock-tank fluid volume records for each production and injection wells in the Alberta Basin. The calculated FVFs were subsequently used to convert the stock tank oil and gas volume records for each well to in-situ reservoir volumes, in accordance with Equation 1. No correction was applied to produced and injected water volumes reported for each well since water (including water containing dissolved gas) is considered essentially incompressible under most reservoir conditions [81]. Steam volumes were also uncorrected since steam is measured and reported in cold-water-equivalent volumes. Steam injected into the subsurface is used for thermal oil recovery and ultimately becomes water in the subsurface. However, in the formation net fluid balance reported below, injected steam is accounted for as a gas since it is in the gas phase at the point of entry into the formation. All data aggregation, processing, and computation was conducted using the R statistical software package *(R: A language and environment for statistical computing*, https://www.R-project.org/, last accessed 14 January 2022).

2.2.3 Calculation of the Distance between the Injection/Production Horizon and the Precambrian Basement

The vertical distance between the injection/production horizon of each well and the Precambrian basement (i.e., the depth to Precambrian basement) was calculated using the TVD of each well and the depth of the Precambrian basement, obtained from the Alberta Geological

Survey's Precambrian Structure depth contours available in Pana et al. [82]. The depth to the Precambrian basement (i.e., a measure of the proximity of the injection/production horizon to the basement) was calculated by subtracting the TVD of each well from the depth of the Precambrian basement in the geographic location of the corresponding well.

2.2.4 Calculation of the Net Fluid Balance in Each Sub-Region and Stratigraphic Horizon Relative to the Precambrian Basement in the Alberta Basin

Production/injection wells and the associated calculated in-situ volumetric data were grouped geographically by PSAC area and stratigraphically in 1 km increments of vertical depth to the Precambrian basement. The in-situ liquid and gas net fluid balance volume (i.e., the volume injected—volume removed) for each geographic and stratigraphic horizon was then calculated and plotted as a function of vertical distance from the Precambrian basement.

These records were then grouped by decade, for the period January 1960-December 2020, to identify significant trends that may have occurred because of market or other changes in types and scales of industrial activity. In some cases, net fluid balance volumes are represented as the cube root of cubic meters in the charts, which is necessary to show the net change (positive or negative) in in-situ fluid balance as well as extreme changes in net volumes. The vertical scale represents the vertical depth to the Precambrian basement (i.e., not the TVD) averaged geographically across the entire PSAC area.

2.2.5 Calculation of In-Situ Formation Pressure Changes in the Alberta Basin over the Period 1960-2020

In Alberta, an oil or gas pool is essentially an accumulation of oil or gas that is (structurally) separate from another such accumulation, and approximately 65,000 oil and gas pools exist in the Alberta Basin [83], [84]. A common feature of many of the conventional oil and gas pools located in stratigraphic traps is the presence and hydrodynamic support of underlying regional saline aquifers [85], [86]. Measurement of the initial (virgin) and subsequent annual in-situ pool pressures is a regulatory requirement for all oil and gas operators; consequently, an extensive public dataset is also available in the geoSCOUT® database. However, while this dataset contains approximately 325,000 in-situ pool pressure-data records, these only cover approximately 7,000 distinct oil and gas pools. Pressure variations in such pools indicate pressure variations in the hydraulically connected underlying saline aquifer systems that

support the hydrocarbon columns and therefore are likely to be indicative of large-scale subsurface pressure changes across this basin. The available hydrocarbon pool pressure data was examined to assess the possibility of its use for an evaluation of long-term subsurface pressure trends across the basin.

The first recorded and most recent pressure measurements for corresponding depth intervals in each pool were identified and extracted from the available data, using R. The variance between the first recorded in-situ pressure measurement and the most recent pressure measurement (as a function of the first recorded pressure measurement) was then calculated for each depth horizon for which data was available in each pool. Pools with a pressure increase (i.e., most recent pressure > initial pressure at same depth interval in the same pool) were grouped into a pressure increase category. In contrast, pools with a pressure decrease (i.e., most recent pressure < initial pressure at same depth interval in the same pool) were grouped into a decrease category in each stratigraphic depth horizon. The calculated pool-pressure variance data were then grouped according to the PSAC area in which they were located and the distance to the Precambrian basement. This data was then used to calculate the average (percentage) pressure increase/decrease and the respective proportion of pools showing changes in each PSAC area and depth increment to the Precambrian basement.

2.3 Results

The calculated net in-situ fluid balances in each geographic area, in 1 km stratigraphic increments from the Precambrian basement, are presented in the subsections below. This information can help inform the development of regional fluid injection and disposal-related policies and manage fluid budgets for the corresponding geographic region in the Alberta Basin. Such policies and fluid budgets may be essential when the current and projected levels of industrial activity and the historical occurrence of seismic activity and seismic hazard potential in each area are considered, as outlined below.

2.3.1 Basin-Wide Total Surface Fluid Balance over the Period 1960-2020

Analysis of the stock-tank volumes of fluids injected and extracted (i.e., produced) from the Alberta Basin over the last 60 years (1960-2020) shows that the volume of both gases and

liquids removed (on average) exceeded the respective volumes of each injected fluid over the same period by approximately an order of magnitude (Table 1).

Table 1. Summary of calculated industrial fluid injection and production stock-tank volumes in the Alberta Basin (1960-2020). Source data extracted from geoLOGIC Systems databases © 2020.

	Gases (m^3)	**Liquids (m^3)**
Total produced	$6.84x10^{12}$	$2.46x10^{10}$
Total injected	$7.97x10^{11}$	$2.01x10^{10}$
Difference	$-6.05x10^{12}$	$-4.53x10^{09}$

Table 1 shows that, at a regional scale the basin has so far experienced extensive depressurization (depletion) due to oil and gas production during the period 1960-2020. Furthermore, analysis of the decade-by-decade net (volume injected minus volume withdrawn) stock-tank gas and liquids over this period indicates that depletion of both liquids and gases accelerated progressively over most of the last six decades (Table 2).

Table 2. Calculated decade-level variations in net industrial fluid injection and production stock-tank volumes in the Alberta Basin. Source data extracted from geoLOGIC Systems databases © 2020.

Decade	**Net Gas (m^3)**	**Net Liquid (m^3)**
1960–1969	$-3.82x10^{11}$	$-3.03x10^{08}$
1970–1979	$-7.18x10^{11}$	$-3.96x10^{07}$
1980–1989	$-8.34x10^{11}$	$-1.82x10^{08}$
1990–1999	$-1.38x10^{12}$	$-4.24x10^{08}$
2000–2009	$-1.47x10^{12}$	$-7.93x10^{08}$
2010–2019	$-1.16x10^{12}$	$-2.50x10^{09}$
Totals	$-5.56x10^{12}$	$-3.94x10^{09}$

This observation is consistent with the expected trend of increasing extraction rates of combined hydrocarbon fluids from the Alberta Basin for the period in which published data are available (1972-2015) [69]. However, actual depletion rates depend on the type, geographic location, depth, and scale of industrial activities, which can fluctuate significantly within short periods (as a function of market fluctuations, regulatory and policy changes, and other factors).

2.3.2 Basin-Wide Total Stock-Tank Fluid Balance Trends over the Period 1960-2020 and Potential Implications

Figure 2 shows the analysis of the annual net (stock-tank volume injected—stock-tank volume extracted) gas and liquid balance in the Alberta Basin over the period 1960-2020. This

figure shows that while removal has historically exceeded injection over the last 60 years and the depletion rate has increased over time, significant recent changes in both trends are evident.

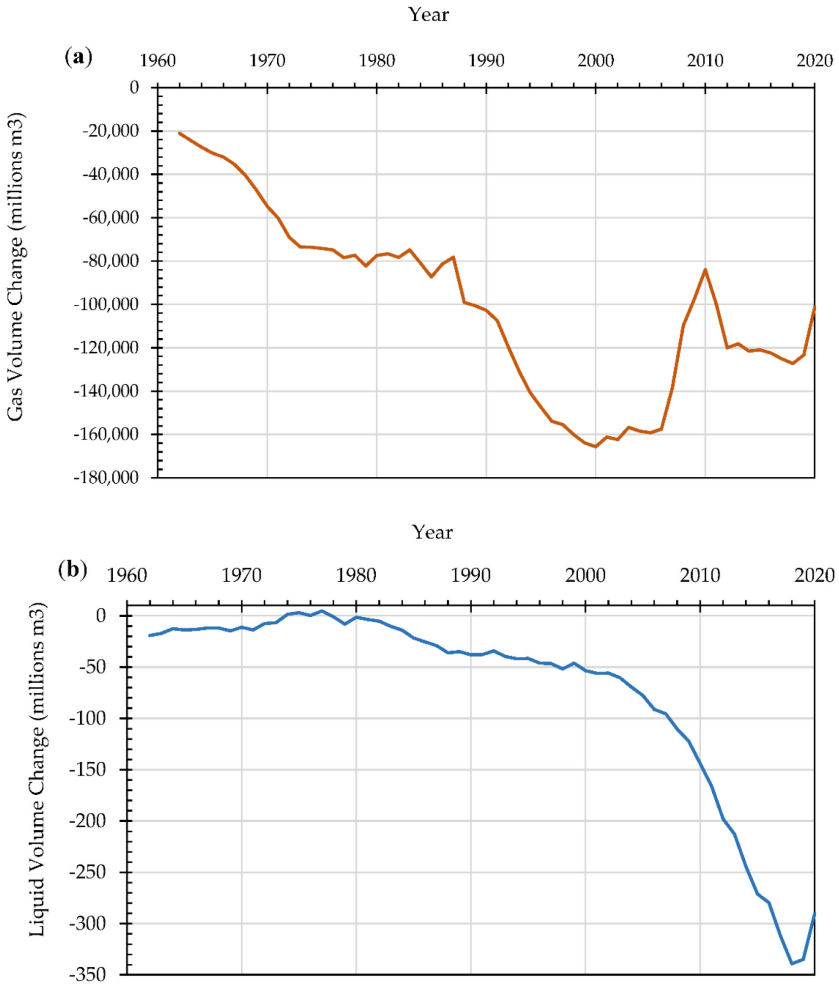

*Figure 2. Calculated net stock tank (**a**) gas balance (gas injected - gas produced) (**b**) liquid balance (liquid injected - liquid produced) trends in the Alberta Basin for the period 1960-2020. Source data extracted from geoLOGIC Systems databases © 2020.*

The change in trend in the net gas balance over the period 2006-2010 correlates with the development and expansion of the thermal bitumen industry and the increase in large volume (steam and non-condensable) gas-phase injection characteristic of this industry. Figure 2 also shows an abrupt reversal in the historical depletion trend in net gas and liquid balances over the last two years (2018-2020). This result indicates that there may be recent changes occurring in the type and scale of industrial activity occurring in the basin that can reverse the basin-wide depletion trends that have been occurring over the last 60 years.

Major, policy-driven changes in the type of energy produced and consumed in Canada are developing, which may change how pore space in the Alberta Basin has been used since the development of the oil and gas industry. The proposed *Net-Zero Emissions Accountability Act* formalizes Canada's objective to achieve net-zero emissions in all sectors of society by 2050 [87]. The subsurface injection of captured CO_2 from major industrial emissions is fundamental for achieving this goal [88]. Therefore, the possibility exists that fluid injection into the Alberta Basin could substantially exceed fluid removal within the next 30 years.

However, the volume removed from the basin can be used to derive an upper-bound estimate of a theoretical sustainable storage capacity within depleted oil and gas formations since a current key regulatory criterion used in approving injection projects is the requirement that the post-injection formation pressure shall not exceed the original virgin reservoir pressure [86], [89]. A simple comparison (at standard temperature and pressure) of Alberta's annual (2017) CO_2 emissions of 273 Mt of CO_2 [90] and the net gas difference presented in Table 1 above show that approximately 10 years of captured industrial CO_2 emissions would be equivalent to all net gas extracted from the Alberta Basin over the last 60 years. Other initiatives such as the use of natural gas to produce blue hydrogen in Alberta as a substitute for liquid transportation fuels would require approximately 203 Mt/year of carbon capture and storage capacity [91], which would exceed the net gas balance from the Alberta Basin in approximately 10 years. Meanwhile, one gigawatt of installed open-loop geothermal electricity generation (operating at a water flow rate of 20 kg/s to produce one megawatt of electric power [92]) has the potential to reinject in eight years the same amount of fluid as the net liquids balance of the basin over the last 60 years.

These simple calculations highlight the need for a strategic evaluation of the proposed future use of the subsurface in this basin, since the scale of future injection can reverse the historical basin depletion trend that has occurred to date. This depletion trend may have been instrumental in the success of large-scale injection to date in this basin, and fluid volume injection greater than fluid volume removed from this basin (i.e., basin re-pressurization) could increase associated future capacity, containment, and induced seismicity risks. Sustained basin-wide fluid injection consistently exceeding fluid removal over long periods increases the likelihood of recipient formations being exposed to pressures above their initial discovery

pressures, which could increase the probability of loss of injection containment and induced seismicity [43], [93]–[95]. Large-scale injection of fluids into deep, laterally extensive, virgin pressure (i.e., un-depleted) formations can result in significant and extensive pressure changes (because of the low pore compressibility of these formations) unless such pressure build-up is attenuated by basin-scale migration of resident brine into and through the caprock, basement rock, and lateral flow boundaries [43]. Additionally, the magnitude of the pressure build-up response to industrial-scale carbon sequestration should be carefully evaluated against the regional-scale hydrologic conditions because of the capacity of such pressure build-up to trigger the large-scale movement of brine vertically and laterally at a regional scale [43]. Such pressure build-up and fluid displacement also increase the risk of loss of injection containment from legacy wells that were poorly abandoned [96]. Previous basin-scale hydrological studies have noted that saline aquifers in the Alberta Basin are interconnected laterally and vertically at a regional scale and provide hydrodynamic drive to most oil and gas formations [97]. Large-scale lateral or vertical movement of brine would thus be undesirable because of the potential to affect regional hydrology and current oil and gas extraction activities.

Therefore, large-scale injection from net-zero activities could overwhelm long-term disposal capacity within the Alberta Basin and adversely affect disposal activities essential for the oil sands, shale oil, and other industries. Basin-scale migration of fluids could trigger changes to regional hydrological regimes, affecting top/bottom water in thermal oil sands extraction or water drive in conventional oil and gas operations, which could adversely impact the economics of such activities. However, there is still debate on the degree of interaction between the basin-scale saline flow systems in the deformed and undeformed parts of the basin, between the basement and sedimentary succession and the true magnitude and direction of formation water flow in the various flow systems [97]–[99]. Consequently, the actual impacts of basin-scale changes in formation pore pressures may be difficult to predict accurately unless the regional and basin-scale hydrological understanding is improved. Recent studies have suggested that vertical connectivity between discrete regional flow systems may be greater than previously hypothesized in some cases, while stratigraphic fluid density contrasts may control the mobility of deep saline fluids [97]–[99]. Uncertainty on the basin-scale interaction between the saline flow systems and the associated driving forces can have important implications on the stability of storage and disposal zones and the sustainability of water withdrawal [97]–[99]. Currently, the

onus is on project proponents to evaluate the suitability of the receiving formation and potential risks arising from high volume injection at a project scale within the basin [73], [86], [89].

High-volume fluid injection into underpressured or pressure-depleted subsurface formations is considered attractive from an earthquake triggering perspective because of the lower pore pressures at the start of injection, which reduce injection operating costs and allow for the injection of large volumes of fluid before pressures increase to virgin reservoir pressures [100]. However, as previously noted, large-scale injection into such formations should be avoided when they are within 1 km of the Precambrian basement or where evidence exists to indicate a hydraulic connection with the Precambrian basement [10], [47], [48], [56]–[58]. Limited unknown geologic hazards are typically encountered during large-scale fluid injection into depleted producing formations not in proximity to or in contact with the basement rocks. Over a century of experience in the natural gas storage industry has shown few failures, the majority of which occurred because of well-bore integrity problems [95], [101]–[104].

2.3.3 Assessment of the Net In-Situ Fluid Balance in Area AB1

Area AB1 comprises the eastern flank of the Rocky Mountains foothills (Figure 1) and includes the deepest part of the Alberta Basin, with a sediment depth exceeding 6 km in some locations. The predominant geologic interest in this area has historically been, and is expected to continue to be, dry gas [71]. This area has also been the most seismically active region in the province from 1922 up to 2010 due to regional tectonic activity in the Rocky Mountain region [105]–[107]. One of the first recorded injection-induced seismic events of concern in Alberta (the Magnitude 5.1 Snipe Lake event) occurred in this area in 1970 [108], [109]. Oil and gas-related induced seismicity has also occurred in this area (near Rocky Mountain House) since the 1970s and has been attributed to extensive gas extraction from (i.e., depletion of deep) Devonian carbonate reservoirs at depths of approximately 4 km (approximately 2 km above the Precambrian basement) [109], [110].

Figure 3 (a, b) show the calculated net in-situ gas and liquid balances across AB1 over the last six decades. This analysis indicates that over this period, the total volumes of liquid and gas extracted exponentially exceeded the respective volumes injected at all depth intervals relative to the Precambrian basement. During the past six decades, extensive gas depletion is notable in the depth zone approximately 2–4 km from the Precambrian basement across AB1.

This result is consistent with extensive regional gas production activity over this period [71]. While a similar trend is noted in the net liquid balance in this area, the level of depletion is lower in the stratigraphic horizons adjacent to the Precambrian basement, and the volume of liquids injected even marginally exceeded the volume of liquids extracted in the deeper stratigraphic horizons during the 1970s and 1980s.

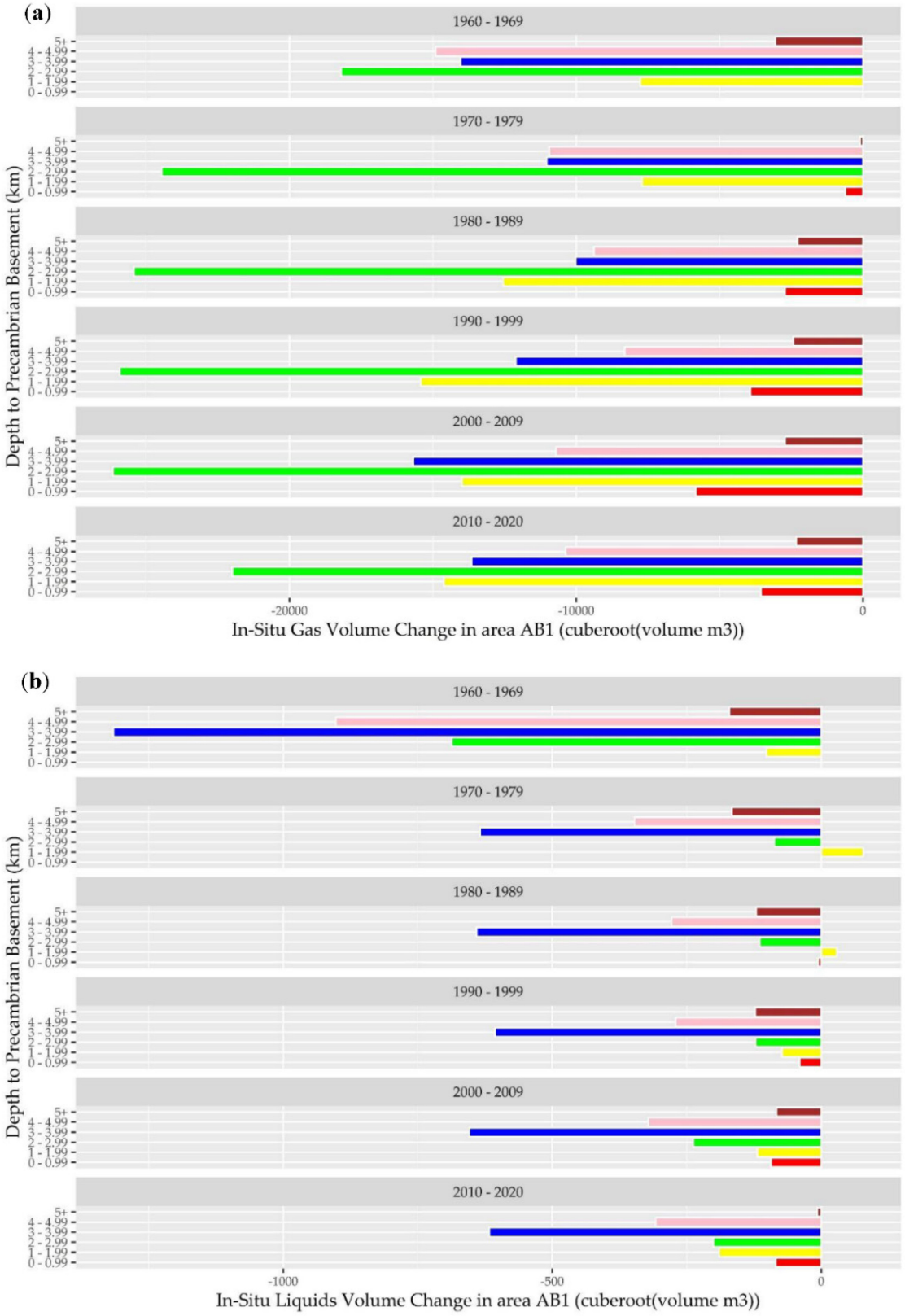

*Figure 3. Calculated net in-situ (**a**) gas and (**b**) liquid balance for area AB1 over the period January 1960-December 2020. Red bars: < 1 km depth from Precambrian basement; Yellow bars: 1-2 km depth from Precambrian basement; Green bars: 2-3 km*

depth from Precambrian basement; Blue bars: 3-4 km from Precambrian basement; Pink bars: 4-5 km depth from Precambrian basement; Brown bars: 5+ km depth from Precambrian basement. Source data extracted from geoLOGIC Systems databases ©2020.

Therefore, the net fluid balance trend for this PSAC area indicates that there is an extensive net negative fluid balance within the stratigraphic horizons located at the depth interval of 2–4 km from the Precambrian basement. However, this analysis also indicates that net fluid balance within the stratigraphic horizons located up to 2 km from the Precambrian basement within PSAC 1 has experienced limited fluid depletion. Consequently, far greater sustainable fluid storage capacity is available in the stratigraphic horizons located 2-4 km from the Precambrian basement. Conversely, fluid injection and storage capacity are limited in the 0-2 km stratigraphic intervals in area AB1.

2.3.4 Assessment of the Net In-Situ Fluid Balance in Area AB2

Area AB2 is located adjacent to the eastern flank of the Rocky Mountain Foothills (Figure 1) and contains the second deepest part of the Alberta Basin, with a sediment depth exceeding 6 km in some locations. The predominant geologic interests in this area are tight oil, wet gas, and natural gas liquids (mostly in the Duvernay Formation [111], Figure 1), and production activity is anticipated to increase significantly in this area over the next decade [71]. Most of the oil and gas-related induced seismicity that has occurred in the Alberta Basin to date has occurred within this area and has been linked to hydraulic fracturing injection, with some events associated with water disposal or production-related depletion [62], [110], [112]–[114].

Figure 4 (a, b) shows the calculated net in-situ gas and liquid balances across AB2 over the last six decades. This analysis indicates that the total volumes of both liquids and gases extracted also exponentially exceeded the respective volumes injected at all depth intervals relative to the Precambrian basement in this area. In addition, accelerating liquids and gas depletion rates are evident in the stratigraphic zones from approximately 3 km above to the top of the Precambrian basement. This trend is also consistent with the current deep basin tight oil and gas industrial activity in this area [71].

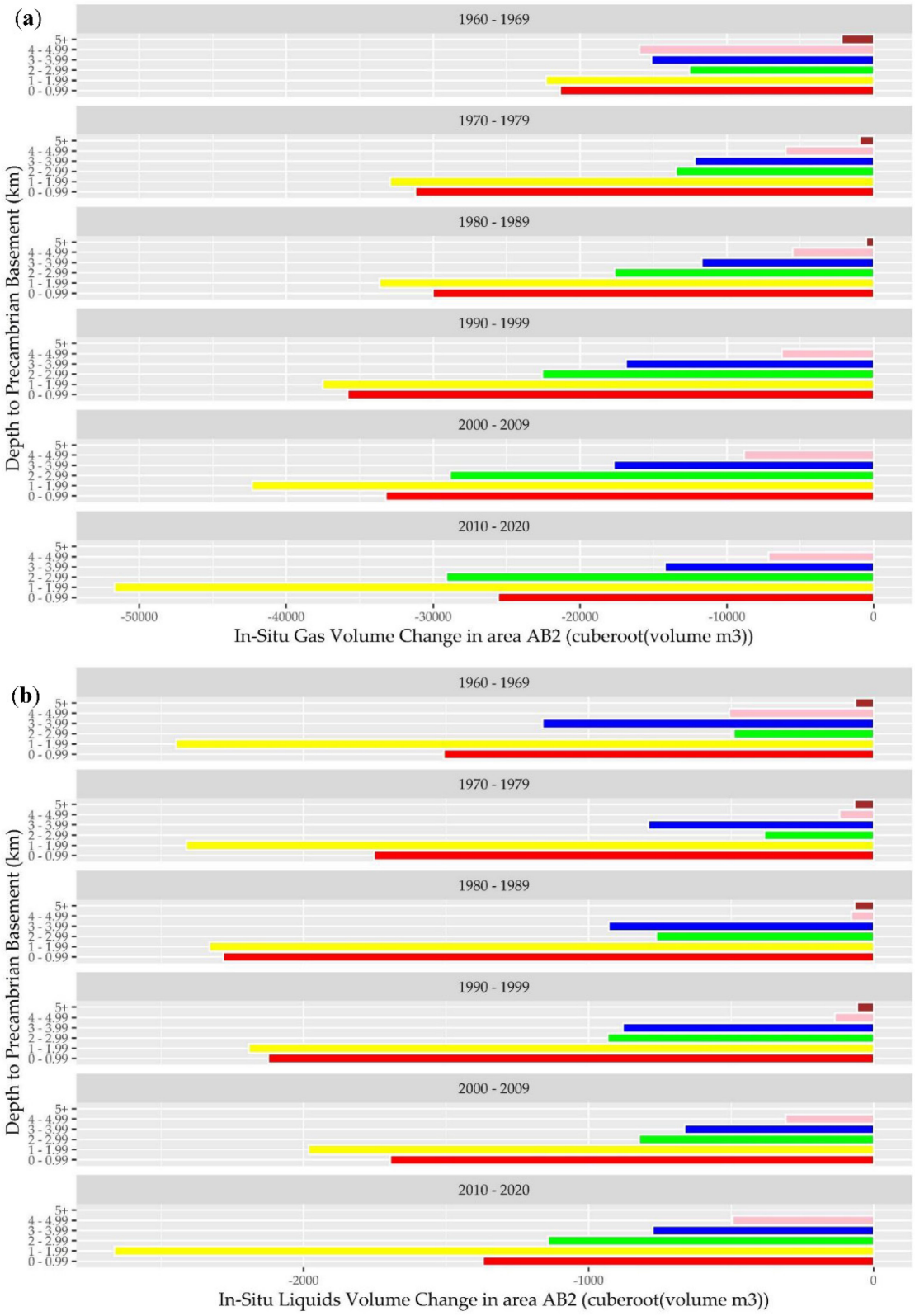

*Figure 4. Calculated net in-situ (**a**) gas and (**b**) liquid balance for AB2 over the period January 1960-December 2020. Red bars: < 1 km depth from Precambrian basement; Yellow bars: 1-2 km depth from Precambrian basement; Green bars: 2-3 km depth*

from Precambrian basement; Blue bars: 3-4 km from Precambrian basement; Pink bars: 4-5 km depth from Precambrian basement; Brown bars: 5+ km depth from Precambrian basement. Source data extracted from geoLOGIC Systems databases ©2020.

The net fluid balance trend across AB2 shows an extensive net negative fluid balance in the stratigraphic horizons located within 3 km of the Precambrian basement. However, this analysis also indicates that the shallowest stratigraphic horizons in PSAC 2 have experienced limited fluid depletion. Consequently, there may be substantially greater sustainable fluid storage capacity within the stratigraphic intervals located within 3 km of the Precambrian basement within this area. Figure 4 (a, b) may provide an upper-bound estimate of the sustainable fluid storage capacity in these stratigraphic intervals in AB2.

2.3.5 Assessment of the Net In-Situ Fluid Balance in Area AB3

Area AB3 is in southeastern Alberta (Figure 1) and encompasses a shallower part of the Alberta Basin with a sediment depth of up to 3 km. The predominant geologic interests in this area are dry gas, and heavy and light crude. While traditional conventional oil and gas production activity has decreased over the last decade, light oil production is projected to increase in the next decade as operators benefit from low production costs and established infrastructure in this area [71].

Figure 5 (a, b) shows the calculated in-situ net gas and liquid balances across AB3 over the last six decades. This analysis indicates that the total volumes of both liquids and gases extracted exponentially exceeded the respective volumes injected at all depth intervals relative to the Precambrian basement in this area. Accelerating depletion of liquids and gas is evident in all zones, with shallow gas depletion consistently increasing over the last six decades. Over the last decade, the depletion rate decelerated in the deeper stratigraphic horizons in this area. This trend is consistent with the oil and gas industrial activity and forecasts in this area [71].

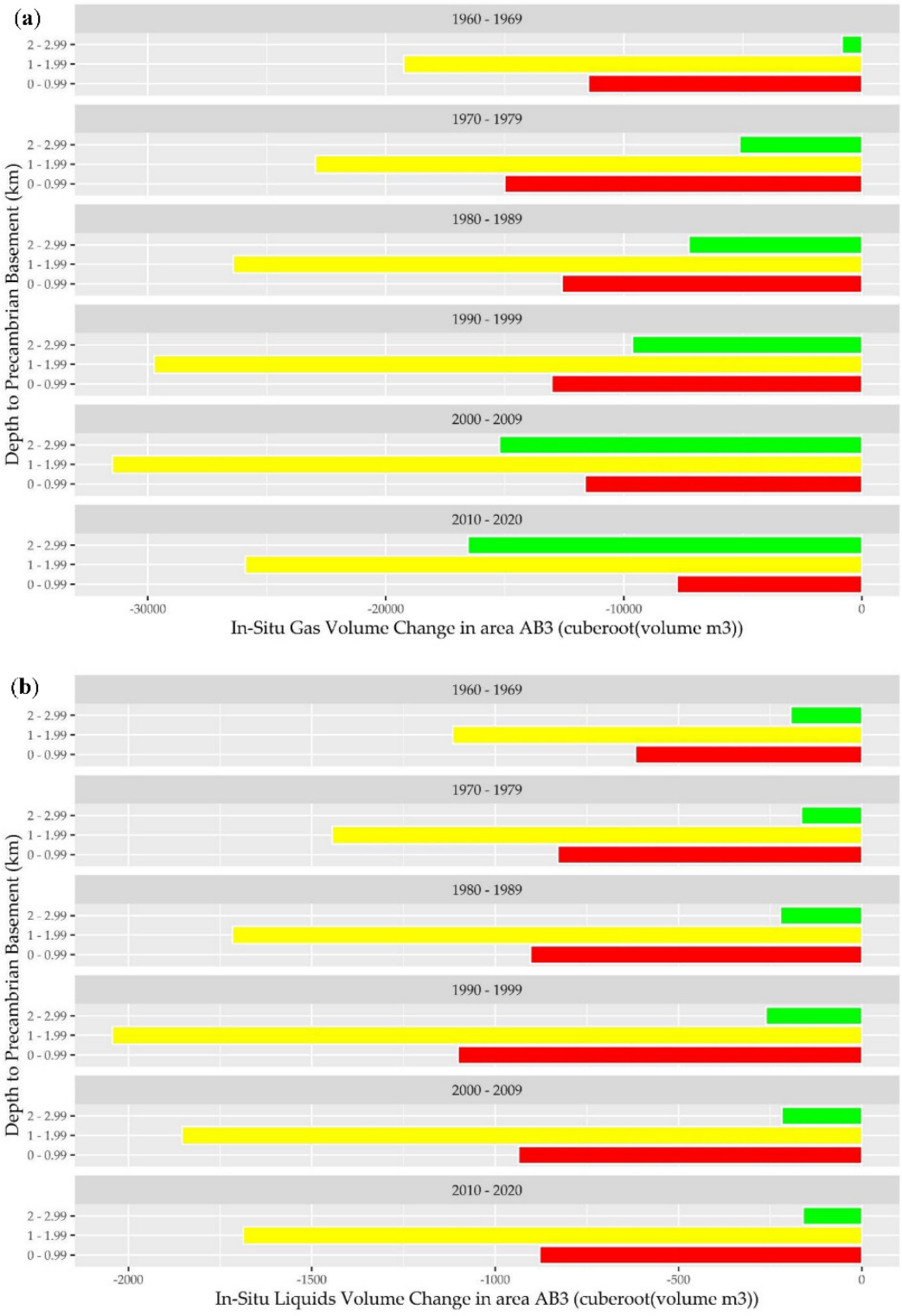

*Figure 5. Calculated net in-situ (**a**) gas and (**b**) liquid balance for AB3 over the period January 1960-December 2020. Red bars: < 1 km depth from Precambrian basement; Yellow bars: 1-2 km depth from Precambrian basement; Green bars: 2-3 km depth from Precambrian basement. Source data extracted from geoLOGIC Systems databases © 2020.*

The net fluid balance trend across AB3 indicates an extensive net negative fluid balance (and sustainable fluid storage capacity) available in all stratigraphic horizons in this area.

2.3.6 Assessment of the Net In-Situ Fluid Balance in Area AB4

Area AB4 is in east-central Alberta (Figure 1) and encompasses a shallower part of the basin with a sediment depth of up to 3 km. The predominant geologic interests in this area are light and ultra-heavy crude, with limited shallow dry gas. While conventional oil and gas production activity has decreased over the last decade in this area, production of light crude is expected to increase over the next decade [71].

Figure 6 (a, b) shows the calculated net gas and liquid balances across AB4 over the last six decades. This analysis indicates that the total volumes of both liquids and gases extracted also exponentially exceeded the respective volumes injected at all depth intervals relative to the Precambrian basement in this area.

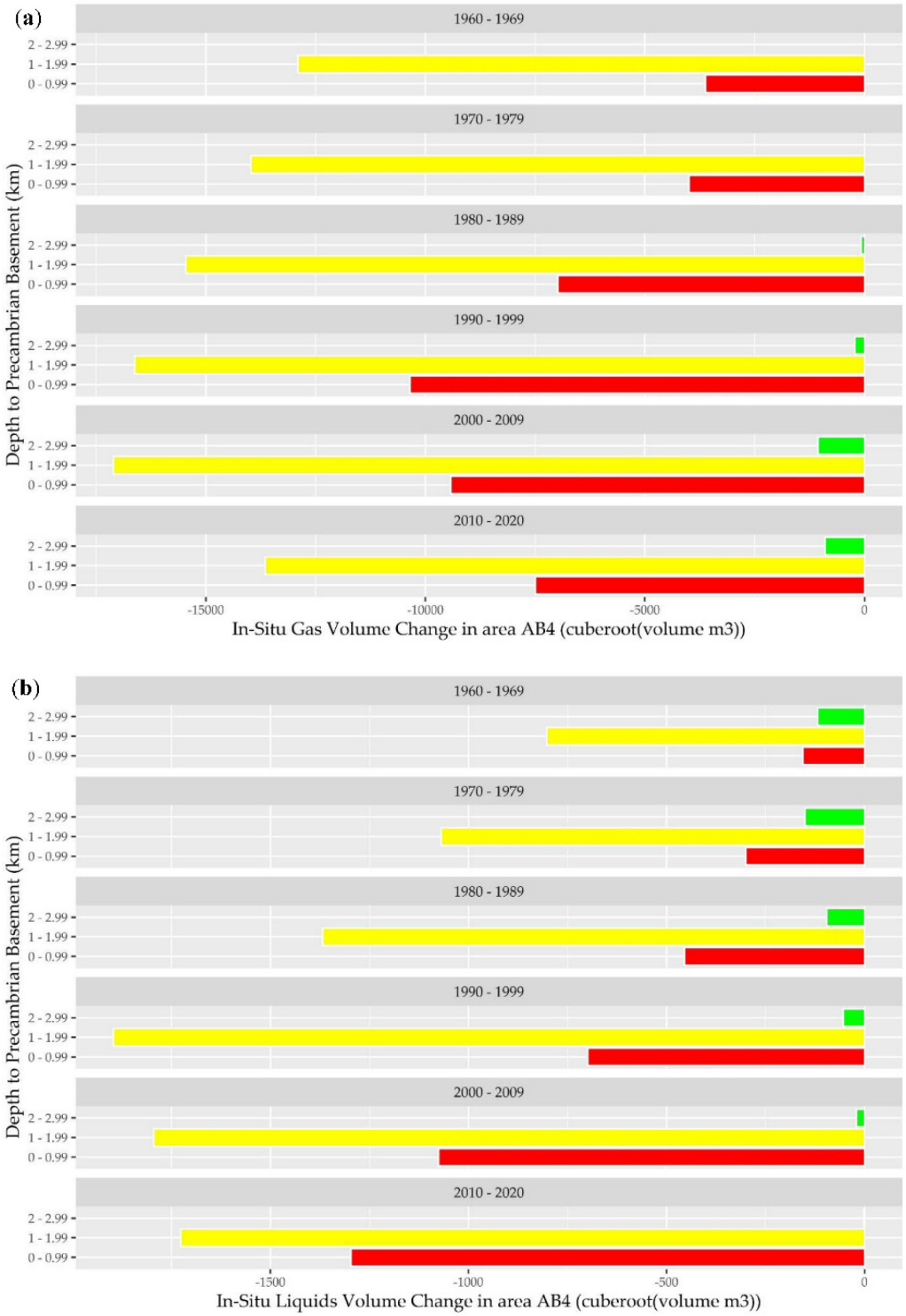

*Figure 6. Calculated net in-situ (**a**) gas and (**b**) liquid balance for AB4 over the period January 1960-December 2020. Red bars: < 1 km depth from Precambrian basement; Yellow bars: 1-2 km depth from Precambrian basement; Green bars: 2-3 km depth from Precambrian basement. Source data extracted from geoLOGIC Systems databases © 2020.*

Extensive gas depletion over six decades is evident in all stratigraphic horizons, with a gas depletion-rate deceleration occurring in the last two decades. However, the consistent six-decade exponential increase in liquids depletion adjacent to the Precambrian basement in this area is notable. While there is extensive sustainable fluid storage capacity within the near-Precambrian basement intervals in this area, this exponentially increasing depletion trend may be significant in assessing regional subsurface storage capacity or near-basement saline aquifer flow characteristics in AB4.

2.3.7 Assessment of the Net In-Situ Fluid Balance in Area AB5

Area AB5 is in central Alberta in the center of the basin (Figure 1) and encompasses an area with a sedimentary cover of up to 4 km deep. The predominant geological interests in this area have historically been conventional oil and gas. However, they have evolved to tight oil in the east-southeastern region and subsurface fluid injection and storage-related activities in the central area.

Figure 7 (a, b) shows the calculated net in-situ liquid and gas balances across AB5 over the last six decades. This analysis also indicates that the total volumes of both liquids and gases extracted exponentially exceeded the respective volumes injected at all depth intervals relative to the Precambrian basement in this area. Extensive gas depletion over the past six decades is notable in the deeper stratigraphic horizons. However, in the stratigraphic zones adjacent to the Precambrian basement, the depletion rates for liquids have consistently decelerated over the last five decades, while gas depletion rates have also decelerated over the last three decades.

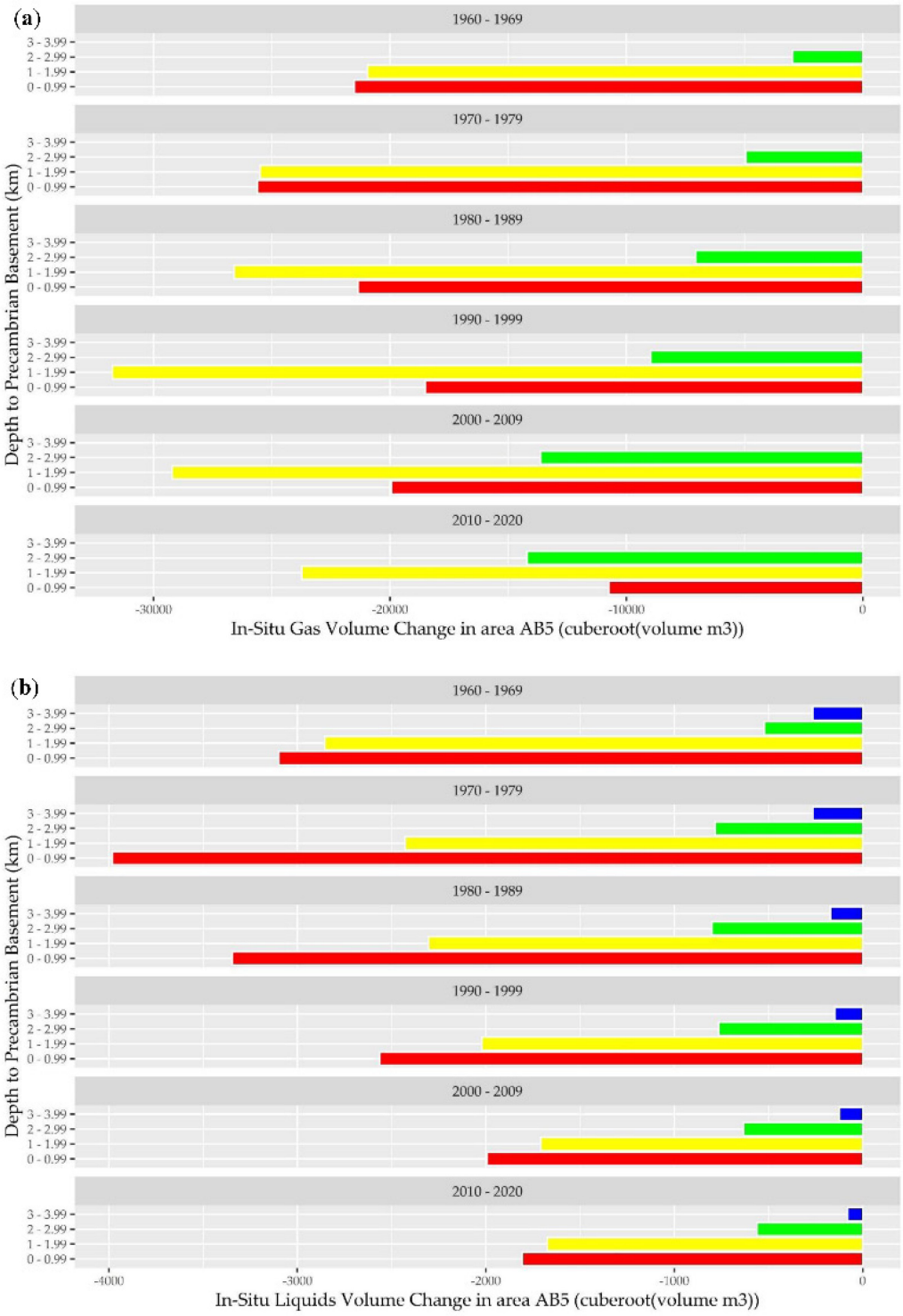

*Figure 7. Calculated net in-situ (**a**) gas and (**b**) liquid balance for AB5 over the period January 1960-December 2020. Red bars: < 1 km depth from Precambrian basement; Yellow bars: 1-2 km depth from Precambrian basement; Green bars: 2-3 km depth from Precambrian basement; Blue bars: 3-4 km from Precambrian basement. Source data extracted from geoLOGIC Systems databases © 2020.*

While extensive sustainable fluid storage capacity appears to exist within this area, increasing injection rates and decreasing extraction rates may be reversing the historical regional depletion trend. This trend may be of significance in assessments of regional subsurface storage capacity and near-basement saline aquifer flow characteristics for this area, especially considering the potential for large-scale fluid injection in the basal saline aquifers from future carbon capture and storage activities [88], [115], [116].

2.3.8 Assessment of the Net In-Situ Fluid Balance in Area AB6

Area AB6, located in northeastern Alberta, overlaps the Athabasca Oil Sands Region (Figure 1) and encompasses an area with sedimentary cover of up to 2 km deep. The predominant geologic interest in this area is its laterally extensive bitumen deposits, which are extracted using mining and steam-based technologies (steam-assisted gravity drainage and cyclic steam stimulation - SAGD and CSS). These deposits produced approximately three million barrels per day of bitumen in 2020 [71].

A comprehensive understanding of the regional (saline) groundwater systems is important for the success of both thermal and mining production technologies in this area since imprecise knowledge of the regional hydrogeology can impact bitumen extraction project feasibility [117]–[119]. The commercial feasibility of both SAGD and CSS bitumen production methods requires long-term stability and predictability of groundwater interaction with production activities over the project lifetime since unanticipated groundwater variations can materially impact operating (such as steam generation or pit dewatering) costs and project revenues (by altering the volume of recoverable oil) [117], [120]–[123]. Thus, comprehensive knowledge of current regional saline aquifer flow systems and future changes of such systems (e.g., created by new large-scale injection projects, for instance) could be necessary for the continued commercial success of bitumen production projects in this area. Thermal projects extract large quantities of saline source water for bitumen production while mining projects conduct extensive pit dewatering, and both inject large amounts of spent process water within this region, which has the potential to alter regional-scale hydrogeological regimes [117]. However, hydrogeological studies are currently conducted on a project level and a case-by-case basis and the cumulative impacts of all projects on regional groundwater systems have not been quantified to date [76], [118]. Therefore, changes to the saline regional-scale hydrodynamic flow

regimes (particularly hydrostatic head increases) may be undesirable because of the potential to affect the feasibility of current and future bitumen extraction in this area.

Figure 8 (a, b) shows the calculated in-situ net liquid and gas balances across AB6 over the last six decades. The in-situ thermal projects in this area are located at around 600 m depth, which is within 1 km of the Precambrian basement. The sedimentary depth in the eastern section of this area varies between 0.5 and 1.5 km [124], [125]. This analysis shows that extensive gas depletion occurred in all stratigraphic horizons in this area during the first four decades, reflecting gas production. However, this trend reversed in the lower stratigraphic horizon within the last two decades, with net gas injection substantially exceeding gas extraction while the gas depletion trend continued in the upper stratigraphic horizon. The increase in net gas balance in the lower stratigraphic horizon corresponds to the period of development and growth of the SAGD industry in this area and reflects the injection of steam and non-condensable gases for bitumen production. However, the reservoir pressure-balanced nature of SAGD operations suggests that there may be limited potential for the increase in gas injection in the lower stratigraphic horizons to interact with the regional hydrodynamic flow systems in this area. Additionally, the potential for industrial-scale fluid injection into such shallow areas may be further constrained by regulatory requirements in Alberta which stipulate that CO_2 sequestration can only occur in formations that are located at depths of greater than 1 km [126].

This area's calculated in-situ net liquid balance shows exponentially increasing liquids extraction within both stratigraphic zones, with a substantial increase within the last decade. This result includes an increase in bitumen production, source water extracted for steam generation, and spent process water injected from operations in this area.

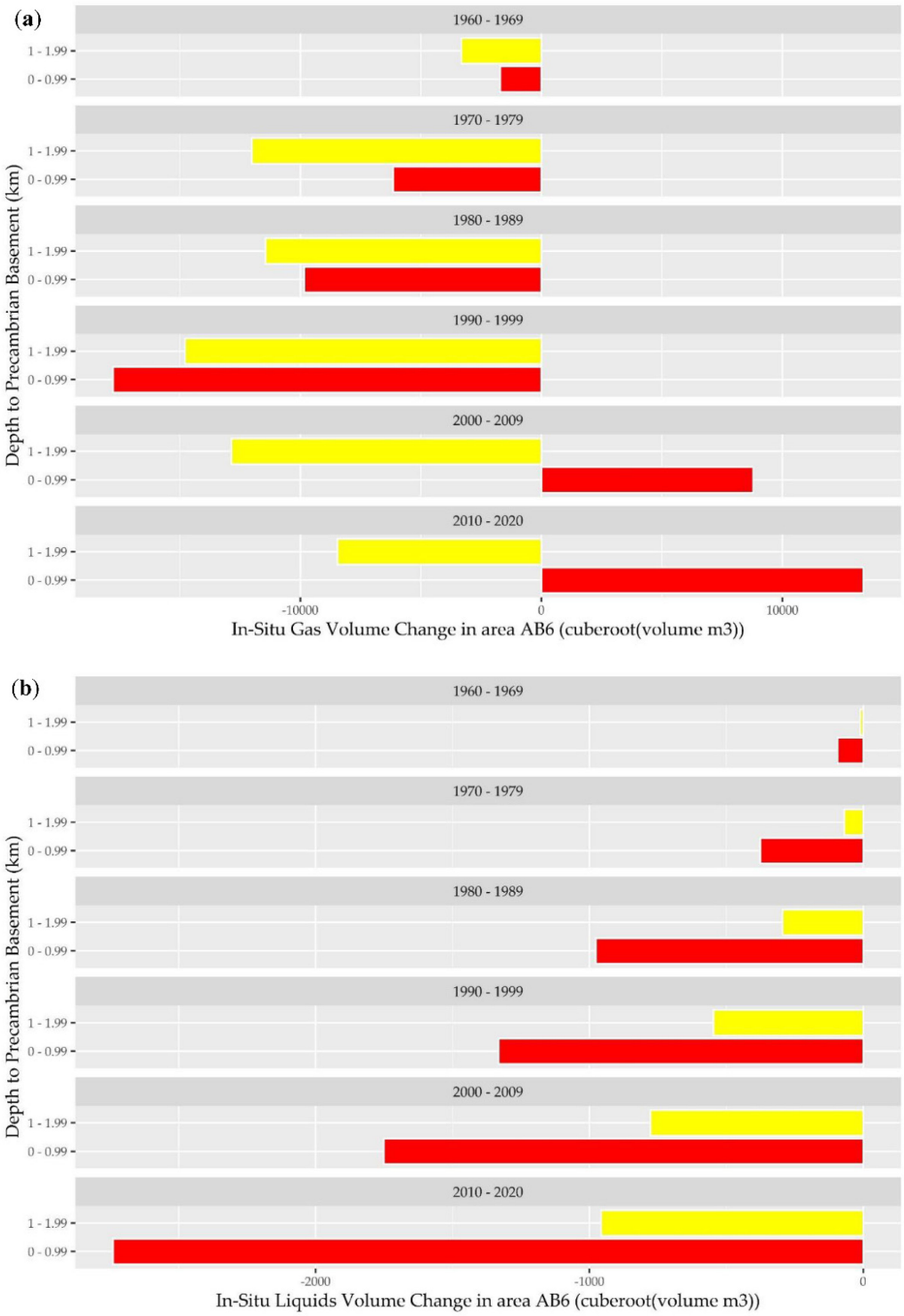

*Figure 8. Calculated net in-situ (**a**) gas and (**b**) liquid balance for AB6 over the period January 1960-December 2020. Red bars: < 1 km depth from Precambrian basement; Yellow bars: 1-2 km depth from Precambrian basemen. Source data extracted from geoLOGIC Systems databases © 2020.*

It is possible that the closed-circuit mechanics of gas injection and the large-scale saline water withdrawal characteristic of thermal bitumen recovery could mitigate the potential for a pore pressure increase in the Precambrian basement zone within this area, and therefore reduce the possibility for induced seismicity triggered by pore pressure increase. In addition, in-situ stress levels are anticipated to be lower in the Precambrian basement within this area because of the shallow depth, which reduces the probability of occurrence of large magnitude induced events. However, the trend and scale of liquid and gas net fluid balance changes in this area in the last two decades may warrant an analysis of the potentially complex interaction between the net fluid balance and the regional-scale hydrodynamic flow systems. Such an analysis may help estimate the sustainable net fluid balance capacity of this area and the potential to accommodate other types of subsurface activities in conjunction with current operations. In addition, an analysis of the impacts (if any) to the regional-scale hydrodynamic flow systems could be instrumental in developing a future regional-scale subsurface capacity management strategy. Recent watershed-scale studies conducted in this area provide first-order estimates of sustainable yields for near-surface (<150 m deep) aquifers and could help future assessments of cross-formation flows and cumulative effects [127].

2.3.9 Assessment of the Net In-Situ Fluid Balance in Area AB7

Area AB7 is in northwestern Alberta (Figure 1) and encompasses an area with sediments up to 4 km deep. The predominant geologic interests in this area have historically been conventional oil, gas, and bitumen but have more recently evolved to tight oil and gas in the southwestern region.

Figure 9 (a, b) shows the calculated in-situ net liquid and gas balances over the last six decades in area AB7. This analysis indicates that total volumes of gases and liquids exponentially exceeded the respective volumes injected at all depths relative to the Precambrian basement.

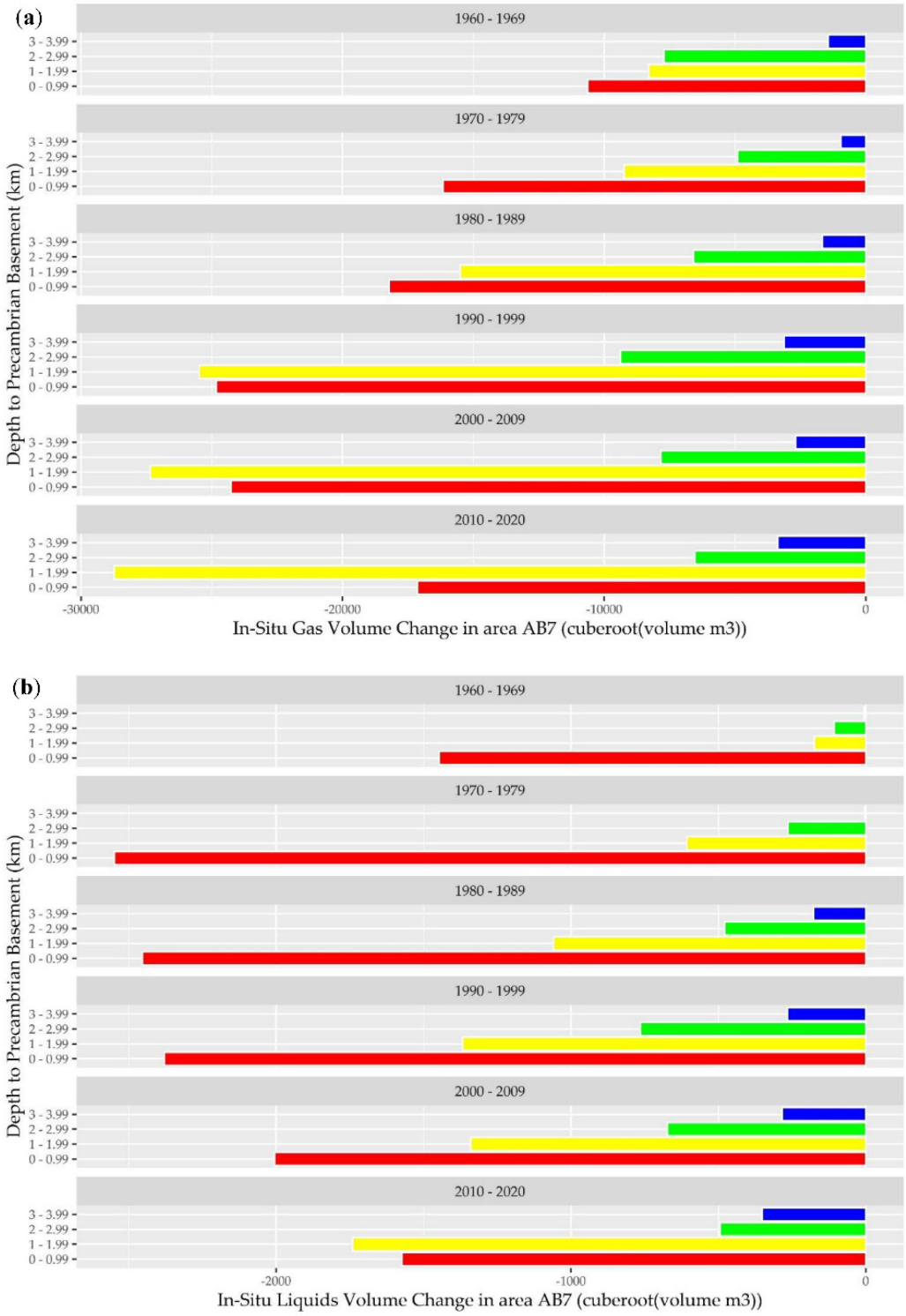

*Figure 9. Calculated net in-situ (**a**) gas and (**b**) liquid balance for AB7 over the period January 1960-December 2020. Red bars: < 1 km depth from Precambrian basement; Yellow bars: 1-2 km depth from Precambrian basement; Green bars: 2-3 km depth from Precambrian basement; Blue bars: 3-4 km from Precambrian basement. Source data extracted from geoLOGIC Systems databases © 2020.*

Extensive extraction of both liquids and gases and associated depletion are notable in the stratigraphic zones up to approximately 2 km from the Precambrian basement. However, the depletion rate of both liquids and gases in the near-basement stratigraphic zone in this area has shown a consistent exponential decrease in the last two decades. While there appears to be significant potential for sustainable storage capacity within formations in this area, this trend may be of significance in regional assessments.

2.3.10 Trends in Calculated Net In-Situ Fluid Balance within Each Area

While the assessment above summarizes the net fluid balance in each area, it can obscure recent or short-term changes in fluid injection/extraction patterns within each area. The annual in-situ gas and liquid fluid balance trends over the last 60 years, presented in Figures 10 to 12, are useful for identifying short-term and recent variations.

Figure 10 shows the annual net gas balance trend over the period 1960-2020 in each area. This figure indicates that while depletion is evident in all areas, the annual gas depletion trend appears stable in areas AB1, AB3, and AB4, while gas depletion is accelerating in areas AB2 and AB7.

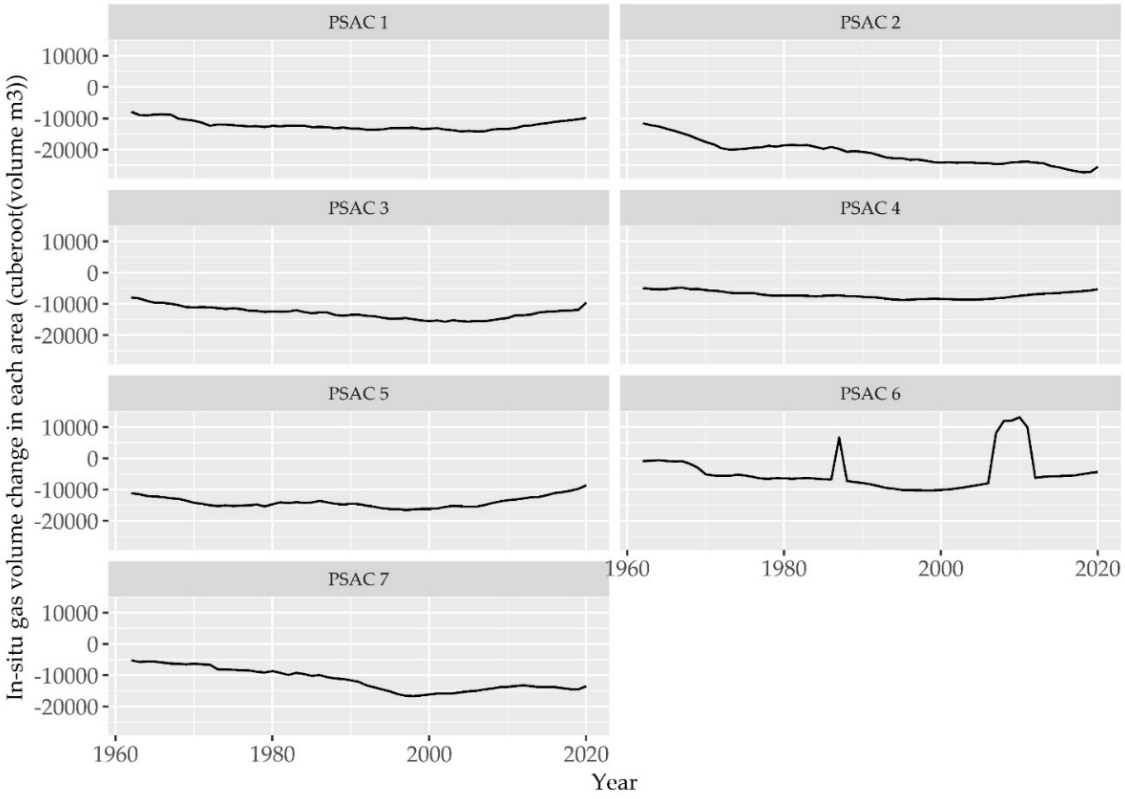

Figure 10. Calculated net annual gas balance trend in the Alberta Basin. Source data extracted from geoLOGIC Systems databases © 2020.

However, the annual gas depletion trend deceleration is notable in areas AB5 and AB6. The short-term spikes in gas injection volumes shown in AB6 are not data processing artifacts since they correlate with annual variations in steam and other (non-steam) gas-phase injection volumes (Figure 11).

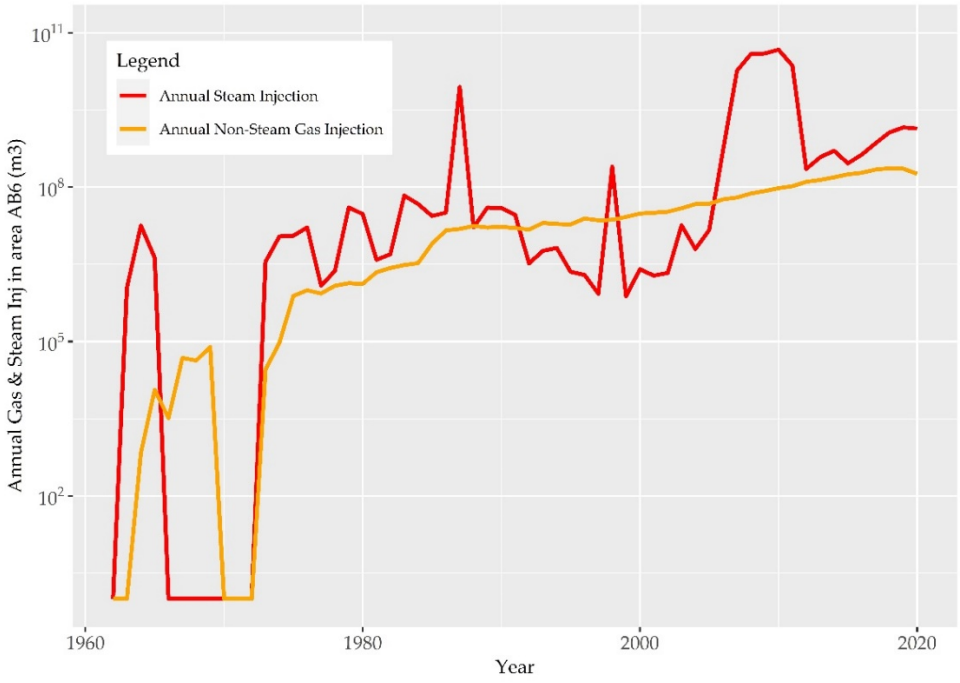

Figure 11. Calculated annual variations in steam and other gas phase injection volumes in area AB6. Source data extracted from geoLOGIC Systems databases © 2020.

The volume of steam and gas injected is a function of bitumen recovery technology and the project's commercial performance criteria, which vary temporally as a function of oil and gas market conditions for the corresponding period. Figure 12 shows the annual net liquid balance trend over the same period in each area. This figure shows that liquid depletion is also prevalent in all areas, with stable liquid depletion levels evident in AB1, AB2, AB3, AB4, and AB7. However, an accelerated liquids depletion trend is notable in area AB6, while AB5 shows a consistent deceleration in the depletion trend.

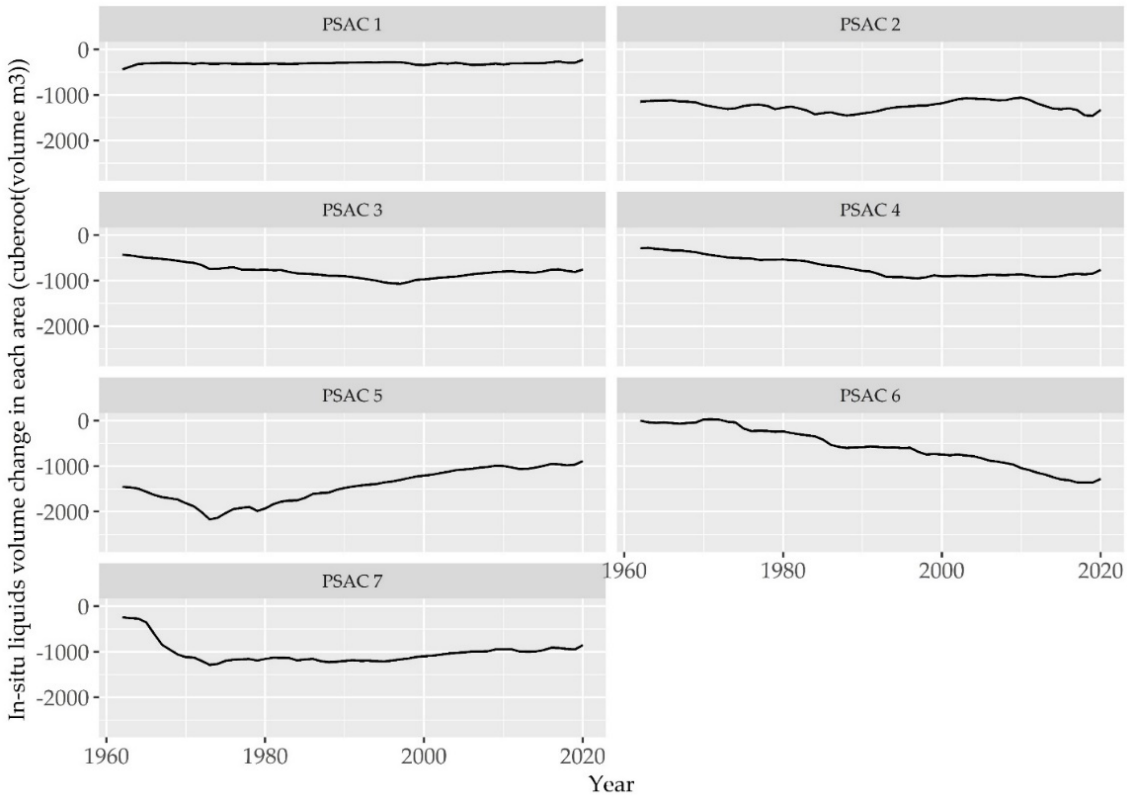

Figure 12. Calculated net annual liquid balance trend in the Alberta Basin. Source data extracted from geoLOGIC Systems databases © 2020.

This analysis indicates that notable regional-scale changes in annual net fluid balance trends appear to be occurring in areas AB5 and AB6 that could be of significance in future sustainable basin subsurface storage capacity assessments and pore space policy considerations. Regional-scale management of subsurface fluid-injection cumulative effects may be warranted in the future to maintain a sustainable fluid budget (and storage capacity) in these areas and mitigate adverse effects on current subsurface pore space users. This need may be critical, especially under scenarios of potential large-scale increases in fluid injection, such as those contemplated by net-zero initiatives that propose carbon capture and storage in these areas.

2.3.11 In-Situ Formation Pressure Changes in the Alberta Basin over the Period 1960-2020

Industrial-scale injection of fluids into or removal of fluids from the subsurface have the potential to trigger basin-scale changes in hydrologic flow systems [128]. Despite its historical economic importance and the extent of industrial activity, limited basin-scale studies have been completed on the hydrologic flow systems and their interconnectivity within the Alberta Basin. Moreover, such studies have been done in a piecemeal fashion both geographically and

stratigraphically [129]. The entire WCSB is, however, generally accepted to be a classic example of a gravity-driven flow basin [72], [123], [130] because of the overall elevation diminution from the southwest to the northeast.

Within the Alberta Basin, Bachu (1995) proposed that the basin-scale flow is controlled by two mega-hydrodynamic (stratigraphic) flow systems consisting of a deeper (pre-Cretaceous) northeastward carbonate dominated (high salinity) aquifer flow system and a shallower (post-Jurassic) southwestward sandstone (lower salinity) aquifer flow system, as shown in Figure 13 [123]. According to Bachu (1995), the deep (high salinity) aquifer flow system is driven by basin topography with a recharge in Montana and the Alberta Rocky Mountains and discharge in northeastern Alberta and Saskatchewan, while the shallower (post-Jurassic) southwestward sandstone (lower salinity) aquifer flow system is driven by erosional rebound in intervening shale sequences. These mega-hydrodynamic flow systems hydraulically connect at a regional-scale west to east along pre-Cretaceous unconformities in the central portion of the basin, and salinity-gradient controlled buoyancy retards cross-formation flow of waters driven by hydraulic head gradients in each and between these two systems [123], [129]. Vertical cross-formation flow through high permeability carbonate (Upper Devonian Wabamun and Grosmont) sequences creates a long-range regional-scale drain effect and forms sub-hydrostatic (underpressured) systems, which control regional-scale flow systems and are fundamental for hydrodynamic trapping of hydrocarbons and injected waste fluids [123], [129].

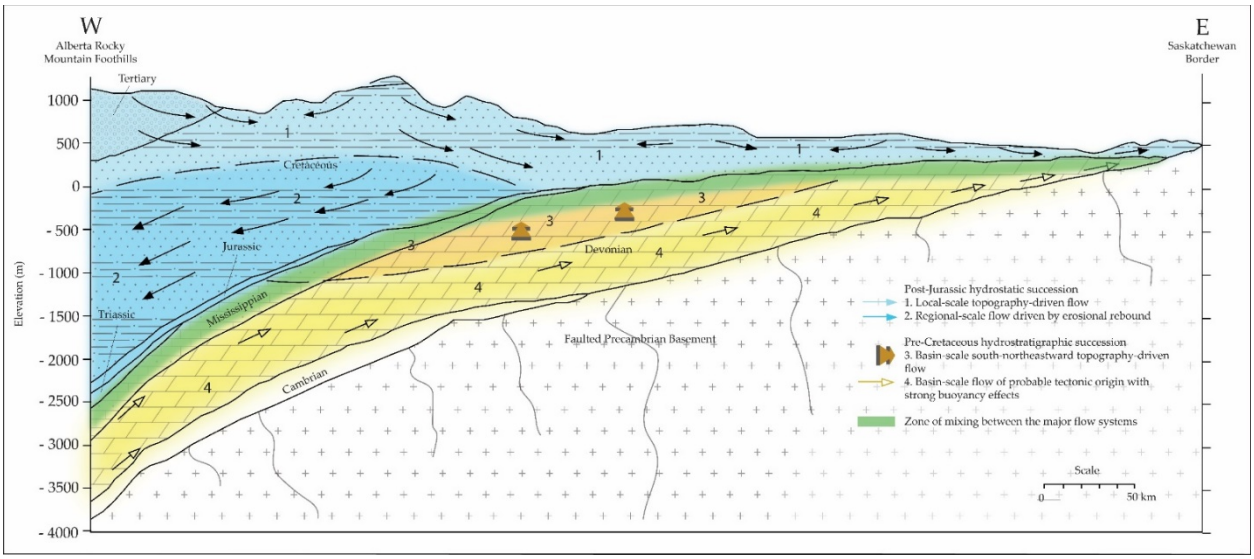

Figure 13. Illustration of the two mega-hydrodynamic regimes in the Alberta Basin. Adapted from Bachu, 1995. ©AAPG Bulletin 1995 and reprinted by permission from the Amercian Association of Petroleum Geologists (AAPG) whose permission is required for further use.

Large-scale alteration of hydraulic heads in the regional sub-hydrostatic systems or the salinity of either flow system could alter the flow of formation waters between these two mega-hydrodynamic regimes. Basin-scale or regional alteration of the hydraulic head or brine density of either or both mega-hydrodynamic flow systems can likely alter fluid interaction with the Precambrian basement since the basal saline aquifers are a part of the pre-Cretaceous flow system, and these directly overly the Precambrian basement. An industrial-scale CO_2 injection project, for instance, (without brine management) can materially increase saline aquifer formation pressures and displace brine at a basin (100 km) scale over its injection lifetime, even though the injected fluid plume linear dimensions may be constrained to under 10 km [43], [44], [128].

Such changes could affect the feasibility of conventional oil, thermal bitumen, and oil sands extraction (by changing hydraulic heads, altering stratigraphic/hydrodynamic traps, impacting top/bottom water or basal pressure) as well as increase the potential for the occurrence of crystalline basement related induced seismicity (by increasing pore pressure in basement faults). Proposed industrial-scale net zero and decarbonization initiatives that utilize CO_2 sequestration could potentially induce such regional or basin-scale alterations of the hydraulic head and density within the Alberta Basin, depending on the cumulative volumes injected over time, unless the injection volumes and net fluid balance are sustainably managed. Additionally,

since major surface water drainage systems are interconnected with both flow systems [129] and high salinity brine discharges into some drainage systems [77], hydraulic head increases have the potential to increase saline mass flux discharge rates into surface water systems. Hydraulic head increases also increase the risk of loss of containment of injected waste and saline fluids from deep formations, through legacy (improperly) abandoned wells, to shallow groundwater or surface [96], [131].

Table 3 shows the calculated pressure changes in hydrocarbon pools (for which data was available) over the last 60 years across the various PSAC areas in the Alberta Basin, relative to the distance to the Precambrian basement.

Table 3. Calculated reservoir pressure change in select pools in the Alberta Basin (1960-2020). Source data extracted from geoLOGIC Systems databases © 2020.

Area	Distance from Precambrian Basement (m)	Number of Pools with Comparable Pressure Data	Percentage of Pools Showing Increased Reservoir Pressure (%)	Average Increase (%)	Percentage of Pools Showing Decreased Reservoir Pressure (%)	Average Decrease (%)
AB1	5+	7	14	15	86	−46
AB1	4–4.99	18	11	91	89	−36
AB1	3–3.99	36	28	22	72	−49
AB1	2–2.99	47	13	35	87	−50
AB1	1–1.99	3	33	21	67	−42
AB1	0–0.99	1	0	0	100	−66
AB2	5+	1	0	0	100	−20
AB2	4–4.99	23	13	19	87	−51
AB2	3–3.99	79	15	80	85	−44
AB2	2–2.99	323	24	95	76	−52
AB2	1–1.99	996	22	70	78	−51
AB2	0–0.99	110	18	58	82	−46
AB3	2–2.99	92	36	117	64	−45
AB3	1–1.99	1351	23	50	77	−44
AB3	0–0.99	36	31	78	69	−28
AB4	1–1.99	884	21	45	79	−40
AB4	0–0.99	11	0	0	100	−68
AB5	3–3.99	2	0	0	100	−66
AB5	2–2.99	114	33	128	67	−45
AB5	1–1.99	1288	26	75	74	−42
AB5	0–0.99	25	40	108	60	−32
AB6	1–1.99	232	22	57	78	−39
AB6	0–0.99	238	15	38	84	−41

AB7	3–3.99	13	31	72	69	−39
AB7	2–2.99	63	17	133	83	−49
AB7	1–1.99	506	24	62	76	−42
AB7	0–0.99	400	28	85	73	−36

Table 3 indicates that in-situ pressure has decreased on average in most pools for which data is available across each of the stratigraphic depth horizons used in this assessment. However, this assessment also indicates that the in-situ pressure may have increased substantially in select pools in some areas. This increase is noticeable in AB5, in which approximately one-third of the pools appear to have experienced in-situ pressure increases of over 100% in the 2–3 km and 0–1 km depth to Precambrian basement range. This observation is consistent with the findings of the net fluid balance assessment above and suggests that a detailed regional fluid budget evaluation may be necessary within AB5 to maintain a sustainable fluid budget in the future. A net fluid balance approach may be a useful tool for such an assessment, as well as in subsequent associated regional management strategies.

However, several researchers have previously noted that the data quality of the in-situ formation-pressure measurement records is quite variable, with over 85% of this pressure data being rejected as being of low quality in one case [117], [132]. An analysis of the annual pressure survey records from select pools indicates considerable scatter in the bottomhole pressure recordings contained in the data set originating from the pool pressure surveys (Figure 14).

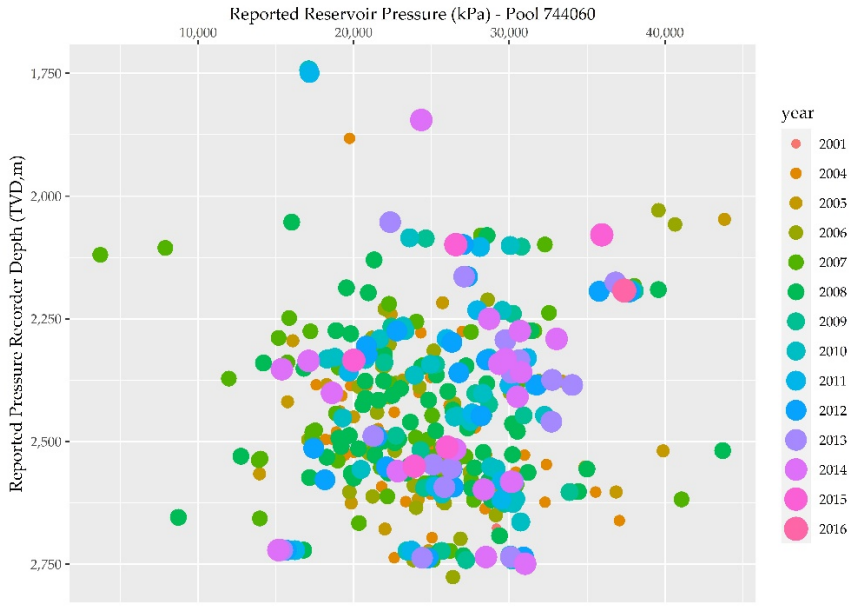

Figure 14. Examples of data scatter in the pool pressure-survey records contained in the geoSCOUT™ database. Source data extracted from geoLOGIC Systems databases © 2020.

Bottomhole pressure data is collected in active (producing/injecting) pools using pressure-recording equipment located in production or injection wells, and current rules stipulate minimum production/injection well shut-in requirements to obtain a stabilized reservoir pressure [133]. However, the possibility may exist that, in some cases (especially in an active commercial production environment), production well shut-in requirements may not always be stringently followed, leading to insufficient length of shut-in and recording of unstabilized reservoir pressures. Therefore, there is some uncertainty regarding the actual magnitude of in-situ formation pressure changes since the quality of the pool-pressure survey records is uncertain.

2.4 Discussion

This assessment shows that widely available measured production and injection volumetric data collected for production and royalty accounting purposes can be useful for evaluating basin-scale net fluid balance. Such an assessment may be a valuable complementary tool for assessing induced seismicity hazards (in near-Precambrian basement injection intervals), the potential for regional-scale hydrologic flow system changes and sustainable regional or basin-scale fluid storage capacity in industrial-scale fluid-injection scenarios. Such an assessment could also be an essential policy and regulatory tool for managing sustainable basin-scale fluid budgets.

Table 4 shows the net in-situ fluid balance in the Alberta Basin, and this information is also presented graphically in accompanying Figures 15 and 16. Table 4 (and Figures 15 and 16) show that oil and gas production has resulted in extensive in-situ fluid deficits in all regions and stratigraphic zones of interest in the Alberta Basin. However, the largest fluid deficits available in Alberta are due to gas production from the oil and gas reservoirs in the upper stratigraphic zones (located more than 1 km from the Precambrian basement) in AB1, AB2, AB3, AB5, and AB7 (Figure 15). In the stratigraphic zones located within 1 km from the Precambrian basement, relatively large fluid deficits are only present in AB2, AB5, and AB7. Consequently, significantly larger sustainable storage capacity for injected fluids in the near Precambrian basement interval is available in AB2, AB5, and AB7, compared to other areas in this basin.

These fluid deficits have also resulted in significant depletion (depressurization) of most of the Alberta oil pools assessed in this study, which enhances their apparent suitability for long-term industrial-scale storage of waste fluids. However, consideration of the net fluid balance in each area within this basin as an indicator of upper capacity limit for injected fluid may help to reduce the potential for occurrence of adverse fluid-injection-related subsurface effects. Specifically, active consideration of the magnitude of the net fluid balance in the near-Precambrian basement stratigraphic intervals (particularly in seismogenic areas in this basin) could be an important component of the array of efforts to mitigate the potential for future industrial-scale fluid-injection activities generating induced seismicity of concern.

Table 4. Calculated net in-situ fluid deficits in the Alberta Basin (as of December 31, 2020). Source data extracted from geoLOGIC Systems databases © 2020.

Area	0–0.99 from the Precambrian Basement		All Other Depth Zones	
	Net Gas Deficit (10^9 m^3)	Net Liquid Deficit ($10^9 m^3$)	Net Gas Deficit ($10^9 m^3$)	Net Liquid Deficit ($10^9 m^3$)
AB1	−324	0	−117,144	−5
AB2	−166,562	−38	−447,808	−87
AB3	−11,165	−4	−122,121	−29
AB4	−2,820	−4	−20,713	−22
AB5	−52,007	−161	−121,545	−70
AB6	−3,742	−29	−9,225	−2
AB7	−46,116	−60	−68,361	−13

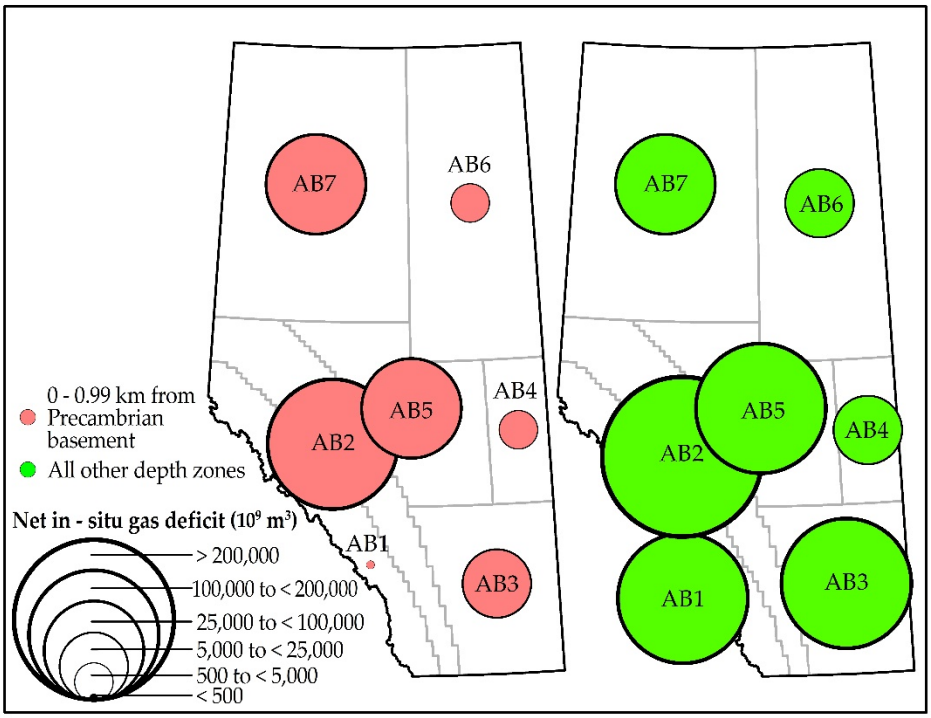

Figure 15. Calculated net in-situ gas deficit in the Alberta Basin (as of December 31, 2020). Source data extracted from geoLOGIC Systems databases © 2020.

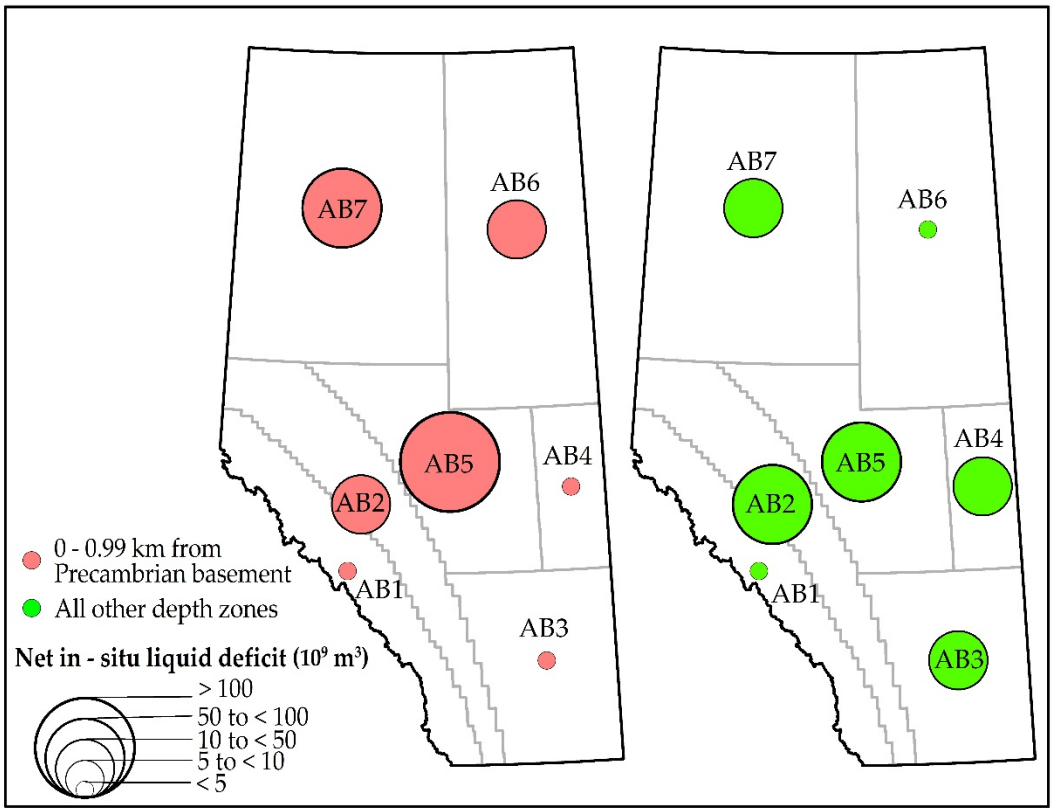

Figure 16. Calculated net in-situ liquid deficit in the Alberta Basin (as of December 31, 2020). Source data extracted from geoLOGIC Systems databases © 2020.

Since a negative fluid balance can be correlated to a lower injection-induced seismicity hazard, then the extensive capacity in the near Precambrian basement zone within areas AB2, AB5, and AB7, and the limited capacity in this zone in all other areas, may be observations worth considering in risk assessments conducted for industrial-scale injection projects proposed in these areas. Conversely, however, while the extensive fluid deficits are evident in the stratigraphic zones located more than 1 km above the Precambrian basement, the extent of the vertical separation between the base of groundwater protection and the proposed injection zone may also be a parameter that could be useful in such risk assessments.

Maintaining a formational, regional, or basin-scale net negative fluid balance in the near-Precambrian basement zone may be an essential part of a basin fluid budget management strategy to limit subsurface pore pressure increase and potential for loss of containment and induced seismicity, as well as a valuable tool in evaluating the sustainable fluid storage capacity of a basin. However, in basins in which interconnected buoyancy-driven flow systems exist, the impact of regional-scale fluid density changes may be important to consider, in addition to

assessment of the net fluid balance and fluid budget. In such basins, regional-scale changes in formation fluid density from industrial-scale fluid injection or fluid transfers increase the likelihood of basin-wide changes in hydrologic flow systems, which could impact other pore space users. Therefore, basin-scale net fluid balance and the implications of regional-scale formation-fluid density changes could be key factors limiting the sustainable fluid storage capacity of such basins under industrial-scale fluid injection scenarios.

2.5 Conclusions

The net fluid balance in the Alberta Basin may be an important consideration in future assessments of its capacity as a storage repository for injected fluids produced from evolution in the energy landscape to meet future energy needs (i.e., massive CO_2 injection projections). The average net fluid balance in this basin has been negative over the last 60 years, primarily because oil and gas extraction consistently exceeded injection in the basin over this period (Figure 2 a, b), which may have helped to mitigate hazards associated with high-volume fluid disposal activities to date. However, energy transition and net-zero initiatives increase the probability of a future positive, sustained net fluid balance from increasing industrial-scale injection of large volumes of fluids exceeding dwindling oil and gas removal from the basin. A positive net fluid balance may increase the likelihood of occurrence of larger induced seismic events, as well as regional-scale changes to the two mega-hydrodynamic flow systems in this basin.

A net fluid balance strategy for the management of fluid-injection-project cumulative effects may help to reduce the potential for the occurrence of pore pressure and reservoir induced seismicity occurrence, in addition to mitigating potential adverse impacts to current industrial pore space users. Currently, areas AB5 and AB6 appear to have experienced significant changes to the net fluid balance over the last two decades. In AB5, gas depletion rates have decreased by an order of magnitude in the near-Precambrian basement zone during this period. In AB6, gas injection has increased by 350% and liquids extraction by approximately 350% in the near-Precambrian basement zone over the last two decades. Therefore, future cumulative effects management attention may be required if these trends continue in these two regions. In addition to an assessment of the net fluid balance, regional-scale assessments should also consider the hydrogeological impacts of large-scale changes in formation brine density, considering its

apparent importance in controlling flow between the two mega-hydrodynamic flow systems in the Alberta Basin.

Assessment of the cumulative effects of sustained large volume fluid injection and extraction projects within a complex and hydraulically interconnected basin may be important to mitigate unintended effects. Such cumulative effects include the potential for basin-scale reservoir pressurization, which has been traditionally overlooked in carbon capture and storage capacity assessments conducted to date [134], [135]. Basin-scale considerations, such as regional reservoir pressurization and net fluid balance, may be limiting factors that could constrain maximum sustainable (safe) fluid storage capacity in Alberta. Future assessments could also consider the distance to the base of groundwater protection as a proxy for fluids moving out of the injection horizons towards non-saline groundwater formations.

This research provides the first known estimate of regional sustainable fluid storage capacity in this basin as well as a methodology to estimate regional net fluid balance, using currently available data. The methodology and estimates presented herein may be useful to other researchers in evaluating sustainable regional storage capacity and the potential for induced seismicity generation from large-scale fluid injection in Alberta and similar basins.

3.0 Assessment of the Brittle-Ductile State of Major Injection and Confining Formations in the Alberta Basin[2]

Abstract

Subsurface interaction between critically stressed seismogenic faults and anthropogenic fluid injection activities has caused several earthquakes of concern over the last decade. Proactive detection of the reverse and strike-slip faults inherent in the Alberta Basin is difficult, while identification of faults likely to become seismogenic is even more challenging. This paper presents a conceptual framework to evaluate the seismogenic potential of undetected faults, within the stratigraphic sequence of interest, during the site selection stage of fluid-injection projects. This method uses the geomechanical properties of formations present at sites of interest and their current state of stress to evaluate whether hosted faults are likely to be brittle or ductile since the hazard posed by faults in brittle-state formations is generally significantly higher than that of faults in ductile-state formations. This analysis used data from approximately 3,100 multi-stress triaxial tests to calculate the Mogi-equivalent brittle–ductile state line for 51 major injection and confining formations in the Alberta Basin and in-situ stress and pore pressure data from approximately 1,200 diagnostic fracture-injection tests to assess the last known brittle-ductile state of each formation. Analysis of these data shows that the major injection formations assessed in the Alberta Basin were in a ductile state, with some confining (caprock) formations in a brittle state at the time of the stress measurements. Once current site-specific in-situ stress data are available, this method enables site-specific assessment of the current brittle-ductile state of geologic formations within the zone of influence of large-volume fluid-injection projects and an evaluation of the associated potential for fault seismogenesis.

[2] This chapter was published in the Special Issue State of the Art Geo-Energy Technology in North America of Energies: Samaroo, M.; Chalaturnyk, R.; Dusseault, M.; Chow, J.F.; Custers, H. Assessment of the Brittle–Ductile State of Major Injection and Confining Formations in the Alberta Basin. Energies 2022, 15, 6877. https://doi.org/10.3390/en15196877.

3.1 Introduction

The presence of proximal geologic faults is a key hazard to many types of infrastructure projects, including major infrastructure projects located on the ground surface (e.g., water retention dams), in the subsurface (e.g., tunnels) and those that utilize the subsurface (e.g., subsurface fluid disposal, energy storage, geothermal projects). Critically stressed faults are of particular importance in infrastructure hazard assessments since small changes in subsurface stresses or pore pressure can trigger fault reactivation, resulting in ground displacement, earthquakes, and out-of-zone migration of subsurface fluids.

However, critically stressed faults appear to be pervasive, even in seismically quiescent intraplate continental regions [100], [136] and intraplate earthquakes can pose a non-negligible infrastructure hazard in such regions because of a paucity of seismic-resistant infrastructure in these historically aseismic locations [137]. Fault hazard assessment in such regions is challenging because of the lack of a fundamental scientific framework to understand seismogenesis, inadequate historical seismic records and the paradox between low strain accrual and sudden moment (energy) release of a stick-slip nature [138]. Fault hazard assessments conducted for fluid-injection projects located in such regions usually focus on the identification and avoidance of (known) faults or the curtailment of injected fluid volumes/pressures to limit induced seismicity occurrence in cases where (usually unknown) critically stressed faults have been intercepted or previously triggered [1].

Within the Alberta Basin, strike-slip and reverse faults are common [139], [140], with brittle slip along these types of faults responsible for the major induced seismic events that have occurred to date [141], [142]. In the Precambrian basement that underlies the Alberta Basin, extensive fracturing has been postulated to exist mostly at the sub-seismic scale, consisting of deeper brittle fault detachments and offsets overlain by broad zones of folded and fractured sedimentary strata [143]. Detection of such types of faults (i.e., reverse, and vertical to sub-vertical strike-slip faults) using conventional seismic methods is difficult because of low offsets and limited extent (i.e., below the seismic resolution limit) [144]. Most of the anthropogenic induced seismicity that has occurred to date in the USA and Canada has been caused by the inadvertent interception and triggering of such previously undetected/unmapped faults [145], [146]. Fluid-injection-project fault hazard assessments that rely solely on identification and

avoidance of known faults may therefore possess some inherent uncertainty regarding future induced seismicity generation potential. The availability of a screening method to assess fault seismicity-hazard potential at the site selection stage of fluid-injection projects can therefore be a useful hazard mitigation tool.

Over the last decade, there has been increasing evidence that geological/geomechanical factors largely control induced seismicity hazard (i.e., felt-induced seismicity), but the controlling factors have been unclear [147], [148]. Pore pressure increase, for instance, has often been cited as a primary factor in induced seismicity generation [61]. However, recent research noted that only 10% of an extensive fault trace triggered in the Dallas-Fort Worth Basin was seismogenic (with seismicity occurring at relatively low levels of pore pressure increase), while approximately 90% of this fault trace was not seismogenic at all levels of pore pressure increase [149]. Additionally, in this case the pore pressure increase required to trigger faults proximal to disposal operations was much higher (ΔP = 0.34 MPa) than that required to trigger distal faults (ΔP = 0.04 MPa) [16]. While the importance of geomechanical features in fault seismogenesis has been recognized [150], there has been limited progress in identifying the main causal factors for fault seismogenicity. The increasing use of machine learning tools to analyze large datasets in this field has resulted in the creation of new lumped parameters (e.g., geologic susceptibility, integrated geological index, combined geomechanical index, etc. [48], [57], [151]), which have been proposed to account for the combined seismogenic influence of all geologic/geomechanical features. While such methods can be useful in hindcast analyses, there is an important need to identify specific (field-measurable) geomechanical parameters that control fault seismogenic slip to enable site-specific data collection and induced seismicity risk assessment prior to the construction/operation of fluid-injection projects.

The upper 10-15 km of the continental crust hosts most of the crustal displacement and seismogenic faults, with the seismogenicity of this zone generally attributed to (brittle) fracture and/or stick-slip displacement in brittle rock and fault sequences [152]–[154]. The lower crust is considered ductile, with its rock sequences displaying plastic/viscous behavior, and faults in this zone are aseismic [152], [153]. In faults that extend over the brittle-ductile zones, progressive displacement within the ductile zone can result in strain accumulation within the brittle zone and subsequent seismogenic shear across the entire fault system [155]. Earthquake seismic hazard is

generally associated with stick-slip displacement within brittle faults, while slip/displacement of ductile faults is generally aseismic and poses negligible seismic hazard [156]. Relatively small changes in confining stress can cause sedimentary rock sequences to transition from a (brittle) seismogenic state (i.e., unstable, stick-slip) to a (ductile) aseismic state and vice versa, with this mechanism postulated to primarily account for earthquake activity in deep sedimentary sequences [157].

While mature fault zones are generally weak, fault and host-rock deformation mechanisms and rheology can vary considerably over short distances (i.e., inside or outside the localized deformation zone) and timescales (earthquake recurrence cycles), since these depend on thermodynamic conditions, rock properties and mechanical state [158]. Variations in material composition along a fault can also determine if fault displacement is seismogenic (i.e., if fault movement is seismic or aseismic) even within fault sections considered brittle [158]–[160]. Ductile fault host-rock behavior is possible at depths of less than 5 km under conditions of high differential stress [161], pore pressure [161], confining pressure [162], porosity [163] and clay content [164]. Ductile rock sequences are likely to host ductile faults since the fault is expected to display the rheological behavior of the host material [165], and consequently slip along such fault is expected to be aseismic. Conversely, brittle rock sequences are likely to host brittle faults [165], with slip along such faults anticipated to be brittle.

In some cases (physical/chemical), alteration of the rocks in the fault zone may alter the behavior of the fault shear-zone, either increasing [166] or decreasing [167] its brittleness relative to the host rock formation. For instance, higher dolomite mineral content in a carbonate formation increases formation and shear zone brittleness [168], with previous research linking the occurrence of some fluid-injection-induced seismic events to specific dolomitized regions of deep (high confining stress and pore pressure) Devonian platform carbonates present throughout the Alberta Basin [169]. While these extensive, highly fractured (low clay content, low porosity) carbonate formations are important hydrocarbon and fluid disposal reservoirs [170], under certain conditions, these deep (often brittle) carbonates can be nucleation sites for significant earthquakes [171]. Therefore, the ability to assess (at the site screening stage) the seismogenic potential of carbonate formations within the zone of influence of large-scale fluid injection projects in this basin could help mitigate future fluid-injection project seismic risk.

Prior work indicated that the location of fluid-injection-induced earthquakes in Alberta is primarily influenced by geologic factors [57], [62]. This research assesses the relative brittleness and the brittle-ductile limits of most of the major injection formations and confining sequences (caprock and under burden) in the Alberta Basin, using a Mogi-equivalent relationship and rock mechanical properties obtained from multi-stress triaxial testing. Subsequently, a conceptual framework to evaluate the in-situ brittle-ductile state of each formation with reference to its Mogi-equivalent line is presented and its use demonstrated, using available in-situ stress and formation pore pressure measurements.

The results presented indicate that, at the time of the in-situ stress and pore pressure measurements, the major injection formations assessed were in the ductile state, with some caprock formations in the brittle state. However, the in-situ stress data available for most of the deep (carbonate-rich) formations in seismogenic regions are likely outdated since they predate recent localized high-volume fluid injection trends occurring in this basin [1], and changes in fluid injection/extraction are known to alter the stress condition in rocks [172]. This analysis indicates that one such formation (the Belloy) that was historically depleted and close to its brittle state has experienced notable induced seismic events triggered by recent industrial-scale fluid disposal activities. This conceptual framework could be useful, in conjunction with contemporaneous site-specific (in-situ stress and pore pressure) data, to evaluate the seismogenic potential of future industrial-scale fluid-injection project sites in carbonate-rich stratigraphic sequences in this and other global sedimentary basins.

3.2 Materials and Methods

The extensive history of oil and gas development in the Alberta Basin, combined with the province's policies on data collection and open data access, resulted in the creation of one of the world's most comprehensive collections of publicly available geoscience data. This includes operational data such as fluid production and injection volumes, formation pressures and well logs, as well as geological, geomechanical, chemical and other types of laboratory analyses. The Alberta Energy Regulator (AER) maintains lists of data types and availability on its website (https://www.aer.ca/providing-information/data-and-reports/activity-and-data last accessed 19 September 2022), with the data catalog for tests conducted on almost all core samples collected in the Alberta Basin located at https://static.aer.ca/prd/documents/sts/GOS-REPS.xlsb (last

accessed 19 September 2022). Submission of all laboratory core-test data for all cores collected is a component of regulatory requirements in the province and therefore mandatory for operators in Alberta. However, there is currently no standard submission format for the different types of laboratory core tests conducted, and consequently significant variability exists in the type and format of data provided. A significant amount of data curation and interpretation was required to compile the database used for regional analyses across the basin.

3.2.1 Identification of Major Injection Formations in the Alberta Basin

Injection fluid operational data were used to identify all wells in Alberta that have injected any volume of fluid into the subsurface over the period from January 1960 to December 2021, along with the type and volume (at surface conditions) of fluid injected and the injection stratigraphic zone (i.e., target receiving formation). This analysis showed that approximately 33,000 wells injected approximately 25 cubic kilometers (km^3) of water, 692 km^3 of gas and 3.35 km^3 of cold-water-equivalent steam (all measured at surface conditions) into the subsurface in Alberta during this period. These wells were then grouped according to the lithology and geologic age (era and period) of the injection formation and the proportion of the total basin-wide volume of each type of fluid injected into each lithological group in each geologic age calculated. The results of this analysis are presented in Section 3.3.

3.2.2 Determination of the Mogi-Equivalent Brittle-Ductile State Limits for Major Formations and Confining Sequences in the Alberta Basin

The AER's Reservoir Evaluation and Productivity Studies (REPS) core and drill cutting material sampling database (as of December 2021) contained approximately 600 individual reports (in secure pdf format) that included laboratory core triaxial tests. However, only a third of these reports contained the results of multiple single-stage triaxial tests conducted at different confining stresses on plug samples retrieved from the same core interval (i.e., multi-stress triaxial tests); the remainder consisted of only one single-stage triaxial tests conducted (only at the confining stress of interest to the particular study - usually only at the confining stress corresponding to the minimum horizontal stress of the target reservoir) at each core interval. Additionally, many reports contained the results of multiple sets of core triaxial tests conducted on samples from different stratigraphic horizons within the same well. Figure 17a below shows the triaxial core-sample well locations, the type of triaxial test data available and the location

density of fluid-injection wells across the basin. Figure 17b shows the relative locations of known significant fluid-injection-induced seismic events that have occurred in the Alberta Basin to date.

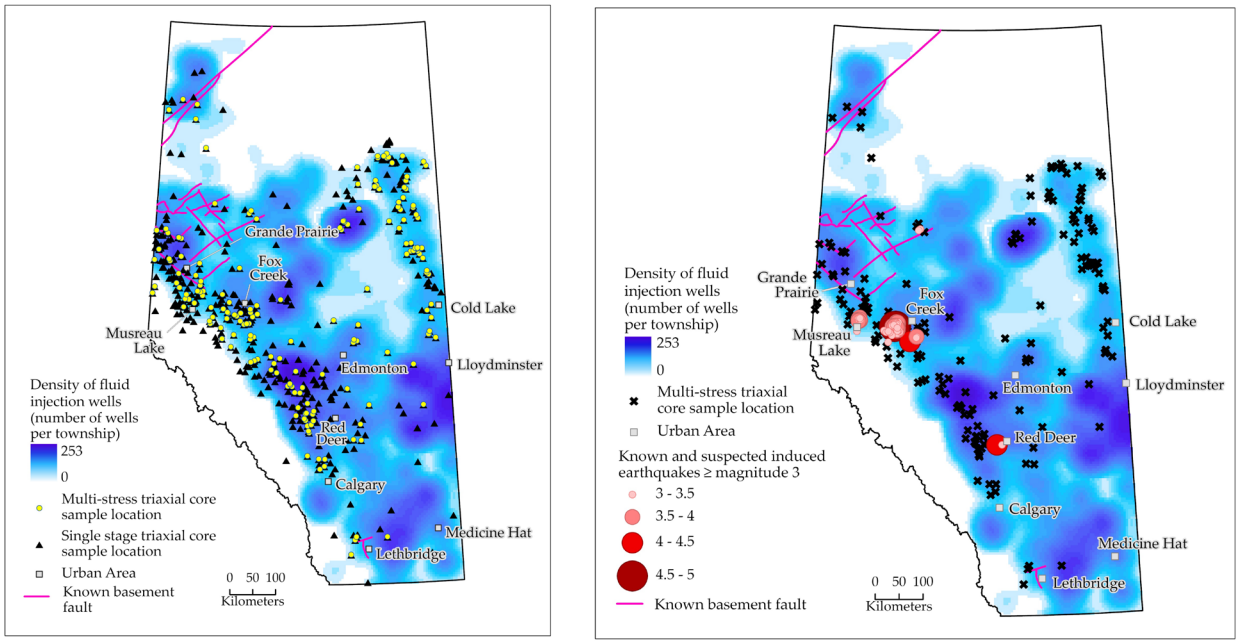

(a) **(b)**

*Figure 17. **(a)** Location of (approximately 600) triaxial core sample wells (triangles), (approximately 200) multi-stress triaxial core sample wells (circles) and density of approximately 33,000 wells reporting some fluid injection over the period 1960-2021. **(b)** Location of known and suspected significant fluid-injection-induced earthquakes that have occurred in the Alberta Basin to date. Known regional basement faults are indicated by red lines.*

The sets of multi-stress triaxial data were contained in individual reports, each corresponding to a single well (or an individual sample in some cases). Manual data extraction, processing and data entry were required to aggregate the data and enable further analysis. Additionally, while each core-test laboratory report contained the unique well identifier (UWI) for each source well and the core sampling intervals, the originating formation details were missing in many cases. This necessitated a geological review of the corresponding well logs for approximately 40% of the multi-stress triaxial core sample wells to identify the geologic formations and lithologies corresponding to each of the core samples tested. Additionally, in approximately 30% of the laboratory reports, only raw triaxial data were available; in such cases, processing and interpretation of the data were required to obtain the required formation geomechanical parameters. Approximately 3,000 sets of multi-stress triaxial tests corresponding

to most of the major lithological sequences in the Alberta Basin (Table 5) were compiled using this data.

Table 5. Summary of the number of multi-stress triaxial tests used in this analysis and the source lithologies.

Geologic Era	Major Lithology	No. of Wells	No. of Multi-Stress Triaxial Core Tests	Proportion of Analyses (%)
Mesozoic	Shale	56	490	16
Mesozoic	Sandstone	58	716	24
Mesozoic	Limestone	17	147	5
Paleozoic	Calcareous shale	67	1,105	37
Paleozoic	Calcareous sandstone	7	67	2
Paleozoic	Limestone	42	413	14
Paleozoic	Anhydrite	13	77	3
Total		260 [1]	3,015	

[1] In some cases multiple core samples were collected from the same well.

Table 5 shows that approximately 91% of the multi-stress triaxial tests available were conducted in low permeability (calcareous shale, calcareous sandstone, or shaly limestone) lithologies, generally with the objective of measuring geomechanical properties important for hydraulic fracturing design (for tight oil exploitation) or caprock characterization (for thermal oil exploitation) in cases of shallow shale formations. The other major category of multi-stress triaxial test data available was collected for the purposes of subsurface salt cavern design, and the wells drilled for these purposes provided geomechanical data for multiple adjacent formations in each area of interest. This information was then used to build an Excel database containing the core-sample originating formation, core depth and laboratory-measured parameters for each sample, including confining stress (σ_3), failure stress (σ_1), unconfined compressive strength (C_o), Young's modulus (E), Poisson's ratio (υ), porosity (n), cohesion (c), angle of internal friction (φ) and Biot's coefficient (α). While most of the reports examined indicated that the laboratory triaxial tests were conducted under drained conditions, this information was not included in approximately 30% of the laboratory test reports reviewed.

This database was then used to determine confining stress at the brittle-ductile transition (σ_3*) and to calculate the empirical Mogi-equivalent ductility parameter (d) for each formation in accordance with the methods provided by Walton, 2021 [21]. First, the confining stress at the brittle-ductile transition (σ_3*) for each formation was determined by reviewing the stress-strain curves of each of the (approximately 3,000 triaxial tests), using the method shown in Figure 18.

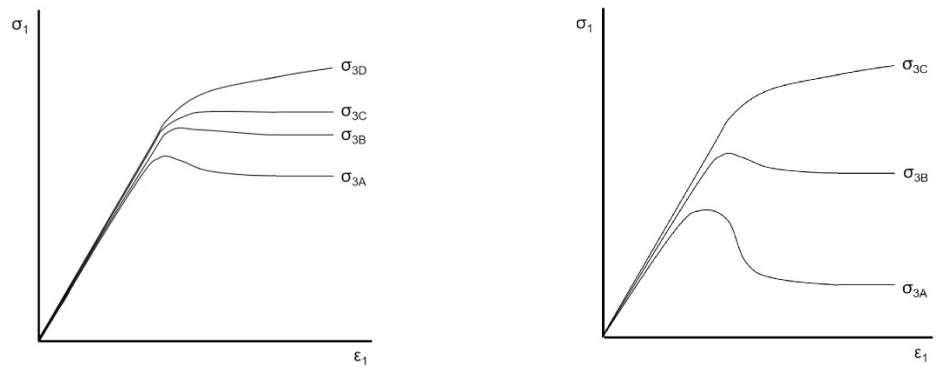

(**a**) (**b**)

Figure 18. Illustration showing how multi-stress (drained) triaxial stress–strain curves were used to determine the principal and confining stresses at the brittle-ductile transition (σ_3) for each formation (**a**) Result of triaxial tests conducted (on core plugs obtained from same core sample) at varying confining stresses with good confining stress resolution; $\sigma_3^* = \sigma_{3C}$ (**b**) Result of triaxial tests conducted (on core plugs obtained from same core sample) at varying confining stresses with poor confining stress resolution; $\sigma_{3B} < \sigma_3^* < \sigma_{3C}$. Modified from Walton, 2021, and used with permission.*

The empirical Mogi-equivalent ductility parameter (d) was then calculated using equation 14:

$$d = (\sigma_1 - \sigma_3^*)/\sigma_3^*, \qquad (14)$$

where σ_1 and σ_3^* are the principal and confining stresses, respectively, at the Mogi-equivalent brittle-ductile transition limit.

While the empirical Mogi-equivalent ductility parameter (d) provides a useful index for the relative brittleness of rocks, it is highly dependent on the strength of the rock [21]. Walton (2021) notes that it is necessary to normalize the ductility parameter by the unconfined compressive strength (C_o) of the rock to obtain a normalized ductility parameter (termed d*) that is independent of the unconfined compressive strength of the rock. This modified ductility parameter includes both rock strength (i.e., C_o) and material parameters (d), is directly comparable to existing brittleness indices, and can be used to quantitatively compare the brittleness of different rock formations [21]. Walton (2021) also notes that the d* evaluated based on the stress-strain curves in the ductile regime can be considered an inherent material property and a rock mechanical index directly proportional to the modified Hoek-Brown material constant (m) commonly used for rock mass strength characterization [173].

The average unconfined compressive strength of each rock formation was calculated using the Excel database, and the modified Mogi-equivalent ductility parameter (d*) then calculated in accordance with equation 15:

$$d^* = d/C_o, \quad (15)$$

where C_o is the average measured unconfined compressive strength of the corresponding rock formation (in MPa). The results of this analysis are presented in Section 3.3.

3.2.3 Determination of the Brittle-Ductile State Parameter and Brittle-Ductile Stress Index for Each Major Injection Formation and Confining Sequence in the Alberta Basin

The standard Mogi-equivalent ductility parameter (d) provides the confining stress limit at which the transition from brittle fracture to ductile flow can be expected to occur [174] in each of the 51 formations assessed in the Alberta Basin, while the modified d* provides a quantitative measure of the relative brittleness of the formations assessed. However, it is necessary to evaluate the relationship between its initial in-situ stress state and its Mogi-equivalent state limit to determine whether a formation is likely to be in a brittle or ductile state at its initial in-situ stress regime. Such an evaluation also can provide an indication of whether sections of geologic faults contained within such formations are likely to be in a brittle or ductile state, since hosted faults are likely to reflect the Mogi-equivalent state of the host formation (especially in the low-porosity, low-clay content formations such as the deep carbonates of the Alberta Basin). Therefore, an evaluation of the brittle/ductile state of a formation can help provide an indication of the probability of the existence of brittle faults within rock sequences and consequently an indication of potential seismic hazards.

A method was devised based on an approach analogous to the definition of the state parameter of the critical state concept for rock [22], using the formation-specific Mogi-equivalent line (in this case assumed to be analogous to the critical-state line) for each formation to evaluate its last-known in-situ stress state relative to its Mogi-equivalent line. This concept is used to derive two associated parameters, called the Brittle-Ductile State Parameter (χ) and the Brittle-Ductile Stress Index (I_{BD}) as shown in Figure 19 and equations 16 to 19. These two parameters can be used to assess whether a formation at its current in-situ stress state may be in the brittle or ductile regime in relation to its Mogi-equivalent state limit and by extension whether it is likely to host brittle (potentially seismogenic) or ductile (potentially aseismic) faults.

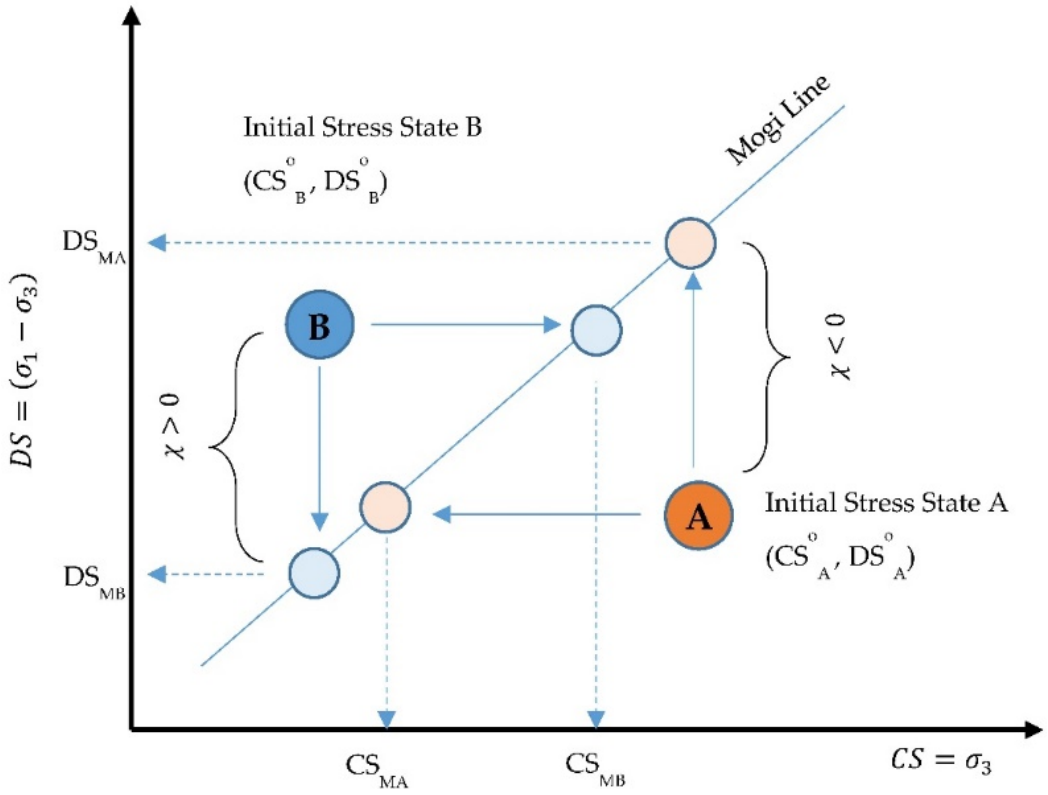

Figure 19. Concept and method used to derive the Brittle-Ductile State Parameter (χ) and the Brittle-Ductile Stress Index (I_{BD}). DS = Deviator stress; CS = Confining Stress; A and B are formations at initial confining and deviator stress states (CS^0, DS^0).

In Figure 19, Formation A at an initial confining stress CS^0_A and deviator stress DS^0_A is in the ductile regime with respect to its Mogi-equivalent line. Since the Mogi-equivalent line relationship (i.e., the ductility parameter d, which is the gradient of the Mogi-equivalent line in Figure 19) is known, equation 14 above can be used to calculate the equivalent confining (CS_{MA}) and deviator (DS_{MA}) stresses at the Mogi-equivalent line for the initial stress state (CS^0_A, DS^0_A) of Formation A in accordance with the following relationships:

$$DS_{MA} = (\sigma_1 - \sigma_3)_{MA} = d * {\sigma_3}^0_A, \qquad (16)$$

$$CS_{MA} = \sigma_{1MA} = \sigma_{1A} / (d + 1), \qquad (17)$$

The calculated in-situ equivalent confining (CS_{MA}) and deviator (DS_{MA}) stresses at the Mogi-equivalent line for Formation A can then be used to calculate the Brittle-Ductile State Parameter (χ) and the Brittle-Ductile Stress Index (I_{BD}) for Formation A according to the relationships provided in equations 18 and 19:

$$\chi = (\sigma_1 - \sigma_3)^0_A - (\sigma_1 - \sigma_3)_{MA}, \quad (18)$$

$$I_{BD} = (\sigma_3{}^0_A / \sigma_{3MA}), \quad (19)$$

where χ is the Brittle-Ductile State Parameter, which provides a measure of the distance to the Mogi-equivalent line under conditions of constant confining stress, while I_{BD} provides a measure of the distance to the Mogi-equivalent line under conditions of constant deviator stress.

Similarly, the Brittle-Ductile State Parameter (χ) and the Brittle-Ductile Stress Index (I_{BD}) can be calculated for Formation B's initial stress state shown in Figure 19, using equations 16 to 19. A negative χ value indicates that the formation is in the ductile regime (based on its initial stress state), whereas a positive χ value indicates that the formation is in the brittle regime (based on its initial stress state). Values of I_{BD} of less than one indicate that the initial stress state of the formation is within the brittle range, while (I_{BD}) values of greater than one indicate that the initial stress state of the formation is within the ductile range.

3.2.4 Estimation of the In-Situ Stress State of Each Major Injection and Confining Formation in the Alberta Basin

An extensive database of in-situ vertical and minimum horizontal stress measurements exists for various formations of interest to the hydrocarbons, disposal, and cavern storage industries in Alberta. Density logs are routinely collected to meet operational and regulatory requirements in the hydrocarbon industry, and integration of these logs to the depth of interest provides a reliable estimate of the vertical stress (gradient) at the target zone [175]. Mini-fracture tests (also referred to as minifrac, diagnostic fracture injection tests or DFITs) required for operational (e.g., fracture design [176]) and regulatory (e.g., AER's Directive 40 [133]) requirements typically provide reliable estimates of the magnitude of the in-situ minimum horizontal stress [177]. Formation pressure tests are routinely conducted to meet operational and regulatory requirements and can provide reliable estimates of the formation pore pressure (gradients) for most formations in the Alberta Basin [1]. Additional sources of minifrac, vertical stress and pore pressure data include the published reports listed in the Data Availability section.

While comprehensive vertical, minimum horizontal stress and pore pressure data are publicly available for many formations in the Alberta Basin, these data are widely distributed across many different sources, such as regulatory, industry, academic and scientific publications.

The vertical, minimum horizontal stress and pore pressure data contained in the publications listed in the Data Availability section were consolidated into a single Excel database and then used to compute the complete stress state of the individual formations using the methods described below. In approximately 30% of the cases, UWIs were provided, but the corresponding formations were not listed. In such cases, geological interpretation of the specific well logs was required to identify each corresponding formation for the in-situ stress/pore pressure measurements. Additionally, data vintages varied widely, with relatively recent data available for formations of interest to the tight (e.g., the Montney and Duvernay) and thermal (e.g., Clearwater caprock, McMurray reservoir) hydrocarbon industries, while data for other (e.g., deep carbonate) formations were collected up to several decades ago.

Determination of the χ and the I_{BD} requires the full stress tensor (i.e., σ_1, σ_2 and σ_3). The frictional limits theorem can be used to estimate the upper limit of the magnitude of the maximum horizontal stress (i.e., σ_1) under (critically stressed) reverse and strike-slip faulting conditions, which are responsible for the occurrence of felt-induced seismicity in the Alberta Basin [113]. This theorem assumes that the maximum in-situ stress is horizontal and is limited by the frictional strength of faults within the rock mass, as shown in equations 20 and 21 below [178], [179]:

$$\sigma_{1\ max} = f(\mu) * (\sigma_3 - P_p) + P_p, \qquad (20)$$

$$f(\mu) = [(1+ \mu^2)^{1/2} + \mu]^2, \qquad (21)$$

where μ is the coefficient of internal friction and P_p is the formation pore pressure. The coefficient of internal friction is the tangent of the angle of internal friction of the formation core sample (i.e., tan (φ)) and is calculated from the formation core triaxial laboratory test database, while formation pore pressure and minimum stress measurements (which can be either horizontal or vertical) are available from the in-situ test database compiled above. Therefore, assuming that geologic faults are present and in a critically stressed state, the complete in-situ stress state of each formation can be estimated using equations 20 and 21, in conjunction with the measured in-situ stress (i.e., vertical stress, minimum horizontal stress and pore pressure) and the triaxial test database. Critically stressed faults appear to be prevalent across all continental regions [136], and

direct/indirect triggering of such faults has been the main causal factor for fluid-injection-induced seismicity in this basin [180].

Ranges of minimum horizontal stress and pore pressure (gradient) measurements were available for individual formations, depending on the characteristics of the lithology, location, measurement method and vintage of the data. The minimum and maximum stress and pore pressure measurements for each formation were used to create a low and a high range of minimum horizontal stress, vertical stress, and formation pore pressure for the corresponding depth range of each formation. The combinations of low and high σ_3, σ_v and P_p values were then used to calculate the corresponding maximum horizontal stress for each scenario, resulting in a minimum and maximum value for each of σ_1, σ_2, σ_3 and P_p at the corresponding formation depth. Only reverse ($\sigma_v = \sigma_3$) and strike-slip ($\sigma_v = \sigma_2$) stress regimes have been considered in this analysis since only these cases have been linked to the occurrence of felt-induced seismicity in the Alberta Basin [113], [142], [181]–[183].

This approach resulted in four possible combinations of confining stress (CS = σ_3) and deviator stress (DS = $\sigma_1 - \sigma_3$) that could be used to calculate the χ and the I_{BD}. These are (i) a high CS-high DS (HCS-HDS), (ii) a high CS-low DS (HCS-LDS), (iii) a low CS-high DS (LCS-HDS), and (iv) a low CS-low DS (LCS-LDS). The use of the LCS-HDS combination maximizes the χ and minimizes the I_{BD} for each formation, and this combination was used as the default (conservative case) analysis scenario. This scenario is also consistent with the observations of previous work, which noted that low confining stress (and high deviator stress) in deep carbonate formations is associated with an increased probability of induced seismicity occurrence in the Alberta Basin [57].

3.3 Results

In the sub-sections below, the data analyzed is used to identify the geologic formations most utilized for fluid injection in the Alberta Basin. The (calculated) modified Mogi-equivalent ductility (d*) parameters are presented and used to evaluate the relative brittleness/ductility of these formations and to identify the most brittle and most ductile injection and confining formations in this basin. The calculated χ and I_{BD} parameters and the measured in-situ stress

reported in the existing literature are used to evaluate the brittleness of the major injection formations at the time of in-situ data collection.

3.3.1 Major Injection Formations in the Alberta Basin

Table 6 below presents the summary of major injection formations identified in the Alberta Basin and the relative proportion of fluid volumes (measured at surface conditions) injected into each type of formation.

Table 6. Geologic formations receiving the largest volumes of injected fluids in the Alberta Basin and the relative proportion of fluid volumes (measured at surface conditions) injected over the period January 1960 to December 2021. Steam injected is reported in cold-water equivalent volumes at surface conditions.

Geologic Formation	Water Injected [1]	Gas Injected [1]	Steam Injected [1]
Paleogene sands (Swan Hills)	17.1%	14.0%	0%
Lower Cretaceous sandstones (McMurray, Clearwater, Cardium, Viking, Nikanassin)	30.6%	9.8%	97.9%
Jurassic sandstones (Sawtooth)	11.5%	15.1%	0%
Triassic carbonates (Charlie Lake, Halfway)	0.4%	1.0%	0%
Triassic siltstones (Montney, Doig)	0.3%	0.6%	0%
Permian sandstones (Belloy)	0.2%	0%	0%
Carboniferous carbonates (Banff, Debolt, Elkton, Livingston, Turner Valley)	0.7%	1.8%	0%
Devonian carbonates (Arcs, Grosmont, Keg River, Leduc, Muskeg, Nisku, Slave Point, Wabamun, Winterburn)	29.2%	43.3%	1.4%
Devonian sandstones (Granite Wash, Gilwood)	4.1%	0.6%	0%
Cambrian sandstones (Basal Sandstone Unit)	0.3%	0%	0.8%
Total volumes injected in above-listed formations	23.8 km^3	596.7 km^3	3.41 km^3
Total fluid volumes injected into all formations in the Alberta Basin	25.2 km^3	692.2 km^3	3.41 km^3

[1] Totals may not add to 100% due to rounding. Fluid volumes are reported in cubic kilometers (i.e., km^3 = cubic kilometers).

Table 6 shows that approximately 94% of the water, 88% of the gases and 100% of the steam that have been injected into the Alberta Basin over the past six decades were injected into 27 major formations. Most of these fluids were injected into three Lower Cretaceous sandstones and nine Devonian carbonate hydrocarbon reservoirs that have been extensively exploited, resulting in significant historical formation pressure depletion [1]. These formations are located at intermediate depths, generally sandwiched between extensive regional low permeability (confining) formations, and possess the geologic characteristics required to isolate injected fluid from both the ground surface and the Precambrian basement. These carbonate-rich formations, along with their confining geologic units (generally low permeability shales or mudstones), form the focus of the subsequent geomechanical data analyses conducted in this study.

Notably, Table 6 does not account for the geographic extent of the listed formations and consequently for differences in the geographic distribution of the injection fluid volumes. For instance, the Cretaceous, Devonian, and Triassic formations listed are geographically extensive, present in most of the Alberta Basin, and the fluid volumes injected are correspondingly geographically distributed [1]. Conversely, the (regional) Permian (e.g., Belloy) and Carboniferous carbonate (e.g., Debolt) formations have a limited geographic distribution with injection volumes concentrated in specific areas. Despite the apparent marginal contribution at a basin-scale, at a regional-scale these formations support large volumes of industrial-scale fluid-injection activities, especially over the last decade (Figure 20).

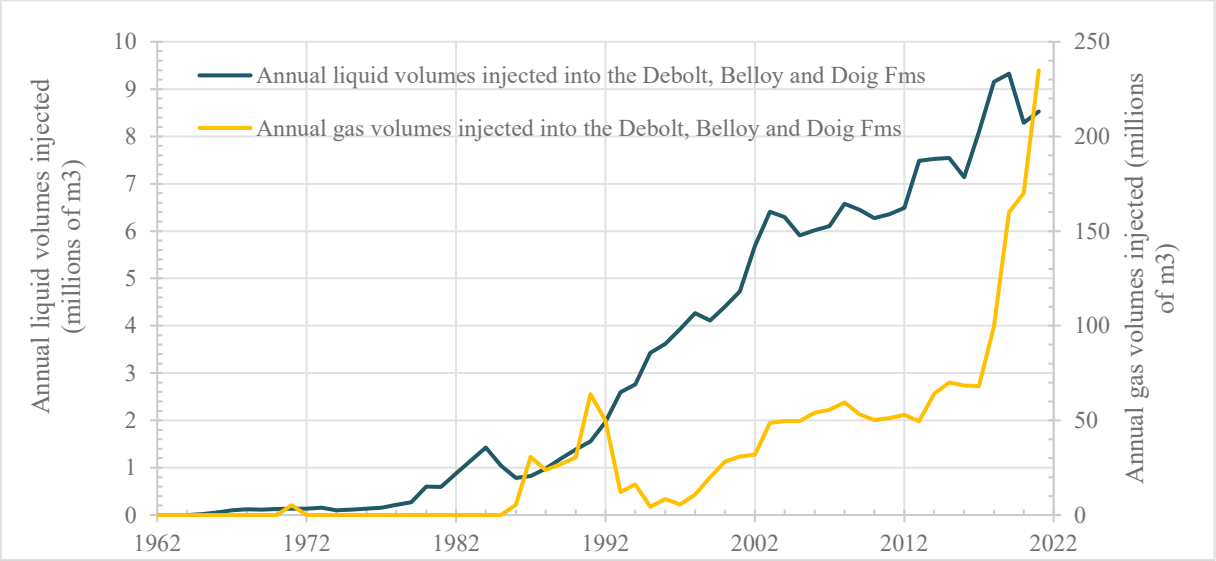

Figure 20. Annual fluid volumes (measured at surface conditions) injected into three regional (i.e., limited geographic extent) formations in the Alberta Basin.

Figure 20 shows that fluid injection into some of these regional disposal formations has increased notably over the last decade, as the hydrocarbon industry in Alberta and the types of subsurface activities conducted in its subsurface have evolved. Significant future increase in fluid-injection volumes in these regional formations is expected over the next decade to support energy transition and net-zero energy objectives [1], which has the potential to considerably alter the stress and pore pressure states of these formations.

3.3.2 Determination of the Mogi-Equivalent Brittle-Ductile State Limits and Relative Brittleness of Major Injection and Confining Formations in the Alberta Basin

Table 7 presents the summary of the laboratory-measured geomechanical properties used to calculate the empirical (d) and modified (d*) Mogi-equivalent ductility parameters.

Table 7. Summary of laboratory triaxial test data, empirical and modified Mogi-equivalent ductility parameter for major injection and confining formations in the Alberta Basin.

Formation *	No. of Wells	No. of Core Tests	Major Core Lithology	TVD from (m)	TVD to (m)	Mean UCS (MPa)	Mean n (%)	Mean φ	Mean μ	σ_1 (MPa)	σ_3* (MPa)	d	d*
Lea Park [2,4]	1	6	Clayey shale	1,524	1,531	0.04	13	28	0.5	38	18	1.1	28.9
Cardium [3,4]	4	21	Sandstone, carbonate cement	1,794	2,477	49	5	37	0.8	184	19	8.5	0.17
Second White Specks [2,3,4]	11	194	Calcareous siltstone	323	2,782	79	3	31	0.6	252	42	5.0	0.06
Fish Scales [2,4]	1	12	Silty shale	469	471	15	21	32	0.6	25	5	4.5	0.30
Dunvegan [3,4]	1	16	Dolomitic siltstone	1,751	1,823	224	5	38	0.8	185	10	17.0	0.08
Viking [3,4]	3	28	Calcareous sandstone	507	2,182	39	19	37	0.8	133	23	4.8	0.12
Joli Fou [2,4]	2	11	Silty shale	287	599	19	16	25	0.5	4	1	2.5	0.13
Falher G, H [3,4]	1	56	Silica cemented sandstone	2,928	3,064	107	8	33	0.7	312	42	6.4	0.06
Upper Clearwater [2,4]	10	73	Silty shale	96	243	2	35	28	0.5	7	3	1.3	0.61
Lower Clearwater [2,4]	24	154	Silty claystone, some siltstone	243	651	20	38	32	0.6	20	7	1.9	0.09
Spirit River [3,4]	1	18	Calcareous sandstone	2,875	2,892	93	9	33	0.6	234	27	7.7	0.08
Lower Mannville [3,4]	4	81	Calcareous sandstone	1,398	2,778	107	12	41	0.9	201	19	9.5	0.09
Ostracod [3,4]	4	8	Calcareous sandstone	2,663	2,692	131	4	40	0.8	276	26	9.6	0.07
Shallow Wilrich [2,4]	1	4	Silty clay shale	574	575	5	22	36	0.7	36	8	3.3	0.62
Deep Wilrich [2,3,4]	1	20	Argillaceous siltstone	2,660	2,695	137	3	38	0.8	279	40	6.0	0.04
Wabiskaw [3,4]	6	30	Silty mudstone	148	417	3	36	40	0.9	11	4	1.6	0.64
McMurray [3,4]	5	23	Weak sandstone	182	455	1	36	32	0.6	11	4	1.6	1.46
Nikanassin [3,4]	4	24	Sandstone	2,280	3,385	90	4	50	1.2	497	30	15.6	0.17
Fernie [2,4]	3	12	Calcareous shale	1,845	3,064	79	4	29	0.6	174	36	3.8	0.05
Nordegg [3,4]	12	95	Argillaceous limestone	1,464	3,079	149	4	38	0.8	214	34	5.2	0.03
Charlie Lake [2,3,4]	5	52	Dolomitic siltstone	1,478	2,241	85	12	52	1.3	206	18	10.4	0.12
Doig [3,4]	2	20	Dolomitic sandstone	2,406	2,990	59	4	53	1.3	224	18	11.2	0.19
Montney [2,3,4]	23	373	Dolomitic siltstone,	823	3,264	155	4	44	1.0	318	22	13.5	0.09
Belloy [3,4]	2	20	Dolomitic siltstone	2,476	2,672	164	9	44	1.0	316	42	6.5	0.04
Mt. Head [3,5]	1	8	Argillaceous limestone	2,393	2,405	108	6	40	1	417	37	10.3	0.10
Banff [2,3,5]	2	14	Dolomitic, silty mudstone	1,550	1,740	123	5	30	1	158	15	9.9	0.08
Exshaw [2,3,5]	3	19	Silty, argillaceous dolomite	1,754	2,419	179	3	48	1	313	23	12.4	0.07
Wabamun [1,3,5]	2	24	Micritic limestone,	2,238	2,374	124	3	38	1	205	15	12.6	0.10

Ireton [1,2,5]	4	39	Calcareous shale	1,594	3,995	78	5	29	1	181	20	8.1	0.10
Leduc [1,3,5]	2	20	Vuggy dolostone	1,618	1,851	103	6	48	1	214	17	11.4	0.11
Duvernay Innisfail [1,2,3,5]	2	22	Calcareous, silty mudstone	1,819	2,017	100	8	33	1	175	22	7.0	0.07
Duvernay Kaybob [2,3,5]	22	599	Calcareous silty mudstone	2,274	4,070	71	8	40	1	164	14	10.9	0.15
Duvernay W. Green [2,3,5]	15	122	Calcareous mudstone	2,796	3,524	44	5	41	1	138	10	12.8	0.29
Majeau Lake [1,2,5]	1	22	Calcareous shale	3,233	3,439	76	7	36	1	187	40	3.7	0.05
Muskwa [1,2,5]	5	32	Calcareous, silty shale	1,459	2,190	73	8	43	1	78	10	6.9	0.10
Waterways [2,5]	3	13	Calcareous shale	498	767	69	4	49	1	80	5	15.0	0.22
Slave Point [3,5]	7	60	Micritic limestone,	324	1,366	81	6	43	1	181	5	35.3	0.43
Fort Vermillion [2,5]	3	31	Anhydrite, interbedded calcareous shale	402	778	112	3	47	1	186	10	17.6	0.16
Watt Mt. [3,5]	11	165	Anhydrite, interbedded siltstone, dolomite	343	2,198	79	0	42	1	124	9	13.2	0.17
Muskeg [2,5]	3	17	Dolomite, interbedded shales	739	1,523	78	4	44	1	85	5	15.9	0.20
Keg River [3,5]	6	49	Dolomite, interbedded anhydrite	1,014	1,778	104	3	50	1	175	20	7.8	0.07
Contact Rapids [2,5]	5	54	Calcareous mudstone	1,012	1,814	76	7	51	1	123	15	7.2	0.09
Cold Lake Limestone [2,5]	2	16	Clastic limestone	1,383	1,796	156	3	41	1	322	15	20.5	0.13
Cold Lake Shale [2,5]	3	36	Argillaceous dolostone	956	1,830	85	4	40	1	132	16	7.1	0.08
Ernestina Lake Anhydrite [2,5]	10	138	Calcareous, silty anhydrite	1,068	1,132	136	0	32	1	194	10	18.4	0.14
Ernestina Lake Limestone [2,5]	10	88	Calcareous, argillaceous limestone	963	1,837	78	0	42	1	111	10	10.1	0.13
Basal Red Beds [3,5]	1	16	Calcareous siltstone, anhydrite stringers	1,494	1,609	92	6	42	1	86	5	16.2	0.18
Basal Sandstone Unit [3,5]	5	51	Fine grained, calcareous sandstone	2,050	2,732	45	14	42	1	123	11	10.5	0.23

* Only formations for which multi-stress triaxial testing data were available are listed. [1] Poor confining stress resolution. [2] Confining formation. [3] Injection formation. [4] Mesozoic-era formation. [5] Paleozoic-era formation. "TVD from" and "TVD to" indicate sampling location depth intervals. TVD: total vertical depth from ground surface. n: porosity

The empirical Mogi-equivalent ductility parameter (d) for formations in the Alberta Basin (Table 7) indicates that most of the 51 formations evaluated are relatively ductile, which (in combination with extensive basin-wide pressure depletion [1]) may help to explain the relative success of sustained historical high-volume fluid injection in this basin to date [184]. Approximately 72% of the empirical ductility values in Table 7 are significantly higher than the typical ranges reported for similar types of rocks in the existing literature (e.g., Walton, 2021). Walton (2021) noted that silicate rocks tend to have d values in the range of 0.9 – 4.1, while the

d values of carbonate-based rocks range from 3.5 to 10.7 (in the case of marble). The higher d values of rocks in the Alberta Basin are likely a function of the high carbonate content, porosity and heterogeneity of its lithological sequences compared to those reported in the literature. For instance, the limestone/dolomite content of the Alberta Basin sandstone core samples presented in Table 7 ranged from 5% to more than 30%, whereas the Berea sandstone samples referenced in the published literature [21] only contained up to 2% dolomite [185] (i.e., far less than that of the Alberta Basin sandstones). Additionally, carbonate presence was pervasive in all core sample results examined, with limestone/dolomite content ranging from 5% to above 80%. Secondary porosity is also likely a significant contributing factor to the higher d values in the Alberta Basin since the degree of faulting and fracturing is directly correlated to the ductility of (dolomitic) rocks under conditions of high confining pressure [186]. The injection formations listed above are all depleted hydrocarbon reservoirs, which have elevated secondary porosity and pervasive dolomitic mineral content (in the core samples tested, as shown in Table 7). Geological heterogeneity in the Alberta Basin is also high, with most of the core samples contained in Table 7 consisting of layered, interbedded lithological sequences and mixed clastic rock types, which is unique compared to the (relatively homogeneous) samples tested, and results reported in the existing literature in this field.

Analysis of the d* values in Table 7 shows that the Upper Clearwater, Lea Park and shallow Wilrich shales appear to be the most ductile, whereas the lower Clearwater and the Joli Fou appear to be the most brittle of the confining sequences in the Mesozoic era. Examination of the d* values for Mesozoic-era formations also suggests that the Nordegg, Belloy, Deep Wilrich and Falher appear to be the most brittle injection formations in this era, while the most ductile injection formations of this era appear to be the Wabiskaw/McMurray, Doig, Cardium and Nikanassin. Examination of the d* values of formations in the Paleozoic era indicates that the Majeau Lake, Exshaw, Duvernay Innisfail and Keg River appear to be the most brittle injection formations, whereas the Slave Point, Duvernay Willesden Green, Basal Sandstone Unit, and Basal Red Beds appear to be the most ductile formations of this era.

An analysis of the current χ and I_{BD} (using the current site-specific in-situ stress conditions relative to the respective Mogi-equivalent line) is required to assess the probability that such formations within the area of interest of a fluid-injection project could be brittle/ductile

under the current in-situ stress conditions. Such an analysis would involve collecting current in-situ stress and pore pressure data from lithological sequences at sites of interest and then calculating the χ and the I_{BD} to assess the site-specific brittle-ductile state of the stratigraphic sequences at each site. The historical stress and pore pressure data available for formations in the Alberta Basin is used in the section below to calculate the last-known brittle-ductile state of each formation to demonstrate the utility of the conceptual framework developed in this study.

3.3.3 Determination of the Brittle-Ductile State Parameter and Brittle-Ductile Stress Index for Major Injection Formation and Confining Sequences in the Alberta Basin

Table 8 shows the calculated historical χ and I_{BD} for major injection and confining formations in the Alberta Basin. Since the χ and I_{BD} provided below are based on the formation stress-state at the time of the in-situ stress and pore pressure data collection (using the LCS-HDS scenario), the formation regime provided in Table 8 is only applicable for the geographic location and period in which the minifrac data were collected. Regional changes in the net fluid balance have been occurring in specific formations and regions in this basin over the last decade, and such activity can alter formation stresses. Therefore, current site-specific in-situ stress data are required to assess the current brittle-ductile state of stratigraphic sequences, and site-specific multi-stress triaxial core analyses are required to account for site-specific geological heterogeneities that may exist within the project area of interest. Additionally, this list does not include formations for which insufficient in-situ stress and pore pressure data were available at the time of this analysis.

Table 8. Assessment of the χ (Brittle-Ductile State) and I_{BD} (Brittle-Ductile Stress Index) of major formations in the Alberta Basin (at the time of in-situ stress and pore pressure data measurements under the LCS-HDS scenario).

Formation [1]	TVD (m)	d	Max In-Situ σ_1 (MPa)	Min In-Situ σ_3 (MPa) [4]	Year Minifrac Data Collected	Max In-Situ DS (MPa)	DS on Mogi Line (MPa)	CS on Mogi Line (MPa)	χ (MPa)	I_{BD}	Formation Regime [3]
Lea Park	325	1.1	15.6	6.8	2011	9	7	7	1	0.9	Brittle
Cardium	2742	8.5	147.4	34.3	2012	113	291	16	−178	2.2	Ductile
Second White Specks	3300	5.0	123.3	54.5	2011	69	272	21	−203	2.7	Ductile
Fish Scales	1644	4.5	82.3	26.9	2011	55	121	15	−66	1.8	Ductile
Dunvegan	1974	17.0	85.6	27.9	2016 [2]	58	474	5	−416	5.9	Ductile
Viking	2875	4.8	153.5	39.1	2019	114	188	26	−73	1.5	Ductile
Joli Fou	750	2.5	29.7	13.5	2019	16	34	8	−18	1.6	Ductile
Falher G, H	2147	6.4	65.5	30.9	2016 [2]	35	198	9	−163	3.5	Ductile
Upper Clearwater	304	1.3	15.4	4.6	2019	11	6	7	5	0.7	Brittle
Spirit River	2892	7.7	110.0	34.4	2019	76	265	13	−189	2.7	Ductile
Lower Mannville	2510	9.5	124.1	29.9	2019	94	284	12	−189	2.5	Ductile

Ostracod, Ellerslie	3005	9.6	131.5	46.3	2016 [2]	85	444	12	−359	3.7	Ductile
Shallow Wilrich Shale	575	3.3	33.8	8.3	2019	25	27	8	−2	1.1	Ductile
Deep Basin Wilrich	2695	6.0	168.7	38.8	2016 [2]	130	231	24	−101	1.6	Ductile
Wabiskaw	194	1.6	17.7	2.3	2019	15	4	7	12	0.3	Brittle
McMurray	291	1.6	16.0	3.4	2019	13	6	6	7	0.6	Brittle
Nikanassin	3211	15.6	143.9	43.8	2016 [2]	100	682	9	−582	5.0	Ductile
Fernie	2429	3.8	84.9	38.9	2016 [2]	46	148	18	−102	2.2	Ductile
Nordegg	3093	5.2	125.3	47.3	2016 [2]	78	246	20	−168	2.3	Ductile
Charlie Lake	1487	10.4	111.3	29.0	2005 [2]	82	301	10	−219	3.0	Ductile
Doig	2358	11.2	382.4	37.5	2004 [2]	345	421	31	−76	1.2	Ductile
Montney	2987	13.5	113.7	41.2	2018	73	556	8	−484	5.3	Ductile
Belloy	1940	6.5	194.2	30.5	2004 [2]	164	198	26	−34	1.2	Ductile
Mount Head	2393	10.3	189.7	43.3	2004 [2]	146	445	17	−298	2.6	Ductile
Banff	1550	9.9	74.7	29.5	2016 [2]	45	291	7	−245	4.3	Ductile
Exshaw Limestone/Shale	3066	12.4	230.1	58.3	2004 [2]	172	720	17	−548	3.4	Ductile
Wabamun	3822	12.6	178.8	52.0	2005 [2]	127	655	13	−528	4.0	Ductile
Ireton	2542	8.1	81.6	39.7	2016 [2]	42	321	9	−279	4.4	Ductile
Leduc	2677	11.4	161.3	37.0	2000	124	420	13	−296	2.8	Ductile
Duvernay Innisfail	1964	7.0	85.6	27.9	2019	58	194	11	−136	2.6	Ductile
Duvernay Kaybob	3442	10.9	142.5	50.5	2019	92	549	12	−457	4.2	Ductile
Duvernay Willesden Green	3800	12.8	103.1	64.6	2019	38	827	7	−788	8.6	Ductile
Majeau Lake	3916	3.7	104.0	57.4	2002	47	211	22	−164	2.6	Ductile
Muskwa	1565	6.9	97.8	20.8	2016 [2]	77	144	12	−67	1.7	Ductile
Waterways	2197	15.0	161.1	38.0	2016 [2]	123	570	10	−447	3.8	Ductile
Slave Point	1500	35.3	59.5	18.3	2014 [2]	41	646	2	−604	11.2	Ductile
Watt Mountain	2198	13.2	139.3	33.5	1982	106	441	10	−335	3.4	Ductile
Muskeg	1905	15.9	128.8	29.0	2013	100	462	8	−362	3.8	Ductile
Keg River/Winnepegosis	1531	7.8	56.4	24.6	2016 [2]	32	192	6	−161	3.8	Ductile
Basal Red Beds	1194	16.2	82.4	18.7	2009	64	304	5	−240	3.9	Ductile
Basal Sandstone Unit	2669	10.5	188.2	45.2	2009	143	475	16	−332	2.8	Ductile

[1] Only formations with available in-situ stress data are listed. [2] Indicates year stress data was published; actual date of stress data collection was sometime between late 1970 and 2015. [3] At time/location of the in-situ stress data collection. [4] Lowest measured confining stress for formation.

Table 8 indicates that only 4 (Lea Park, Upper Clearwater, Wabiskaw and McMurray) of the 41 major injection and confining formations assessed in the Alberta Basin appeared to be in the brittle regime, while all others were in a ductile regime (under an LCS-HDS scenario) at the time of in-situ stress data collection. This is somewhat expected, since brittleness has been previously reported in the Clearwater shales [187] and shaly sections of the Wabiskaw Formation [188], whereas brittle behavior is typical of the locked sands of the McMurray Formation [189], [190]. However, this analysis also suggests that some major injection/confining formations, such as the Belloy, Doig, Muskwa, Majeau Lake, Duvernay Innisfail, Shallow and Deep Wilrich, Joli Fou and Fish Scales, could be close to a brittle state (at the time of the in-situ stress and pore pressure measurements). Additionally, this analysis indicates that the Duvernay

Willesden Green could be considerably more ductile than the Duvernay Kaybob and Innisfail, which offers additional insights into the relative seismic quiescence [191] of the former and the seismogenicity [62] of the latter formation sequences when subjected to high-volume fluid injection.

A comparative (graphical) assessment of the information contained in Table 8 (shown in Figure 21) can be a useful tool for regional screening of the relative potential for seismogenicity in a stratigraphic sequence of interest. For instance, this assessment using vintage data indicates that high-volume fluid injection in the Slave Point formation may be less likely to trigger seismogenic fault slip than similar activities in the Belloy formation (at the time of the in-situ stress and pore pressure data collection). While current in-situ stress and pore pressure data would be required for assessment of the current brittle-ductile state of formations in a stratigraphic sequence of interest, such data are routinely collected during the project site screening/selection stage for most large-scale fluid-injection projects.

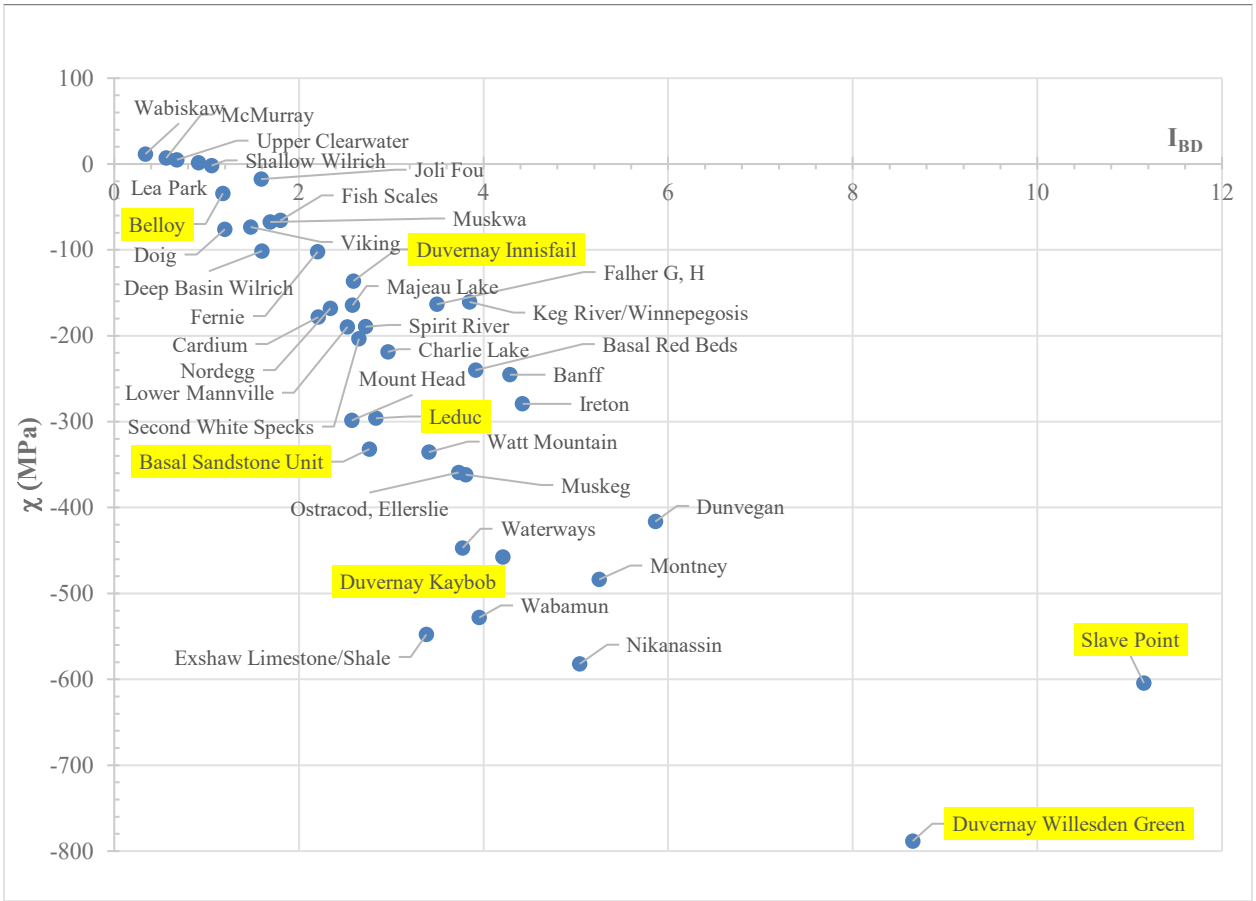

Figure 21. Comparative analysis of the χ and I_{BD} of major formations in the Alberta Basin (at the time of in-situ stress and pore pressure data measurements and under the LCS-HDS scenario).

Table 8 also shows that the vintage of the in-situ stress measurements used in this assessment varies significantly, ranging from data collected in the late 1970s up to 2019. Most of the earlier data were collected for basin-wide stress and acid gas storage studies, whereas most of the recent in-situ stress and pore pressure data available was obtained from low permeability formations (collected for hydraulic fracturing design or thermal caprock characterization purposes). Over this period, extensive fluid extraction and injection activities occurred in this basin, with large-scale fluid extraction resulting in regional formation depletion in most areas and, in some areas, large-scale injection resulting in local formation pore pressure increase [1]. Large-scale fluid injection can lead to formation pore pressure and temperature changes, cause formation deformation, and substantially alter total formation stresses in every direction [192].

Therefore, an assessment of the current brittle-ductile state of a formation using our method described above requires an assessment of the current in-situ stress state of the

formations of interest. Consequently, while the assessments in Table 8 provide the brittle-ductile state of the formations at the time of (in-situ stress) data collection, continuous and evolving injection and production activity occurring within this basin are likely to have altered the stress state in these formations. However, current site-specific (in-situ stress, pore pressure, geological and geomechanical) data collection is typically required to support the project design, risk assessment and regulatory application process for fluid-injection projects. The use of this method, in conjunction with such site-specific and recent data, can provide an assessment of the current brittle-ductile state of the formations of interest and the potential for seismic/aseismic slip in hosted faults.

3.4 Discussion

Aseismic creep has been postulated to be the main process driving natural earthquake swarms in shallow strike-slip faults globally, with interconnected vertically stacked creep and dynamic rupture (brittle failure) processes responsible for seismogenicity in some major faults such as the San Andreas [193]. Most of the world's seismicity in sedimentary cover occurs in carbonate sequences, driven by fault creep and rupture, which transitions from slow, stable (ductile) slip to rapid unstable (stick; brittle) slip at confining stresses above in-situ conditions typically present at depths of 3-5 km (i.e., temperatures above 65 $^{\circ}$C and confining stresses above 60 MPa) [194]. This range of in-situ conditions is analogous to those that exist in deep carbonate-rich injection/confining formations of interest in the Alberta Basin (Table 8), in which this proposed method is anticipated to be applicable.

Shallow strike-slip faults are prevalent in the Alberta Basin, and swarm-type seismicity is characteristic of some of the major Alberta events triggered by fluid injection [195]. Aseismic creep in ductile formations triggering brittle faults within carbonate sequences has been postulated to be the main driver of fluid-injection-induced seismicity in this and other basins [164]. Current models for assessing and managing induced seismic risk may be inadequate in such cases since large events have been observed to occur outside the pressure influence zone and on faults considered not optimally oriented for slip (as in the case of the January 12, 2016, M_w 4.1 Fox Creek earthquake [141]). The faults on which seismicity occurred in the Fox Creek case extended across most of the stratigraphic sequences, whereas the larger seismogenic events all occurred in the overlying (carbonate) Leduc Formation, while fault slip within the Kaybob

Duvernay (shale injection) Formation was largely aseismic [196]. Aseismic slip has also been noted as a viable mechanism to explain the occurrence of recent far-field fluid-injection-induced seismic events in both Alberta and British Columbia, with aseismic slip occurring within the Montney and concurrent seismogenic slip in the underlying (carbonate) Belloy/Debolt formations [197], [198].

This analysis shows that (for an LCS-HDS stress scenario) the overlying Leduc (carbonate) Formation is less ductile (χ = −296 MPa, I_{BD} = 2.8) than the underlying Kaybob Duvernay (shale) Formation (χ = −457 MPa, I_{BD} = 4.2), and consequently more likely to host seismogenic fault slip (Table 8) within this stratigraphic sequence. In the case of seismic events triggered by hydraulic fracturing in Alberta and British Columbia, virtually all large induced seismic events triggered by injection into the (deep) Montney Formation (χ = −484 MPa, I_{BD} = 5.3) were located in the underlying Belloy (χ = −34 MPa, I_{BD} = 1.2) and Debolt (no data available) formations. Meanwhile, virtually all large induced seismic events triggered by stimulation activity in the Kaybob Duvernay (χ = −457 MPa, I_{BD} = 4.2) were located in the overlying Leduc Formation (χ = −296 MPa, I_{BD} = 2.8) [72]. Conversely, large-scale fluid injection occurring in the shallow Montney (i.e., outside of the zone of influence of the Belloy/Debolt) was observed to trigger (aseismic) slip equivalent to a Magnitude 5.0 earthquake, which resulted in measurable surface displacement but no detectable seismicity [198]. This analysis indicates that such a response could be expected since both the Montney and Kaybob Duvernay are more ductile than the Belloy and Wabamun (under an LCS-HDS scenario; no data were available for the Debolt Formation; Table 8). Table 9 shows that the major fluid-injection-induced seismic events that have occurred to date in Alberta and British Columbia have occurred in the least ductile (underlying/overlying) formation(s) in the stratigraphic sequence adjacent to the fluid injection zone.

Table 9. Summary of recent significant induced earthquake sequences in Alberta and British Columbia.

Location (Year)	Largest Magnitude	Trigger Activity [1]	Injection Zone	Injection Zone d*	Earthquake Zone	Earthquake Zone d*
Musreau Lake (2018–2020)	3.9	WD [199]	Ireton	0.10	Nisku Precambrian	ND ND [2]
Peace River (2018–2020)	3.2	WD [142]	Leduc	0.11	Leduc Precambrian	0.11 ND [2]
Red Deer (2019)	4.2	HF [142]	Duvernay Willesden Green	0.29	Leduc	0.11

Fox Creek (2016)	4.8	HF [142]	Kaybob Duvernay	0.15	Leduc	0.11
Fox Creek (2016)	4.1	HF [164]	Kaybob Duvernay	0.15	Wabamun Winterburn	0.10 ND
Cardston (2011–2012)	3.0	HF [200]	Exshaw	0.07	Wabamun Precambrian	0.10 ND [2]
Cordel Field (1994–2008)	4.0	WD [110]	Turner Valley	ND	Turner Valley Precambrian	ND ND [2]
Montney (2018) [3]	4.45	HF [198], [201]	Montney	0.09	Belloy Debolt	0.04 ND
Montney (2015) [3]	4.55	HF [198]	Montney	0.09	Belloy	0.04
Montney (2015) [3]	3.55	HF [198]	Montney	0.09	Belloy	0.04
Montney (2014) [3]	3.9	HF [145]	Montney	0.09	Belloy	0.04
Montney (2013) [3]	4.21	HF [198]	Montney	0.09	Belloy	0.04

[1] HF: Hydraulic fracturing. WD: Wastewater disposal. [2] The igneous Precambrian basement is likely the most brittle formation in the stratigraphic sequence in the Alberta Basin. [3] Events located in British Columbia. ND: No data available.

Therefore, aseismic slip increasing the stress in and triggering brittle failure in faults hosted in more brittle formations adjacent to the injection zone may be a likely contributing mechanism in the cases outlined above. This analysis provides a method to identify the relative brittleness of injection and confining formations and to assess the potential for brittle failure to occur by computing and comparing the χ and I_{BD} in each formation in the stratigraphic sequence of interest. While this method requires current site-specific in-situ stress and pore pressure data for each major stratigraphic sequence in the zone of influence of injection projects, such measurements are routinely collected as a part of injection project design regulatory requirements in Alberta. Table 10 shows the four major formations closest and furthest from the brittle state at the time of the in-situ stress and pore pressure measurements, which may help guide data collection and hazard assessments for fluid-injection projects proposed in these formations.

Table 10. Alberta Basin injection and confining formations closest and furthest from the brittle state in-situ (based on available historical in-situ stress state and pore pressure measurements).

Geologic Era	Injection Formations Closest to Brittle State [1]	Injection Formations Furthest from Brittle State [1]	Confining Formations Closest to Brittle State [1]	Confining Formations Furthest from Brittle State [1]
Mesozoic	Wabiskaw-McMurray, Belloy, Viking, Doig	Nikanassin, Dunvegan, Ostracod-Ellerslie, Mannville	Clearwater, Lea Park, Wilrich, Joli Fou	Montney, Charlie Lake, Second White Specks, Fernie
Paleozoic	Muskwa, Keg River, Majeau Lake, Basal Red Beds	Slave Point, Wabamun, Muskeg, Watt Mountain	Banff, Exshaw, Ireton, Duvernay Innisfail	Waterways, Duvernay Willesden Green

[1] Some formations can be both injection and confining since high-volume fluid injection occurs in some confining (shale) formations for the purposes of tight hydrocarbon exploitation.

In the absence of current in-situ stress and pore pressure data, the relative brittleness (d*) of the formation sequences in the fluid-injection project area of interest could provide a screening-level indicator of the formations that are likely to be the most brittle in a stratigraphic sequence of interest. Table 11 provides the four most brittle and the four most ductile of the 51 (injection and confining) formations assessed in the Alberta Basin (based on d*; i.e., rock strength and material properties).

Table 11. Four most brittle and most ductile major injection and confining formations in the Alberta Basin, based on rock mechanical properties.

Geologic Era	Most Brittle Injection Formations [1]	Most Ductile Injection Formations [1]	Most Brittle Confining Formations [1]	Most Ductile Confining Formations [1]
Mesozoic	Nordegg, Belloy, Deep Wilrich, Falher G, H	Wabiskaw/McMurray, Doig, Cardium, Nikanassin	Deep Wilrich, Fernie, Second White Specks, Montney	Lea Park, Shallow Wilrich, Upper Clearwater, Fish Scales
Paleozoic	Majeau Lake, Exshaw, Duvernay Innisfail, Keg River	Slave Point, Duvernay Willesden Green, Basal Sandstone Unit, Basal Red Beds	Duvernay Innisfail, Banff, Cold Lake Shale, Contact Rapids	Duvernay Willesden Green, Waterways, Muskeg, Watt Mt.

[1] Some formations can be both injection and confining since high-volume fluid injection occurs in some confining (shale) formations for the purposes of tight hydrocarbon exploitation.

Triaxial core testing is considered a reasonable method of replicating stresses at reservoir conditions [202] but core samples recovered can be biased towards stronger and more competent zones within a stratigraphic sequence. Such more competent units are also more likely to be major stress-bearing members [203], display higher deviator stresses (i.e., high σ_1 and low σ_3), dominate the failure behavior of the rock unit and hosted faults and have been associated with an increased probability of fluid-injection-induced seismicity in the Alberta Basin [57]. However, while these analyses provide a regional-scale perspective of the brittle-ductile state of the stronger (more competent) formations within this basin, site-specific analyses of the stratigraphic sequences present would be required to account for project-scale geological heterogeneities. Additionally, the possibility exists that fault zones within dolomite layers may be even more brittle than the surrounding host rock since embrittlement and localization of brittle deformation of the fault core and the shear zone was previously noted [166], and further research in this area may be warranted.

Assessment of the potential for fluid-injection projects to trigger seismicity has relied on the identification and avoidance of faults within the zone of influence [1]. However, assessment

of the probability of aseismic slip within (more ductile) injection formations loading fault sections and triggering seismogenic slip in far-field, more brittle formations may be an important complement to the hazard assessment process for fluid-injection projects. This complementary assessment may be especially important in the Alberta Basin since the types (strike-slip and reverse) of faults prevalent in this basin can be challenging to detect during the site selection process.

3.5 Conclusions

This research provides an assessment of the relative brittleness/ductility of 51 of the major injection and confining formations in the Alberta Basin, as well as a method to assess the likelihood of a formation being in the brittle or ductile regime, using the current state of in-situ stress and pore pressure.

This analysis indicates that approximately 72% of the formations had ductility significantly higher than typical ranges reported for similar-type rocks in the existing literature. The high ductility of the formations assessed, in conjunction with extensive historical pressure depletion, could be a contributing factor in the success of sustained historical high-volume fluid injection in this basin. However, some of the most brittle formations in the stratigraphic sequences assessed include extensively used injection formations such as the Belloy, Deep Wilrich, Falher, Majeau Lake, Exshaw, Duvernay Innisfail and Keg River, and notable confining formations such as the Lower Clearwater and the Joli Fou shales. Increasing utilization of some of these injection formations (such as the Belloy and Doig) may require closer examination of their current/future brittle-ductile state to mitigate the potential for future seismogenesis.

This analysis shows that the Lea Park, Clearwater, Wabiskaw and McMurray formations were in a brittle state, and the Belloy, Doig, Muskwa, Majeau Lake, Duvernay Innisfail, Shallow and Deep Wilrich, Joli Fou and Fish Scales formations were close to the brittle state at the time the in-situ stress data were collected. Almost all induced seismic events triggered by large-scale fluid injection into the (ductile state) Montney formation in British Columbia occurred in the underlying (close to brittle state) Belloy and Debolt formations.

The data and method presented could be used to assess the potential for (sub)vertical fault sections to be aseismic/seismogenic by evaluating the relative brittleness/ductility and the in-situ

brittle/ductile state of host formations in the stratigraphic sequence of interest. Such information may be valuable during site selection for large-scale fluid-injection projects by providing insight into the far-field seismogenic potential of unknown/undetected fault sections. Increasingly, it is recognized that near-field aseismic fault slip triggering far-field seismic fault slip is an important driving process for injection-induced seismicity both in the Alberta Basin (e.g., [164]) and globally (e.g., [204], [205]).

3.6 Data Availability

In-situ stress measurements are available from: (i) The Alberta Government's OpenData link, located at https://open.alberta.ca/opendata/gda-dig_2016_0040. (ii) Chapter 29 of the Atlas of the Western Canadian Sedimentary Basin, located at https://ags.aer.ca/atlas-the-western-canada-sedimentary-basin/chapter-29-situ-stress. (iii) AER/AGS Report 97 https://static.ags.aer.ca/files/document/REP/REP_97.pdf. (iv) AER/AGS Special Reports 090, 091, 092, 093, 094 & 095, all located at https://ags.aer.ca/products/all-publications. (v) AGS Digital Data 2018-0013, located at https://ags.aer.ca/publication/dig-2018-0013. (vi) Published reports and articles including [183], [206]–[225]. Core-sample triaxial testing lab reports are available on request from the AER's data request catalog, located at https://static.aer.ca/prd/documents/sts/GOS-REPS.xlsb. Fluid-volume injection data is available from the geoSCOUT™ database located at www.geologic.com. All geoSCOUT™ data is © 2022. All hyperlinks were last accessed 4 July 2022.

4.0 Estimating Sustainable Long Term Fluid Disposal Rates in the Alberta Basin[3]

Abstract

Reliable regional-scale permeability data and minimum sustained injectivity rate estimates are key parameters required to mitigate economic risk in the site selection, design, and development of commercial-scale carbon sequestration projects, but are seldom available. Publicly available disposal well data from over 4,000 disposal wells is used to assess and history-match regional permeability estimates and provide the frequency distribution for disposal well injection rates in each of 66 disposal formations in the Alberta Basin. Core data and laboratory analyses from over 3,000 cores are used to construct geological, geomechanical and petrophysical models for 22 of these disposal formations. These models and the history-matched regional permeability estimates are then used to conduct coupled geomechanics and reservoir simulation modeling (using the ResFrac™ numerical simulator) to assess (i) well performance in each formation when injecting carbon dioxide for a 20-year period, (ii) carbon dioxide saturation and reservoir response at the end of the 20-year injection period, and (iii) reliability of the simulated rates compared to an actual commercial sequestration project. This analysis shows that (i) the injection rate from these simulations closely match actual performance of the commercial case, (ii) only 7 of the 22 disposal formations analyzed appear capable of supporting carbon dioxide injectors operating at greater than 200,000 tons per year/well, (iii) three of these formations can support injectors operating at rates comparable to the successful commercial-scale case, and (iv) carbon dioxide presence and a formation pressure increase of at least 25% above pre-injection pressure can be expected at the boundaries of the (12 km x 12 km) model domain at the end of 20 years of injection.

[3] This chapter was published in the Special Issue "State of the Art Geo-Energy Technology in North America" of Energies: Samaroo, M.; Chalaturnyk, R.; Dusseault, M. Estimating Sustainable Long-Term Fluid Disposal Rates in the Alberta Basin. Energies 2022, 16, 2532. https://doi.org/10.3390/en16062532 on March 7, 2023.

4.1 Introduction

Evolution of energy supply policies globally has the potential to fundamentally change subsurface formation pore space utilization in hydrocarbon producing basins across the globe. In the Alberta Basin, large-scale hydrocarbon fluid extraction over the last 60 years has resulted in extensive pressure depletion in most of the higher permeability (i.e., "conventional") oil and gas formations [1]. However, emerging energy policies such as net-zero emissions goals can progressively increase subsurface fluid pressures in such formations, by gradually decreasing (future) fluid extraction rates while increasing (future) fluid injection rates. Additionally, reconciliation of (i) the anticipated volume of fluids to be injected into the subsurface with sustainable subsurface formation capacity, and (ii) injection rates required to support industrial needs with sustainable injection rates supported by the targeted formations is required to support optimal utilization of the existing basin subsurface pore space capacity and minimize risks to project proponents and clients as well as surface (e.g., induced seismicity) and subsurface users [1]. Extensive work has been conducted on developing methods to assess theoretical subsurface capacity for injected fluids such as carbon dioxide at various scales, based mainly on sparse data, probabilistic matrix porosity and permeability estimates (e.g., [116], [226]–[229]). Recent methods have emerged that enable refinement of capacity estimates to account for additional subsurface risk factors, such as subsurface pressure sensitivities (e.g., [1], [230]).

The sustainability of predicted long-term injection rates and the anticipated effect on the injection formations is also a key requirement for the development of long-range plans for future net-zero projects. Reasonable certainty is required that predicted injection rates are realistic, can be sustained for decades and the effects on the receiving formations are negligible or at least predictable. Estimation of such rates is fundamental for engineering and economic purposes, such as determination of number of injectors, pipelines and compression infrastructure requirements, and consequently commercial service rates for future common-use CO_2 sequestration facilities (i.e., hubs). However, so far there has been limited focus on developing methods to estimate sustainable formation-scale long-term injection rates [18], despite the importance of this parameter to the successful long-term operation of high-volume fluid-injection projects. Additionally, greater rigor may be required in evaluating sustainable injection rates, since long-term formation (e.g., thermal) impacts may be more important than short-term

(e.g., pressure) impacts in such projects. For instance, initial results using fully coupled models have suggested that thermal effects can be more important than fluid pressure effects over the long-term in CO_2 injection, and significant errors could be expected when isothermal models are used [18]. Injection of increasingly larger volumes of non-traditional fluids such as CO_2 is anticipated to occur in the Alberta and other sedimentary basins globally as net-zero emissions energy policies are implemented over the next decade.

This study aims to estimate most likely long-term fluid injection rates for key disposal formations in the Alberta Basin under current regulatory constraints (maximum injection pressure up to 90% of the minimum horizontal stress - σ_{hmin}), using actual laboratory (formation core-sample porosity, fluid saturation, uniaxial and triaxial test data), actual field data (formation thickness, pore pressure, minimum and vertical in-situ stress, formation temperature) and a fully coupled compositional three-dimensional integrated hydraulic fracturing and reservoir simulator. A 3D compositional physics-based simulator (ResFrac™) which allows for fully coupled field-scale simulation of the geomechanical effects of sustained fluid injection on a target formation over the entire lifecycle of an injection well is used to simulate long-term CO_2 injection in each formation of interest [231], [232]. While the objective of this work is primarily to help benchmark realistic (sustainable) long-term Alberta Basin formation injection rates, the approach presented can also contribute to the development of a consistent approach (i.e., a standard protocol or workflow) for such assessments. Such a workflow has been identified as an important tool that can help to mitigate both economic and subsurface risks in the underground storage industry [16], [233]. This analysis suggests that, in a geoscience data-rich environment such as the Alberta Basin, the use of such a model and approach can provide reliable indicators of the long-term injection performance of injector wells and formation geomechanical response.

4.2 Materials and Methods

Alberta has one of the most extensive collections of publicly available geoscience and operational data, originating from its long history of hydrocarbon exploitation and open data policies. This includes operational data such as fluid production and injection volumes, formation pressures and well logs, as well as petrophysical, geological, geomechanical, chemical and other types of laboratory analyses conducted on formation cores collected from subsurface projects developed over the last 60 years across the province. Operational data (including

monthly fluid-injection volumes and pump run times for each injection well) are available in the geoSCOUT™ database (available from geoLOGIC Systems https://www.geologic.com/geoscout/ last accessed 09 January 2023). Data from laboratory tests conducted on almost all core samples collected in the Alberta Basin are available on request from the Alberta Energy Regulator (https://static.aer.ca/prd/documents/sts/GOS-REPS.xlsb (last accessed 09 January 2023).

4.2.1 Identification of Key Injection Formations in the Alberta Basin

In Chapter 3, operational data was used to identify the geologic formations that had received the largest proportions of injected fluid in the Alberta Basin over the period January 1962 to December 2021 [234]. This information shows that approximately 87% of the water injected into the Alberta Basin over this period was injected into only 12 geologic formations, comprising the Paleogene sands, the Lower Cretaceous sandstones, the Jurassic sandstones, the Devonian carbonates, and the Devonian sandstones (Table 12). Water volumes injected into these formations include reinjection of produced water into active production reservoirs (e.g., as part of pressure maintenance and enhanced oil operations) as well as water injected into formations without associated hydrocarbon recovery (i.e., water disposal).

Table 12. Key recipient formations for all types of fluid injection in the Alberta Basin over the period January 1962 to December 2021. After Samaroo et al., 2022, and used with permission. Detailed production/injection and net fluid balance data for these formations are contained in Samaroo et al, 2022.

Lithotype and Geologic Formation	Water Injected[1]	Gas Injected[1]	Steam Injected[1]
Paleogene sands (Swan Hills)	17.1%	14.0%	0%
Lower Cretaceous sandstones (McMurray, Clearwater, Cardium, Viking, Nikanassin)	30.6%	9.8%	97.9%
Jurassic sandstones (Sawtooth)	11.5%	15.1%	0%
Triassic carbonates (Charlie Lake, Halfway)	0.4%	1.0%	0%
Triassic siltstones (Montney, Doig)	0.3%	0.6%	0%
Permian sandstones (Belloy)	0.2%	0%	0%
Carboniferous carbonates (Banff, Debolt, Elkton, Livingston, Turner Valley)	0.7%	1.8%	0%
Devonian carbonates (Arcs, Grosmont, Keg River, Leduc, Muskeg, Nisku, Slave Point, Wabamun, Winterburn)	29.2%	43.3%	1.4%
Devonian sandstones (Granite Wash, Gilwood)	4.1%	0.6%	0%
Cambrian sandstones (Basal Sandstone Unit)	0.3%	0%	0.8%
Total volumes injected in above-listed formations	**23.8 km^3**	**596.7 km^3**	**3.41 km^3**
Total fluid volumes injected into all formations in the Alberta Basin	**25.2 km^3**	**692.2 km^3**	**3.41 km^3**

[1] Totals may not add to 100% due to rounding. Fluid volumes are reported in cubic kilometers (i.e., km^3 = cubic kilometer = 10^9 m^3), measured at surface conditions. Steam volume reported in cold-water equivalent volume.

While the 12 key injection formations identified above have historically been the recipients of the highest total injection volumes, significant changes in fluid injection types and

patterns are anticipated to occur over the next decade [1]. These changes are likely to result in a substantial increase in future fluid-injection volumes, distributed over formations that were not previously considered major injection targets and without concurrent associated fluid (hydrocarbon) recovery (i.e., an increase in fluid disposal). Therefore, all formations listed in Table 12 above could be considered future injection targets and consequently formations of interest to this study.

4.2.2 Historical Water Disposal Injection Rates in Formations of Interest

The geoSCOUT^{TM} database also contains the monthly fluid injection, fluid license type and run-time records for all licensed wells in the Alberta Basin for the period 1960 to present. Well license regulatory requirements in Alberta [235] stipulate (among other conditions) that the purpose of the well (e.g., disposal, production, observation, etc.), current status and the fluid type (e.g., water, CO_2, methane, etc.) must be specified, and corresponding monthly volumes reported when operational. All injection wells with a (historical or current) status corresponding to water disposal, the monthly volumes injected (in m^3), injection runtime (in hours), injection well unique well identifier (UWI) and the injection formation were extracted from this database. Injection wells classified in the water disposal category are standalone injectors, and are not associated with hydrocarbon extraction operations, such as waterflooding, pressure maintenance or other enhanced oil recovery activities. Disposal wells are exempt from the pool-associated regulatory obligations for replacement of formation fluids and pressure maintenance in hydrocarbon reservoirs (i.e., voidage replacement ratios [86]) and consequently are considered representative of the type of operations associated with CO_2 sequestration injection.

Injection records with zero monthly volume or zero monthly hours were then removed, and the wells grouped by injection formation to create formation-specific databases consisting of approximately 4,000 injection wells and 1,000,000 data records. The monthly water disposal injection rate for each well in m^3/hour was then calculated by dividing the injection volume in m^3 by the corresponding monthly runtime in hours. Characteristic injection rate statistical parameters required for determining the most likely injection rate (mean, mode, median, variance, standard deviation and max) and the injection rate frequency distribution were then calculated for each formation of interest. These injection rate statistical parameter results are

presented in Section 4.3, and the injection-rate frequency distribution for each formation is provided in Appendix A.

4.2.3 Geological, Geomechanical and Petrophysical Data for Formations of Interest

The database of geological, geomechanical and petrophysical properties for selected cores from the major confining and injection formations in the Alberta Basin created in Chapter 3 was leveraged for this study. This dataset contains geological, geomechanical and petrophysical laboratory tests conducted on approximately 3,000 cores collected from 260 wells, as well as in-situ minimum horizontal and vertical stress, reservoir pore pressure, and temperature data for major injection and confining formations in the Alberta Basin. Sufficient information was contained in this dataset to construct 3D geological, geomechanical and petrophysical models for 26 of the injection formations shown in Table 12. The key parameters used to construct the respective geological, geomechanical and petrophysical ResFrac™ models for each of the 26 injection formations (14 Mesozoic and 12 Paleozoic) are listed in Tables 13 and 14.

Table 13. Stratigraphic zones and minimum-maximum ranges of geological, geomechanical and petrophysical parameters used to construct geomechanical models for Mesozoic Era formations of interest. Upper and lower numbers represent the minimum and maximum ranges of values for each parameter across the core sample depth interval.

Formation	Core Depth Interval (m)	ϕ	S_w (%)	P_o (MPa/km)	ν	σ_h (MPa)	E (MPa)	k (m^2)	ρ (kg/m^3)	σ_t (MPa)	t (^0C)	σ_v (MPa/km)	σ_c (MPa)
Upper Cardium	1,794	0.04	0.35	7.10	0.12	22	13,872	2.60×10^{-16}	2,149	6	54	22.7	55
	1,810	0.11	0.35	7.10	0.31	23	54,174	2.77×10^{-15}	2,149	19	54	22.7	261
Lower Cardium	2,156	0.07	0.14	7.10	0.10	27	18,621	9.87×10^{-18}	2,149		65	22.7	
	2,477	0.12	0.15	7.10	0.30	31	59,966	2.76×10^{-16}	2,149		74	22.7	
Pouce Coupe	1,751	0.03	0.07	11.14	0.19	22	27,540	3.95×10^{-19}	2,542		53	22.7	185
	1,823	0.06	0.13	11.14	0.31	23	55,020	3.95×10^{-19}	2,639		55	22.7	250
Viking	2,176	0.21	0.40	7.70	0.06	30	13,790	5.97×10^{-17}	2,290		65	22.2	144
	2,182	0.23	0.40	7.70	0.19	30	57,290	4.59×10^{-16}	2,570		65	22.2	144
Falher	2,928	0.06	0.40	7.10	0.07	42	3,360	3.95×10^{-18}	2,550	6	108	23.7	21
	3,064	0.12	0.40	7.10	0.41	44	47,150	4.05×10^{-17}	2,550	15	113	23.7	248
Notikewin	2,876	0.08	0.35	7.84	0.21	34	17,950	3.95×10^{-17}	2,550	5	106	23.5	84
	2,892	0.10	0.35	7.84	0.31	34	32,760	5.92×10^{-16}	2,640	9	107	23.5	101
Middle Mannville	2,332	0.09	0.43	7.84	0.19	28	18,459	1.48×10^{-18}			86	22.1	70
	2,455	0.09	0.43	7.84	0.57	29	44,974	1.16×10^{-16}			91	22.1	147
Lower Mannville	2,714	0.07	0.57	7.84	0.19	32	1,170	2.76×10^{-17}	2,554		100	22.1	105
	2,778	0.07	0.57	7.84	0.31	33	45,814	1.16×10^{-16}	2,699		103	22.1	194
Nikanassin	3,362	0.06	0.27	9.50	0.02	46	22,389	4.93×10^{-17}	2,615		134	24.8	
	3,385	0.08	0.78	9.50	0.11	46	63,612	9.87×10^{-16}	2,669		135	24.8	
Upper Charlie Lake	1,478	0.04	0.00	7.49	0.20	29	2,687	2.08×10^{-18}			72	25.2	32
	1,587	0.23	0.00	7.49	0.27	31	32,530	1.35×10^{-13}			78	25.2	60
Lower Charlie Lake	1,980	0.10	0.11	7.49	0.08	39	7,053	4.67×10^{-16}	2,326		97	25.2	37
	2,241	0.25	0.81	7.49	0.36	44	53,967	4.93×10^{-13}	2,617		110	25.2	218
Upper Doig	2,406	0.09	0.47	7.90	0.11	38	36,966	4.93×10^{-14}	2,590		118	21.2	52
	2,451	0.09	0.47	7.90	0.32	39	60,414	4.93×10^{-14}	2,650		120	21.2	111
Lower Doig	2,956	0.07	0.45	7.90	0.11	47	10,246	3.95×10^{-16}	2,523		145	21.2	36
	2,990	0.07	0.45	7.90	0.34	48	37,521	3.40×10^{-14}	2,595		147	21.2	37
Belloy	2,476	0.06	0.79	10.05	0.26	48	22,770	2.55×10^{-18}	2,476	6	128	22.8	108
	2,672	0.13	0.84	10.05	0.33	48	74,976	1.18×10^{-14}	3,093	22	131	22.8	211

Table header key: **ϕ**: Total porosity; **S_w**: Water saturation; **P_o**: Pore pressure gradient; **ν:** Poisson's ratio; **σ_h**: minimum horizontal stress: **E**: Young's modulus; **k**: Permeability; **ρ:** bulk density; **σ_t:** tensile strength; **t**: Reservoir temperature; **σ_v**: Vertical stress gradient; **σ_c:** Unconfined compressive strength.

The data shown in Tables 13 and 14 represent a summary of the minimum and maximum ranges of each of the parameters required to construct a geomechanical model for each formation. Each formation depth interval contains multiple core samples, with higher resolution data corresponding to the stratigraphic variations within each respective core depth interval. This detailed stratigraphic data (i.e., the core testing results from the 3,000 laboratory core tests summarized in Chapter 3) was imported into the ResFrac™ software and used to construct the corresponding 3D stratigraphic, geomechanical and petrophysical models for each formation of interest.

Table 14. Stratigraphic zones and minimum-maximum ranges of geological, geomechanical and petrophysical parameters used to construct geomechanical models for Paleozoic Era formations of interest. Upper and lower numbers represent the minimum and maximum ranges of values for each parameter across the depth interval.

Formation	Depth (m)	ϕ	S_w (%)	P_o (MPa/km)	ν	σ_h (MPa)	E (MPa)	k (m^2)	ρ (kg/m^3)	σ_t (MPa)	t (^{0}C)	σ_v (MPa/km)	σ_c (MPa)
Wabamun	2,238	0.03	0.01	6.39	0.13	30.4	12,828	5.76×10^{-20}	2,584	4	67	23.15	50
	2,380	0.07	0.73	6.39	0.45	32.4	115,172	3.33×10^{-14}	2,931	11	71	23.15	192
Leduc	1,618	0.02	0.15	7.87	0.08	22.4	17,655	9.87×10^{-18}	2,803	3	49	22.75	18
	1,855	0.10	0.58	7.87	0.74	25.6	119,241	4.42×10^{-13}	2,842	9	56	22.75	29
Upper Slave Point	595	0.04	0.44	5.40	0.14	7.3	23,520	6.95×10^{-13}	2,490	3	18	23.71	96
	795	0.15	0.58	5.40	0.28	9.7	75,430	2.06×10^{-12}	2,620	10	24	23.71	169
Lower Slave Point	1,323	0.03	0.44	5.40	0.08	16.1	15,240	5.00×10^{-16}	2,610	5	50	23.71	86
	1,366	0.07	0.58	5.40	0.22	16.7	57,690	2.38×10^{-12}	2,680	16	52	23.71	86
Upper Muskeg	739	0.10	0.76	7.90	0.13	11.3	24,320	7.00×10^{-17}	2,580	5	22	21.05	63
	744	0.25	0.86	7.90	0.24	11.3	47,520	2.17×10^{-13}	2,820	8	22	21.05	63
Lower Muskeg	1,510	0.09	0.75	7.90	0.18	23.0	47,200	7.00×10^{-17}	2,744	5	59	21.05	52
	1,523	0.21	0.88	7.90	0.49	23.2	83,200	2.17×10^{-13}	2,865	9	59	21.05	160
Upper Keg River	1,014	0.09	0.15	9.01	0.19	16.3	2,120	4.18×10^{-13}	2,620	7	43	22.88	70
	1,046	0.38	0.24	9.01	0.27	16.8	53,830	2.22×10^{-12}	2,670	10	44	22.88	140
Middle Keg River	1,510	0.15	0.18	9.01	0.18	24.3	47,200	1.86×10^{-13}	2,620	7	63	22.88	52
	1,522	0.36	0.25	9.01	0.49	24.5	83,200	1.96×10^{-12}	2,667	11	64	22.88	52
Lower Keg River	1,739	0.09	0.15	9.01	0.06	28.0	38,370	1.59×10^{-13}	2,621	7	73	22.88	58
	1,778	0.38	0.25	9.01	0.36	28.6	92,500	2.21×10^{-12}	2,667	11	75	22.88	177
Red Beds	1,494	0.02	1.00	9.79	0.10	23.5	14,280	3.56×10^{-22}	2,546	3	67	23.32	41
	1,625	0.05	1.00	9.79	0.31	25.5	64,800	1.59×10^{-21}	2,598	8	73	23.32	92
Basal Sandstone Unit	2,050	0.05	1.00	9.50	0.11	41.2	9,900	6.91×10^{-16}	2,620	2	82	23.43	36
	2,265	0.19	1.00	9.50	0.36	45.5	29,500	1.48×10^{-14}	2,700	5	91	23.43	98

Key: **ϕ**: Total porosity; **S_w**: Water saturation; **P_o**: Pore pressure gradient; **ν:** Poisson's ratio; **σ_h**: minimum horizontal stress: **E**: Young's modulus; **k**: Permeability; **ρ:** bulk density; **σ_t:** tensile strength; **t**: Reservoir temperature; **σ_v**: Vertical stress gradient; **σ_c:** Unconfined compressive strength.

While extensive geomechanical data was available for the specified depth intervals listed in Tables 13 and 14, in some cases there was insufficient core laboratory test data over the core (run) interval for petrophysical parameters such as permeability, porosity, and water saturation. In such cases a value (generated using a random function generator) constrained between the minimum and maximum values from immediately adjacent (upper and lower) depth intervals

was assigned to the missing variable to complete the petrophysical model for the corresponding stratigraphic zone. The relative locations of disposal and sample core wells across Alberta are shown in Figure 22.

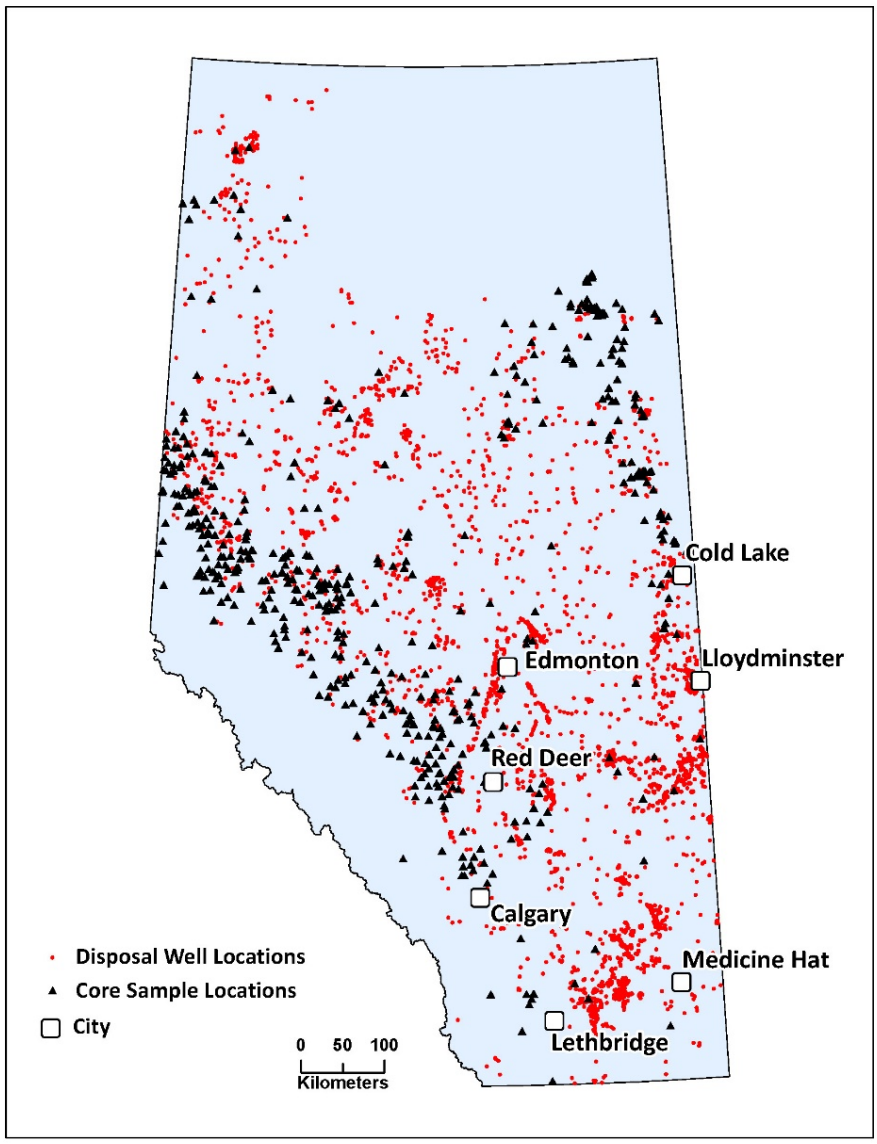

Figure 22. Relative locations of water disposal and core sample wells used in this study. Red dots indicate geographic locations of the approximately 4,000 water disposal wells while black triangles indicate the geographic locations of the approximately 260 core sample wells.

4.2.4 Common Injection Parameters Used in All Simulations.

The injection well configuration used in all ResFrac™ models was based on the actual design of the Radway CO_2 injectors used at the commercial-scale Quest Carbon Capture and Storage (CCS) Project in Alberta, and a representative injector well completion report for these

wells is available in [236]. The CO_2 injector is assumed to be vertical for all formation models, with a perforated zone length of approximately one third of the formation thickness (up to a maximum perforated zone length of 35 m to maintain consistency with the wellbore design of the CO_2 injectors used at the Quest CCS project). Other common injection parameters used in all simulations, along with the corresponding sources/references are provided in Table 15 below.

Table 15. Common injection parameters used in all simulations.

Parameter	Value
Well geometry	Vertical [236]
Maximum horizontal stress σ_{HMAX} azimuth	45.5 °C [237]
Injection well casing internal diameter	0.15037 m [236]
Perforated zone length	1/3 of formation thickness, to a maximum of 35 m [236]
Perforation shot density	17 shots per meter [236]
Perforation hole diameter	0.0106 m [236]
Matrix (x and y) dimensions	12 km x 12 km
No. of matrix elements in x direction	100
No. of matrix elements in y direction	100
Matrix region z dimension	Thickness of cored region of formation
Maximum matrix element size (z)	1 m
Matrix boundary conditions	Closed
Vertical permeability	0.1 x horizontal permeability [238]
Fluid model	Compositional
BHP injection constraint	90% of σ_{hmin} [89]
Injection simulation run time	20 years [239]
CO_2 density	761 kg/m^3 [239]
Brine density	1,193 kg/m^3 [239]
Brine salinity	320,000 ppm [239]
Relative permeability model	Brooks-Corey [240]
Average annual injection fluid temperature	15 °C [241]
Biot coefficient (Mesozoic Formations)	0.7 [242]
Biot coefficient (Paleozoic Formations)	0.6 [243]
Geothermal gradient	Formation specific in-situ measurements
Formation heat capacity	1 kJ/kg-K [244]
Formation thermal conductivity	2.5 W/m-K [244]
Formation coefficient of linear thermal expansion	1 x 10^{-5} 1/°C [244]
Fracture toughness	0 [244]

While limited injection fluid temperature records were available, the annual average injection fluid temperature of 15 °C was selected to represent the average annual temperature observed ([241], [245]) in other CO_2 injection operations in Alberta. The maximum bottomhole injection pressure constraint selected (i.e., 90% of the formation σ_{hmin}) represents the regulatory criteria [89] applicable to disposal wells operating in Alberta. While the constraint of maximum injection pressure equals to 90% of σ_{hmin} used ensures regulatory compliance, it does not account for the potential to trigger slip on critically stressed faults that may exist in the proximity of the

reservoir. In cases where such critically stressed faults are present, an injection pressure threshold lower than 90% of σ_{hmin} may be required to mitigate the likelihood of triggering fault slip within the reservoir and/or adjacent formations [246]. Future enhancements to this workflow could include investigation of this geomechanical risk factor and the potential impacts to estimated injection rates. Closed (i.e., no flow) boundary conditions were used in all simulations to replicate conditions in which there may be multiple independent CO_2 injection projects operating adjacent to each other, with pressure buildup constraints at common boundaries, as well as to evaluate most-likely worst-case pressure-buildup conditions. While it is recognized that the (supercritical) CO_2 storage capacity of a saline formation can be sensitive to its irreducible water saturation and capillary entry pressure [247], the same ResFrac^{TM} simulator relative permeability defaults were used for all simulations as formation specific information was unavailable at the time of this study, since the main interest in this case is injection rate estimation. Additionally, the sensitivity of storage capacity to these factors at formation depths greater than 1.2 km is an area of emerging research (e.g., [248]), and future enhancements to this study could include the impact of these factors on injection rates. The simulation duration of 20 years was selected to mirror the typical design life of a commercial-scale CO_2 injection project operating in the Alberta Basin [239]. A 12 km x 12 km domain was selected to represent the dimensions of a regional-scale injection formation, while enabling completion of all simulations within the maximum number of simulator hours allocated to the University of Alberta (12,000 hours) under the terms of the software academic license.

These common injection parameters and relationships were used to complete the dataset required to construct the corresponding ResFrac™ 3D models for each of the 26 formations of interest, and to conduct the reservoir simulations are described in the sections below.

4.2.5 Reservoir Simulation

ResFrac™ is a three-dimensional physics-based, integrated hydraulic fracturing and reservoir simulation numerical model consisting of a geologic model containing the properties of the formation, a compositional fluid flow model containing the phase behavior and fluid flow characteristics of the formation, a wellbore geometry model containing the wellbore architecture used for injection, and a fluid injection operations model containing the fluid injection operations over the lifecycle of the well [231]. ResFrac™ was designed as a practical engineering tool that

can be used to create a reasonable representation of the physical processes occurring during field-scale fluid injection (and hydraulic fracturing), to understand, predict and optimize fluid injection operations quantitatively and qualitatively [244].

The ResFrac™ model fully couples (implicitly) subsurface injection and (multi-phase) fluid flow processes with injection-induced thermal and mechanical stresses in the matrix in three dimensions (x, y and z) to evaluate well injection and production rates (while considering the effects of fluid-phase composition on fluid flow), as well as the dimensions and location of any subsurface fractures created during injection [232]. The compositional model optimizes computational efficiency by assuming that (i) fluid flow (wellbore to elements and between elements) is governed by a combination of Darcy and non-Darcy (Forchheimer) flow, (ii) the stress state of each element can be approximated by the boundary element method, which assumes small-strain conditions within each element, that each element is elastically homogenous and isotropic and deformation of each element is linear-elastic, (iii) fractures generated are planar at field scale, and can initiate and propagate arbitrarily, and (iv) porothermoelastic stress changes in the model domain do not affect the total volumetric strain [231], [232], [244]. Additionally, all model domains were constructed under the (simplified) assumption that stratigraphic layers corresponding to core samples exhibited vertical transverse isotropy across the entire model domain. Model outputs include quantification of daily injection rates for injection fluids, fluid saturation and formation pressure across the model domain as well as the dimensions of any large-scale planar fractures (i.e., larger than the dimension of the smallest mesh element) generated over the simulation period. A detailed technical description/evaluation of the initial/boundary conditions and the governing/constitutive equations used in the ResFrac^{TM} model to simulate matrix (hydraulic and thermal) fracture initiation and propagation, multiphase fluid flow, thermal transport, stress shadowing, and porothermoelastic responses from temperature/pressure change in the matrix are outside of the scope of this work but can be found in the ResFrac^{TM} Technical Writeup document [244].

Models were constructed with variable mesh spacing, with denser 45 m x 45 m x 1 m (x - y - z) elements close to the injection well and gradually increasing to kilometer-scale (x-y) spacing towards the edges of the model domain. Mesh elements in the z-direction were maintained at 1 m thickness, to account for vertical stratigraphic data resolution and geological

variations. A mesh refinement strategy of increasing resolution in the near-wellbore region is considered an effective method for generating reliable results in large-domain simulation models, while maintaining geomechanical model computational efficiency [17]. Figure 23 shows a diagram of the mesh strategy used to optimize model run times while maintaining near-wellbore simulation reliability.

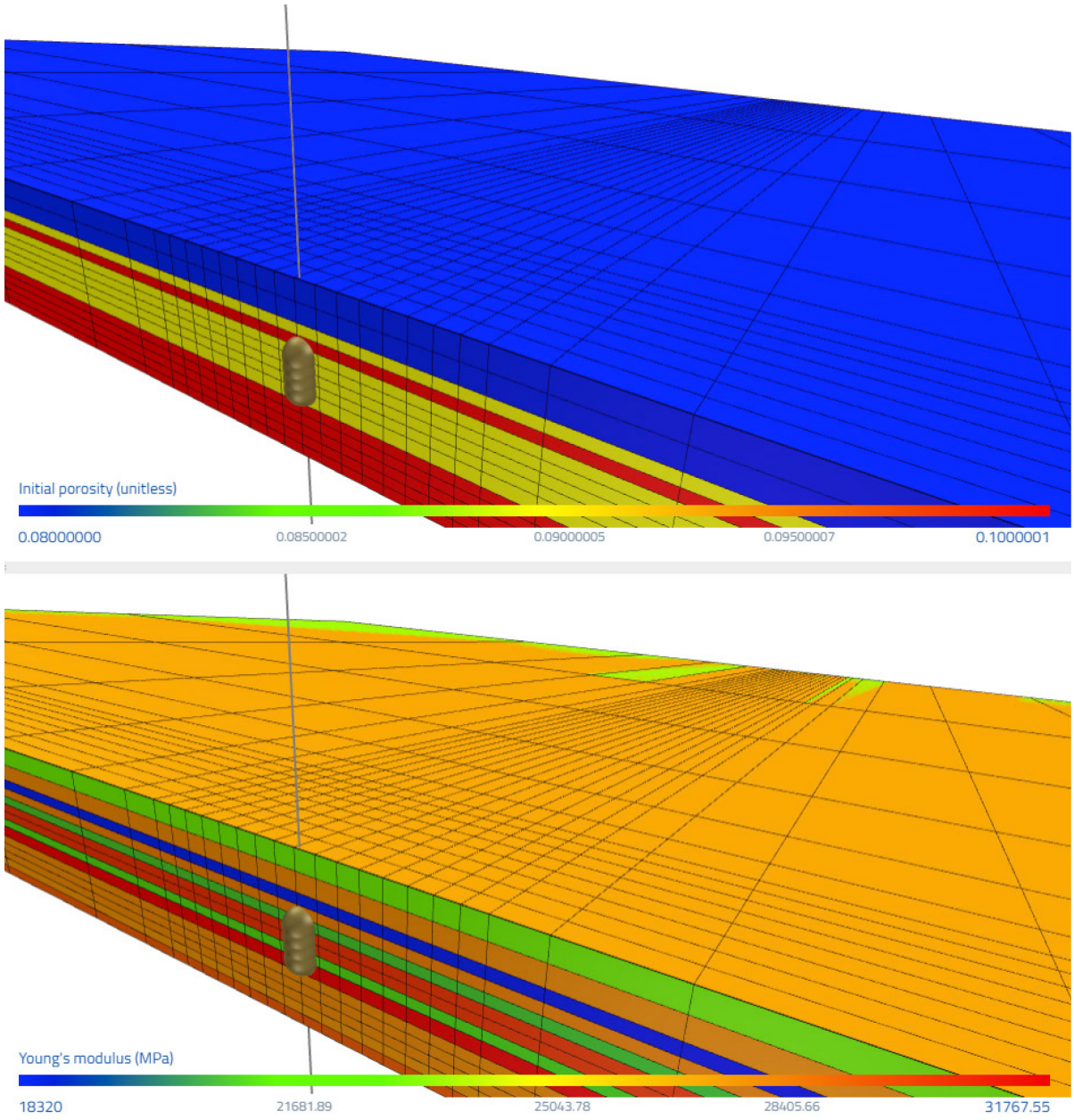

Figure 23. Cross-section of matrix mesh configuration used in the 12 km x 12 km ResFrac™ model domain, showing mesh refinement surrounding the injector wellbore. Wellbore and perforations are indicated by a grey vertical line and cylinder in the center of the model and stratigraphic sequence. Note: not to scale – vertical exaggeration applied for visualization purposes.

Two identical 3D models were constructed for each of the 26 formations listed in Tables 13 and 14, with one model containing brine as an injection fluid and the other CO_2. Formations located at a depth of less than 1 km were removed from this analysis, since Alberta's regulations stipulate that such formations cannot be used for the purposes of CO_2 sequestration [126]. The brine model for each formation was then run for an injection period of 20 years at a maximum bottomhole pressure constraint of 90% of σ_{hmin}. The output from each brine model run was evaluated and the model (i.e., the global permeability adjustment parameter) was adjusted iteratively to match the historically observed injectivity. The settings of the CO_2 injection fluid model were then adjusted to mirror those of the history-matched model. The resulting CO_2 injection model was then run for a 20-year period, and the injection rate, dimensions of any subsurface fractures created, CO_2 saturation, and pressure increase at the domain boundary noted. Model run durations varied between one hour to up to 96 hours, depending on the number of elements (i.e., formation thickness) and formation permeability, with a total of approximately 11,000 hours of simulator time used.

4.2.6 History Matching of Modeled and Historical Injectivity Rates and Model Calibration

Laboratory permeability measurements obtained from core (and/or core plug) samples generally do not account for the impact of sampling bias and geological heterogeneities such as fractures, planes of weakness and other preferential flow paths and consequently require correction (i.e., upscaling) before they can be used at the formation or regional scale [249]–[252]. Core plug derived permeability measurements have been noted to underestimate regional-scale permeability measurements by up to six orders of magnitude in regions in Alberta [125]. Previous work has noted that in one specific case in Alberta (the Viking Formation) the upper range (i.e., the maximum) of the core plug permeability data is likely more representative of the actual field-scale fluid flow conditions [252]. However, limited regional-scale permeability data is currently available, and assessment of this parameter can be challenging, especially in dual-porosity systems and fractured rock formations. History-matching of modeled and actual flow rates in regional well networks is considered a reliable method of assessing the kilometer-scale impact of geological heterogeneities, such as fracture networks [253]. The ResFrac™ model contains a global permeability multiplier variable, which allows for an efficient adjustment of all the permeability values across the entire geologic model domain by a specified scalar constant.

The use of this variable facilitates rapid adjustment of core-scale permeability and iterative (trial and error) model re-runs to obtain a match to field-scale permeability, when required.

Each formation model was initially run with water as the injection fluid and a global permeability multiplier of 1 for an injection period of 20 years, and the stabilized water injection rates obtained compared with the median historical water (injection) disposal rate for the corresponding formation. The global permeability multiplier variable was then adjusted (using trial and error) to increase or decrease the model's stabilized water injection rate to approximate the corresponding median historical injection rate for the corresponding formation. This process was repeated iteratively until the model's 20-year stabilized water injection rate closely matched (+/- 10%) the historical median rate for the corresponding formation, with an average of five model runs required to obtain a history match.

Table 16 shows the global permeability multiplier and the history-matched regional-scale permeability values obtained for each formation. It is assumed that these disposal wells were not creating/propagating subsurface fractures during operation, since regulatory criteria in Alberta stipulate that fluid disposal wells must always operate below the fracture gradient [89]. However, the possibility exists that thermally induced fractures could have occurred in some cases, especially if there were substantial differences between the injected fluid and receiving formation temperatures.

Table 16. History-matched regional-scale permeability for formations of interest.

Formation	Depth Interval (from – to; m)	Average Core-scale Permeability (m^2)	Global Permeability Multiplier Required for History Match	History-Matched Regional-scale Permeability (m^2)
Upper Cardium [1]	1,794 - 1,810	1.23×10^{-15}	100	1.23×10^{-13}
Lower Cardium [1]	2,156 - 2,477	2.50×10^{-16}	10	2.50×10^{-15}
Pouce Coupe (Dunvegan) [1]	1,751 - 1,823	3.95×10^{-19}	100,000	3.95×10^{-14}
Viking [1]	2,176 - 2,220	2.31×10^{-16}	75	$1{,}73 \times 10^{-14}$
Falher [1]	2,928 - 3,064	1.69×10^{-17}	1,000	1.69×10^{-14}
Notikewin [1]	2,876 - 2,892	1.44×10^{-16}	300	4.31×10^{-14}
Middle Mannville [1]	2,332 - 2,455	4.03×10^{-17}	3,000	1.21×10^{-13}
Lower Mannville [1]	2,714 - 2,778	6.52×10^{-17}	10,000	6.52×10^{-13}
Nikanassin [1]	3,362 - 3,385	5.70×10^{-16}	5,000	2.85×10^{-12}
Upper Charlie Lake [1]	1,478 - 1,587	1.18×10^{-14}	0.05	5.89×10^{-16}
Lower Charlie Lake [1]	1,980 - 2,241	1.91×10^{-13}	0.01	1.91×10^{-15}
Upper Doig [1]	2,406 - 2,451	4.93×10^{-14}	1	4.93×10^{-14}
Lower Doig [1]	2,957 - 2,990	1.05×10^{-14}	30	3.15×10^{-13}
Belloy [1]	2,476 - 2,672	4.63×10^{-15}	300	1.39×10^{-12}
Wabamun [2]	2,238 - 2,380	2.26×10^{-15}	100,000	2.26×10^{-10}
Leduc [2]	1,618 - 1,855	2.74×10^{-14}	20	5.48×10^{-13}
Lower Slave Point [2]	1,323 - 1,366	5.71×10^{-13}	0.5	2.86×10^{-13}

Lower Muskeg [2]	1,510 - 1,523	7.02×10^{-14}	1	7.02×10^{-14}
Upper Keg River [2]	1,014 - 1,046	1.26×10^{-12}	1	5.61×10^{-13}
Middle Keg River [2]	1,510 - 1,522	1.34×10^{-12}	0.3	4.81×10^{-13}
Lower Keg River[2]	1,739 - 1,778	1.13×10^{-12}	0.1	1.32×10^{-13}
Basal Sandstone Unit [2]	2,050 - 2,265	3.55×10^{-15}	30	1.11×10^{-13}

[1] Mesozoic formations. [2] Paleozoic formations.

The global permeability multiplier values above were then entered into the corresponding ResFrac™ CO_2 injection model for each formation, thereby adjusting permeabilities in all stratigraphic layers across the entire model domain. This permeability accounts for sample bias and the impact of formation-scale heterogeneities and discontinuities often underrepresented in laboratory core and core plug samples [254] and is considered a reliable method of accounting for the kilometer-scale impact of geological heterogeneities, such as fracture networks [253].

4.2.7 Estimation of Carbon Dioxide Injection Rates and Formation Geomechanical Impacts

Each CO_2 injection model, containing the calibrated (regional scale) permeability values, was then run with the bottomhole injection pressure constraint of 90% of σ_{hmin} for an injection period of 20 years. The ResFrac™ model outputs allow the user to track the mass fraction rate of CO_2 injected over time, as well as the surface area of new fractures generated over the lifetime of the injection sequence. An example of the output of the model is shown in Figure 24.

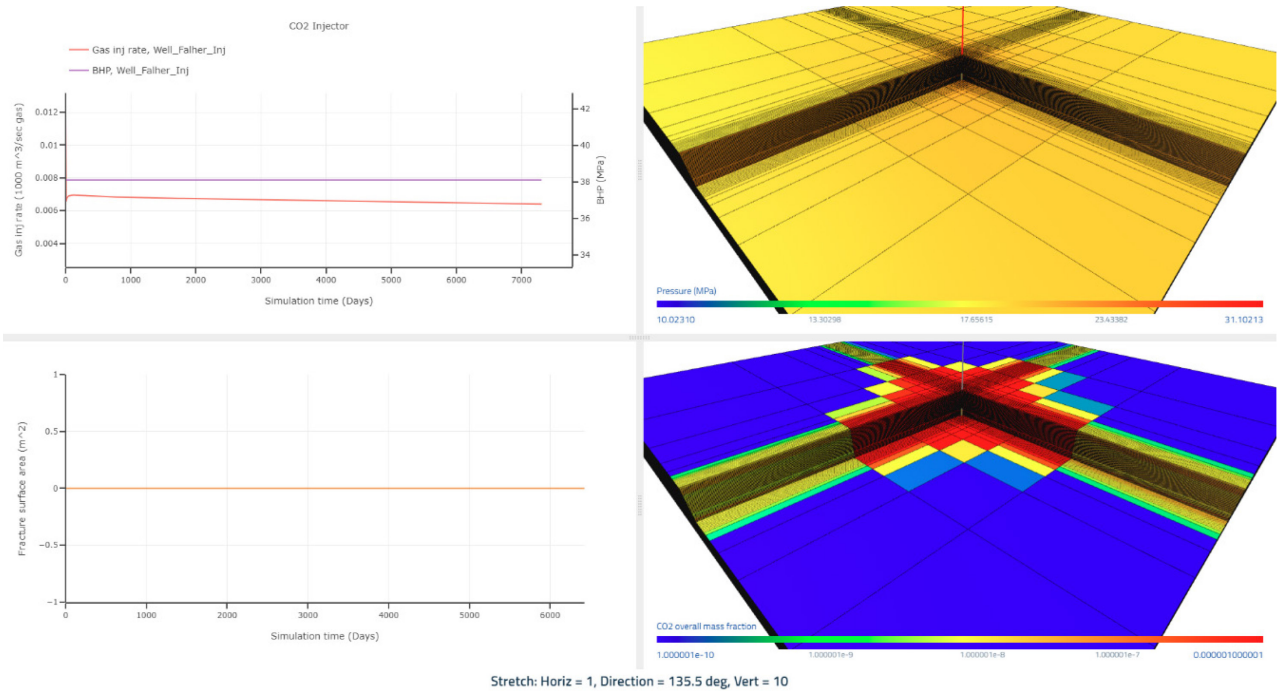

Figure 24. Example of the ResFrac™ model output for a CO_2 injector simulation in the Falher Formation. Upper right-hand frame: Pressure distribution in the model domain. Bottom right-hand frame: CO_2 mass fraction distribution in the model domain.

Upper left-hand frame: CO_2 injection rate and bottomhole pressure. Lower left-hand frame: Fracture surface area created over injection lifecycle.

The injection pressure was increased to 10% above the fracture gradient for a subsample of formations, to verify that the simulator could detect the occurrence of fracturing during injection simulations. These simulations were then run for 20 years and the fracture surface area, gas injection rate and fracture aperture outputs of the simulator examined to ensure that the occurrence of fracturing was reflected in the fracture surface area output parameter of the model. The output of one of these simulations is shown in Figure 25.

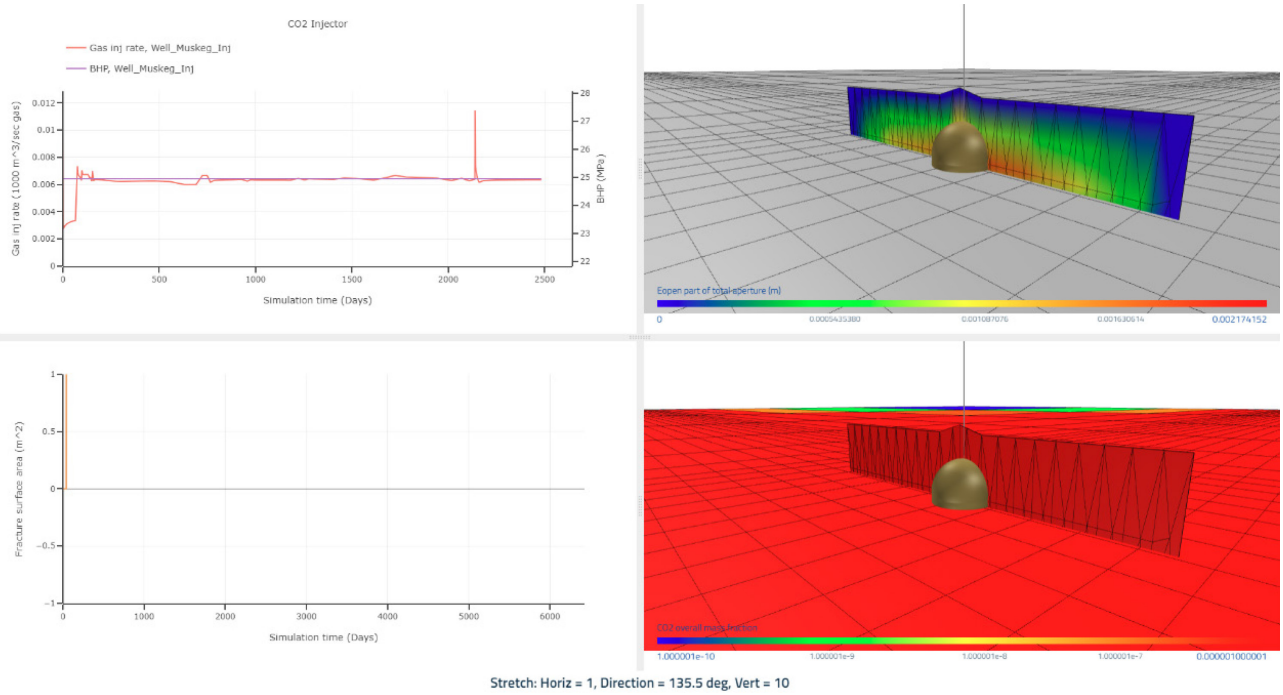

Figure 25. Example of the ResFrac™ model output for a CO_2 injector simulation in the Muskeg Formation conducted under an injection pressure = 1.1 x σ_{hmin}. Upper right-hand frame: Horizontal section across the center of the matrix region and perforations showing fracture element (blue rectangle) and fracture aperture generated. Bottom right-hand frame: Horizontal section across the center of the matrix region and perforations showing CO_2 mass fraction distribution in the fracture element generated and the model domain. Upper left-hand frame: CO_2 injection rate and bottomhole pressure. Note instability (fluctuations) in CO_2 injection rate. Lower left-hand frame: Total fracture surface area created over injection lifecycle. Note fracture surface area generated is non-zero.

These simulations showed that the occurrence of fracturing during the simulation period can be detected by both instability in the model's (CO_2) gas injection rate parameter output and the generation of non-zero values in the fracture surface area parameter output (Figure 25). Therefore, both model output parameters were examined carefully for evidence of the occurrence of fracturing for all simulations conducted. The stabilized (i.e., minimum) CO_2 injection rates

over the 20-year injection simulation period and the fracture surface area for each formation were then tabulated and the results are presented in Section 4.3 below.

4.3 Results

The sections below present the results of the benchmark water injection rate and the CO_2 injection rates analyses obtained from the calibrated models for each of the formations of interest in the Alberta Basin.

4.3.1 Historical Water Injection Rates in Formations of Interest

Table 17 presents the analysis of the historical water injection rates of all licensed disposal wells that have operated in each of 66 disposal formations in the Alberta Basin over the last 60 years (January 1962-December 2022). The injection rate frequency distribution for wells in each formation is included in Appendix A.

Table 17. Historical water injection rates and key statistical parameters for water disposal wells operating in each of the formations of interest in the Alberta Basin during the period January 1962-December 2022.

Geologic Era	Formation	Historical Water Injection Rates (m^3/hr)						No. of Injectors
		Mean	Mode	Median	Variance	Std. Dev.	Max	
Upper Cretaceous [2]	Belly River	2.2	0.6	1.0	10	3.1	60	49
Upper Cretaceous [2]	Cardium	5.9	0.8	1.1	92	9.6	64	28
Upper Cretaceous [2]	Dunvegan [1]	5.3		4.0	72	8.5	70	2
Lower Cretaceous [2]	Viking Sandstone	4.9	3.0	2.6	43	6.6	65	89
Lower Cretaceous [2]	Paddy	11.2	3.0	9.5	117	10.8	206	20
Lower Cretaceous [2]	Cadotte	6.6	13.5	3.3	78	8.9	63	56
Lower Cretaceous [2]	Peace River	8.5	4.2	6.7	65	8.1	35	10
Lower Cretaceous [2]	Colony	3.8	5.3	2.3	16	4.0	48	11
Lower Cretaceous [2]	McLaren Sandstone	19.5	9.9	13.1	276	16.6	71	12
Lower Cretaceous [2]	Notikewin	2.8	0.6	1.9	15	3.9	28	33
Lower Cretaceous [2]	Grand Rapids	7.7	2.7	2.4	387	19.7	287	49
Lower Cretaceous [2]	Clearwater Sandstone	8.2	0.4	3.2	154	12.4	132	44
Lower Cretaceous [2]	Sparky	4.7	0.4	2.5	35	6.0	38	77
Lower Cretaceous [2]	Falher	8.3	14.5	9.0	65	8.0	37	2
Lower Cretaceous [2]	Rex	9.5	20.7	2.6	230	15.2	115	6
Lower Cretaceous [2]	Lloydminster Sandstone	12.4	0.1	9.9	166	12.9	477	123
Lower Cretaceous [2]	Glauconitic Sandstone	26.3	1.0	18.1	789	28.1	1,178	270
Lower Cretaceous [2]	Ostracod	11.3	0.3	5.1	148	12.2	48	5
Lower Cretaceous [2]	Cummings	39.8	0.0	20.1	3,354	57.9	1,718	103
Lower Cretaceous [2]	Dina	36.6	0.0	23.6	2,072	45.5	2,290	358
Lower Cretaceous [2]	Detrital [1]	17.9		19.4	43	6.5	32	3
Lower Cretaceous [2]	Spirit River	5.4	1.3	1.8	29	5.4	21	8
Lower Cretaceous [2]	Bluesky	4.4	1.0	1.6	82	9.1	84	39
Lower Cretaceous [2]	Wabiskaw Sandstone	17.8	0.1	1.8	809	28.5	120	15
Lower Cretaceous [2]	McMurray Sandstone	19.9	0.0	8.9	1,006	31.7	1,102	233

Lower Cretaceous [2]	Cadomin	14.0	11.6	10.2	165	12.9	49	18
Lower Cretaceous [2]	Gething	4.3	0.3	1.0	94	9.7	68	16
Lower Cretaceous [2]	Sunburst	17.7	0.0	14.3	241	15.5	126	122
Lower Cretaceous [2]	Ellerslie	31.4	0.1	17.0	1,460	38.2	282	205
Lower Cretaceous [2]	Taber	11.2	0.8	8.5	111	10.6	73	97
Lower Cretaceous [2]	Nikanassin	9.5	10.8	9.7	24	4.9	25	3
Jurassic [2]	Sawtooth	22.2	0.1	17.8	453	21.3	655	200
Jurassic [2]	Nordegg	7.0	13.7	4.0	51	7.1	45	19
Triassic [2]	Baldonnell	5.0	15.5	2.6	26	5.1	21	5
Triassic [2]	Boundary Lake	0.9	0.0	0.5	5	2.3	18	4
Triassic [2]	Charlie Lake	3.1	1.6	1.7	20	4.5	49	14
Triassic [2]	Halfway	5.7	0.3	2.5	49	7.0	45	7
Triassic [2]	Doig	4.1	5.1	4.8	2	1.5	6	2
Triassic [2]	Montney	5.6	0.0	3.2	69	8.3	90	27
Permian [2]	Belloy	10.8	1.0	8.1	125	11.2	245	100
Mid-Carboniferous [2]	Debolt	9.6	0.4	4.8	181	13.5	115	48
Mid-Carboniferous [2]	Livingstone	12.5	6.2	9.2	143	12.0	69	24
Mid-Carboniferous [2]	Elkton	14.5	1.3	4.6	811	28.5	391	29
Mid-Carboniferous [2]	Turner Valley	3.2	4.0	2.1	19	4.4	50	15
Lower Carboniferous [2]	Shunda	3.3	2.0	1.8	20	4.5	54	7
Lower Carboniferous [2]	Pekisko	5.9	2.0	3.6	43	6.5	102	57
Lower Carboniferous [2]	Banff	9.5	0.8	6.4	101	10.1	67	56
Upper Devonian [3]	Blueridge	16.5	17.6	17.7	121	11.0	56	4
Upper Devonian [3]	Wabamun	13.9	0.7	4.3	866	29.4	321	229
Upper Devonian [3]	Nisku	19.1	0.0	9.4	1,870	43.2	933	265
Upper Devonian [3]	Arcs	10.6	12.2	7.5	253	15.9	367	26
Upper Devonian [3]	Grosmont	6.8	0.5	2.1	151	12.3	280	51
Upper Devonian [3]	Peechee [1]	6.3		7.1	6	2.4	10	2
Upper Devonian [3]	Camrose	3.6	7.0	2.7	13	3.6	42	5
Upper Devonian [3]	Leduc	53.9	0.1	21.3	5,232	72.3	1,353	338
Upper Devonian [3]	Duvernay [1]	7.3		6.8	39	6.2	47	2
Upper Devonian [3]	Cooking Lake	18.1	0.1	15.5	281	16.7	169	19
Upper Devonian [3]	Cairn	10.0	16.5	8.0	56	7.5	47	10
Middle Devonian [3]	Slave Point	16.5	0.0	11.7	513	22.7	636	74
Middle Devonian [3]	Gilwood	12.2	13.3	10.8	96	9.8	109	13
Middle Devonian [3]	Keg River	19.6	0.6	7.0	3,854	62.1	873	135
Middle Devonian [3]	Muskeg	5.9	3.4	4.7	47	6.8	111	7
Middle Devonian [3]	Contact Rapids [1]	5.9		5.3	9	3.0	26	1
Lower Devonian [3]	Lotsberg *	294.7 *		287.7 *	14,129 *	118.9 *	614 *	3*
Lower Devonian [3]	Granite Wash	10.9	0.0	8.8	116	10.8	213	22
Cambrian [3]	Basal Sandstone Unit	49.5	5.4	39.7	1,798	42.4	348	45

* Injection wells in this formation are associated with salt cavern disposal operations and injection rates are representative of operational requirements and not geological constraints. [1] Insufficient number of wells to calculate mode. [2] Mesozoic Era. [3] Paleozoic Era.

While the data presented in Table 17 constitutes a useful reference of the water injection rate activity in each of the listed formations, visualization of key trends in the data is simpler when this information is plotted as a stacked bar chart, as presented in Figure 26.

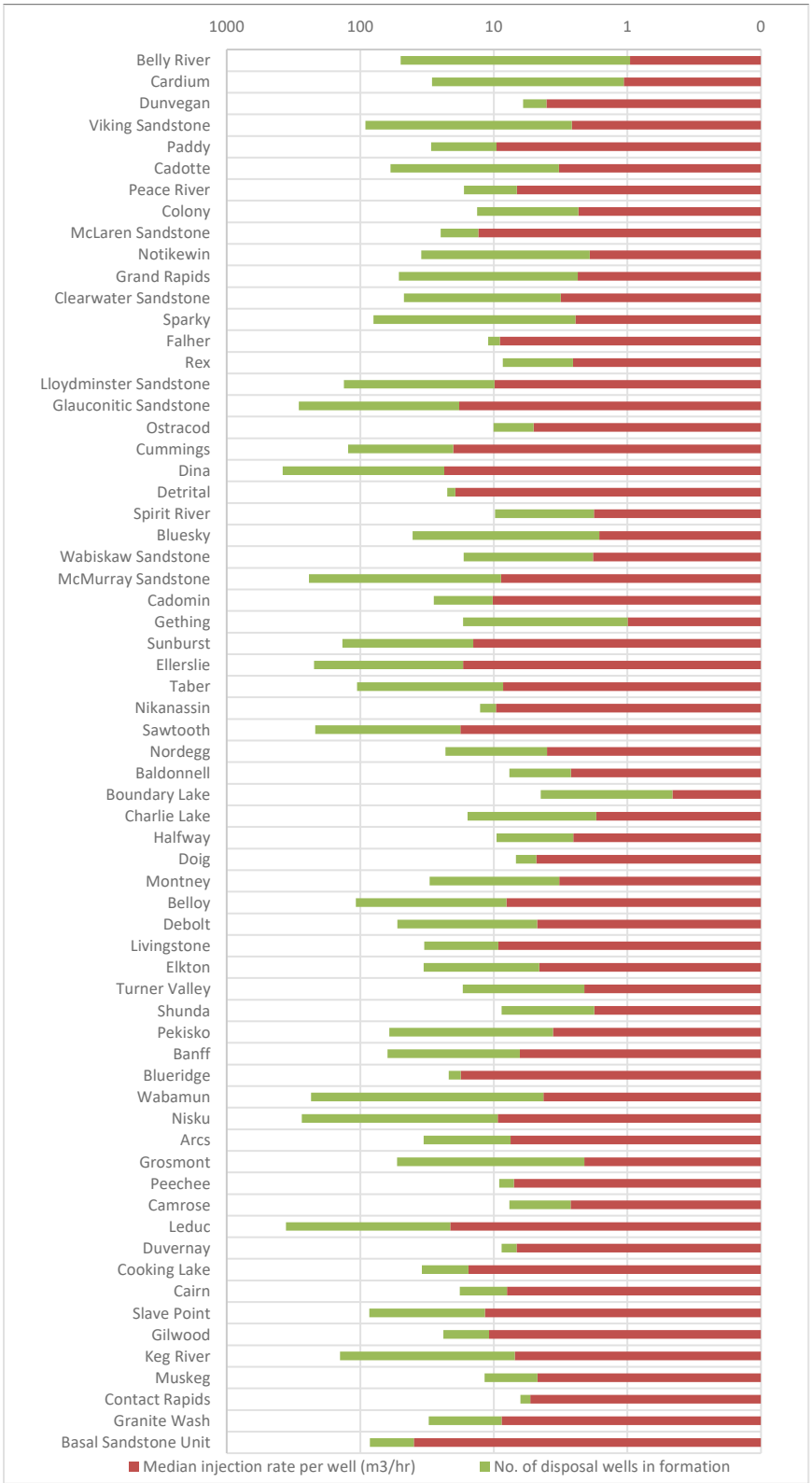

Figure 26. Comparison of median water injection rates and number of disposal wells in formations of interest in the Alberta Basin (for period January 1962-December 2022).

Table 17 shows that several cases of extreme (outlier) maximum injection rate values exist in the database, which can affect the representativeness of the calculated mean. Examination of the injection rate frequency distributions for all formations of interest (Appendix A) shows that these are predominantly positively skewed, with the presence of outlier values. In such cases of skewness, the median is the preferred measure of central tendency since it is a resistant parameter and less likely to be affected by outliers in the dataset. Therefore, the median value was selected as the most likely injection rate and hence a more appropriate benchmark for comparing injection rates across formations in this study, as well as for subsequent calibration of the geological model and to history match the water injection reservoir simulation for each formation of interest.

Figure 26 shows that only 20% (13) of the (66) listed disposal formations recorded median water disposal injection rates exceeding 10 m^3/hour (approximately 1,500 barrels per day (bpd)). Wells located in the Lower Cretaceous (Glauconitic, Cummings, Dina, Detrital, Ellerslie) and (Sawtooth) Jurassic sandstones and three Devonian carbonate (Blueridge, Leduc and Cooking Lake) formations showed higher than average median injection rates (around 20 m^3/hour; 3,000 bpd) and the highest concentrations of water disposal injectors. The highest median water disposal injection rates (around 40 m^3/hour; 6,000 bpd) in the Alberta Basin were recorded by wells located in the Basal Cambrian (Sandstone) Unit. However, geological heterogeneities that can significantly enhance secondary porosity and local-scale permeability common in many of the formations listed above ([249], [251], [255]) are likely contributors to the presence of injection rate outliers noted in Table 17.

4.3.2 Estimated Regional-Scale Permeability, Individual Injector Carbon Dioxide Injection Rates and Formation Geomechanical Impacts

Table 18 presents the regional-scale permeability required to history match the median per-well water disposal rates in each of the 22 formations (for which sufficient data was available) to both establish the median individual-well water disposal rate and to construct 3D geomechanical and petrophysical models. This table shows that the history-matched (upscaled) regional-scale permeability values derived in this study are in general consistent with those – derived from drill stem tests – contained in the previous studies referenced in Table 18. However, while the permeability values presented are considered regional scale, they may be

subject to sample bias and are likely only representative of the areas within Alberta for which both core and water disposal data were collected (shown in Figure 21). Within such areas the permeability estimates provided can be used as a reasonable approximation of the long-term regional-scale fluid flow and injectivity characteristics (at 90% of σ_{hmin}) of the 22 formations contained in Table 18. This information may be useful in the planning, site selection, and design stages of future large-scale fluid disposal projects in the Alberta Basin and can help to mitigate economic risks associated with formation-scale injectivity uncertainty.

The use of this history-matched regional-scale permeability data and the 3D geomechanical and petrophysical (ResFrac™) models enabled estimation of the injectivity performance of a single CO_2 injector (operating at an injection pressure of 90% of σ_{hmin}) located in the center of a 12 km x 12 km block of each of the 22 formations listed in Table 18. This table also shows the modeled estimates of the sustained (minimum) annual CO_2 injection rates for a single injection well operating in each of the formations of interest for a period of 20 years.

Table 18. Modeled annual CO_2 injection rates for a single injector well operating for 20 years at 90% of σ_{hmin} in each of the formations of interest in the Alberta Basin.

Formation	Depth Interval (from – to; m)	History-Matched Regional-scale Permeability Estimates (m^2)	Average Well-scale Permeability reported in Previous Studies (m^2)	Modeled Sustained 20-year CO_2 Injection Rates per Injector Well (tpa*)	Fracture Surface Area Generated (m^2)
Upper Cardium	1,794 - 1,810	1.23×10^{-13}	8.33×10^{-14} [29]	90,212	0
Lower Cardium	2,156 - 2,477	2.50×10^{-15}	2.16×10^{-16} [37]	22,439	0
Pouce Coupe/Dunvegan	1,751 - 1,823	3.95×10^{-14}	9.87×10^{-14} [38]	134,202	0
Viking	2,176 - 2,220	1.73×10^{-14}	1.83×10^{-14} [39 – 40]	48,826	0
Falher	2,928 - 3,064	1.69×10^{-14}	2.96×10^{-14} [41]	166,552	0
Notikewin	2,876 - 2,892	4.31×10^{-14}	2.96×10^{-14} [42]	33,838	0
Middle Mannville	2,332 - 2,455	1.21×10^{-13}	4.93×10^{-13} [42]	184,184	0
Lower Mannville	2,714 - 2,778	6.52×10^{-13}	4.93×10^{-13} [42]	484,058	0
Nikanassin	3,362 - 3,385	2.85×10^{-12}	1.97×10^{-16} [43]	323,565	0
Upper Charlie Lake	1,478 - 1,587	5.89×10^{-16}	5.09×10^{-15} [44]	37,102	0
Lower Charlie Lake	1,980 - 2,241	1.91×10^{-15}	1.48×10^{-15} [44]	32,782	0
Upper Doig	2,406 - 2,451	4.93×10^{-14}	1.38×10^{-14} [44]	156,845	0
Lower Doig	2,957 - 2,990	3.15×10^{-13}	1.38×10^{-14} [44]	118,147	0
Belloy	2,476 - 2,672	1.39×10^{-12}	5.33×10^{-14} [45]	192,471	0
Wabamun	2,238 - 2,380	2.25×10^{-12}	2.40×10^{-14} [40], [46]	130,794	0
Leduc	1,618 - 1,855	5.48×10^{-13}	5.0×10^{-13} [36]	327,794	0
Lower Slave Point	1,323 - 1,366	2.86×10^{-13}	2.93×10^{-13} [36]	202,459	0
Lower Muskeg	1,510 - 1,523	7.02×10^{-14}	9.87×10^{-16} [47]	50,462	0
Upper Keg River	1,014 - 1,046	1.31×10^{-12}	8.98×10^{-14} [40]	297,922	0
Middle Keg River	1,510 - 1,522	4.81×10^{-13}	8.98×10^{-14} [40]	236,957	0

Lower Keg River	1,739 - 1,778	1.32×10^{-13}	8.98×10^{-14} [40]	187,215	0
Basal Sandstone Unit	2,050 - 2,265	1.23×10^{-13}	9.87×10^{-13} [20]	423,821	0

* tpa: tonnes per annum.

In all simulations conducted, zero fracture surface area was generated, which indicates that the sustained injection of CO_2 (over a 20-year period at 90% of σ_{hmin} and a temperature of 15 $^{\circ}$C) into the 22 formations listed in Table 18 is unlikely to result in the creation of large-scale thermally induced planar fractures. However, given the relatively large mesh element size in the near-wellbore region (45 m x 45 m x 1 m; x-y-z) it is possible that smaller (i.e., below mesh element resolution) thermally induced fractures could have occurred during the simulation but not have been detected by the model because of the (relatively large) mesh element resolution. Zero fracture surface area was consistently recorded in all simulations conducted, which indicated that conditions for the propagation of such fractures beyond the mesh element size (45 m x 45 m x 1 m) are unlikely to have existed during the simulation.

Table 18 shows that there are several disposal formations that may be capable of supporting the operation of high-rate CO_2 injectors for 20-year periods, at rates comparable to those experienced at the only commercial-scale carbon sequestration project operating in Alberta currently (i.e., the Quest project). These include regionally extensive Mesozoic sandstones such as the Middle and Lower Mannville, Nikanassin, Pouce Coupe/Dunvegan, Falher, Doig and Belloy, which are relatively ductile [13] depleted formations likely to be hydraulically isolated from the Precambrian basement [1]. As shown in Chapters 2 and 3, formation ductility, pressure depletion and hydraulic isolation from the Precambrian basement are major factors that can reduce the potential for generation of large-magnitude induced seismicity during sustained industrial-scale fluid disposal activities. Additionally, Table 18 shows that the regionally extensive (depleted) Devonian carbonate formations also located distant from the Precambrian basement (such as the Wabamun, Leduc, Slave Point and Keg River) could sustain CO_2 injection rates comparable to those demonstrated at the Quest project. The generation of large magnitude induced seismicity and the loss of (lateral and/or vertical) containment are considered critical failure modes that can permanently and materially impact the chances of success of a large-scale CO_2 injection project [7].

In all simulations presented in Table 18, a single CO_2 injector operating for 20 years resulted in the presence of CO_2 distributed throughout the 12 km x 12 km model domain at

varying levels of saturation, especially in the higher permeability stratigraphic horizons. Figure 27 shows an example of the simulation output for the Middle Mannville formation.

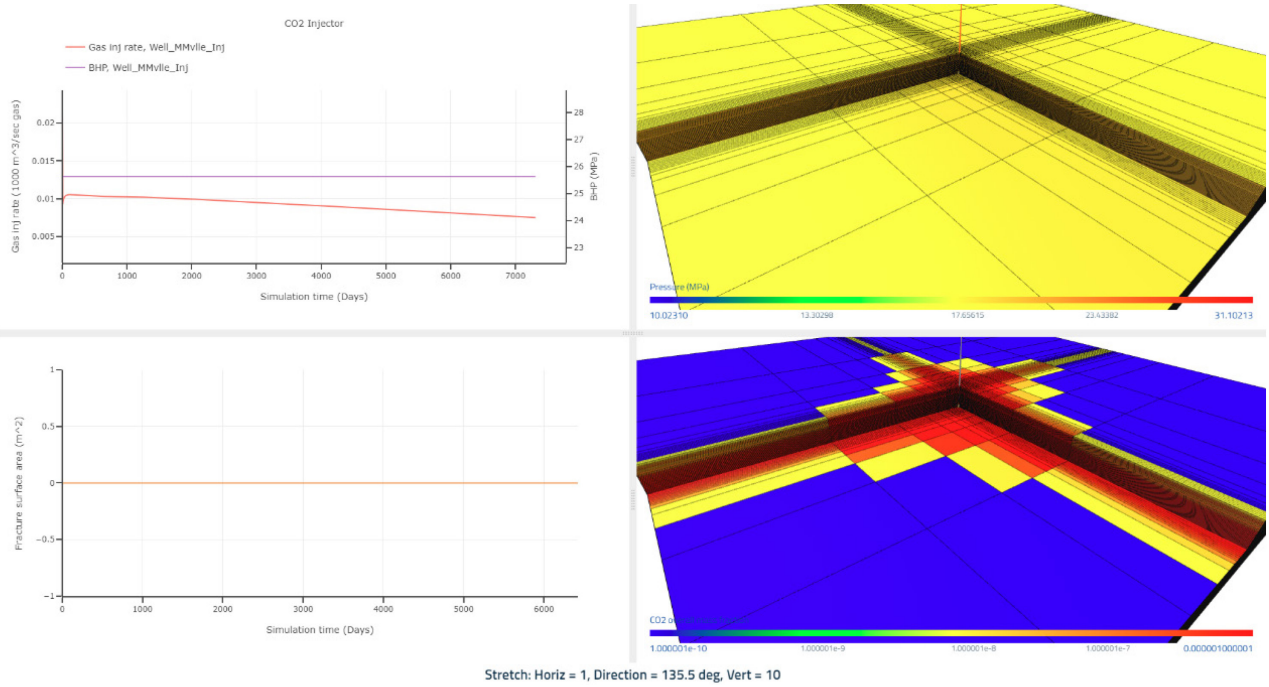

Figure 27. ResFrac™ model output for case of CO_2 injection into the Middle Mannville Formation for a 20-year period (with a bottomhole pressure limit of 90% of σ_{hmin}). Upper left: Bottomhole pressure and gas injection rate. Lower left: Fracture surface area generated. Upper right: Reservoir pressure at year 20. Lower right: CO_2 mass fraction in the model domain at year 20.

Additionally, in all simulations it was observed that the reservoir pressure at the matrix boundary (located 12 km from the injection well) had increased by a minimum of 25% by the end of the 20-year simulation period. The gradual increase in reservoir pressure at the (no-flow) matrix boundary resulted in a corresponding decrease in modeled injectivity over the simulation history, as shown in Figure 27. Under the closed (no-flow) boundary conditions used in these simulations, a single CO_2 injector operating for 20 years is therefore likely to result in a simulated reservoir pressure increase of at least 25% at a radius of at least 12 km (i.e., size of matrix region) from the injector well location for all the formations modeled. However, this is likely representative of a worst-case scenario since actual boundary conditions are not likely to be closed (unless surrounded by other injection operations) and therefore actual reservoir pressure increase is likely to be less than the modeled reservoir pressure increase.

A reliable assessment of the credibility of a simulation requires assessment of the congruence between model predictions, actual observed external data not used in the

development of the model, and prospective/predictive outcomes (i.e., model validation) [256]. In the geoscience field, a history match of a reservoir model to past reservoir performance data is considered a good indicator of model reliability/credibility [257]. History matching requires the use of observed reservoir behavior to estimate reservoir properties which resulted in the behavior [257]. History matching is used in this study to estimate regional-scale permeability for the formations of interest by using the historical water disposal rates in each formation.

Validation of the CO_2 injection rates predicted by these simulations requires a comparison of actual CO_2 injection rates in at least one of the formations assessed. The monthly CO_2 injection rates for the Quest CCS project are available from the date of commissioning of the project in 2015 and are published in the project's Knowledge Sharing Program Records submitted to the Alberta Department of Energy [258]. Figure 28 shows a comparison between the actual monthly CO_2 injection rates for all (three) injectors at this project for the period August 2015 (i.e., Year 0) – December 2021 (i.e., Year 7) to the ResFrac™ model's predicted CO_2 injection rate over a 20-year period for the Basal Sandstone Unit Formation (also referred to as the Basal Cambrian Sands or BCS).

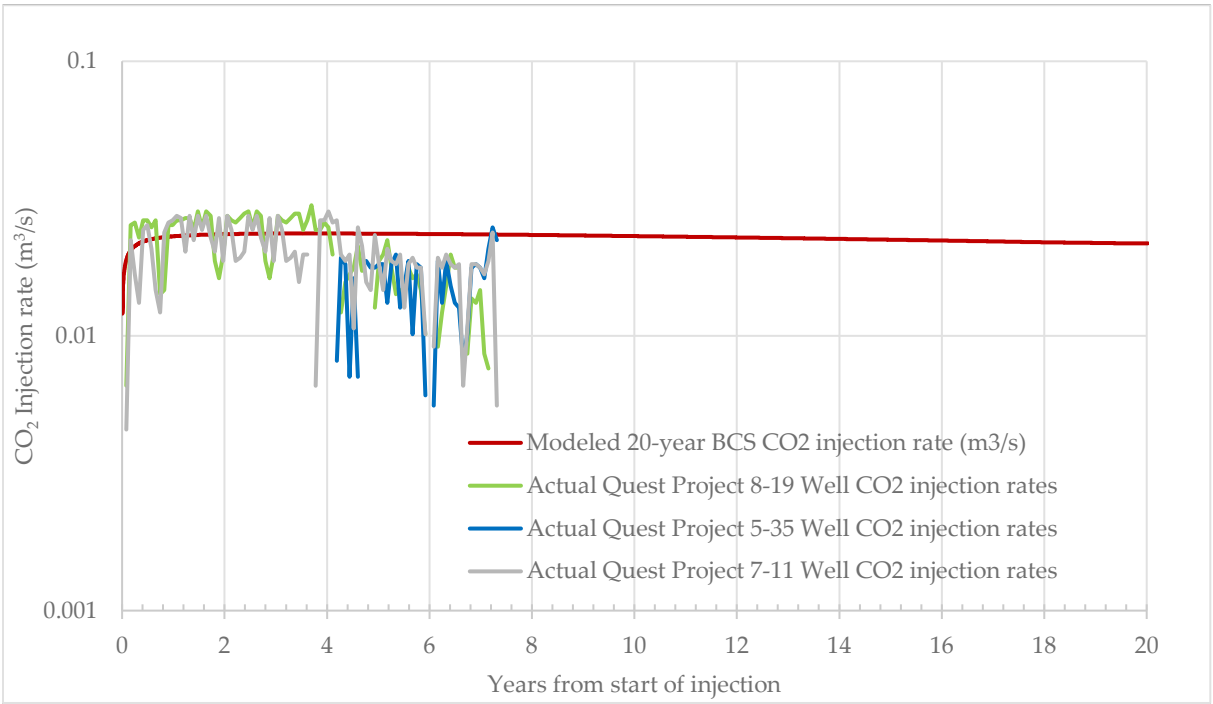

Figure 28. Comparison between the ResFrac™ model's predicted per-well CO_2 injection rate for the Basal Sandstone Unit over a 20-year period (red line) to actual CO_2 injection rates experienced at the three CO_2 injectors operating at the Quest project in

Alberta (grey, blue and green lines). Zero or near-zero injection rates corresponding to operational variables (such as well maintenance/workovers, plant maintenance/turnaround and operational upsets) were removed from the Quest injection records.

Figure 28 shows that the per-well CO_2 injection rates predicted by the ResFrac™ model closely match the actual injection rates of the three CO_2 injectors operating at the Quest project for years 1-4. The decline in Quest injectivity which occurred after Year 4 is associated with the precipitation of halite in the near-wellbore environment at these wells, and injectivity can be restored to original rates by conducting hot water workovers (flushes) [259]. The fluctuation in Quest well injectivity post-Year 4 shown in Figure 28 is therefore considered an operational issue, and not a fundamental geologic limitation. Figure 28 therefore validates that the workflow and simulation methodology developed in this study appear capable of predicting, with a reasonable degree of accuracy, the actual individual CO_2 well injectivity rates (at least) in the Basal Sandstone Unit.

4.4 Discussion

Extensive guidance criteria and methods have been developed for identification and assessment of geologic containment (such as caprock integrity) risks in CO_2 injection projects (e.g., [26], [260]–[262]) and for estimation of gross capacity (e.g., [135], [263]), which are critical factors that determine the suitability of a site for geologic CO_2 storage. Recently, some progress has been made on the estimation of sustainable capacity, which consists of the ability of the storage container to safely maintain the injected CO_2 in the target reservoir for geologic time, while minimizing impacts to other current and future surface and subsurface users (e.g., [1]). However, the regional economic feasibility of commercial-scale CO_2 injection and storage is largely controlled by both the available (sustainable) formation storage capacity in the region and the ability to consistently inject (into the subsurface) the desired CO_2 volumes required to meet project goals at rates that minimize the number of injector wells over the lifetime of the project [233]. The importance of these parameters is reflected in the current selection criteria for CO_2 sequestration sites, which provide guidelines for both capacity (i.e., reservoir thickness and porosity) and injectivity (i.e., permeability, reservoir pore pressure and fracture pressure) [263]. However, in many cases there is high confidence in permeability estimates at the local-scale but limited confidence in regional-scale permeability estimates, which limits the ability to assess the probability of successful well performance over the multi-decade operating life of large volume fluid disposal projects, such as commercial-scale CO_2 sequestration projects [264]. In addition to

injection well performance, other key sources of uncertainty specific to CO_2 sequestration projects include the geomechanical response of target disposal formations and the expected (CO_2 and pressure) plume behavior over several decades of injection [265]. Disposal well injectivity is therefore a key risk in commercial-scale CO_2 sequestration projects, with high confidence required in assessments of both long-term storage capacity, the minimum per-well injection rates, and the maximum number of wells before such projects can obtain corporate financial approvals to proceed and secure commercial sequestration service contracts with emitters (clients).

Extensive efforts have been focused on estimating regional and basin-scale carbon sequestration capacity both globally and within Alberta (e.g., [266]–[270]), but there has been significantly less attention directed to the need to improve the reliability of injectivity rates [18], despite the critical importance of this parameter [15]. The inability of CO_2 injector wells to achieve the minimum design injection rate compromises project economics and can ultimately result in project economic failure. Therefore, the ability to minimize long-term injection rate uncertainty (i.e., estimate realistic long-term injection rates) can contribute significantly to reducing economic risk for CO_2 sequestration projects. Design injection rates vary depending on several site-specific factors including well construction and operation cost, with the minimum individual well design injection rate in the Quest project in Alberta established at 394,000 tonnes-per-annum/well (tpa/well) in 2012 [271], while injection rates below 25,000 tpa/well per annum were considered uneconomic in the case of projects contemplated in Europe [272]. However, carbon penalties in Canada have since increased substantially from approximately $15/ton in 2012 [273] (year of the final investment decision of the Quest project) to $65/ton in 2023, which is likely to significantly reduce the minimum injectivity rate threshold per injector well required for positive return rates in CO_2 sequestration projects.

Consequently, if an arbitrary injection rate threshold of 100,000 tpa/well is assumed for the Alberta Basin, then 15 of the 22 disposal formations analyzed appear to be capable of supporting CO_2 sequestration wells operating at this rate for 20 years without incurring large-scale (thermally induced) fracturing. If this threshold is increased to 200,000 tpa/well then only 7 of the 22 formations appear to be capable of supporting sustained CO_2 injection at this rate for 20-year periods. These 7 formations include previously overlooked geographically extensive

Mesozoic sandstones and carbonates that appear to be capable of supporting injectors operating at rates equivalent to those at the only commercial-scale CO_2 sequestration (Quest) project. Additionally, these Mesozoic formations are depleted (a result of over six decades of hydrocarbon extraction), are more likely to be hydraulically isolated from the Precambrian basement [1] and are more ductile [234]. Geologic sealing capacity (i.e., containment) uncertainty is also lower in these formations, since these formations are predominantly legacy oil and gas reservoirs which have successfully contained fluid under pressure over geologic timescales, and extensive geologic and petrophysical characterization datasets are publicly available. The combination of these factors can reduce the likelihood of sustained industrial-scale fluid injection into these formations generating induced seismicity of concern as well as reduce geologic uncertainty, when compared to injection into (previously unexploited and underexplored) saline aquifers overlying the Precambrian basement. The generation of induced seismicity and loss of containment are considered the two critical failure modes for large-scale CO_2 sequestration projects [7].

Deep saline aquifers have been the main targets for large-scale CO_2 sequestration, based on their lack of legacy wellbore penetrations, extensive geographic extent, depth, thickness, and potential pore volume capacity [274]. However, in the Alberta Basin there is very limited geologic data available on the Basal Sandstone Unit (the deep saline aquifer of interest) despite its extensive geographic coverage, while its stratigraphic location on top of the Precambrian basement increases its likelihood of a hydraulic connection with high seismogenic hazard Precambrian fault systems. The lack of geologic data increases uncertainty while its proximity to the Precambrian basement and virgin reservoir pressure increases the potential of generating induced seismicity of concern, especially if scenarios of multiple CO_2 sequestration projects operating simultaneously in the same formation over multi-decade periods are contemplated [1]. Therefore, the ability of the geographically extensive and ultrathick intermediate-depth Mesozoic sandstone and carbonate formations in Alberta to support long-term CO_2 injection rates comparable to those of the deep saline aquifers may be of interest to policymakers, project developers and regulators in the province. The history-matched permeability and the simulated CO_2 injection rate estimates presented in this study may also be useful to project developers to help manage injectivity and economic risk in CO_2 sequestration projects proposed within the Alberta Basin.

However, it should be noted that the presence of legacy oil and gas wellbores in these (intermediate depth) Mesozoic formations can increase containment risk and project operating (monitoring, measurement, and verification) costs. Such risks could be managed by a combination of upgrading wellbore abandonment to meet modern standards and maintaining pressure in the sequestration horizon below the original (virgin) formation pressure throughout the project lifecycle and post-closure [275]. Additionally, while only vertical wells and injection pressure below the fracture gradient were considered in this simulation study, individual well injectivity rates can be increased (nominally) by using horizontal injector wells and (significantly) by hydraulic fracture stimulation of the injection formations [233].

The CO_2 injection pressure strategy (i.e., injection pressure limit = 90% of σ_{hmin}) and consequently the injection estimates presented are based on the requirements for regulatory compliance in the Alberta Basin. However, substantially lower injection pressures may be required in cases in which there are critically stressed faults present in or in proximity to the disposal formations, even when such formations are depleted, to avoid triggering fault slip [246]. Substantial injection pressure reduction is likely to result in substantial injection rate reduction, and such an investigation represents an opportunity for a future refinement to the results presented in this study.

While this study focused on estimation of long-term CO_2 injection rates in the Alberta Basin, the workflow used can be applied in many hydrocarbon producing basins in which there is an extensive amount of geoscience data. The use of such a method to estimate regional-scale CO_2 injection rates can help to reduce project design injectivity uncertainty and economic risk, since the history match of modeled and actual flow rates in regional well networks is a reliable method of accounting for kilometer-scale impact of geological heterogeneities [253]. A summary of the workflow developed is provided in Figure 29.

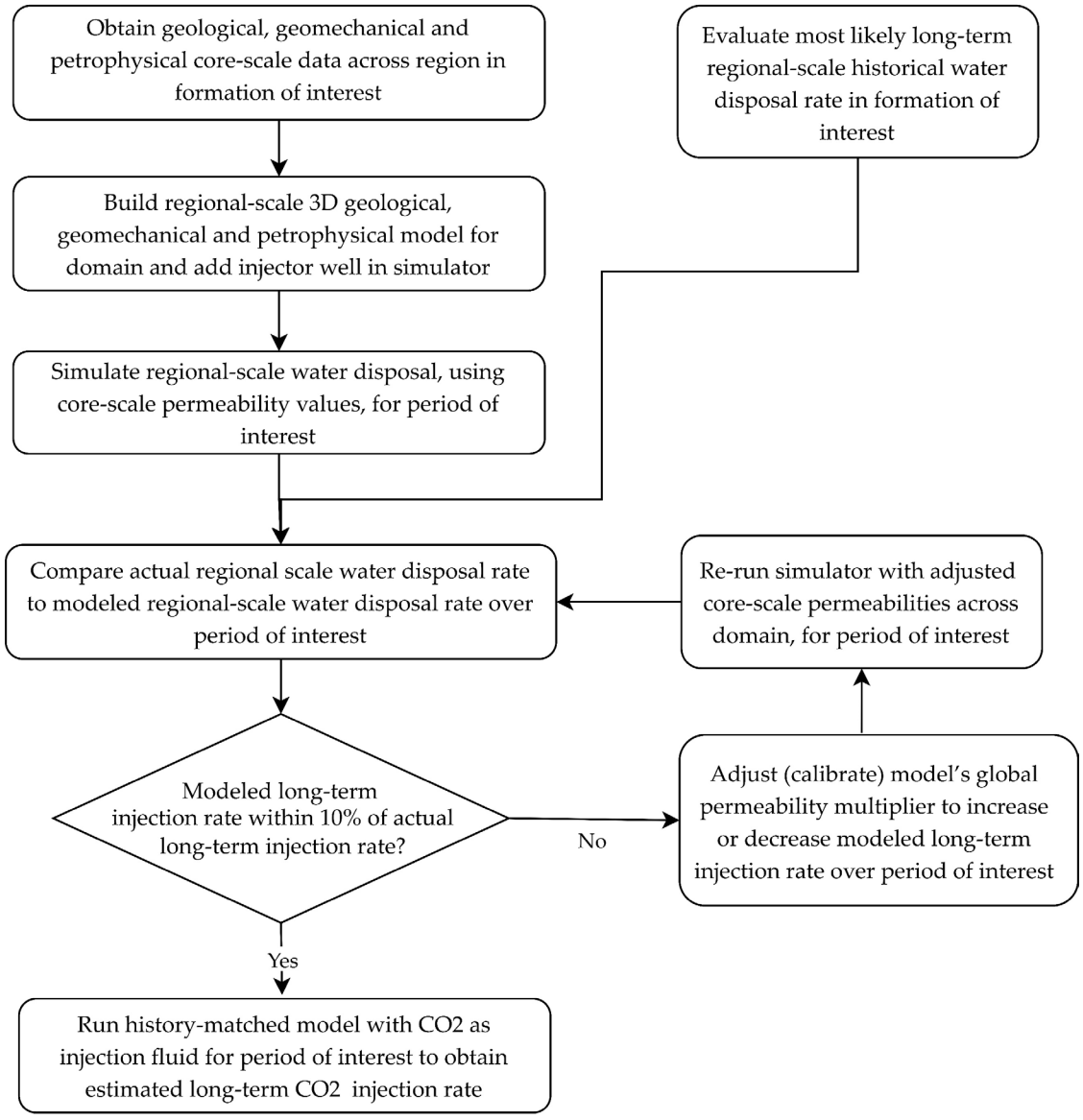

Figure 29. Summary of workflow used in this study to estimate long-term regional CO_2 injection rates in the Alberta Basin.

The geomechanical, geological, petrophysical and water disposal data and the reservoir simulator used in this study (and represented in the workflow in Figure 29) are commonly required for hydrocarbon operational activities and are therefore generally available in hydrocarbon producing basins. The method described above can therefore be of interest to CO_2 injection project proponents, regulators, and policy makers considering the development of industrial-scale sequestration projects in such locations.

4.5 Conclusions

This analysis shows that there is large variability in the range of factors required to upscale laboratory measured (core-scale) permeability to history-match regional-scale permeability across the Alberta Basin, with formation-specific correction factors ranging over six orders of magnitude (from 0.1 to 1 x 10^5). This observation is consistent with the formation-scale estimates of upscaling factors obtained from well-scale drill stem testing conducted in two select areas of the Alberta Basin (the Peace River [251] and the Pembina Cardium [249]).

This analysis also indicates that, when populated with formation-specific geology/geomechanics/petrophysics and history-matched permeability parameters, physics-based compositional 3D geomechanical models (such as ResFrac™) appear to be capable of providing useful indicators of likely well and reservoir performance for commercial-scale CO_2 sequestration projects. These simulations also show that, when injection pressures are constrained to 90% of σ_{hmin}, only 7 of the 22 disposal formations assessed in the Alberta Basin are capable of sustaining CO_2 injection at commercial-scale rates (i.e., greater that around 200,000 tpa/well) over a 20-year period. Sustained injection of CO_2 into these formations (at an injection fluid temperature of 15 °C) appears unlikely to result in large-scale thermally induced fracturing over a 20-year injection period. Some of these formations appear to also be capable of sustaining commercial-scale long-term CO_2 injection rates, comparable to those of the principal CO_2 sequestration target formation in Alberta (the Basal Sandstone Unit). Commercial-scale CO_2 sequestration into such formations may present a lower induced seismicity hazard, because of the greater likelihood of hydraulic isolation from the high seismogenic-hazard Precambrian basement.

This analysis also indicates that, under the conditions used in this study, (i) the presence of CO_2 at varying levels of saturation can be expected throughout the (higher permeability stratigraphic layers in the) 12 km x 12 km model domains for all formations analyzed, and (ii) a minimum pressure increase of at least 25% over initial formation pressure can be expected (under closed boundary conditions) at the boundaries of the model domain (radius of 12 km from the injector well) at the end of the 20-year injection period. The methods and workflow utilized in this study can be used for the estimation of long-term CO_2 injectivity rates and geomechanical

effects in any geoscience-data rich sedimentary basin, and consequently may be of value to project developers, regulators, and policy makers globally.

5.0 Conclusions and Recommendations

Net-zero energy and energy transition associated changes to industrial activities are likely to materially alter the nature and type of subsurface activities conducted in sedimentary basins globally over the next decade. These changes will require evolution of the processes used by project proponents and regulators to evaluate and manage risks not previously considered and to ensure that the pore space resource in such basins is sustainably managed for the benefit of current and future users. Considering the scale of the activity envisaged, basin-scale risk assessment principles are required to ensure sustainable management of pore space resources rather than the individual project-centric assessment strategy currently used. Basin-scale reservoir re-pressurization and/or gigaton scale displacement of reservoir fluids in a hydraulically connected mega-hydrodynamic flow system can trigger permanent adverse impacts to current and future subsurface pore space and basin users. The negative net fluid balance and high ductility characteristics of most of its injection and confining formations (at the time of the in-situ measurements) may have been significant contributors to the success rate of high-volume fluid-injection activities historically conducted in the Alberta Basin. Inclusion of these parameters in the site selection risk assessment and lifecycle risk management stages of project development and regulatory processes may be useful in ensuring that future injections continue to be successful.

The net fluid balance method developed and proposed in this research represents an initial step in the development of future best practices for the assessment of sustainable subsurface fluid injection capacity in hydraulically interconnected sedimentary basins. Future enhancements to this approach include assessment of the potential for migration of fluids into non-saline environments, investigation of the geomechanical effects of re-pressurizing depleted formations to virgin pressures and investigation of the potential long-term effects of a positive net fluid balance in virgin pressure formations, and the associated pressure and capacity implications.

Evaluation of the current Brittle-Ductile State (χ) and Brittle-Ductile Index (I_{BD}) parameters developed in this research could help project developers and regulators evaluate the potential for seismogenicity in targeted injection reservoirs and confining (caprock, lateral and under-burden) geologic layers at the project site selection stages. This can help alleviate the

potential for fluid-injection projects to trigger induced seismicity of concern and presents a proactive approach for avoidance of induced seismicity compared to the current reactive approach of managing induced seismicity occurrence after project development and operation. Improvement of the vertical resolution of seismic event detection is likely to help improve the accuracy of identification of seismogenic formations within fault traces and help to refine and validate this risk assessment method.

In addition to sustainable storage capacity, high-confidence estimates of long-term regional-scale CO_2 injectivity rates underpin the economic justification and commercial contracts for commercial-scale sequestration projects. The workflow developed in this research for generation of high confidence injectivity estimates is likely to be useful to project developers in the site selection process to help mitigate project economic risk. However, regulators may require larger scale models to evaluate the cumulative effects of multiple discrete industrial-scale injection projects operating in a single regional-scale formation (i.e., tens of kilometers scale), which is challenging to accomplish with the computing resources currently available.

Detailed studies are recommended to improve understanding of the regional-scale hydrologic link between surface water bodies, shallow groundwater, and deep saline aquifers and to assess the scale of anthropogenic-induced changes (if any) on the regional hydrologic balance within areas AB4, AB6 and AB7. A detailed regional fluid budget evaluation of area AB5 is also recommended, to evaluate if future pore space management adjustments may be required to maintain a sustainable fluid budget in this area.

It is recommended that the hazard assessment process for (future) fluid-injection projects also include an assessment of the probability of aseismic slip within (more ductile) injection formations loading fault sections and triggering seismogenic slip in far-field, more brittle formations. Such assessment may be especially important in the Alberta Basin since the types (strike-slip and reverse) of faults prevalent in this basin can be challenging to detect during the site selection process.

Future investigation of the potential for long-term fluid injection conducted at the Alberta regulatory pressure limit of 90% of σ_{hmin} to trigger slip on critically stressed faults, especially in depleted reservoir environments, is also recommended. Additionally, the long-term

geomechanical impact of differences between injection fluid and receiving formation temperatures may also be warranted. Such investigations could help determine if there could be situations in which these variables could constitute geomechanical risk factors in long-term industrial fluid-injection projects.

6.0 References

[1] M. Samaroo, R. Chalaturnyk, M. Dusseault, R. Jackson, A. Buhlmann, and H. Custers, "An Assessment of the Net Fluid Balance in the Alberta Basin," *Energies*, vol. 15, no. 3, pp. 1–32, 2022, doi: 10.3390/en15031081.

[2] J. A. Schremmer, "Utah Law Review Pore Space Property," *Utah Law Rev.*, vol. 1, no. 1, pp. 0–72, 2021, doi: https://doi.org/10.26054/0D- SPTA-CFJW.

[3] R. L. Gresham and O. L. Anderson, "Legal and commercial models for pore-space access and use for geologic CO2 sequestration," *Univ. Pittsburgh Law Rev.*, vol. 72, no. 4, pp. 701–777, 2011, doi: 10.5195/LAWREVIEW.2011.170.

[4] IEA, "Net Zero by 2050: A Roadmap for the Global Energy Sector," *Int. Energy Agency*, p. 224, 2021, [Online]. Available: https://www.iea.org/reports/net-zero-by-2050.

[5] Canada Energy Regulator, "Canada's Energy Future 2021: Energy Supply and Demand," 2021. [Online]. Available: https://www.cer-rec.gc.ca/en/data-analysis/canada-energy-future/2021/canada-energy-futures-2021.pdf.

[6] S. Krevor *et al.*, "Subsurface carbon dioxide and hydrogen storage for a sustainable energy future," *Nat. Rev. Earth Environ.*, 2023, doi: 10.1038/s43017-022-00376-8.

[7] T. Warner *et al.*, "Overview of Failure Modes and Effects Associated with CO2 Injection and Storage Operations in Saline Formations (DOE/NETL-2020/2634)," Pittsburgh, PA, 2020. [Online]. Available: https://www.energy.gov/sites/default/files/2021/01/f82/DOE-LPO_Carbon_Storage_Report_Final_December_2020.pdf.

[8] W. C. Walton and C. F. Mclane, "Aspects of groundwater supply sustainable yield," *GroundWater*, vol. 51, no. 2, pp. 158–160, 2013, doi: 10.1111/gwat.12001.

[9] National Academy of Sciences, "Induced Seismicity Potential in Energy Technologies," National Academies Press, Washington, DC, 2015. doi: 10.17226/13355.

[10] B. R. Scanlon, R. C. Reedy, M. B. Weingarten, and K. E. Murray, "Managing basin-scale fluid budgets to reduce injection-induced seismicity from the recent U.S. Shale oil revolution," *Seismol. Res. Lett.*, vol. 90, no. 1, pp. 171–182, Feb. 2019, doi: 10.1785/0220180223.

[11] R. J. Walters, M. D. Zoback, J. W. Baker, and G. C. Beroza, "Characterizing and Responding to Seismic Risk Associated with Earthquakes Potentially Triggered by Fluid Disposal and Hydraulic Fracturing," *Seismol. Res. Lett.*, vol. 86, no. 4, pp. 1110–1118, 2015, doi: 10.1785/0220150048.

[12] Golder Associates, "Literature Review of Global Pit Lakes: Pit Lakes - Case Studies (Report No. 1777450)," Calgary, AB, AB, 2017. [Online]. Available: https://cosia.ca/sites/default/files/attachments/Literature Review of Global Pit Lakes_0.pdf.

[13] S. R. Buss, A. W. Herbert, K. M. Green, and C. Atkinson, "Contaminant fluxes from hydraulic containment landfills - a review (Science Report SC0310/SR)," 2004. [Online]. Available: https://assets.publishing.service.gov.uk/government/uploads/system/uploads/attachment_data/file/291583/scho0904bhxx-e-e.pdf.

[14] M. Bianchi, H. H. Liu, and J. T. Birkholzer, "Radionuclide transport behavior in a generic geological radioactive waste repository," *Groundwater*, vol. 53, no. 3, pp. 440–451, 2015, doi: 10.1111/gwat.12171.

[15] T. McGuire, "Tundra SGS – Critical Importance of Site-Specific Injectivity Testing for Carbon Dioxide Injection Well Simulation Calibration," *SSRN Electron. J.*, no. October, 2022, doi: 10.2139/ssrn.4274242.

[16] R. A. Schultz *et al.*, "Underground energy-related product storage and sequestration: site characterization, risk analysis, and monitoring," *Geol. Soc. London, Spec. Publ.*, vol. 528, no. 1, 2023, doi: 10.1144/SP528-2022-66.

[17] S. M. Ghaderi, D. W. Keith, and Y. Leonenko, "Feasibility of Injecting Large Volumes of CO2 into Aquifers," *Energy Procedia*, vol. 1, no. 1, pp. 3113–3120, 2009, doi: 10.1016/j.egypro.2009.02.092.

[18] S. H. Hajiabadi, P. Bedrikovetsky, S. Borazjani, and H. Mahani, “Well Injectivity during CO2 Geosequestration: A Review of Hydro-Physical, Chemical, and Geomechanical Effects,” *Energy and Fuels*, vol. 35, no. 11, pp. 9240–9267, 2021, doi: 10.1021/acs.energyfuels.1c00931.

[19] J. Schuenemeyer, “Methodology for the 2005 USGS Assessment of Undiscovered Oil and Gas Resources, Central North Slope, Alaska,” Menlo Park, California, 2005. [Online]. Available: http://pubs.usgs.gov/of/2005/1410/.

[20] M. K. Verma and K. J. Bird, “Role of reservoir engineering in the assessment of undiscovered oil and gas resources in the National Petroleum Reserve, Alaska,” *Am. Assoc. Pet. Geol. Bull.*, vol. 89, no. 8, pp. 1091–1111, 2005, doi: 10.1306/04040504055.

[21] G. Walton, “A New Perspective on the Brittle–Ductile Transition of Rocks,” *Rock Mech. Rock Eng.*, vol. 54, no. 12, pp. 5993–6006, 2021, doi: 10.1007/s00603-021-02595-9.

[22] N. G. Gerogiannopoulos and E. T. Brown, “The critical state concept applied to rock,” *Int. J. Rock Mech. Min. Sci.*, vol. 15, no. 1, pp. 1–10, 1978, doi: 10.1016/0148-9062(78)90716-7.

[23] T. Aven and O. Renn, “Improving government policy on risk: Eight key principles,” *Reliab. Eng. Syst. Saf.*, vol. 176, no. April, pp. 230–241, Aug. 2018, doi: 10.1016/j.ress.2018.04.018.

[24] L. M. Jones, “Resilience by Design: Bringing Science to Policy Makers,” *Seismol. Res. Lett.*, vol. 86, no. 2A, pp. 294–301, Mar. 2015, doi: 10.1785/0220150010.

[25] D. J. Evans, “An appraisal of Underground Gas Storage technologies and incidents, for the development of risk assessment methodology,” *Br. Geol. Surv. Open Rep. OR/07/023*, p. 287, 2007.

[26] R. J. Pawar *et al.*, “Recent advances in risk assessment and risk management of geologic CO2 storage,” *Int. J. Greenh. Gas Control*, vol. 40, no. July 2016, pp. 292–311, Oct. 2015, doi: 10.1016/j.ijggc.2015.06.014.

[27] S. Bourne, S. Crouch, and M. Smith, “A risk-based framework for measurement, monitoring and verification of the Quest CCS Project, Alberta, Canada,” *Int. J. Greenh. Gas Control*, vol. 26, pp. 109–126, 2014, doi: 10.1016/j.ijggc.2014.04.026.

[28] U.S. DOE, “Final Risk Assessment Report for the FutureGen Project Environmental Impact Statement,” vol. 2006, no. April, p. 398, 2007, [Online]. Available: https://www.energy.gov/sites/prod/files/EIS-0394-DEIS-RiskAssessmentReport-2007.pdf.

[29] I. J. Duncan, “Developing a Comprehensive Risk Assessment Framework for Geological Storage of CO2,” 2014. [Online]. Available: https://www.osti.gov/servlets/purl/1170168.

[30] S. A. Smith, J. A. Sorensen, E. N. Steadman, and J. A. Harju, “Acid gas injection and monitoring at the Zama oil field in Alberta, Canada: A case study in demonstration-scale carbon dioxide sequestration,” *Energy Procedia*, vol. 1, no. 1, pp. 1981–1988, 2009, doi: 10.1016/j.egypro.2009.01.258.

[31] S. A. Smith, J. A. Sorensen, E. N. Steadman, and J. A. Harju, “Plains CO2 Reduction (PCOR) Partnership (Phase II) – Zama Field Validation Test Regional Technology Implementation Plan - Task 3 Deliverable D52,” Morgantown, West Virginia, 2010. [Online]. Available: https://undeerc.org/pcor/newsandpubs/pdf/SAS-D52_Zama_RTIP-Re-revised-June10FINAL.pdf.

[32] Shell Canada Quest Subsurface Team, “Quest Storage Development Plan,” Edmonton, AB, 2011. [Online]. Available: https://open.alberta.ca/dataset/46ddba1a-7b86-4d7c-b8b6-8fe33a60fada/resource/5555eb2e-6d86-4419-97a3-8d3de7c5b702/download/storagedevelopmentplan.pdf.

[33] J. P. Jones, J. R. Brydie, and E. H. Perkins, “Investigation of potential far field impacts on freshwater resources related to CO2 storage: A case study of the HARP project site in Alberta, Canada,” in *Energy Procedia*, 2013, vol. 37, pp. 3792–3799, doi: 10.1016/j.egypro.2013.06.275.

[34] M. Soltanzadeh, “Regional-Scale Geomechanical Characterization of the Devonian Sedimentary Succession West of the Athabasca Area in Support of Potential CO2 Storage Operations,” Edmonton, AB, 2014. [Online]. Available: https://albertainnovates.ca/focus-areas/clean-resources/project-library/.

[35] H. L. Longworth, G. C. Dunn, and M. Semchuck, “Underground disposal of acid gas in Alberta, Canada: regulatory concerns and case histories,” *SPE Proc. - Gas Technol. Symp.*, pp. 181–192, 1996, doi:

10.2523/35584-ms.

[36] A. A. Alshuhail, D. C. Lawton, and H. J. Isaac, “Geophysical characterization of the Devonian Nisku Formation for the Wabamun Area CO2 sequestration project (WASP), Alberta, Canada,” in *Energy Procedia*, 2011, vol. 4, pp. 4696–4703, doi: 10.1016/j.egypro.2011.02.431.

[37] Enhance Energy and Northwest Redwater Partnership, “The Alberta Carbon Trunkline and Clive Injection Facility Knowledge Sharing Report 2016,” Edmonton, AB, AB, 2017. [Online]. Available: https://open.alberta.ca/dataset/f66db190-751e-4ad2-8a26-60809244a28e/resource/a94e61ab-8333-4f95-8380-a023fd12f849/download/ccsactlreport2016.pdf.

[38] S. Goodarzi and A. Settari, “Geomechanical Modelling and Analysis Wabamun Area CO2 Sequestration Project (WASP),” Calgary, Alberta, 2010. [Online]. Available: https://www.ucalgary.ca/wasp/Geomechanical Numerical Modeling.pdf.

[39] Alberta Energy, “Summary Report of the Regulatory Framework Assessment,” Edmonton, AB, 2012. [Online]. Available: https://open.alberta.ca/dataset/5483a064-1ec8-466e-a330-19d2253e5807/resource/ecab392b-4757-4351-a157-9d5aebedecd0/download/6259895-2013-carbon-capture-storage-summary-report.pdf.

[40] J. S. Nakai, M. Weingarten, A. F. Sheehan, S. L. Bilek, and S. Ge, “A Possible Causative Mechanism of Raton Basin, New Mexico and Colorado Earthquakes Using Recent Seismicity Patterns and Pore Pressure Modeling,” *J. Geophys. Res. Solid Earth*, vol. 122, no. 10, pp. 8051–8065, Oct. 2017, doi: 10.1002/2017JB014415.

[41] P. O. Ogwari, H. R. DeShon, and M. J. Hornbach, “The Dallas-Fort Worth Airport Earthquake Sequence: Seismicity Beyond Injection Period,” *J. Geophys. Res. Solid Earth*, vol. 123, no. 1, pp. 553–563, 2018, doi: 10.1002/2017JB015003.

[42] R. J. Walters, M. D. Zoback, J. W. Baker, and B. Greg, “Scientific principles affecting protocols for site-characterizaion and risk assessment related to the potential for seismicity triggered by saltwater disposal and hydraulic fracturing,” pp. 1–80, 2015, [Online]. Available: https://scits.stanford.edu/sites/g/files/sbiybj13751/f/scitsguidelines_final_spring2015_0.pdf.

[43] Q. Zhou and J. T. Birkholzer, “On scale and magnitude of pressure build-up induced by large-scale geologic storage of CO2,” *Greenh. Gases Sci. Technol.*, vol. 47, pp. 36–47, 2011, doi: 10.1002/ghg3.

[44] J. T. Birkholzer, C. M. Oldenburg, and Q. Zhou, “CO2 migration and pressure evolution in deep saline aquifers,” *Int. J. Greenh. Gas Control*, vol. 40, pp. 203–220, 2015, doi: 10.1016/j.ijggc.2015.03.022.

[45] S. M. Ghaderi and Y. Leonenko, “Reservoir modeling for Wabamun lake sequestration project,” *Energy Sci. Eng.*, vol. 3, no. 2, pp. 98–114, 2015, doi: 10.1002/ese3.60.

[46] K. W. Chang and P. Segall, “Injection-induced seismicity on basement faults including poroelastic stressing,” *J. Geophys. Res. Solid Earth*, vol. 121, no. 4, pp. 2708–2726, 2016, doi: 10.1002/2015JB012561.

[47] M. Kozłowska, M. R. Brudzinski, P. Friberg, R. J. Skoumal, N. D. Baxter, and B. S. Currie, “Maturity of nearby faults influences seismic hazard from hydraulic fracturing,” *Proc. Natl. Acad. Sci. U. S. A.*, vol. 115, no. 8, pp. E1720–E1729, Feb. 2018, doi: 10.1073/pnas.1715284115.

[48] T. Hincks, W. Aspinall, R. Cooke, and T. Gernon, “Oklahoma’s induced seismicity strongly linked to wastewater injection depth,” *Science (80-.).*, vol. 7911, no. February, pp. 1–46, 2018, doi: 10.1126/science.aap7911.

[49] M. R. Brudzinski and M. Kozłowska, “Seismicity induced by hydraulic fracturing and wastewater disposal in the Appalachian Basin, USA: a review,” *Acta Geophys.*, vol. 67, no. 1, pp. 351–364, 2019, doi: 10.1007/s11600-019-00249-7.

[50] J. Rutqvist *et al.*, “Fault activation and induced seismicity in geological carbon storage – Lessons learned from recent modeling studies,” *J. Rock Mech. Geotech. Eng.*, vol. 8, no. 6, pp. 789–804, Dec. 2016, doi: 10.1016/j.jrmge.2016.09.001.

[51] D. Dempsey and J. Suckale, “Physics-based forecasting of induced seismicity at Groningen gas field, the Netherlands,” *Geophys. Res. Lett.*, vol. 44, no. 15, pp. 7773–7782, Aug. 2017, doi: 10.1002/2017GL073878.

[52] T. H. W. Goebel and M. Shirzaei, “More Than 40 yrs of Potentially Induced Seismicity Close to the San Andreas Fault in San Ardo, Central California,” *Seismol. Res. Lett.*, vol. 92, no. January, pp. 187–198, 2020, doi: 10.1785/0220200276.

[53] F. R. Walsh and M. D. Zoback, “Oklahoma’s recent earthquakes and saltwater disposal,” *Sci. Adv.*, vol. 1, no. 5, Jun. 2015, doi: 10.1126/sciadv.1500195.

[54] F. R. Walsh and M. D. Zoback, “Probabilistic assessment of potential fault slip related to injection induced earthquakes: Application to north-central Oklahoma, USA,” *Geology*, vol. 44, no. 12, pp. 991–994, 2016, doi: 10.1130/G38275.1.

[55] L. Quinones *et al.*, “Tracking induced seismicity in the Fort Worth basin: A summary of the 2008–2018 north Texas earthquake study catalog,” *Bull. Seismol. Soc. Am.*, vol. 109, no. 4, pp. 1203–1216, Aug. 2019, doi: 10.1785/0120190057.

[56] R. J. Skoumal, M. R. Brudzinski, and B. S. Currie, “Proximity of Precambrian basement affects the likelihood of induced seismicity in the Appalachian, Illinois, and Williston Basins, central and eastern United States,” *Geosphere*, vol. 14, no. 3, pp. 1365–1379, Jun. 2018, doi: 10.1130/GES01542.1.

[57] S. Pawley *et al.*, “The Geological Susceptibility of Induced Earthquakes in the Duvernay Play,” *Geophys. Res. Lett.*, vol. 45, no. 4, pp. 1786–1793, Feb. 2018, doi: 10.1002/2017GL076100.

[58] T. H. W. Goebel and E. E. Brodsky, “The spatial footprint of injection wells in a global compilation of induced earthquake sequences,” *Science (80-.).*, vol. 361, no. 6405, pp. 899–904, 2018, doi: 10.1126/science.aat5449.

[59] A. Mcgarr, “Seismic Moment and Volume Change,” *J. Geophys. Res. B Solid Earth*, vol. 81, no. 8, 1976.

[60] L. De Barros, F. Cappa, Y. Guglielmi, L. Duboeuf, and J. R. Grasso, “Energy of injection-induced seismicity predicted from in-situ experiments,” *Sci. Rep.*, vol. 9, no. 1, Dec. 2019, doi: 10.1038/s41598-019-41306-x.

[61] A. McGarr and A. J. Barbour, “Wastewater Disposal and the Earthquake Sequences During 2016 Near Fairview, Pawnee, and Cushing, Oklahoma,” *Geophys. Res. Lett.*, vol. 44, no. 18, pp. 9330–9336, 2017, doi: 10.1002/2017GL075258.

[62] R. Schultz, G. Atkinson, D. W. Eaton, Y. J. Gu, and H. Kao, “Hydraulic fracturing volume is associated with induced earthquake productivity in the Duvernay play,” *Science (80-.).*, vol. 359, no. 6373, pp. 304–308, 2018, doi: 10.1126/science.aao0159.

[63] G. Kwiatek *et al.*, “Controlling fluid-induced seismicity during a 6.1-km-deep geothermal stimulation in Finland,” *Sci. Adv.*, vol. 5, no. 5, 2019, doi: 10.1126/sciadv.aav7224.

[64] Oklahoma Corporation Commission, “Earthquake Response Summary Recent Actions,” Oklahoma Cita, OK, 2017. [Online]. Available: http://www.occeweb.com/News/01-04-16EQ ADVISORY.pdf.

[65] E. Hand, “Injection wells blamed in Oklahoma earthquakes: Regulators in several states start to limit wastewater disposal to reduce risks of induced tremors,” *Science (80-.).*, vol. 345, no. 6192, pp. 13–14, 2014, doi: 10.4159/harvard.9780674594159.c7.

[66] A. McGarr *et al.*, “Coping with earthquakes induced by fluid injection,” *Science (80-.).*, vol. 347, no. 6224, pp. 830–831, 2015, doi: 10.1126/science.aaa0494.

[67] C. Langenbruch and M. D. Zoback, “Response to Comment on ‘How will induced seismicity in Oklahoma respond to decreased saltwater injection rates?,’” *Sci. Adv.*, vol. 3, no. 8, pp. 1–10, 2017, doi: 10.1126/sciadv.aao2277.

[68] J. W. B. and G. C. B. J. Walters, M. D. Zoback, “Characterizing and Responding to Seismic Risk Associated with Earthquakes Potentially Triggered by Saltwater Disposal and Hydraulic Fracturing,” *Seismol. Res. Lett.*, vol. 86, no. 4, pp. 1110–1118, 2015, doi: https://doi.org/10.1785/0220150048.

[69] M. Teare, S. Miller, S. Overland, R. Marsh, and C. Tamblyn, “ST98-2015: Alberta’s Energy Reserves 2014 and Supply/Demand Outlook 2015-2024,” Calgary, AB, 2015. [Online]. Available: https://www.aer.ca/providing-information/data-and-reports/statistical-reports/st98.

[70] R. Mansell, M. Moore, J. Winter, and M. Krzepkowski, “Size, Role and Performance in the Oil and Gas Sector,” *Univ. Calgary Sch. Public Policy SPP Res. Pap.*, vol. 5, no. 23, pp. 1–77, 2012, doi: 10.2139/ssrn.2115955.

[71] Alberta Energy Regulator, “ST98 Alberta Energy Outlook,” *ST98*, 2020. https://www.aer.ca/providing-information/data-and-reports/statistical-reports/st98/executive-summary/data (accessed Apr. 07, 2021).

[72] C. A. Connolly, L. M. Walter, H. Baadsgaard, and F. J. Longstaffe, “Origin and evolution of formation waters, Alberta Basin, Western Canada Sedimentary Basin,” *Appl. Geochemistry*, vol. 5, no. 4, pp. 375–395, 1990, doi: 10.1016/0883-2927(90)90016-X.

[73] R. J. Cox, “Subsurface disposal of produced waters: An Alberta perspective,” in *Produced Water. Technological/Environmental Issues and Solutions*, vol. 46, J. P. Ray and F. R. Engelhardt, Eds. Springer Science & Business Media, 1992, pp. 1–606.

[74] The National Academies of Sciences Engineering and Medicine, “Flowback and Produced Waters: Opportunities and Challenges for Innovation,” in *Proceedings of a Workshop*, 2017, doi: 10.17226/24620.

[75] N. Gaurina-Međimurec, B. Pašić, P. Mijić, and I. Medved, “Deep underground injection of waste from drilling activities—An overview,” *Minerals*, vol. 10, no. 4, 2020, doi: 10.3390/min10040303.

[76] P. Gosselin *et al.*, “The Royal Society of Canada Expert Panel: Environmental and Health Impacts of Canada’s Oil Sands Industry,” Ottawa, ON, 2010. [Online]. Available: http://www.rsc.ca/documents/expert/RSC_ExP_ExecutiveSummary_ENG_Dec14_10_FINAL_v5.pdf.

[77] S. Jasechko, J. J. Gibson, S. Jean Birks, and Y. Yi, “Quantifying saline groundwater seepage to surface waters in the Athabasca oil sands region,” *Appl. Geochemistry*, vol. 27, no. 10, pp. 2068–2076, 2012, doi: 10.1016/j.apgeochem.2012.06.007.

[78] R. C. Burruss, “Development of a probabilistic assessment methodology for evaluation of carbon dioxide storage - USGS Open File Report 2009-1035,” 2009. [Online]. Available: http://www.usgs.gov/pubprod.

[79] D. J. Miller, “Geology of Possible Petroleum Provinces in Alaska,” *Geol. Surv. Bull.*, vol. 1094, p. 131, 1959, [Online]. Available: https://pubs.usgs.gov/bul/1094/report.pdf.

[80] S. Zhou, H. Huang, and Y. Liu, “Biodegradation and origin of oil sands in the western Canada sedimentary basin,” *Pet. Sci.*, vol. 5, no. 2, pp. 87–94, 2008, doi: 10.1007/s12182-008-0015-3.

[81] T. L. Osif, “Effects of Salt, Gas, Temperature, and Pressure on the Compressibility of Water.,” *Soc. Pet. Eng. AIME, SPE*, no. February, pp. 175–181, 1984, doi: 10.2118/13174-pa.

[82] D. I. Pană, “EUB/AGS Earth Sciences Report 2002-02: Precambrian Basement of the Western Canada Sedimentary Basin in Northern Alberta,” Edmonton, AB, AB, 2002. [Online]. Available: http://www.ags.gov.ab.ca/publications/a.

[83] Province of Alberta, *Oil and Gas Conservation Act: Revised Statutes of Alberta 2000 Chapter O-6*. Alberta, Canada: Queen’s Printer, 2009, pp. 1–88.

[84] Alberta Energy Regulator, “ST103 - Field/Pool List,” Edmonton, AB, 2021. [Online]. Available: https://www.aer.ca/providing-information/data-and-reports/statistical-reports/st103.

[85] S. Creaney *et al.*, “Chapter 31 - Petroleum Generation and Migration in the Western Canada Sedimentary Basin,” in *Geological Atlas of the Western Canada Sedimentary Basin*, G. D. Mossop and I. Shetsen, Eds. Edmonton: Alberta Research Council, 1994, pp. 1–14.

[86] Alberta Energy Regulator, “Directive 065: Resources applications for oil and gas reservoirs,” Alberta Energy Regulator, Edmonton, Alberta, Canada, 2022. [Online]. Available: https://static.aer.ca/prd/documents/directives/Directive065.pdf.

[87] House of Commons of Canada, *Bill C-12: An Act respecting transparency and accountability in Canada’s efforts to acheive net-zero greenhouse gas emissions by the year 2050*. Canada, 2020, p. 16.

[88] Canada Energy Regulator, “Canada Energy Future 2020,” 2020. [Online]. Available: https://www.cer-rec.gc.ca/en/data-analysis/canada-energy-future/2020/index.html.

[89] Alberta Energy Regulator, “Directive 051: Injection and Disposal Wells Well Classifications Completion, Logging and Testing Requirements,” Edmonton, Alberta, 1994. [Online]. Available: https://www.aer.ca/documents/directives/Directive051.pdf.

[90] Environment and Climate Change Canada, “National Inventory Report 1990-2017: Greenhouse Gas Sources and Sinks in Canada,” Ottawa, 2019. [Online]. Available: https://www.canada.ca/en/environment-climate-change/services/climate-change/greenhouse-gas-emissions.html.

[91] D. B. Layzell, C. Young, J. Lof, J. Leary, and S. Sit, “Towards net-zero energy systems in Canada: a key role for hydrogen,” *Transit. Accel. Reports*, vol. 2, no. 3, p. 53, 2020, [Online]. Available: https://www.cesarnet.ca/publications/transition-accelerator-reports/towards-net-zero-energy-systems-canada-key-role-hydrogen%0Ahttps://transitionaccelerator.ca/towards-net-zero-energy-systems-in-canada-a-key-role-for-hydrogen.

[92] J. Banks and N. B. Harris, “Geothermal potential of Foreland Basins: A case study from the Western Canadian Sedimentary Basin,” *Geothermics*, vol. 76, pp. 74–92, Nov. 2018, doi: 10.1016/j.geothermics.2018.06.004.

[93] C. D. Hawkes, P. J. McLellan, U. Zimmer, and S. Bachu, “Geomechanical factors affecting geological storage of CO2 in depleted oil and gas reservoirs,” *Can. Int. Pet. Conf. 2004, CIPC 2004*, 2004, doi: 10.2118/2004-258.

[94] D. R. Schwab, T. S. Bidgoli, and M. H. Taylor, “Characterizing the Potential for Injection-Induced Fault Reactivation Through Subsurface Structural Mapping and Stress Field Analysis, Wellington Field, Sumner County, Kansas,” *J. Geophys. Res. Solid Earth*, vol. 122, no. 10, pp. 10,132-10154, 2017, doi: 10.1002/2017JB014071.

[95] S. Hannis *et al.*, “CO2 Storage in Depleted or Depleting Oil and Gas Fields: What can We Learn from Existing Projects?,” *Energy Procedia*, vol. 114, no. November 2016, pp. 5680–5690, 2017, doi: 10.1016/j.egypro.2017.03.1707.

[96] Teresa L. Watson, “Abandoned wells create liability for future subsurface exploitation,” *Alta. Law Rev.*, vol. 57, no. 4, pp. 1001–1024, 2020, [Online]. Available: https://www.albertalawreview.com/index.php/ALR/article/view/2602/2564.

[97] S. J. Birks, J. W. Fennell, J. J. Gibson, Y. Yi, M. C. Moncur, and M. Brewster, “Using regional datasets of isotope geochemistry to resolve complex groundwater flow and formation connectivity in northeastern Alberta, Canada,” *Appl. Geochemistry*, vol. 101, pp. 140–159, Feb. 2019, doi: 10.1016/j.apgeochem.2018.12.013.

[98] S. Bachu, “Flow systems in the Alberta Basin: Patterns, types and driving mechanisms,” *Bull. Can. Pet. Geol.*, vol. 47, no. 4, pp. 455–474, 1999.

[99] G. Ferguson *et al.*, “The Persistence of Brines in Sedimentary Basins,” *Geophys. Res. Lett.*, vol. 45, no. 10, pp. 4851–4858, May 2018, doi: 10.1029/2018GL078409.

[100] M. D. Zoback and S. M. Gorelick, “Earthquake triggering and large-scale geologic storage of carbon dioxide,” *Proceedings of the National Academy of Sciences of the United States of America*, vol. 109, no. 26. pp. 10164–10168, Jun. 26, 2012, doi: 10.1073/pnas.1202473109.

[101] M. J. Lippmann and S. M. Benson, “Relevance of underground natural gas storage to geologic sequestration of carbon dioxide,” 2002. [Online]. Available: http://escholarship.org/uc/item/5gs5q111.pdf.

[102] J. Nicot and A. H. Chowdhury, “Disposal of brackish water concentrate into depleted oil and gas fields: a case study,” *Desalination*, vol. 181, no. 1–3, pp. 61–74, 2005.

[103] S. Benson *et al.*, “Chapter 5: Underground geological storage,” *IPCC Spec. Rep. Carbon dioxide Capture Storage*, pp. 195–276, 2005.

[104] K. F. Perry, “Natural Gas Storage Industry Experience and Technology: Potential Application to CO2 Geological Storage,” *Carbon Dioxide Capture Storage Deep Geol. Form.*, vol. 2, pp. 815–825, 2005, doi: 10.1016/B978-008044570-0/50135-5.

[105] V. H. Stern, R. J. Schultz, L. Shen, Y. J. Gu, and D. W. Eaton, *Alberta earthquake catalogue, version 1.0:*

September 2006 through December 2010, vol. 15, no. September 2006. 2013.

[106] A. Fereidoni and L. Cui, "Composite Alberta Seismicity Catalog : CASC2014-x." 2015, Accessed: Apr. 08, 2021. [Online]. Available: http://www.inducedseismicity.ca/wp-content/uploads/2015/01/Composite-Alberta-Seismicity-Catalog3.pdf.

[107] R. Schultz, V. Stern, Y. J. Gu, and D. Eaton, "Detection threshold and location resolution of the Alberta Geological Survey earthquake catalogue," *Seismol. Res. Lett.*, vol. 86, no. 2A, pp. 385–397, Mar. 2015, doi: 10.1785/0220140203.

[108] W. G. Milne, "The Snipe Lake, Alberta earthquake of March 8, 1970," *Can. J. Earth Sci.*, vol. 7, no. 6, pp. 1564–1567, 1970, doi: 10.1139/e70-148.

[109] R. J. Wetmiller, "Earthquakes near Rocky Mountain House, Alberta, and their relationship to gas production facilities (Canada)," *Can. J. Earth Sci.*, vol. 23, no. 2, pp. 172–181, 1986, doi: 10.1139/e86-020.

[110] R. Schultz, V. Stern, and Y. J. Gu, "An investigation of seismicity clustered near the Cordel Field, west central Alberta, and its relation to a nearby disposal well," *J. Geophys. Res. Solid Earth*, vol. 119, no. 4, pp. 3410–3423, 2014, doi: 10.1002/2013JB010836.

[111] C. D. Rokosh *et al.*, "ERCB/AGS Open File Report 2012-06 Summary: Summary of Alberta's Shale- and Siltstone-Hosted Hydrocarbon Resource Potential," 2012. [Online]. Available: https://ags.aer.ca/publication/ofr-2012-06.

[112] E. Galloway *et al.*, "Faults and associated karst collapse suggest conduits for fluid flow that influence hydraulic fracturing-induced seismicity," *Proc. Natl. Acad. Sci.*, vol. 115, no. 43, pp. E10003–E10012, Oct. 2018, doi: 10.1073/pnas.1807549115.

[113] R. Schultz, R. Wang, Y. J. Gu, K. Haug, and G. Atkinson, "A seismological overview of the induced earthquakes in the Duvernay play near Fox Creek, Alberta," *J. Geophys. Res. Solid Earth*, vol. 122, no. 1, pp. 492–505, 2017, doi: 10.1002/2016JB013570.

[114] G. M. Atkinson, "Strategies to prevent damage to critical infrastructure due to induced seismicity," *Facets*, vol. 2, no. 1, pp. 374–394, 2017, doi: 10.1139/facets-2017-0013.

[115] W. D. Peck *et al.*, "CO2 storage resource potential of the Cambro-Ordovician Saline System in the western interior of North America," *Energy Procedia*, vol. 37, pp. 5230–5239, 2013, doi: 10.1016/j.egypro.2013.06.439.

[116] S. Bachu, A. Melnik, and R. Bistran, "Approach to evaluating the CO2 storage capacity in Devonian deep saline aquifers for emissions from oil sands operations in the Athabasca area, Canada," *Energy Procedia*, vol. 63, pp. 5093–5102, 2014, doi: 10.1016/j.egypro.2014.11.539.

[117] D. Barson, S. Bachu, and P. Esslinger, "Flow systems in the Mannville Group in the east-central Athabasca area and implications for steam-assisted gravity drainage operations for in-situ bitumen production," *Bull. Can. Pet. Geol.*, vol. 49, no. 3, pp. 376–392, 2001.

[118] A. D. Miall, "Geoscience of climate and energy 13. The environmental hydrogeology of the oil sands, lower Athabasca area, Alberta," *Geosci. Canada*, vol. 40, no. 3, pp. 215–233, 2013, doi: 10.12789/geocanj.2013.40.016.

[119] P. L. Broughton, "Subglacial blowouts in western Canada: insights into extreme meltwater pressures and hydrofracturing," *Boreas*, vol. 47, no. 1, pp. 326–346, 2018, doi: 10.1111/bor.12268.

[120] T. Sperling, "Risk-cost-benefit framework for the design of dewatering systems in open pit mines," University of British Columbia, 1990.

[121] D. A. Walters, A. Settari, and P. R. Kry, "Coupled geomechanical and reservoir modeling investigating poroelastic effects of cyclic steam stimulation in the Cold Lake reservoir," *SPE Reserv. Eval. Eng.*, vol. 5, no. 6, pp. 507–516, 2002, doi: 10.2118/80997-PA.

[122] M. Pooladi-Darvish and L. Mattar, "SAGD operations in the presence of overlying gas cap and water layer - Effect of shale layers," *J. Can. Pet. Technol.*, vol. 41, no. 6, pp. 40–50, 2002, doi: 10.2118/02-06-04.

[123] S. Bachu, “Synthesis and model of formation-water flow, Alberta Basin, Canada,” *Am. Assoc. Pet. Geol. Bull.*, vol. 79, no. 8, pp. 1159–1178, 1995, doi: 10.1306/8d2b2209-171e-11d7-8645000102c1865d.

[124] J. Majorowicz, H. Hofmann, and T. Babadagli, “Deep geothermal heat storage under oilsands - Can we use it to help oilsands industry? New EGS concept proposed,” *Trans. - Geotherm. Resour. Counc.*, vol. 37, no. PART 1, pp. 173–178, 2013.

[125] S. Bachu and R. A. Burwash, “Regional-scale analysis of the geothermal regime in the Western Canada Sedimentary Basin,” *Geothermics*, vol. 20, no. 5–6, pp. 387–407, 1991, doi: 10.1016/0375-6505(91)90028-T.

[126] Government of Alberta, “Carbon Sequestration Tenure Regulation,” Government of Alberta, Canada, 68/2011, 2016. [Online]. Available: https://kings-printer.alberta.ca/1266.cfm?page=2011_068.cfm&leg_type=Regs&isbncln=9780779790500.

[127] J. Klassen and J. E. Liggett, “First-Order Groundwater Availability Assessment for the Upper Peace Region,” Edmonton, AB, 2019. [Online]. Available: https://static.ags.aer.ca/files/document/OFR/OFR_2019_10.pdf.

[128] J. T. Birkholzer and Q. Zhou, “Basin-scale hydrogeologic impacts of CO2 storage: Capacity and regulatory implications,” *Int. J. Greenh. Gas Control*, vol. 3, no. 6, pp. 745–756, Dec. 2009, doi: 10.1016/j.ijggc.2009.07.002.

[129] S. J. Anfort, S. Bachu, and L. R. Bentley, “Regional-scale hydrogeology of the Upper Devonian-Lower Creataceous sedimentary succession, south-central Alberta basin, Canada,” *Am. Assoc. Pet. Geol. Bull.*, vol. 85, no. 4, pp. 637–660, 2001, doi: 10.1306/8626c96f-173b-11d7-8645000102c1865d.

[130] B. Hitchon and M. E. Holter, “Calcium and Magnesium in Alberta Brines,” *Econ. Geol. Rep. 1*, no. July, pp. 1–26, 1971, [Online]. Available: https://ags.aer.ca/publications/ECO_1.html.

[131] T. Benedictus *et al.*, “TNO Report TNO-034-UT-2009-01427: Long Term Integrity of CO2 Storage – Well Abandonment,” 2009. [Online]. Available: https://www.globalccsinstitute.com/archive/hub/publications/98891/long-term-integrity-co2-storage-well-abandonment.pdf.

[132] D. Allan Gray, J. Majorowicz, and M. Unsworth, “Investigation of the geothermal state of sedimentary basins using oil industry thermal data: Case study from Northern Alberta exhibiting the need to systematically remove biased data,” *J. Geophys. Eng.*, vol. 9, no. 5, pp. 534–548, 2012, doi: 10.1088/1742-2132/9/5/534.

[133] Alberta Energy Regulator, *Directive 040: Pressure and Deliverability Testing Oil and Gas Wells*, no. July. Edmonton, AB, Canada, 2020, pp. 1–61.

[134] S. T. Anderson and H. Jahediesfanjani, “Estimating the pressure-limited dynamic capacity and costs of basin-scale CO2 storage in a saline formation,” *Int. J. Greenh. Gas Control*, vol. 88, no. June, pp. 156–167, 2019, doi: 10.1016/j.ijggc.2019.05.031.

[135] S. Thibeau, S. Bachu, J. Birkholzer, S. Holloway, F. Neele, and Q. Zhou, “Using pressure and volumetric approaches to estimate CO2 storage capacity in deep saline aquifers,” *Energy Procedia*, vol. 63, pp. 5294–5304, 2014, doi: 10.1016/j.egypro.2014.11.560.

[136] J. Townend and M. D. Zoback, “How faulting keeps the crust strong,” *Geology*, vol. 28, no. 5, pp. 399–402, 2000, doi: 10.1130/0091-7613(2000)028<0399:HFKTCS>2.3.CO;2.

[137] K. D. Morell, R. Styron, M. Stirling, J. Griffin, R. Archuleta, and T. Onur, “Seismic Hazard Analyses From Geologic and Geomorphic Data: Current and Future Challenges,” *Tectonics*, vol. 39, no. 10, pp. 1–47, 2020, doi: 10.1029/2018TC005365.

[138] S. E. Hough, “Intraplate seismic hazard: Evidence for distributed strain and implications for seismic hazard,” *Intraplate Earthquakes*, pp. 303–327, 2012, doi: 10.1017/CBO9781139628921.013.

[139] G. M. Ross and D. W. Eaton, “Basement reactivation in the Alberta Basin: Observational constraints and mechanical rationale,” *Bull. Can. Pet. Geol.*, vol. 47, no. 4, pp. 391–411, 1999, doi: 10.2113/49.3.426.

[140] J. R. Dietrich, “Seismic stratigraphy and structure of the lower Paleozoic, Central Alberta Lithoprobe Transect,” *Bull. Can. Pet. Geol.*, vol. 47, no. 4, pp. 362–374, 1999.

[141] T. S. Eyre, D. W. Eaton, M. Zecevic, D. D’Amico, and D. Kolos, “Microseismicity reveals fault activation before Mw 4.1 hydraulic-fracturing induced earthquake,” *Geophys. J. Int.*, vol. 218, no. 1, pp. 534–546, 2019, doi: 10.1093/gji/ggz168.

[142] R. Schultz and R. Wang, “Newly emerging cases of hydraulic fracturing induced seismicity in the Duvernay East Shale Basin,” *Tectonophysics*, vol. 779, no. February, p. 228393, 2020, doi: 10.1016/j.tecto.2020.228393.

[143] J. Hope, D. W. Eaton, and G. M. Ross, “Lithoprobe seismic transect of the Alberta Basin: Compilation and overview,” *Bull. Can. Pet. Geol.*, vol. 47, no. 4, pp. 331–345, 1999.

[144] B. W. M. Schulte, H. Lyatsky, and D. Bridge, “Methods of fault detection with geophysical data and surface geology,” *Can. J. Explor. Geophys.*, vol. 44, no. 5, pp. 1–23, 2019, [Online]. Available: https://csegrecorder.com/articles/view/methods-of-fault-detection-with-geophysical-data-and-surface-geology.

[145] X. Bao and D. W. Eaton, “Fault activation by hydraulic fracturing in western Canada,” *Science (80-.).*, vol. 354, no. 6318, pp. 1406–1409, 2016, doi: 10.1126/science.aag2583.

[146] R. J. Skoumal, J. Ole Kaven, and J. I. Walter, “Characterizing seismogenic fault structures in Oklahoma using a relocated template-matched catalog,” *Seismol. Res. Lett.*, vol. 90, no. 4, pp. 1535–1543, 2019, doi: 10.1785/0220190045.

[147] A. K. Shah and G. R. Keller, “Geologic influence on induced seismicity: Constraints from potential field data in Oklahoma,” *Geophys. Res. Lett.*, vol. 44, no. 1, pp. 152–161, Jan. 2017, doi: 10.1002/2016GL071808.

[148] R. Schultz, R. J. Skoumal, M. R. Brudzinski, D. Eaton, B. Baptie, and W. Ellsworth, “Hydraulic fracturing-induced seismicity,” *Reviews of Geophysics*, vol. 58, no. 3. Blackwell Publishing Ltd, pp. 1–43, 2020, doi: 10.1029/2019RG000695.

[149] P. H. Hennings *et al.*, “Pore Pressure Threshold and Fault Slip Potential for Induced Earthquakes in the Dallas-Fort Worth Area of North Central Texas,” *Geophys. Res. Lett.*, vol. 48, no. 15, pp. 1–9, 2021, doi: 10.1029/2021GL093564.

[150] Z. Fan, P. Eichhubl, and J. F. W. Gale, “Geomechanical analysis of fluid injection and seismic fault slip for the Mw 4.8 Timpson, Texas, earthquake sequence,” *J. Geophys. Res. Solid Earth*, vol. 121, no. iv, pp. 3076–3095, 2016, doi: 10.1002/2016JB012821.Received.

[151] G. Hui, S. Chen, Z. Chen, F. Gu, M. Ghoroori, and M. A. Mirza, “Comprehensive Characterization and Mitigation of Hydraulic Fracturing-Induced Seismicity in Fox Creek, Alberta,” *SPE J.*, vol. 26, no. 5, pp. 2736–2747, 2021, doi: 10.2118/206713-PA.

[152] R. H. Sibson, “Earthquake faulting as a structural process,” *J. Struct. Geol.*, vol. 11, no. 1–2, pp. 1–14, 1989, doi: 10.1016/0191-8141(89)90032-1.

[153] A. A. Zhamaletdinov, *On the Nature of the Brittle-Ductile Transition Zone in the Earth’s Crust (Review)*, vol. 2. Springer International Publishing, 2019.

[154] W. F. Brace and J. D. Byerlee, “Stick-Slip as a Mechanism for Earthquakes,” *Science (80-.).*, vol. 153, no. 3739, p. 990, 1966.

[155] C. H. Scholz, “Earthquakes and friction laws,” *Nature*, no. 391, pp. 37–42, 1998.

[156] C. H. Scholz, “Brittle Tectonics: A Non-linear Dynamical System,” in *Encyclopedia of Complexity and Systems Science*, vol. 1, R. Myers, Ed. Springer, 2009, pp. 657–674.

[157] J. D. Byerlee and W. F. Brace, “High Pressure Mechanical Instability in Rocks,” *Science (80-.).*, vol. 164, no. 3880, pp. 713–716, 1969, doi: https://doi.org/10.1126/science.164.3880.713.

[158] R. Bürgmann and G. Dresen, “Rheology of the lower crust and upper mantle: Evidence from rock

mechanics, geodesy, and field observations," *Annu. Rev. Earth Planet. Sci.*, vol. 36, pp. 531–567, 2008, doi: 10.1146/annurev.earth.36.031207.124326.

[159] R. Jolivet, M. Simons, P. S. Agram, Z. Duputel, and Z. K. Shen, "Aseismic slip and seismogenic coupling along the central San Andreas Fault," *Geophys. Res. Lett.*, vol. 42, no. 2, pp. 297–306, 2015, doi: 10.1002/2014GL062222.

[160] M. Abdelmeguid and A. Elbanna, "Sequences of seismic and aseismic slip on bimaterial faults show dominant rupture asymmetry and potential for elevated seismic hazard," *Earth Planet. Sci. Lett.*, vol. 593, p. 117648, 2021, doi: 10.1016/j.epsl.2022.117648.

[161] G. Hirth and N. M. Beeler, "The role of fluid pressure on frictional behavior at the base of the seismogenic zone," *Geology*, vol. 43, no. 3, pp. 223–226, 2015, doi: 10.1130/G36361.1.

[162] J. Aubry, F. X. Passelègue, J. Escartín, J. Gasc, D. Deldicque, and A. Schubnel, "Fault Stability Across the Seismogenic Zone," *J. Geophys. Res. Solid Earth*, vol. 125, no. 8, pp. 1–21, 2020, doi: 10.1029/2020JB019670.

[163] V. Vajdova, W. Zhu, T. M. Natalie Chen, and T. Wong, "Micromechanics of brittle faulting and cataclastic flow in Tavel limestone," *J. Struct. Geol.*, vol. 32, no. 8, pp. 1158–1169, 2010, doi: 10.1016/j.jsg.2010.07.007.

[164] T. S. Eyre *et al.*, "The role of aseismic slip in hydraulic fracturing–induced seismicity," *Sci. Adv.*, vol. 5, no. 8, pp. 1–11, 2019, doi: 10.1126/sciadv.aav7172.

[165] W. M. Behr and J. P. Platt, "Brittle faults are weak, yet the ductile middle crust is strong: Implications for lithospheric mechanics," *Geophys. Res. Lett.*, vol. 41, no. 22, pp. 8067–8075, 2014, doi: 10.1002/2014GL061349.Received.

[166] N. De Paola, C. Collettini, D. R. Faulkner, and F. Trippetta, "Fault zone architecture and deformation processes within evaporitic rocks in the upper crust," *Tectonics*, vol. 27, no. 4, pp. 1–21, 2008, doi: 10.1029/2007TC002230.

[167] N. Brantut, A. Schubnel, J. N. Rouzaud, F. Brunet, and T. Shimamoto, "High-velocity frictional properties of a clay-bearing fault gouge and implications for earthquake mechanics," *J. Geophys. Res. Solid Earth*, vol. 113, no. 10, pp. 1–18, 2008, doi: 10.1029/2007JB005551.

[168] K. S. Mews, M. M. Alhubail, and R. G. Barati, "A Review of Brittleness Index Correlations for Unconventional Tight and Ultra-Tight Reservoirs," *Geosci.*, vol. 9, no. 7, 2019, doi: 10.3390/geosciences9070319.

[169] R. Schultz *et al.*, "Linking fossil reefs with earthquakes: Geologic insight to where induced seismicity occurs in Alberta," *Geophys. Res. Lett.*, vol. 43, pp. 2534–2542, 2016, doi: 10.1002/2015GL067514.Received.

[170] S. N. Ehrenberg and P. H. Nadeau, "Sandstone vs. carbonate petroleum reservoirs: A global perspective on porosity-depth and porosity-permeability relationships," *Am. Assoc. Pet. Geol. Bull.*, vol. 89, no. 4, pp. 435–445, 2005, doi: 10.1306/11230404071.

[171] R. M. Kurzawski, M. Stipp, A. R. Niemeijer, C. J. Spiers, and J. H. Behrmann, "Earthquake nucleation in weak subducted carbonates," *Nat. Geosci.*, vol. 9, no. 9, pp. 717–722, 2016, doi: 10.1038/ngeo2774.

[172] A. McGarr, D. Simpson, and L. Seeber, "40 Case histories of induced and triggered seismicity," in *International Geophysics*, 81A ed., vol. 81, no. PART A, W. H. K. Lee, International Association of Seismology and Physics of the Earth's Interior. Committee on Education., and International Association for Earthquake Engineering., Eds. Academic Press, 2002, pp. 647–661.

[173] V. Hajiabdolmajid, P. K. Kaiser, and C. D. Martin, "Modeling brittle failure of rock," *Int. J. Rock Mech. Min. Sci.*, vol. 34, no. 2, pp. 227–244, 2002, doi: 10.1201/9781315364261-8.

[174] K. Mogi, "Pressure dependence of rock strength and transition from brittle fracture to ductile flow," *Bull. Earthquake Res. Inst.*, vol. 44. pp. 215–232, 1966, [Online]. Available: http://repository.dl.itc.u-tokyo.ac.jp/dspace/handle/2261/12246.

[175] C. D. Hawkes, S. Bachu, K. Haug, and A. W. Thompson, “Analysis of in-situ stress regime in the Alberta Basin, Canada, for performance assessment of CO2 geological sequestration sites,” in *Proceedings of the fourth annual conference on carbon capture and sequestration DOE/NETL, May 2-5, 2005*, 2005, pp. 2–5.

[176] P. J. Mclellan, “In-situ stress prediction and measurement by hydraulic fracturing, Wapiti, Alberta,” *J. Can. Pet. Technol.*, vol. 27, no. 2, pp. 85–96, 1988, doi: 10.2118/87-38-58.

[177] J. S. Bell and S. E. Grasby, “The stress regime of the Western Canadian Sedimentary Basin,” *Geofluids*, vol. 12, no. 2, pp. 150–165, May 2012, doi: 10.1111/j.1468-8123.2011.00349.x.

[178] A. Bailey, E. Tenthorey, and B. Ayling, “Characterising the present-day stress regime of the Georgina Basin,” *Aust. J. Earth Sci.*, vol. 64, no. 1, pp. 121–136, 2017, doi: 10.1080/08120099.2017.1268206.

[179] M. Brudy, M. D. Zoback, K. Fuchs, F. Rummel, and J. Baumgärtner, “Estimation of the Complete Stress Tensor to 8 km Depth in the KTB Scientific Drill Holes: Implications for Crustal Strength,” *J. Geophys. Res.*, vol. 102, no. B8, pp. 1–23, Aug. 1997, doi: 10.1029/96jb02942.

[180] M. van der Baan and F. J. Calixto, “Human induced seismicity and large scale hydrocarbon production in the USA and Canada,” *Geochemistry, Geophys. Geosystems*, vol. 18, no. 7, pp. 2467–2485, 2016.

[181] L. W. Shen, D. R. Schmitt, and R. Schultz, “Frictional Stabilities on Induced Earthquake Fault Planes at Fox Creek, Alberta: A Pore Fluid Pressure Dilemma,” *Geophys. Res. Lett.*, vol. 46, no. 15, pp. 8753–8762, 2019, doi: 10.1029/2019GL083566.

[182] H. Zhang, D. W. Eaton, G. Rodriguez, and S. Q. Jia, “Source-mechanism analysis and stress inversion for hydraulic- fracturing-induced event sequences near Fox Creek, Alberta,” *Bull. Seismol. Soc. Am.*, vol. 109, no. 2, pp. 636–651, 2019, doi: 10.1785/0120180275.

[183] L. W. Shen, D. R. Schmitt, R. Wang, and T. E. Hauck, “States of In Situ Stress in the Duvernay East Shale Basin and Willesden Green of Alberta, Canada: Variable In Situ Stress States Effect Fault Stability,” *J. Geophys. Res. Solid Earth*, vol. 126, no. 6, 2021, doi: 10.1029/2020JB021221.

[184] G. Ferguson, “Deep injection of waste water in the Western Canada Sedimentary Basin,” *Groundwater*, vol. 53, no. 2, pp. 187–194, Mar. 2015, doi: 10.1111/gwat.12198.

[185] B. Menéndez, W. Zhu, and T. Wong, “Micromechanics of brittle faulting and cataclastic flow in Berea sandstone,” *J. Struct. Geol.*, vol. 18, no. 1, pp. 1–16, 1996, doi: https://doi.org/10.1016/0191-8141(95)00076-P.

[186] N. J. Austin, L. A. Kennedy, J. M. Logan, and R. Rodway, “Textural controls on the brittle deformation of dolomite: The transition from brittle faulting to cataclastic flow,” *Geol. Soc. Spec. Publ.*, vol. 243, pp. 51–66, 2005, doi: 10.1144/GSL.SP.2005.243.01.06.

[187] Imperial Oil Resources Ventures Ltd., “Application for Cold Lake Solvent Assisted SAGD Project Expansion: Attachment 2 Cold Lake Expansion Project Fracture Characterization,” Edmonton, AB, AB, 2016. [Online]. Available: https://open.alberta.ca/dataset/8a060768-ed57-47d4-aea3-0fb8577b646e/resource/72cc92f0-ebb9-4848-8e8d-b169ac04b0c2/download/vol1-attachment2.pdf.

[188] F. J. Hein, B. Fairgrieve, and G. Dolby, “Heavy-oil and Oil-sand Petroleum Systems in Alberta and Beyond,” in *AAPG Studies in Geology:*, American Association of Petroleum Geologists, 2012, pp. 207–249.

[189] M. B. Dusseault and N. R. Morgenstern, “Locked sands,” *Q. J. Eng. Geol.*, vol. 12, no. 2, pp. 117–131, 1979, doi: 10.1144/GSL.QJEG.1979.012.02.05.

[190] T. S. Abdelaziz, C. D. Martin, and R. J. Chalaturnyk, “Characterization of locked sand from northeastern Alberta,” *Geotech. Test. J.*, vol. 31, no. 6, pp. 480–489, 2008, doi: 10.1520/gtj101225.

[191] S. H. Mckean, J. A. Priest, and D. W. Eaton, “A geomechanical comparison of the Duvernay and the Montney,” *GeoConvention*, pp. 1–5, 2018.

[192] S. Kim and S. A. Hosseini, “Study on the ratio of pore-pressure/stress changes during fluid injection and its implications for CO2 geologic storage,” *J. Pet. Sci. Eng.*, vol. 149, no. October 2016, pp. 138–150, 2017, doi: 10.1016/j.petrol.2016.10.037.

[193] E. Roland and J. J. McGuire, “Earthquake swarms on transform faults,” *Geophys. J. Int.*, vol. 178, no. 3, pp. 1677–1690, 2009, doi: 10.1111/j.1365-246X.2009.04214.x.

[194] F. X. Passelègue *et al.*, “From fault creep to slow and fast earthquakes in carbonates,” *Geology*, vol. 47, no. 8, pp. 744–748, 2019, doi: 10.1130/G45868.1.

[195] T. S. Eyre, M. Zecevic, R. O. Salvage, and D. W. Eaton, “A long-lived swarm of hydraulic fracturing-induced seismicity provides evidence for aseismic slip,” *Bull. Seismol. Soc. Am.*, vol. 110, no. 5, pp. 2205–2215, 2020, doi: 10.1785/0120200107.

[196] N. Igonin, J. P. Verdon, and D. W. Eaton, “Seismic Anisotropy Reveals Stress Changes around a Fault as It Is Activated by Hydraulic Fracturing,” *Seismol. Res. Lett.*, vol. 93, no. 3, pp. 1–16, 2022, doi: 10.1785/0220210282.Supplemental.

[197] H. Yu, R. M. Harrington, H. Kao, Y. Liu, and B. Wang, “Fluid-injection-induced earthquakes characterized by hybrid-frequency waveforms manifest the transition from aseismic to seismic slip,” *Nat. Commun.*, vol. 12, no. 1, 2021, doi: 10.1038/s41467-021-26961-x.

[198] T. S. Eyre, S. Samsonov, W. Feng, H. Kao, and D. W. Eaton, “InSAR data reveal that the largest hydraulic fracturing-induced earthquake in Canada, to date, is a slow-slip event,” *Sci. Rep.*, vol. 12, no. 1, pp. 1–12, 2022, doi: 10.1038/s41598-022-06129-3.

[199] T. Li *et al.*, “Earthquakes Induced by Wastewater Disposal near Musreau Lake, Alberta, 2018 - 2020,” *Seismol. Res. Lett.*, vol. 93, no. 2A, pp. 1–12, 2021, doi: 10.1785/0220210139.Supplemental.

[200] R. Schultz *et al.*, “The Cardston earthquake swarm and hydraulic fracturing of the Exshaw formation (Alberta Bakken play),” *Bull. Seismol. Soc. Am.*, vol. 105, no. 6, pp. 2871–2884, 2015, doi: 10.1785/0120150131.

[201] R. O. Salvage and D. W. Eaton, “The Influence of a Transitional Stress Regime on the Source Characteristics of Induced Seismicity and Fault Activation: Evidence from the 30 November 2018 Fort St. John ML 4.5 Induced Earthquake Sequence,” *Bull. Seismol. Soc. Am.*, vol. 112, no. 3, pp. 1–20, 2022, doi: 10.1785/0120210210.

[202] E. Fjaer, R. M. Holt, P. Horsrud, A. M. Raaen, and R. Risnes, *Petroleum related rock mechanics*, Second Edi., vol. 9, no. 3. Elsevier B.V, 2008.

[203] V. Roche and M. Van Der Baan, “The role of lithological layering and pore pressure on fluid-induced microseismicity,” *J. Geophys. Res. Solid Earth*, vol. 120, no. 2, pp. 923–943, 2015, doi: 10.1002/2014JB011606.

[204] P. Bhattacharya and R. C. Viesca, “Fluid-induced aseismic fault slip outpaces pore-fluid migration,” *Science (80-.).*, vol. 364, no. 6439, pp. 464–468, 2019, doi: 10.1126/science.aaw7354.

[205] F. Cappa, Y. Guglielmi, C. Nussbaum, and J. Birkholzer, “On the Relationship Between Fault Permeability Increases, Induced Stress Perturbation, and the Growth of Aseismic Slip During Fluid Injection,” *Geophys. Res. Lett.*, vol. 45, no. 20, pp. 11,012-11,020, 2018, doi: 10.1029/2018GL080233.

[206] H. Han, S. Yin, Z. Chen, and M. B. Dusseault, “Estimate of in-situ stress and geomechanical parameters for Duvernay Formation based on borehole deformation data,” *J. Pet. Sci. Eng.*, vol. 196, no. 107994, pp. 1–2, 2021, doi: https://doi.org/10.1016/j.petrol.2020.107994.

[207] A. Cui, K. Glover, and R. Wust, “Elastic and plastic mechanical properties of liquid-rich unconventional shales and their implications for hydraulic fracturing and proppant embedment: A case study of the Nordegg Member in Alberta, Canada,” *48th US Rock Mech. / Geomech. Symp. 2014*, vol. 2, pp. 822–833, 2014.

[208] D. Roney, D. Quirk, A. S. Ziarani, and L. Burke, “Integration of microseismic data, tracer information, and fracture modeling into the development of fractured horizontal wells in the Slave Point Formation,” *Soc. Pet. Eng. - SPE Can. Unconv. Resour. Conf. 2014*, vol. 1, pp. 480–497, 2014, doi: 10.2118/171605-ms.

[209] Statoil Hydro, “Application for Approval of Kai Kos Dehseh Project - SIR Round 3,” Edmonton, AB, 2009. [Online]. Available: https://open.alberta.ca/dataset/7017ad9b-f8da-4ca2-b2be-2f6a073d58f2/resource/02292fca-2bec-4823-ad2d-00104bd09c99/download/kkd-sir-round-3.pdf.

[210] Alberta Innovates Technology Futures, “Appendix D: Geomechancal Analyis of the Effects of CO2 Injection in the Leduc (D3-A) and Nisku (D-2) Reservoirs in the Clive Field,” Edmonton, Alberta, 2019. [Online]. Available: https://open.alberta.ca/dataset/90f61413-0ef1-45a4-9e1c-6bff7c23fd7e/resource/17d13263-5527-4f56-bed9-112fe1353241/download/energy-actl-enhance-energy-clive-leduc-field-mmv-plan-appendices-2019-07.pdf.

[211] Canadian Discovery Ltd., “Characterization of the Belloy and Debolt Water Disposal Zones in the Montney Play Fairway, Northeastern BC,” Victoria, BC, 2015. [Online]. Available: http://cdn.geosciencebc.com/project_data/GBC_Report2015-03/GBCReport2015-03_report.pdf.

[212] S. Goodarzi, A. Settari, S. M. Ghaderi, C. Hawkes, and Y. Leonenko, “The effect of site characterization data on injection capacity and cap rock integrity modeling during carbon dioxide storage in the Nisku saline aquifer at the Wabamun Lake area, Canada,” *Environ. Geosci.*, vol. 27, no. 1, pp. 49–65, 2020, doi: 10.1306/eg.06201919005.

[213] S. Costin, R. Smith, Y. Yuan, D. Andjelkovic, and G. Garcia Rosas, “SPE-196037-MS In-Situ Stresses in Colorado Group, AB, Calculated from Open-Hole Mini-Fracs and FMI Logs,” in *SPE Annual Technical Conference and Exhibition*, 2019, pp. 1–25.

[214] M. L. Morin, “Natural and Drilling Induced Fractures in the Grosmont Formation, Alberta: Implications for the State of Stress,” University of Alberta, 2017.

[215] Imperial Oil Resources Ventures Ltd., “Application for Approval of the Aspen Project: Volume 1,” Edmonton, AB, 2013. [Online]. Available: https://static1.squarespace.com/static/52abb9b9e4b0cb06a591754d/t/5dd7383c761fa94d312c8ccb/1574385753225/xVol1-Project-Description+%28Geology%29.pdf.

[216] Prosper Petroleum Ltd., “Application for approval of the Rigel Oil Sands Project,” Edmonton, AB, 2013. [Online]. Available: https://prosperpetroleum.com/wp-content/uploads/2015/06/Rigel-Oil-Sands-Project-ApplicationB.compressed.pdf.

[217] L. W. Shen, D. R. Schmitt, and K. Haug, “Quantitative constraints to the complete state of stress from the combined borehole and focal mechanism inversions: Fox Creek, Alberta,” *Tectonophysics*, vol. 764, no. May, pp. 110–123, Aug. 2019, doi: 10.1016/j.tecto.2019.04.023.

[218] J. G. Liu, B. Xu, L. Sun, B. Li, and G. J. Wei, “In situ stress field in the Athabasca oil sands deposits: Field measurement, stress-field modeling, and engineering implications,” *J. Pet. Sci. Eng.*, vol. 215, no. January, p. 110671, 2022, doi: 10.1016/j.petrol.2022.110671.

[219] C. Carmen and D. A. Talinga, “Overburden characterization with formation pore pressure and anisotropic stress field estimation in the Athabasca Basin, Canada,” *Interpretation*, vol. 7, no. 4, pp. 761–771, 2019, doi: 10.1190/int-2018-0146.1.

[220] P. R. Kry and J. M. Gronseth, “In-Situ Stresses and Hydraulic Fracturing in the Deep Basin.,” *J. Can. Pet. Technol.*, vol. 22, no. 6, pp. 31–35, 1983, doi: 10.2118/83-06-02.

[221] J. S. Bell and S. Bachu, “In situ stress magnitude and orientation estimates for Cretaceous coal-bearing strata beneath the plains area of central and southern Alberta,” *Bull. Can. Pet. Geol.*, vol. 51, no. 1, pp. 1–28, 2003, doi: 10.2113/gscpgbull.51.1.1.

[222] S. Bachu *et al.*, “The Heartland Area Redwater CO2 storage project (HARP): Results of Phase I site characterization,” *Energy Procedia*, vol. 4, no. 2011, pp. 4559–4566, 2011, doi: 10.1016/j.egypro.2011.02.414.

[223] S. A. R. Keneti and R. C. K. Wong, “Investigation of anisotropic behavior of Montney shale under indirect tensile strength test,” *Soc. Pet. Eng. - Can. Unconv. Resour. Int. Pet. Conf. 2010*, vol. 4, pp. 2583–2591, 2010, doi: 10.2118/138104-ms.

[224] O. Contreras, G. Hareland, and R. Aguilera, “Pore pressure modelling and stress-faulting-regime determination of the Montney shale in the Western Canada Sedimentary Basin,” *J. Can. Pet. Technol.*, vol. 52, no. 5, pp. 349–359, 2013, doi: 10.2118/161770-PA.

[225] B. L. Jimenez, G. Yu, R. Aguilera, and A. Settari, “Calibration of well logs with mini-frac data for

estimating the minimum horizontal stress in the tight-gas Monteith formation of the Western Canada Sedimentary Basin: A case study," *SPE Prod. Oper.*, vol. 30, no. 2, pp. 110–120, Apr. 2015, doi: 10.2118/168594-pa.

[226] S. Bachu, M. Brulotte, M. Grobe, and S. Stewart, "Earth Sciences Report 00-11: Suitability of the Alberta Subsurface for Carbon-Dioxide Sequestration in Geological Media," 2000. [Online]. Available: https://ags.aer.ca/publication/esr-2000-11.

[227] L. G. H. (Bert) van der Meer and F. Yavuz, "CO2 storage capacity calculations for the Dutch subsurface," *Energy Procedia*, vol. 1, no. 1, pp. 2615–2622, Feb. 2009, doi: 10.1016/j.egypro.2009.02.028.

[228] Y. Holubnyak *et al.*, "Calculation of CO2 Storage Capacity for Arbuckle Group in Southern Kansas: Implications for a Seismically Active Region," in *Energy Procedia*, 2017, vol. 114, pp. 4679–4689, doi: 10.1016/j.egypro.2017.03.1599.

[229] J. Kearns *et al.*, "Developing a Consistent Database for Regional Geologic CO2 Storage Capacity Worldwide," in *Energy Procedia*, 2017, vol. 114, pp. 4697–4709, doi: 10.1016/j.egypro.2017.03.1603.

[230] H. Jahediesfanjani, P. D. Warwick, and S. T. Anderson, "Estimating the pressure-limited CO2 injection and storage capacity of the United States saline formations: Effect of the presence of hydrocarbon reservoirs," *Int. J. Greenh. Gas Control*, vol. 79, pp. 14–24, Dec. 2018, doi: 10.1016/j.ijggc.2018.09.011.

[231] M. McClure *et al.*, "Nuances and frequently asked questions in field-scale hydraulic fracture modeling," *Soc. Pet. Eng. - SPE Hydraul. Fract. Technol. Conf. Exhib. 2020, HFTC 2020*, no. 1, pp. 1–20, 2020, doi: 10.2118/199726-ms.

[232] W. McClure, Mark, B. Mohsen, S. Sogo, and H. Jian, "Fully coupled hydromechanical simulation of hydraulic fracturing in 3D discrete-fracture networks," *SPE J.*, vol. 21, no. 4, pp. 1302–1320, 2016, doi: 10.2118/173354-pa.

[233] A. Lucier and M. Zoback, "Assessing the economic feasibility of regional deep saline aquifer CO2 injection and storage: A geomechanics-based workflow applied to the Rose Run sandstone in Eastern Ohio, USA," *Int. J. Greenh. Gas Control*, vol. 2, no. 2, pp. 230–247, 2008, doi: 10.1016/j.ijggc.2007.12.002.

[234] M. Samaroo, R. Chalaturnyk, M. Dusseault, J. F. Chow, and H. Custers, "Assessment of the Brittle – Ductile State of Major Injection and Confining Formations in the Alberta Basin," *Energies*, vol. 15, no. 6877, pp. 1–24, 2022, doi: 10.3390/en15196877.

[235] Alberta Energy Regulator, "Directive 056: Energy Development Applications and Schedules," Alberta Energy Regulator, Calgary, AB Canada, 2021. [Online]. Available: https://static.aer.ca/prd/documents/directives/directive-056.pdf.

[236] Shell Canada Ltd, "Drilling Completion Tour Report Well ID 8-19-059-20W4M," Calgary, AB, 2010. [Online]. Available: https://www.aer.ca/providing-information/about-the-aer/contact-us/information-services-and-facilities/tour-report-request.

[237] K. Reiter and O. Heidbach, "3-D geomechanical-numerical model of the contemporary crustal stress state in the Alberta Basin (Canada)," *Solid Earth*, vol. 5, no. 2, pp. 1123–1149, 2014, doi: 10.5194/se-5-1123-2014.

[238] J. Di, "Permeability Characterization and Prediction in a Tight Oil Reservoir, Edson Field, Alberta," 2015. doi: 10.11575/PRISM/27310.

[239] Shell Canada Ltd. and Shell Canada, "Generation-4 Integrated Reservoir Modeling Report for the Quest CCS Project," Calgary, AB, 2011. [Online]. Available: https://open.alberta.ca/dataset/46ddba1a-7b86-4d7c-b8b6-8fe33a60fada/resource/03c38d0b-5f96-47a5-8f0b-503e62e6240e/download/generation-4integratedreservoirmodelingreport.pdf.

[240] S. Bachu, "Drainage and imbibition CO2/brine relative permeability curves at in situ conditions for sandstone formations in western Canada," in *Energy Procedia*, 2013, vol. 37, pp. 4428–4436, doi: 10.1016/j.egypro.2013.07.001.

[241] P. Tawiah, J. Duer, S. L. Bryant, S. Larter, S. O'Brien, and M. Dong, "CO2 injectivity behaviour under non-isothermal conditions – Field observations and assessments from the Quest CCS operation," *Int. J. Greenh. Gas Control*, Jan. 2019, doi: 10.1016/j.ijggc.2019.102843.

[242] L. P. Qiao, R. C. K. Wong, R. Aguilera, and A. Kantzas, “Determination of Biot’s effective stress parameter for permeability of Nikanassin Sandstone,” *Can. Int. Pet. Conf. 2009, CIPC 2009*, no. 3, pp. 1–5, 2009, doi: 10.2118/2009-105.

[243] R. Suarez-Rivera and E. Fjær, “Evaluating the poroelastic effect on anisotropic, organic-rich, mudstone systems,” *Rock Mech. Rock Eng.*, vol. 46, no. 3, pp. 569–580, 2013, doi: 10.1007/s00603-013-0374-y.

[244] M. McClure, C. Kang, S. Medam, and C. Hewson, “ResFrac Technical Writeup,” 2022. [Online]. Available: http://arxiv.org/abs/1804.02092.

[245] K. Pyo, M. Powell, J. Van Nieuwkerk, and P. West, “CO2 Flooding in Joffre Viking Pool,” *Pet. Soc. Can. Int. Pet. Conf.*, 2003.

[246] L. Meng *et al.*, “Risking fault reactivation induced by gas injection into depleted reservoirs based on the heterogeneity of geomechanical properties of fault zones,” *Pet. Geosci.*, vol. 23, no. 1, pp. 29–38, 2017, doi: 10.1144/petgeo2016-031.

[247] H. Zhao, X. Liao, Y. Chen, and X. Zhao, “Sensitivity analysis of CO2 sequestration in saline aquifers,” *Pet. Sci.*, vol. 7, no. 3, pp. 372–378, 2010, doi: 10.1007/s12182-010-0080-2.

[248] S. Wang and T. K. Tokunaga, “Capillary Pressure-Saturation Relations for Supercritical CO2 and Brine in Limestone/Dolomite Sands: Implications for Geologic Carbon Sequestration in Carbonate Reservoirs,” *Environ. Sci. Technol.*, vol. 49, no. 12, pp. 7208–7217, 2015, doi: 10.1021/acs.est.5b00826.

[249] O. J. Friesen, S. E. Dashtgard, J. Miller, L. Schmitt, and C. Baldwin, “Permeability heterogeneity in bioturbated sediments and implications for waterflooding of tight-oil reservoirs, Cardium Formation, Pembina Field, Alberta, Canada,” *Mar. Pet. Geol.*, vol. 82, pp. 371–387, 2017, doi: 10.1016/j.marpetgeo.2017.01.019.

[250] G. Fowler, M. McClure, and C. Cipolla, “A Utica case study: The impact of permeability estimates on history matching, fracture length, and well spacing,” *Proc. - SPE Annu. Tech. Conf. Exhib.*, vol. 2019-Septe, 2019, doi: 10.2118/195980-ms.

[251] S. Bachu and J. R. Underschultz, “Regional-scale porosity and permeability variations, Peace River Arch Area, Alberta, Canada,” *Am. Assoc. Pet. Geol. Bull.*, vol. 76, no. 4, pp. 547–562, 1992, doi: https://doi.org/10.1306/BDFF886C-1718-11D7-8645000102C1865D.

[252] E. B. Bekele, M. A. Person, B. J. Rostron, and R. Barnes, “Modeling secondary oil migration with core-scale data: Viking Formation, Alberta basin,” *Am. Assoc. Pet. Geol. Bull.*, vol. 86, no. 1, pp. 55–74, 2002.

[253] W. E. Sanford, “Estimating regional scale permeability-depth relations ina fractured-rock terrain using groundwater-flow model calibration,” *Hydrogeol. J.*, vol. 25, no. 2, pp. 405–419, 2017, doi: 10.1007/s10040-016-1483-y.

[254] S. Zheng, P. W. M. Corbett, A. Ryseth, and G. Stewart, “Uncertainty in well test and core permeability analysis: a case study in fluvial channel reservoirs, northern North Sea, Norway,” *Am. Assoc. Pet. Geol. Bull.*, vol. 84, no. 12, pp. 1929–1954, 2000, doi: https://doi.org/10.1306/8626C72B-173B-11D7-8645000102C1865D.

[255] J. E. Amthor, E. W. Mountjoy, and H. G. Machel, “Regional-scale porosity and permeability variations in Upper Devonian Leduc buildups: implications for reservoir development and prediction in carbonates,” *Am. Assoc. Pet. Geol. Bull.*, vol. 78, no. 10, pp. 1541–1558, 1994, doi: 10.1306/a25ff215-171b-11d7-8645000102c1865d.

[256] I. Dahabreh *et al.*, “Modeling and Simulation in the Context of Health Technology Assessment: Review of Existing Guidance, Future Research Needs, and Validity Assessment,” *AHRQ Agency Healthc. Res. Qual.*, p. 98, 2017, [Online]. Available: http://www.epistemonikos.org/documents/a8200a083c5eb3274b5976689871158b216ae1e8.

[257] D. S. Oliver and Y. Chen, “Recent progress on reservoir history matching: A review,” *Comput. Geosci.*, vol. 15, no. 1, pp. 185–221, 2011, doi: 10.1007/s10596-010-9194-2.

[258] Shell Canada Ltd, “Quest Carbon Capture and Storage Project - 2021 Annual Status Report,” Edmonton, AB, 2021. [Online]. Available: https://open.alberta.ca/dataset/d5694c02-019d-4650-8b09-

3b5a9afff181/resource/64c95768-5d47-4662-a54a-3255c1b2d98a/download/quest-annual-status-report-alberta-energy-regulator-2020.pdf.

[259] N. Smith *et al.*, "GHGT-15 Quest CCS facility - Halite Injectivity Damage Remediation in CO2 Injection Wells," *SSRN Electron. J.*, no. March, 2021, doi: 10.2139/ssrn.3820898.

[260] O. Tucker, M. Holley, R. Metcalfe, and S. Hurst, "Containment risk management for CO2 storage in a depleted gas field, UK North Sea," in *Energy Procedia*, 2013, vol. 37, pp. 4804–4817, doi: 10.1016/j.egypro.2013.06.390.

[261] R. Walke, R. Metcalfe, L. Limer, P. Maul, A. Paulley, and D. Savage, "Experience of the application of a database of generic Features, Events and Processes (FEPs) targeted at geological storage of CO2," *Energy Procedia*, vol. 4, pp. 4059–4066, 2011, doi: 10.1016/j.egypro.2011.02.348.

[262] R. Metcalfe *et al.*, "A unified approach to Performance Assessment (PA) of geological CO2 storage," in *Energy Procedia*, Feb. 2009, vol. 1, no. 1, pp. 2503–2510, doi: 10.1016/j.egypro.2009.02.013.

[263] S. Bachu, C. Hawkes, D. Lawton, M. Pooladi-Darvish, and E. Perkins, "CCS Site Characterization Technical Study Report No. 2009/10," Edmonton, Alberta, 2009. [Online]. Available: https://www.globalccsinstitute.com/archive/hub/publications/95881/ccs-site-characterisation-criteria.pdf.

[264] Shell Canada Quest Subsurface Team, "Quest CCS Project: Injectivity Risk and Uncertainty Review," Edmonton, AB, 2011. [Online]. Available: https://open.alberta.ca/dataset/46ddba1a-7b86-4d7c-b8b6-8fe33a60fada/resource/81708751-f63e-4c88-9789-cd48de01f9e2/download/injectivityriskanduncertaintyreview.pdf.

[265] P. Ringrose, S. Greenberg, S. Whittaker, B. Nazarian, and V. Oye, "Building Confidence in CO2 Storage Using Reference Datasets from Demonstration Projects," *Energy Procedia*, vol. 114, no. November 2016, pp. 3547–3557, 2017, doi: 10.1016/j.egypro.2017.03.1484.

[266] W. A. Peck, K. A. Glazewski, R. C. L. Klenner, C. D. Gorecki, E. N. Steadman, and J. A. Harju, "A workflow to determine CO2 storage potential in deep saline formations," *Energy Procedia*, vol. 63, pp. 5231–5238, 2014, doi: 10.1016/j.egypro.2014.11.554.

[267] S. Bachu, "Review of CO2 storage efficiency in deep saline aquifers," *Int. J. Greenh. Gas Control*, vol. 40, pp. 188–202, Oct. 2015, doi: 10.1016/j.ijggc.2015.01.007.

[268] S. Bachu, "Screening and ranking of sedimentary basins for sequestration of CO2 in geological media in response to climate change," *Environ. Geol.*, vol. 44, no. 3, pp. 277–289, Jun. 2003, doi: 10.1007/s00254-003-0762-9.

[269] A. Jafari and S. Bachu, "Evaluation of CO2 storage capacity in Devonian hydrocarbon reservoirs for emissions from oil sands operations in the Athabasca area, Canada," *Energy Procedia*, vol. 63, pp. 5222–5230, 2014, doi: 10.1016/j.egypro.2014.11.553.

[270] F. Riis and E. Halland, "CO2 storage atlas of the Norwegian Continental shelf: Methods used to evaluate capacity and maturity of the CO2 storage potential," *Energy Procedia*, vol. 63, no. 1876, pp. 5258–5265, 2014, doi: 10.1016/j.egypro.2014.11.557.

[271] L. Rock *et al.*, "The Quest CCS Project: 1st Year Review Post Start of Injection," in *Energy Procedia*, 2017, vol. 114, no. November 2016, pp. 5320–5328, doi: 10.1016/j.egypro.2017.03.1654.

[272] J. Carneiro, R. Martinez, I. Suaréz, Y. Zarhloule, and A. Rimi, "Injection rates and cost estimates for CO2 storage in the west Mediterranean region," *Environ. Earth Sci.*, vol. 73, no. 6, pp. 2951–2962, 2015, doi: 10.1007/s12665-015-4029-z.

[273] Government of Alberta, "Specified Gas Emitters Regulation, Alta Reg 139/2007," Canada, 2007. [Online]. Available: https://www.canlii.org/en/ab/laws/regu/alta-reg-139-2007/latest/alta-reg-139-2007.html.

[274] M. A. Celia, S. Bachu, J. M. Nordbotten, and K. W. Bandilla, "Status of CO2 storage in deep saline aquifers with emphasis on modeling approaches and practical simulations," *J. Am. Water Resour. Assoc.*, vol. 5, no. 3, pp. 2–2, 2015, doi: 10.1111/j.1752-1688.1969.tb04897.x.

[275] Enhance Energy Inc., "Clive Leduc Field Monitoring Measurement and Verification Plan," Edmonton, AB,

2019. [Online]. Available: https://open.alberta.ca/dataset/90f61413-0ef1-45a4-9e1c-6bff7c23fd7e/resource/99fae078-1316-432b-8447-acd74bd1abb0/download/energy-actl-enhance-energy-clive-leduc-field-mmv-plan-2019-07.pdf.

7.0 Appendix A (Supplementary Materials)

The figures below provide the per-well water injection rate frequency distributions for the (approximately 4,000) water disposal wells that operated over the period January 1962-December 2022 in each formation of interest in the Alberta Basin. These distributions were used to history match the regional-scale permeability estimates for the formations of interest in this study. They can also be used to constrain long-term per-well ranges of water injection for proposed future water disposal activities in these formations, as well as to estimate the probability that a target water injection rate may be achievable for proposed commercial-scale projects. Such information can help to enhance and calibrate future fluid disposal project design data and models as required for the Alberta Basin.

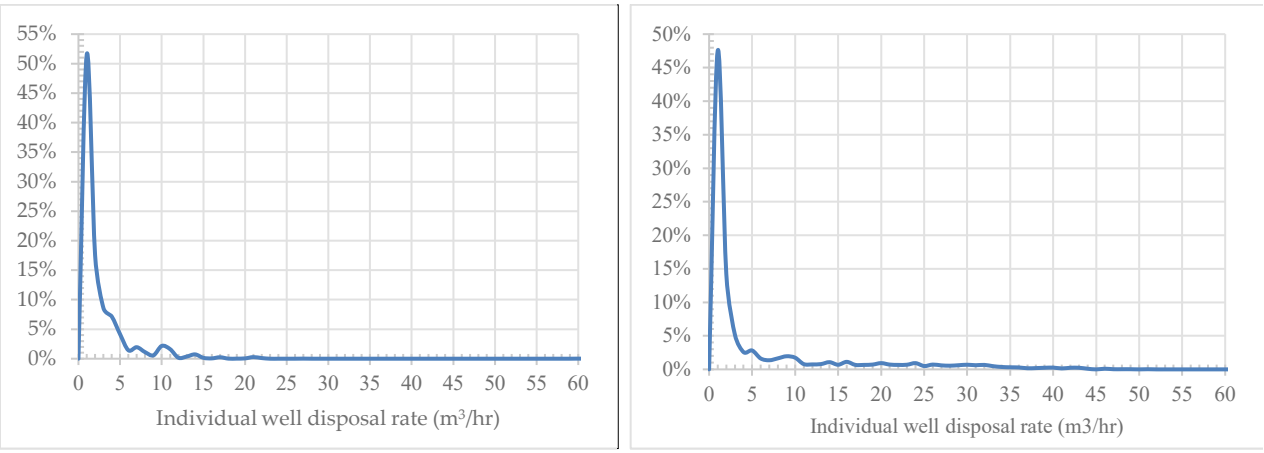

(a) **(b)**

*Figure 30. Historical per-well water injection rate (X-axis) frequency (Y-axis) distributions (January 1962-December 2022) in **(a)** the Belly River Formation; **(b)** the Cardium Formation.*

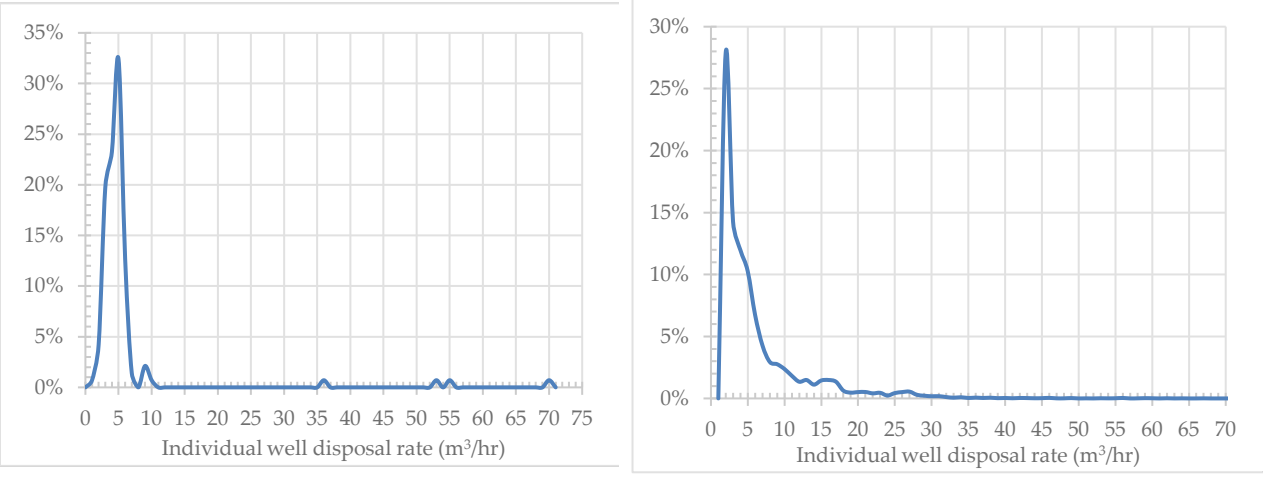

(a) **(b)**

*Figure 31. Historical per-well injection rate (X-axis) frequency (Y-axis) distributions (January 1962-December 2022) in (**a**) the Dunvegan Formation; (**b**) the Viking Formation.*

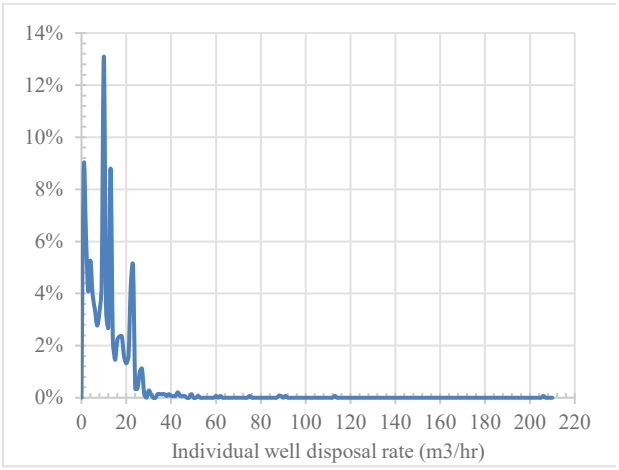

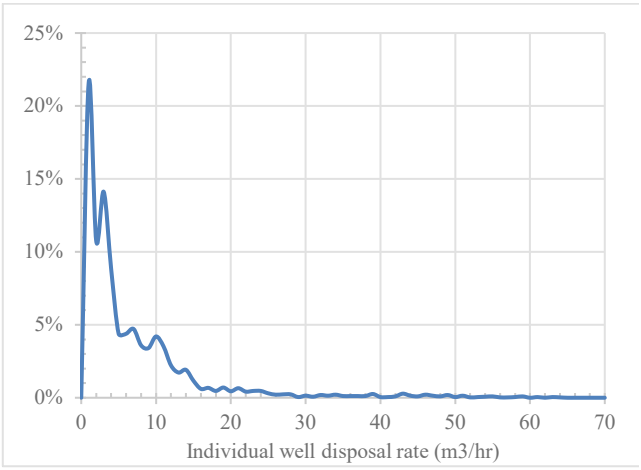

(a) **(b)**

*Figure 32. Historical per-well water injection rate (X-axis) frequency (Y-axis) distributions (January 1962-December 2022) in (**a**) the Paddy Formation; (**b**) the Cadotte Formation.*

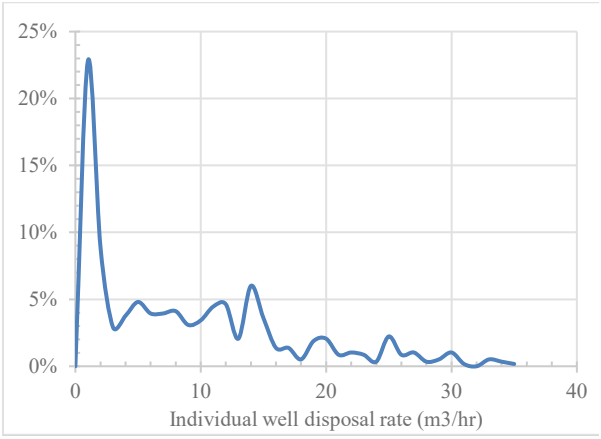

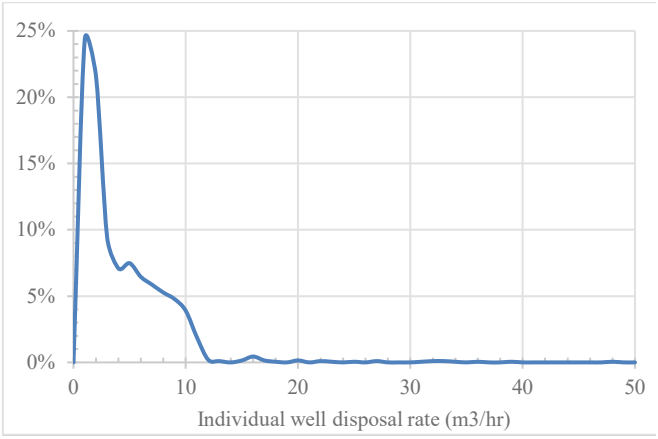

(a) **(b)**

*Figure 33. Historical per-well water injection rate (X-axis) frequency (Y-axis) distributions (January 1962-December 2022) in (**a**) the Peace River Formation; (**b**) the Colony Formation.*

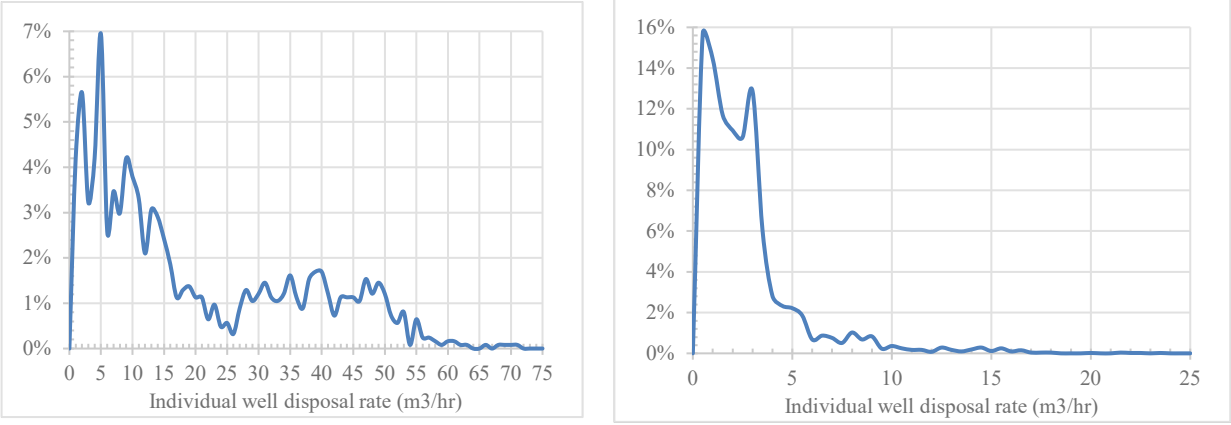

(a) **(b)**

*Figure 34. Historical per-well water injection rate (X-axis) frequency (Y-axis) distributions (January 1962-December 2022) in (**a**) the McLaren Formation; (**b**) the Notikewin Formation.*

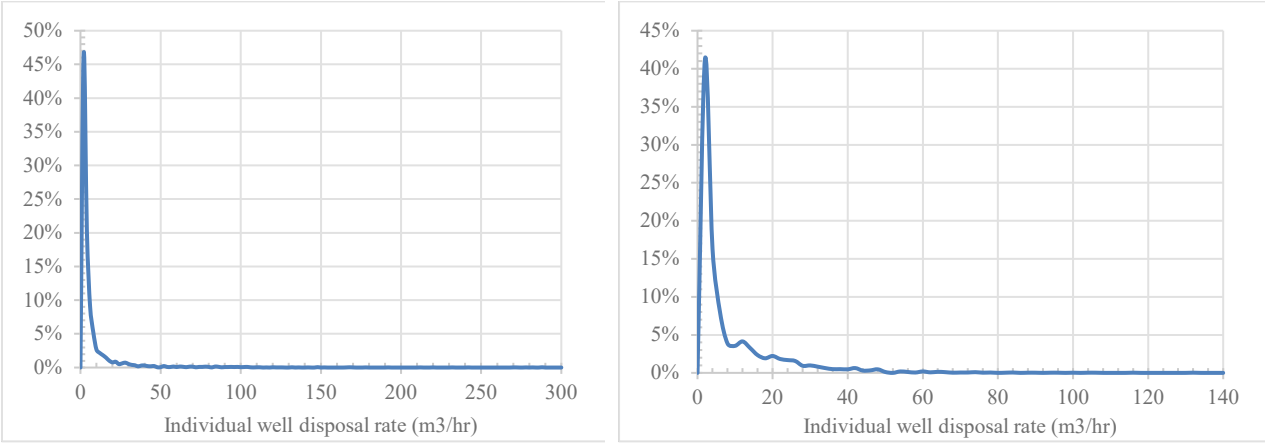

(a) **(b)**

*Figure 35. Historical per-well water injection rate (X-axis) frequency (Y-axis) distributions (January 1962-December 2022) in (**a**) the Grand Rapids Formation; (**b**) the Clearwater Sandstone Formation.*

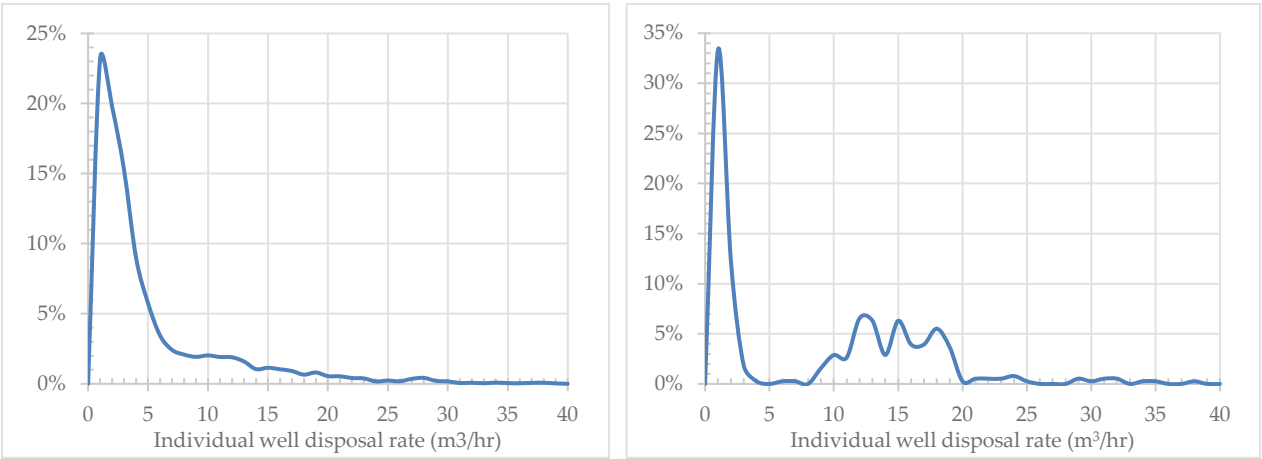

(a) **(b)**

*Figure 36. Historical per-well water injection rate (X-axis) frequency (Y-axis) distributions (January 1962-December 2022) in **(a)** the Sparky Formation; **(b)** the Falher Formation.*

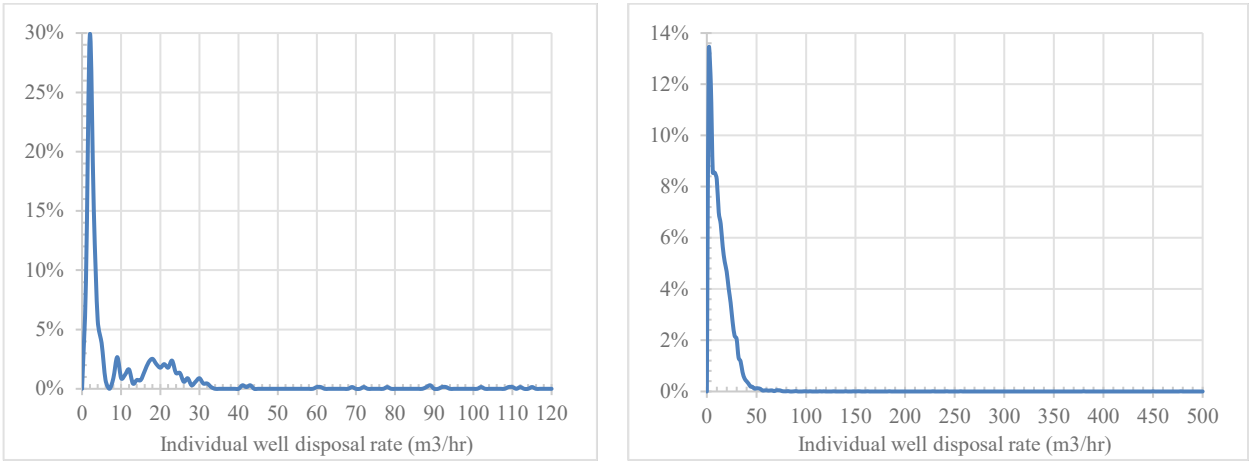

(a) **(b)**

*Figure 37. Historical per-well water injection rate (X-axis) frequency (Y-axis) distributions (January 1962-December 2022) in **(a)** the Rex Formation; **(b)** the Lloydminster Sandstone Formation.*

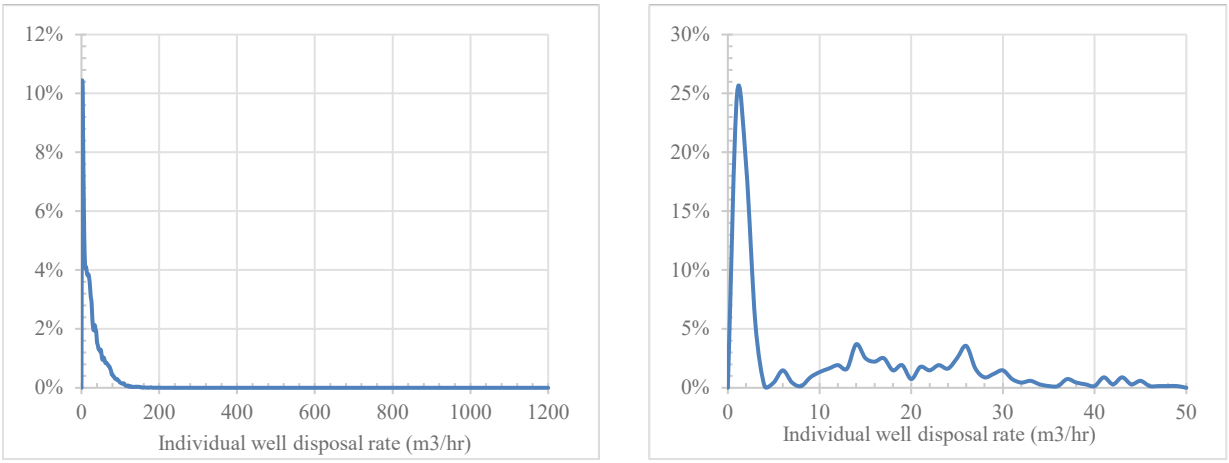

(a) **(b)**

*Figure 38. Historical per-well water injection rate (X-axis) frequency (Y-axis) distributions (January 1962-December 2022) in **(a)** the Glauconitic Formation; **(b)** the Ostracod Formation.*

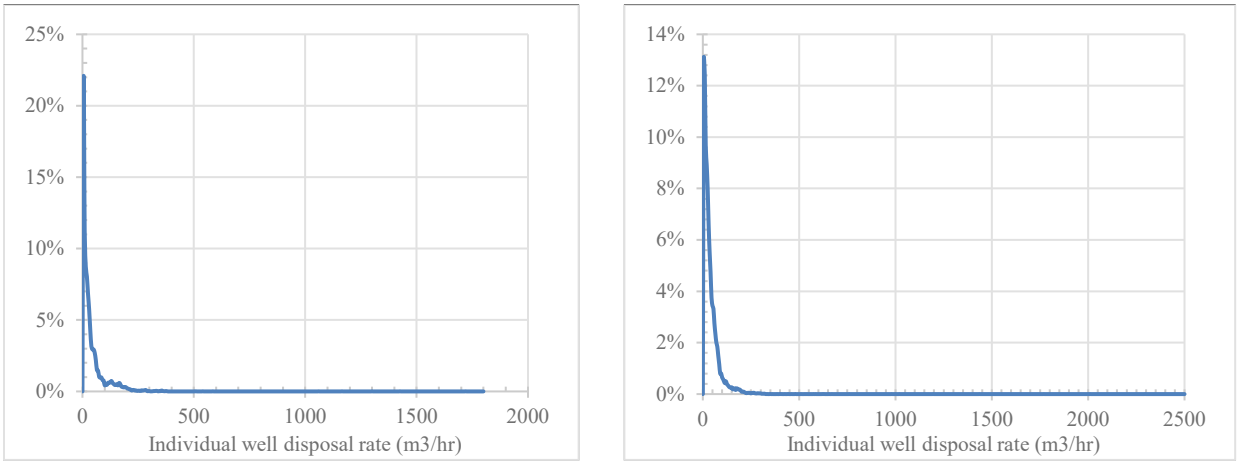

(a) **(b)**

*Figure 39. Historical per-well water injection rate (X-axis) frequency (Y-axis) distributions (January 1962 – December 2022) in (**a**) the Cummings Formation; (**b**) the Dina Formation.*

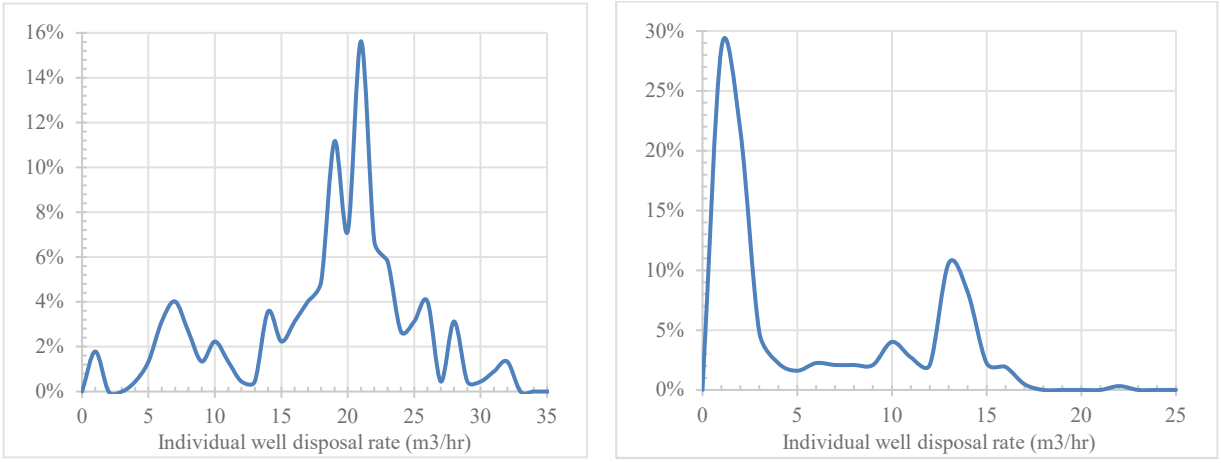

*Figure 40. Historical per-well water injection rate (X-axis) frequency (Y-axis) distributions (January 1962-December 2022) in (**a**) the Detrital Formation; (**b**) the Spirit River Formation.*

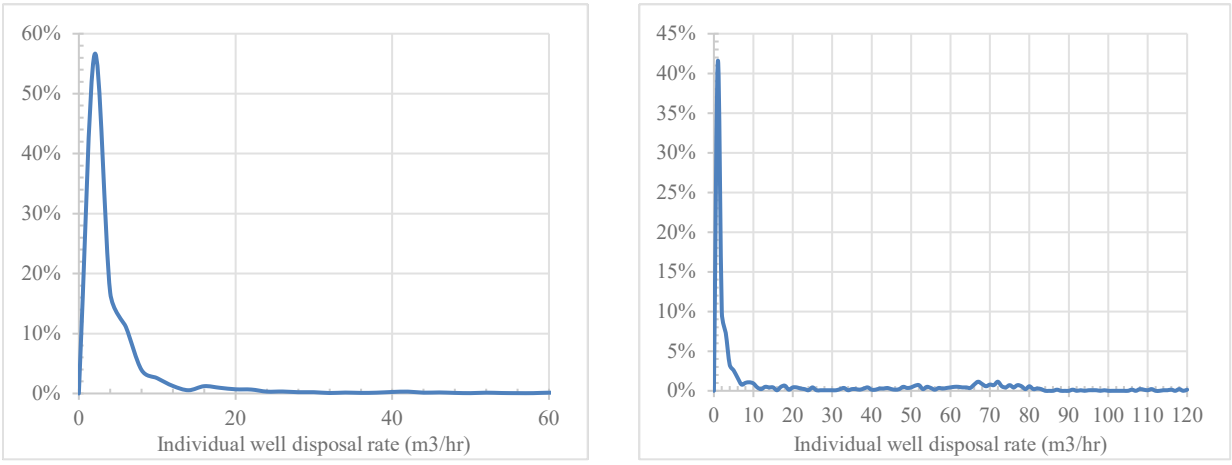

(a) **(b)**

*Figure 41. Historical per-well water injection rate (X-axis) frequency (Y-axis) distributions (January 1962-December 2022) in (**a**) the Bluesky Formation; (**b**) the Wabiskaw Sandstone Formation.*

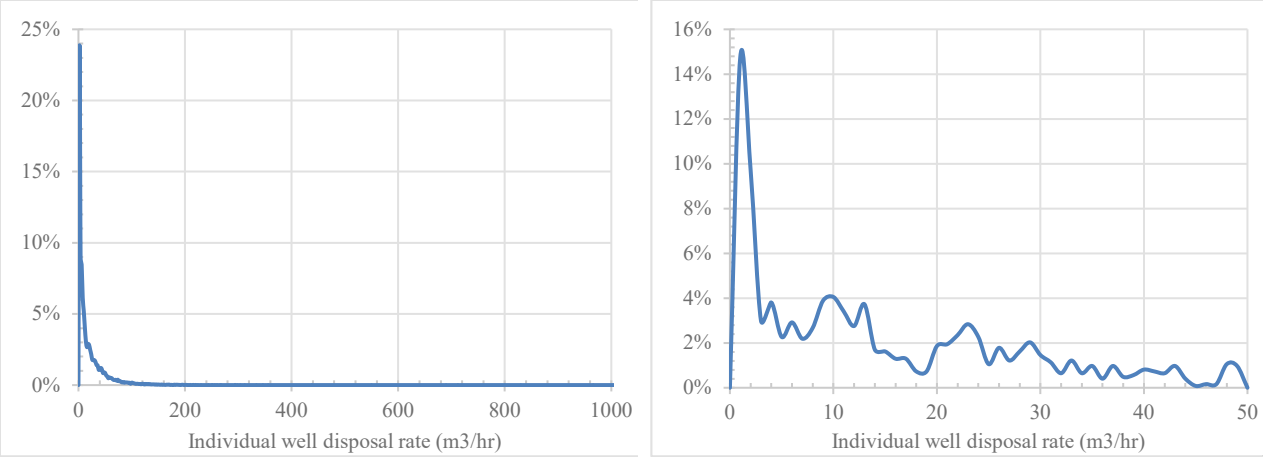

(a) **(b)**

*Figure 42. Historical per-well water injection rate (X-axis) frequency (Y-axis) distributions (January 1962-December 2023) in (**a**) the McMurray Formation; (**b**) the Cadomin Formation.*

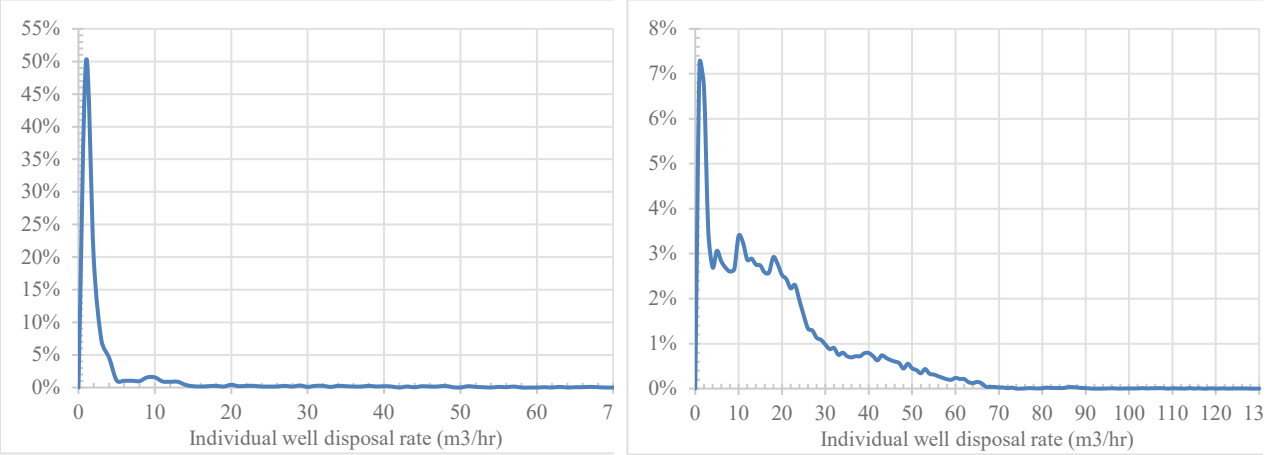

(a) **(b)**

*Figure 43. Historical per-well water injection rate (X-axis) frequency (Y-axis) distributions (January 1962-December 2022) in (**a**) the Gething Formation; (**b**) the Sunburst Formation.*

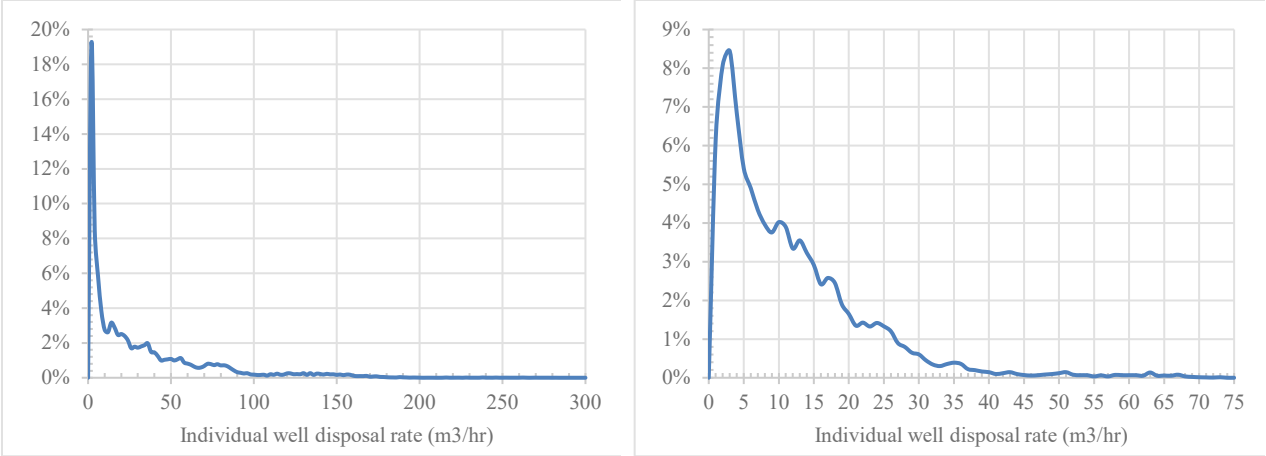

(a) **(b)**

*Figure 44. Historical per-well water injection rate (X-axis) frequency (Y-axis) distributions (January 1962-December 2022) in (**a**) the Ellerslie Formation; (**b**) the Taber Formation.*

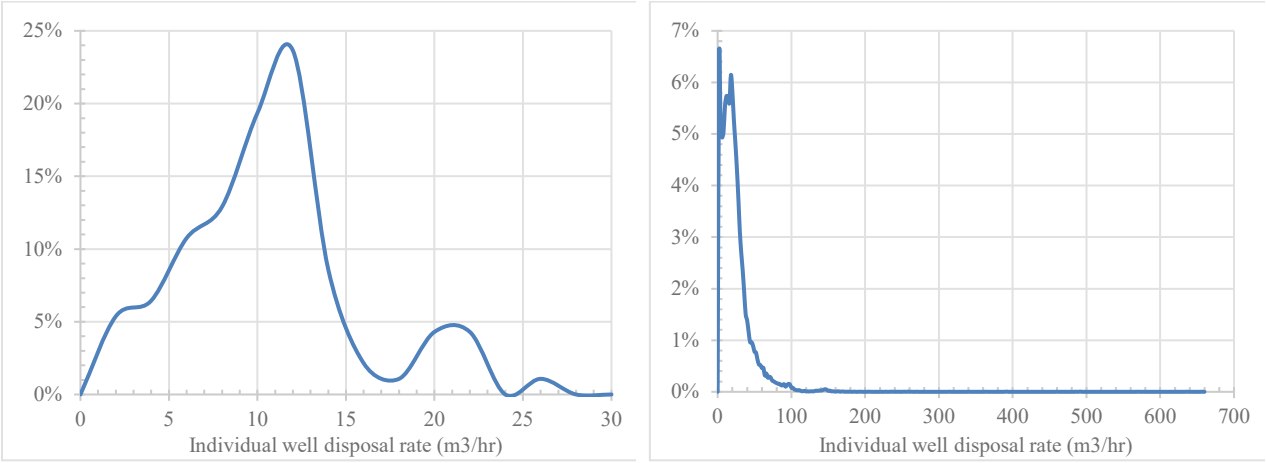

(a) **(b)**

*Figure 45. Historical per-well water injection rate (X-axis) frequency (Y-axis) distributions (January 1962-December 2022) in (**a**) the Nikanassin Formation; (**b**) the Sawtooth Formation.*

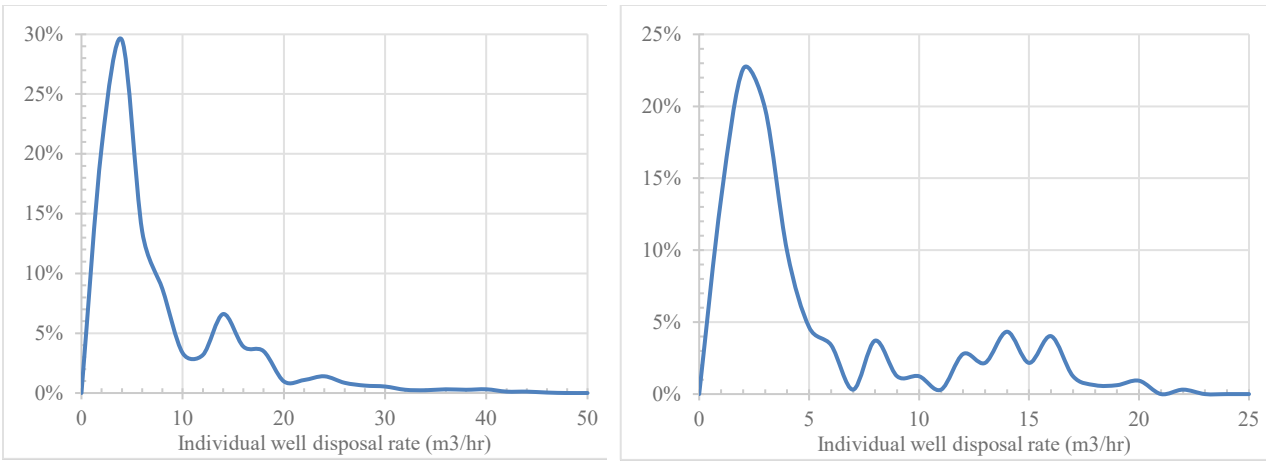

(a) **(b)**

*Figure 46. Historical per-well water injection rate (X-axis) frequency (Y-axis) distributions (January 1962-December 2022) in (**a**) the Nordegg Formation; (**b**) the Baldonnell Formation.*

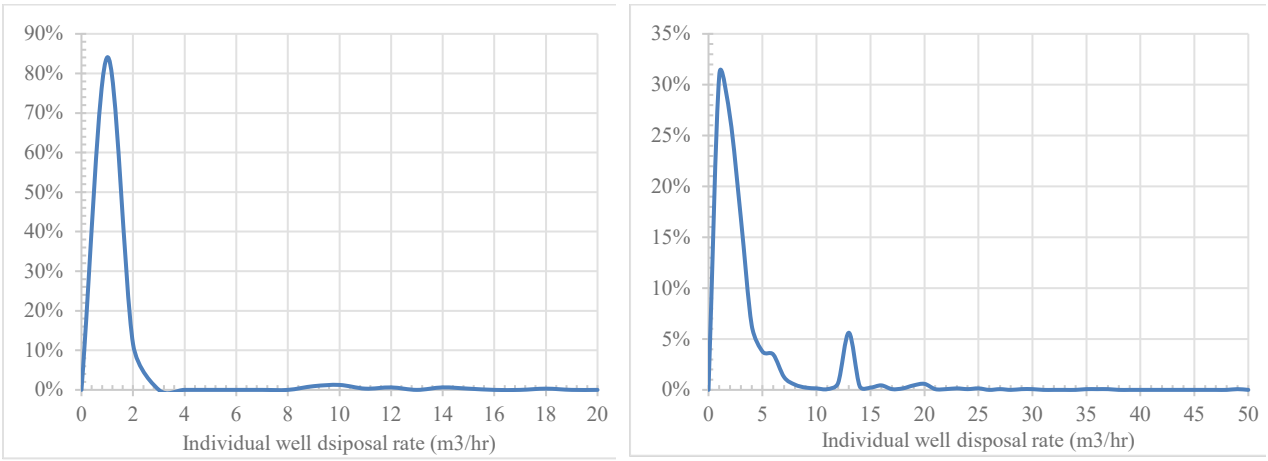

(a) **(b)**

*Figure 47. Historical per-well water injection rate (X-axis) frequency (Y-axis) distributions (January 1962-December 2022) in (**a**) the Boundary Lake Formation; (**b**) the Charlie Lake Formation.*

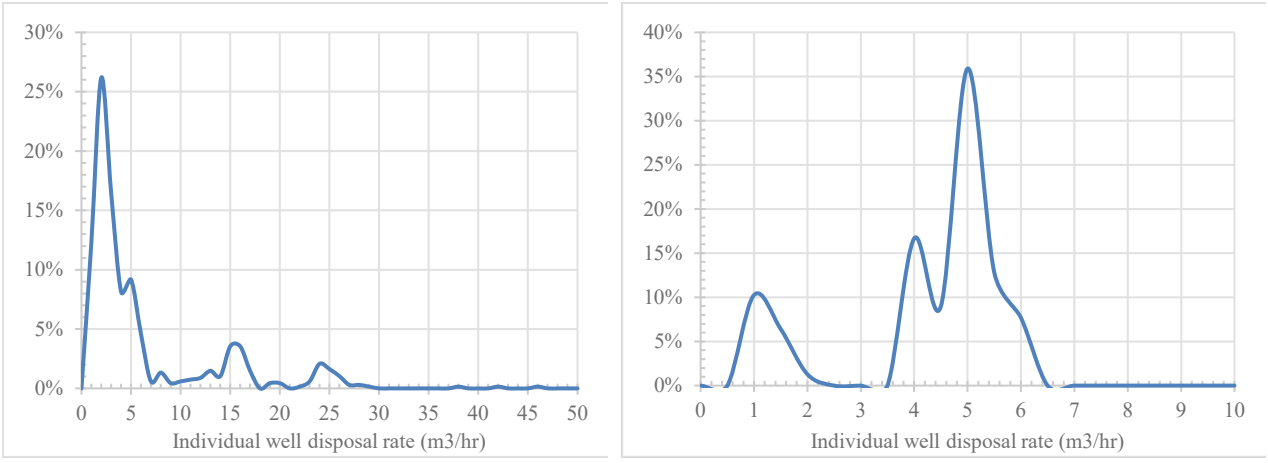

*Figure 48. Historical per-well water injection rate (X-axis) frequency (Y-axis) distributions (January 1962-December 2022) in (**a**) the Halfway Formation; (**b**) the Doig Formation.*

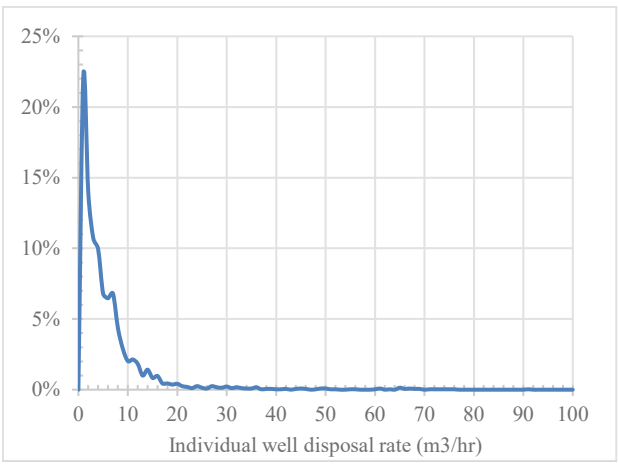

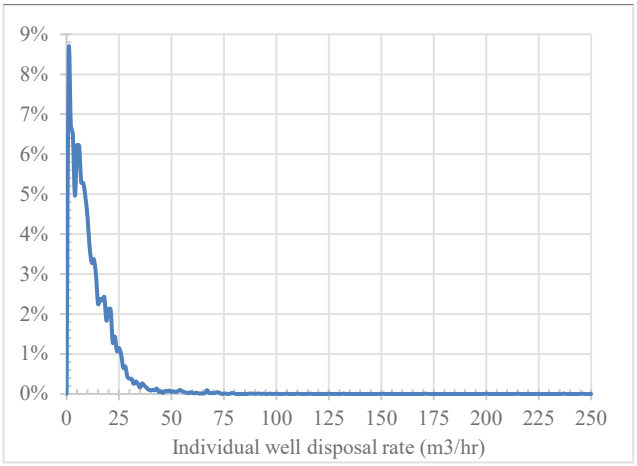

(a) **(b)**

*Figure 49. Historical per-well water injection rate (X-axis) frequency (Y-axis) distributions (January 1962-December 2022) in (**a**) the Montney Formation; (**b**) the Belloy Formation.*

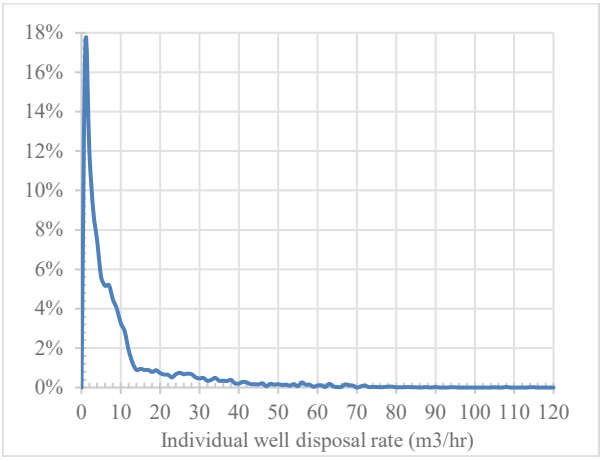

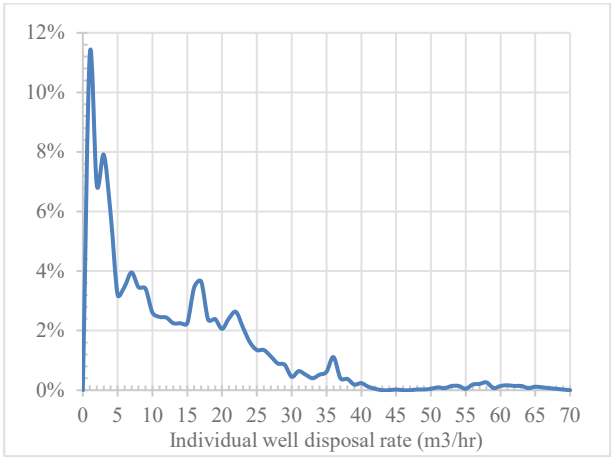

(a) **(b)**

*Figure 50. Historical per-well water injection rate (X-axis) frequency (Y-axis) distributions (January 1962-December 2022) in (**a**) the Debolt Formation; (**b**) the Livingstone Formation.*

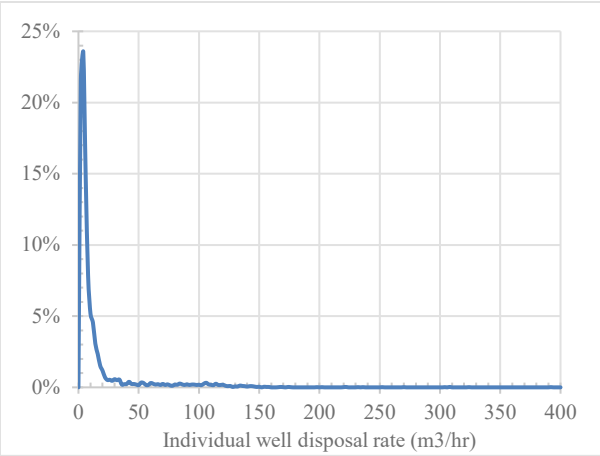

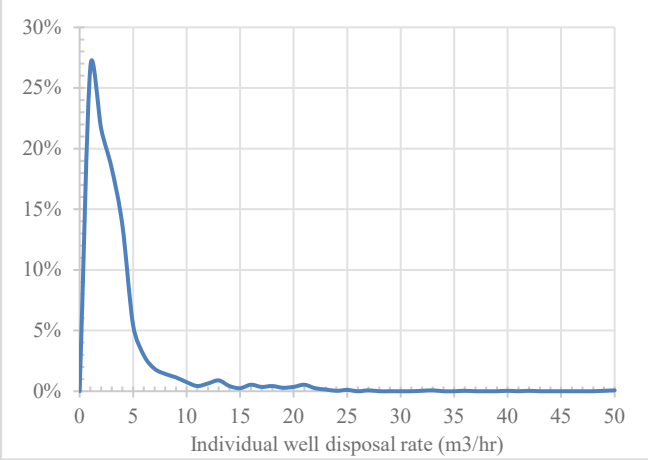

(a) **(b)**

*Figure 51. Historical per-well water injection rate (X-axis) frequency (Y-axis) distributions (January 1962-December 2022) in (**a**) the Elkton Formation; (**b**) the Turner Valley Formation.*

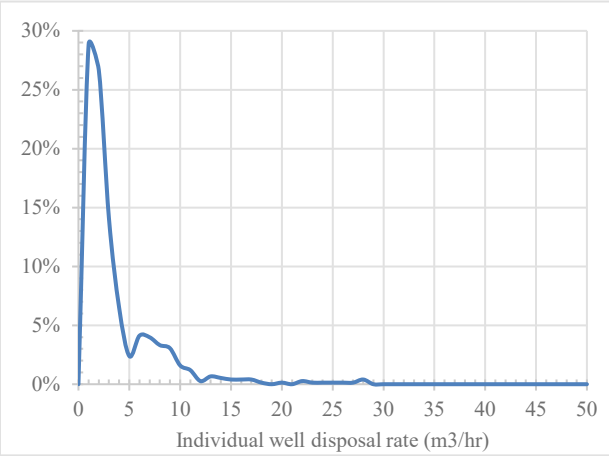

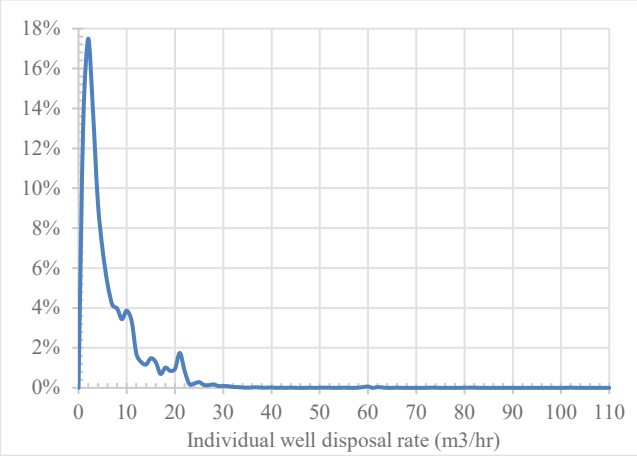

(a) **(b)**

*Figure 52. Historical per-well water injection rate (X-axis) frequency (Y-axis) distributions (January 1962-December 2022) in (**a**) the Shunda Formation; (**b**) the Pekisko Formation.*

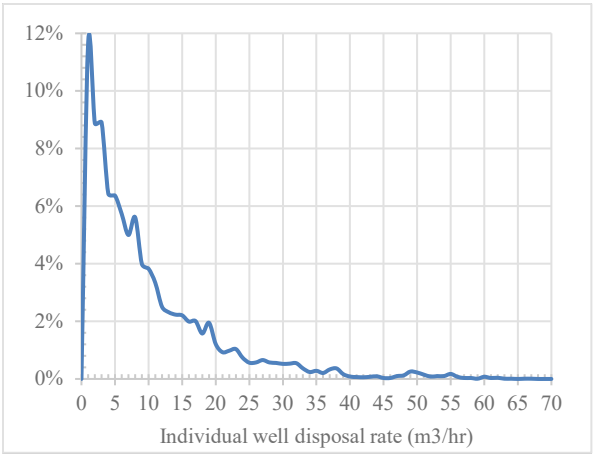

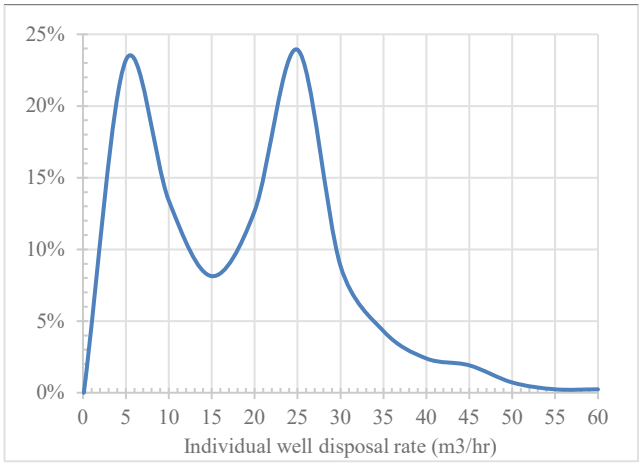

(a) **(b)**

*Figure 53. Historical per-well water injection rate (X-axis) frequency (Y-axis) distributions (January 1962-December 2022) in (**a**) the Banff Formation; (**b**) the Blueridge Formation.*

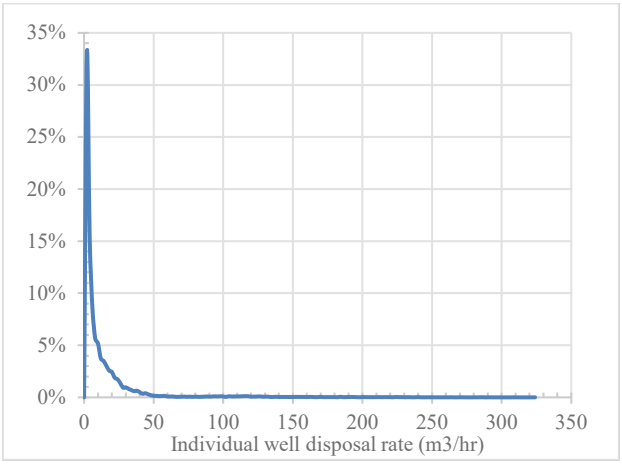

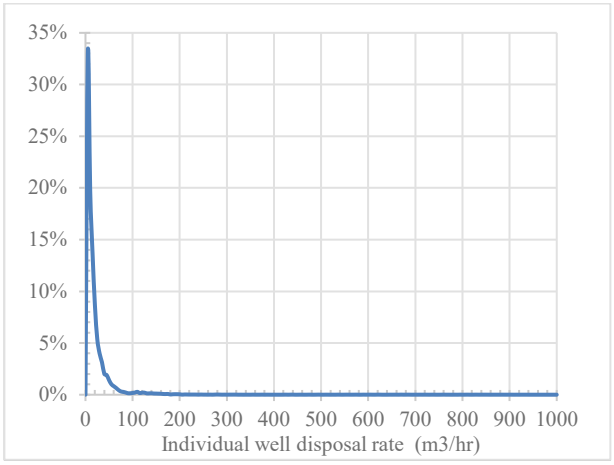

(a) **(b)**

*Figure 54. Historical per-well water injection rate (X-axis) frequency (Y-axis) distributions (January 1962-December 2022) in (**a**) the Wabamun Formation; (**b**) the Nisku Formation.*

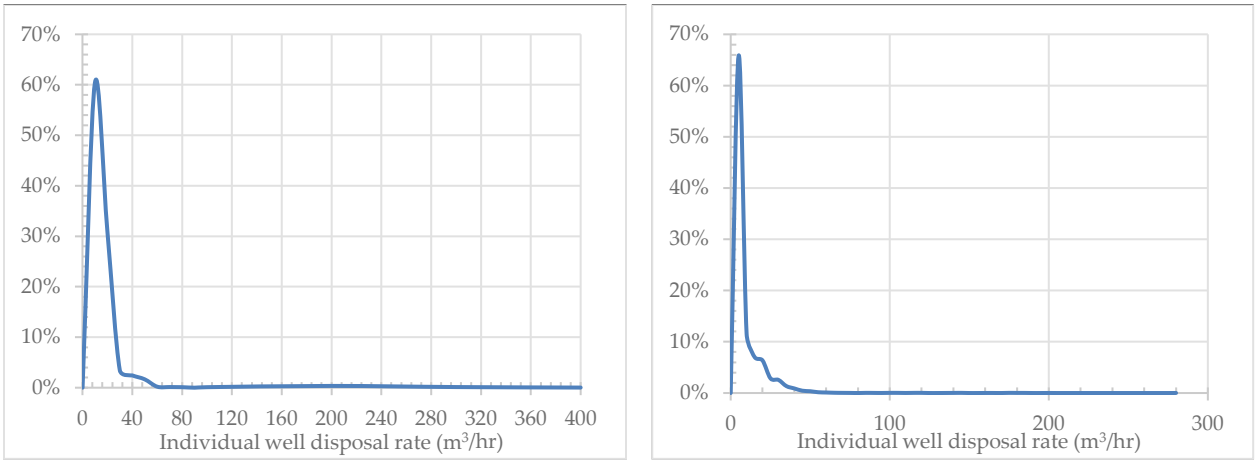

(a) **(b)**

*Figure 55. Historical per-well water injection rate (X-axis) frequency (Y-axis) distributions (January 1962-December 2022) in (**a**) the Arcs Formation; (**b**) the Grosmont Formation.*

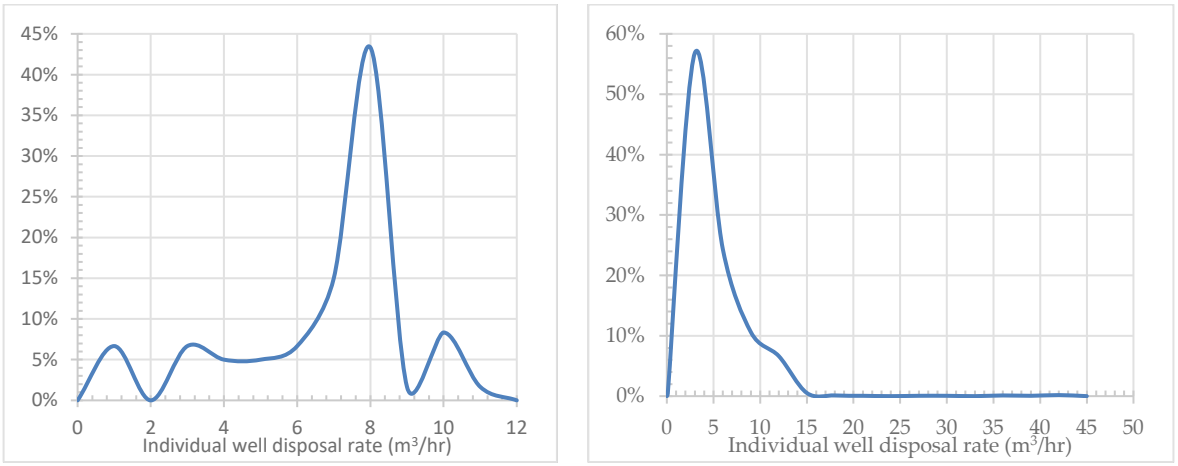

(a) **(b)**

*Figure 56. Historical per-well water injection rate (X-axis) frequency (Y-axis) distributions (January 1962-December 2022) in (**a**) the Peechee Formation; (**b**) the Camrose Formation.*

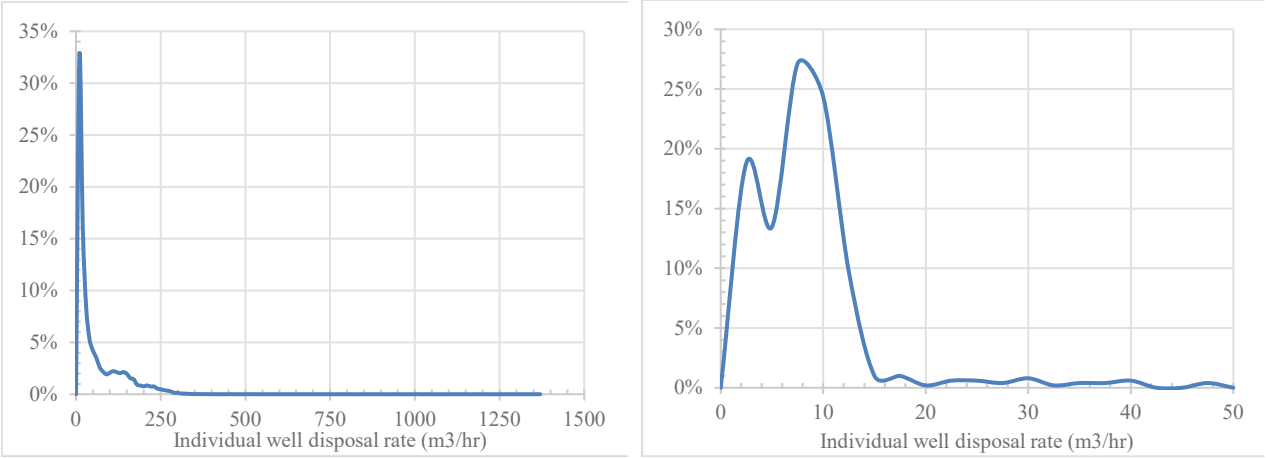

(a) **(b)**

*Figure 57. Historical per-well water injection rate (X-axis) frequency (Y-axis) distributions (January 1962-December 2022) in (**a**) the Leduc Formation; (**b**) the Duvernay Formation.*

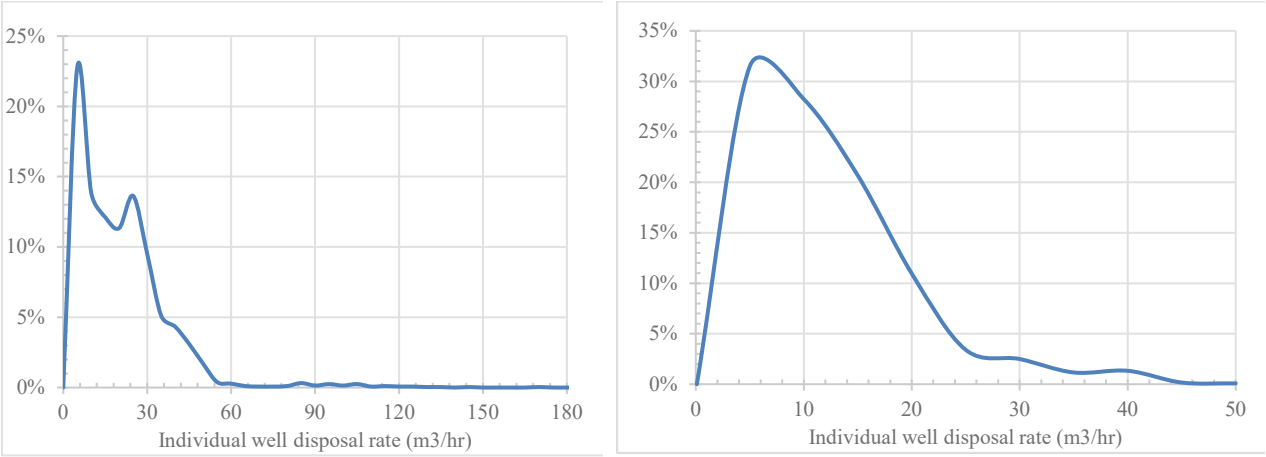

(a) **(b)**

*Figure 58. Historical per-well water injection rate (X-axis) frequency (Y-axis) distributions (January 1962-December 2022) in (**a**) the Cooking Lake Formation; (**b**) the Cairn Formation.*

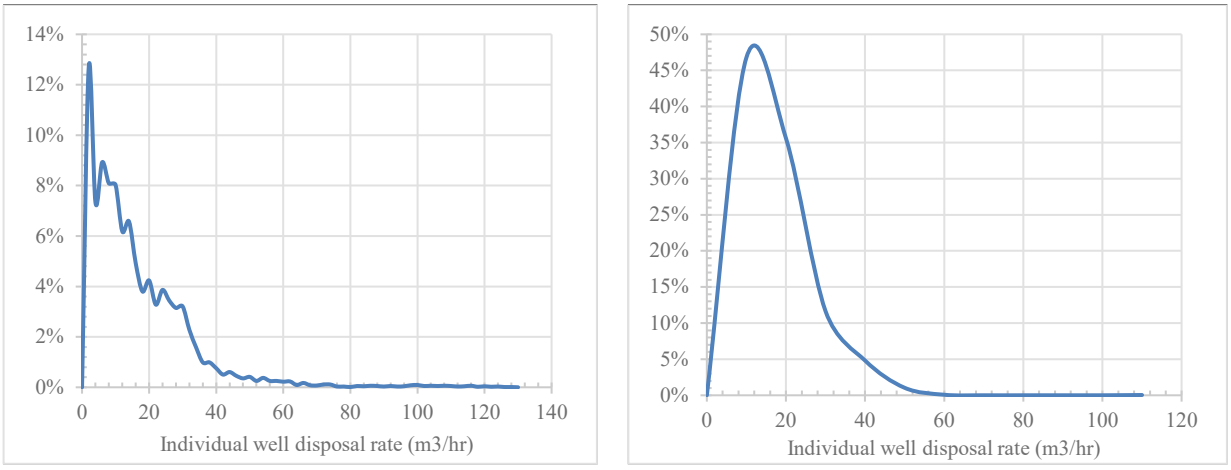

(a) **(b)**

*Figure 59. Historical per-well water injection rate (X-axis) frequency (Y-axis) distributions (January 1962-December 2022) in (**a**) the Slave Point Formation; (**b**) the Gilwood Formation.*

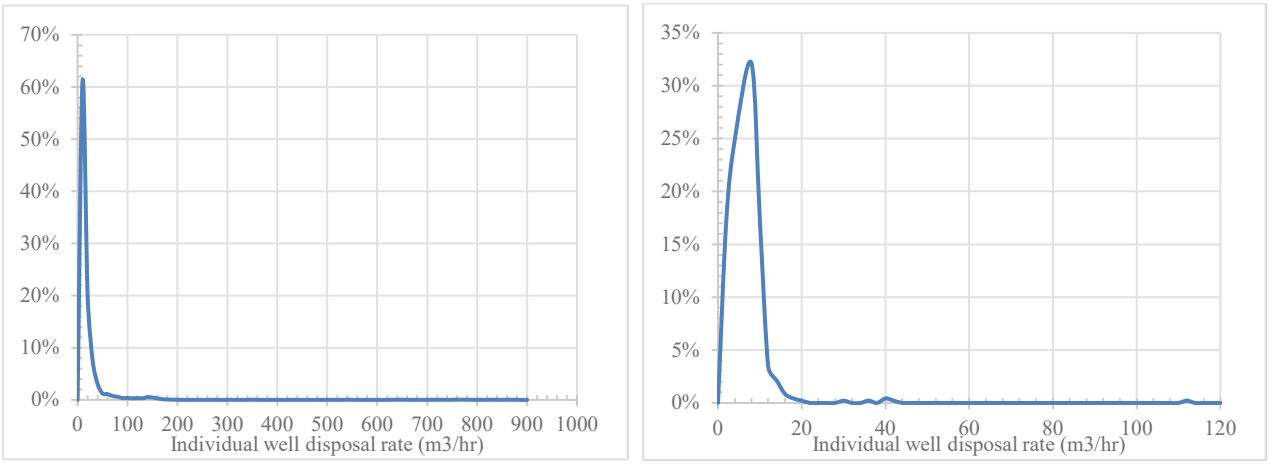

(a) **(b)**

*Figure 60. Historical per-well water injection rate (X-axis) frequency (Y-axis) distributions (January 1962-December 2022) in (**a**) the Keg River Formation; (**b**) the Muskeg Formation.*

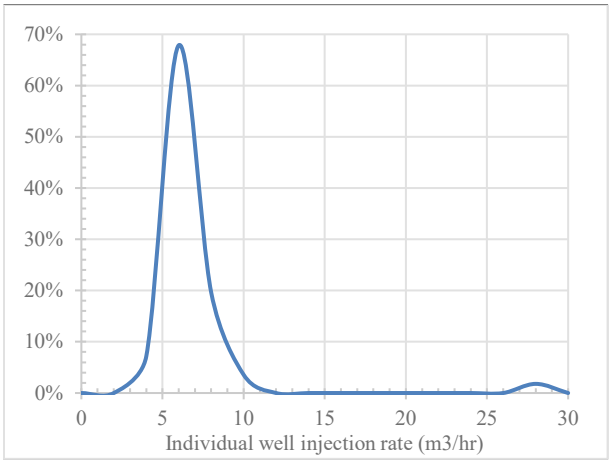

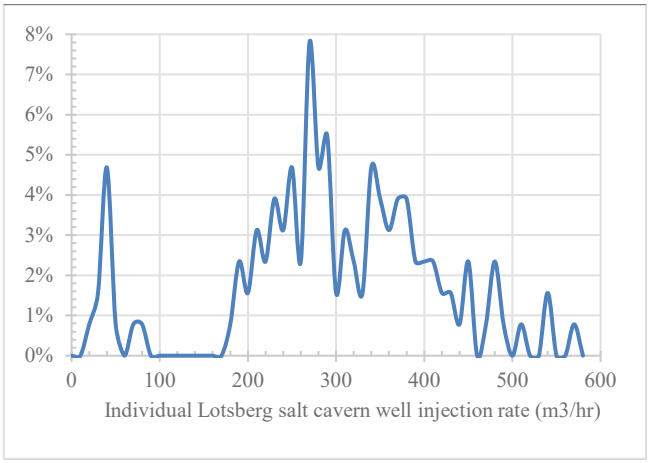

(a) **(b)**

*Figure 61. Historical per-well water injection rate (X-axis) frequency (Y-axis) distributions (January 1962-December 2022) in **(a)** the Contact Rapids Formation; **(b)** the Lotsberg Formation (note that these wells inject into purpose-built waste disposal salt caverns, and not into geologic pore space. The well injection rate variability shown in this figure consequently reflects waste disposal project operational factors (e.g., waste availability, staff availability) and not geologic constraints.*

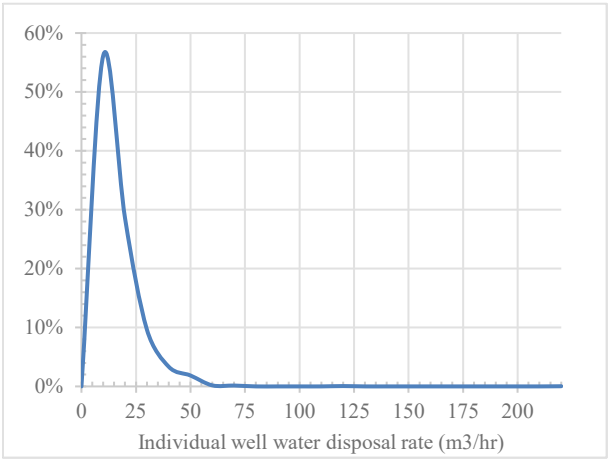

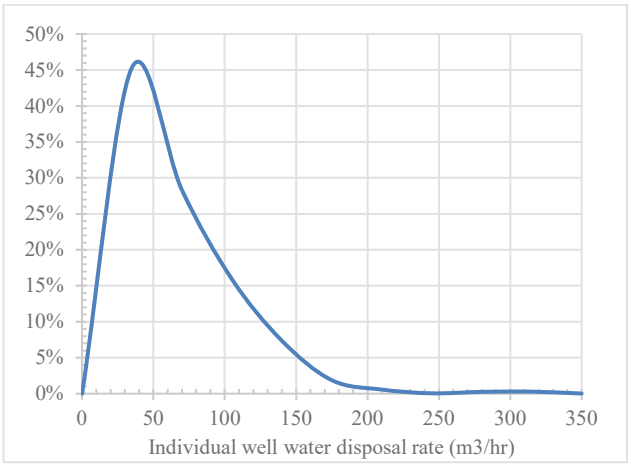

(a) **(b)**

*Figure 62. Historical per-well water injection rate (X-axis) frequency (Y-axis) distributions (January 1962-December 2022) in **(a)** the Granite Wash Formation; **(b)** the Basal Sandstone Unit.*